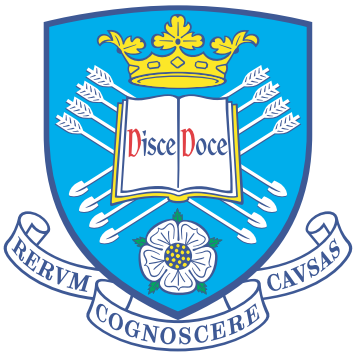

The University Of Sheffield.

Quantum Metrology of Grid Deformations and Squeezed Light

With applications in quantum imaging & quantum information

By

Jasminder Sidhu

Faculty of Natural Sciences
Department of Physics and Astronomy
University of Sheffield

A dissertation submitted to the University of Sheffield in partial fulfilment of the requirements for the degree of Doctor of Philosophy in the Faculty of Natural Sciences.

November 2018

Acknowledgements

I reserve a special thanks to my supervisor Pieter Kok. First for his trust placed in me to join his research group despite my limited experience in the field of quantum information theory, and second for his guidance and support throughout my graduate studies. He has been a fantastic teacher, whose continual optimism has been influential and inspirational. I feel grateful to have worked with him.

I owe thanks to my friends in the theory group: Giuseppe Buonaiuto, David Hurst, Scott Vinay, Luke Heyfron, Emiliano Cancellieri, Mark Howard, Earl Campbell, and Zixin Huang, for helping make the most of my graduate experience. Notable excerpts from memory include David's unique sense of humour, Scott's enthusiasm for debate, Howard's 'charm', Giuseppe's unique persona and Emiliano's special greetings! We all shared countless stimulating discussions and enjoyable times while establishing unnecessary etiquettes to pass onto the next generation of theorists. I would also like to thank others in the LDSD and EPMM group who have been great friends, and stewards for a punctual round-up on Friday evenings to appreciate the grain and hop. Particular thanks are due to Kyriacos Georgiou, Naoum Vaenas, and Rahul Jayaprakash for their support.

Thanks to Mark Quinn and Nigel Clarke for having faith in my ability to lead their undergraduate teaching for a short while, to gain experience in this and to apply for a fellow of higher education award. I did obtain the recognition, but the jury is still out on whether I did a good job.

Thanks are due to Antonios Ktenidis, and especially to Eleni Routoula for encouraging and supporting me during my PhD and for our many coffees together. I hope the closure of Starbuck's chain in Orchard square had nothing to do with our marathon social sit-ins most weekends!

Last, but not least, I would like to acknowledge the Defence, Science and Technology Laboratory (DSTL) who have financially supported my work under the Quantum 2.0 technologies programme. I hope they find this work as interesting as I have.

Author's declaration

I, Jasminder Singh Sidhu, declare that the work in this thesis was carried out in accordance with the requirements of the University's Regulations and Code of Practice for Research Degree Programmes and that it has not been submitted for any other academic award. Except where indicated by specific reference in the text, the work is my own work. Work done in collaboration with, or with the assistance of, others, is indicated as such. Any views expressed are mine.

SIGNED: ..... DATE: .....

Ευτυχισμένοι είναι οι ελεύθεροι και ελεύθεροι είναι οι γενναίοι.
The secret of happiness is freedom, and the secret of freedom, courage.
— Thucydides (460 BC-395 BC)

Some of the research has been published and presented at various conferences.

List of Publications

Jasminder S. Sidhu and Pieter Kok '*Quantum metrology of spatial deformation using arrays of classical and quantum light emitters*', Phys. Rev. A **95**, 063829 (2017)

Jasminder S. Sidhu and Pieter Kok '*Quantum metrology for general Hamiltonian parameters*', arXiv:1802.01601 (2018). (Submitted to Physical Review A.)

Jasminder S. Sidhu and Pieter Kok '*Optimal estimation of complex squeezing in phase space*', in preparation.

Zixin Huang, **Jasminder S. Sidhu**, Chiara Macchiavello, Lorenzo Maccone, and Pieter Kok '*Optimal Gaussian-state quantum illumination measurement*', in preparation.

Conferences

71st Scottish Universities Summer School in Quantum Optics and Quantum Dynamics (SUSSP71) 21 July - 02 August 2015, University of Strathclyde (Scotland) - Poster '*Quantum rulers for geometrical precision metrology*'.

Recent Advances in Quantum Metrology (RAQM2016) 02-04 March 2016, Warsaw (Poland), Co-author of talk presented by Pieter Kok: '*Quantum imaging with correlated photon measurements*'.

23rd Central European conference on quantum optics (CEWQO2016) 27 June - 01 July 2016, Kolymbari (Greece) - Talk and Poster '*Quantum metrology of spatial deformation using arrays of classical and quantum light emitters*'.

24th Central European conference on quantum optics (CEWQO2017) 26-30 June 2017, DTU Lyngby (Denmark) - Poster '*Quantum metrology of spatial deformation using arrays of classical and quantum light emitters*'.

UK Northern Quantum Meeting 2 (NQM2) 15 December 2017, Lancaster University (UK) - Talk '*Quantum metrology of spatial deformation using arrays of classical and quantum light emitters*'.

Physics of Light matter interactions 2018 (PLMCN19) 15-19 May 2018, Chengdu (China) - Poster '*Quantum metrology for arbitrary dynamics*'.

25th Central European conference on quantum optics (CEWQO2018) 21-25 May 2018, UIB-CSIC Palma de Mallorca (Spain) - Poster '*Quantum metrology for arbitrary Hamiltonian dynamics*'.

Organised conferences

Quantum Technologies 2015 (QUTE2015) 31 March 2015. Invited speakers: Christopher Gerry, Pieter Kok, Roger Colbeck, Vincent Boyer, Zlatko Papic, Naomi Nickerson, Henning Schomerus and Ahsan Nazir.

Abstract

In this thesis we make progress towards applications of quantum estimation theory to new physical systems. We first consider two commonly visited problems in quantum metrology: source optimisation and source localisation. For the first, we focus on estimating distances between neighbouring light sources along an array, which undergoes stretching deformations. We evaluate how changing the nature of the sources impacts the estimation precision of d by using the quantum Fisher information (QFI) as a figure of merit. By comparing this quantity for arrays of single photon emitters, coherent, thermal, and entangled sources, we find that the classical coherent and thermal states outperform the single photon emitters. This would be favourable since generating classical states is less resource-expensive to create. However, a quantum enhancement is observed when entanglement is employed. In agreement with separate work, the optimal state is that which entangles the eigenstates corresponding to the maximum and minimum difference eigenvalues of the generator. We demonstrate that not all entangled states can reproduce similar precision enhancements. This insight is reminiscent of previous studies, where entanglement was concluded as a necessary but insufficient resource for quantum metrology

Next, we address the source localisation problem to detect any deformations applied to a grid of sources. Improving this detection depends on our ability to engineer grids that maximise the sensitivity of the QFI matrix. Hence, we derive the generators of local translations of unitary evolutions that describe any general grid deformation, and show that our result is a multi-parameter extension of other results in the literature. We obtain a general result for the quantum Fisher information matrix (QFIM) through these generators for any grid deformation and explore specific spatial maps, including composite stretches, shears, and rotations. Since the QFI matrix depends only on the properties of the probe state and the configuration of the emitters, we explore how we can modify both to enhance our estimation sensitivity to determine the applied grid deformation. Physically motivated, we find the best arrangement of sources that enhances the sensitivity of detection for a set number of sources.

Finally, we consider the optimal estimation of a complex squeezing operation in phase space. The use of squeezed light as a quantum resource is ubiquitous in quantum optics, and a complete characterisation of a complex squeezing operation is pivotal for fundamental reasons. This is a true multi-parameter quantum estimation problem of incompatible observables. Specifically, we find that the symmetric logarithmic derivates (SLDs) for amplitude and directional squeezing do not commute. This prohibits simultaneous optimal estimates of both parameters, even in the asymptotic limit. As a result, we focus on finding separable optimal estimates. The Cramér-Rao bound is determined to provide a theoretical benchmark on the bi-variate estimation precision for general single mode Gaussian probes. Using this and the SLDs, we present a practical experimental implementation that can realise the individual fundamental precision bounds.

Table of Contents

List of symbols

The following list is neither exhaustive nor exclusive, but may be helpful. It contains symbols that have been used frequently or those that may cause confusion. Boldface characters denote vectors or matrices.

$\|x\|$	Norm of x
$\hat{A}^\dagger$	Hermitian conjugate of operator $\hat{A}$
$\hat{a}_j$	Annihilation operator for optical mode j
$\hat{a}_j^\dagger$	Creation operator for optical mode j
$\|n\rangle$	Fock number state with n photons
$\langle\hat{O}\rangle$	Expectation value of operator $\hat{O}$
$\|\alpha\rangle$	Coherent state
ρ_{Th}	Density operator for a thermal state
$\check{\varphi}$	Parameter estimate of φ_j
$\delta\varphi_j$	Variation in estimate of φ_j: $\delta\varphi_j = \check{\varphi}_j - \langle\varphi_j\rangle$
$\Delta\varphi_j$	Error in parameter estimate: $\Delta\check{\varphi}_j = \check{\varphi}_j - \varphi_j$
$\mathrm{Var}[\check{\varphi}_j]$	Variance of estimator
$\mathrm{B}[\check{\varphi}_j]$	Bias of estimator
ν	Number of independent repeat measurements
Λ	Unitary evolution channel
$\hat{\mathscr{E}}$	Positive operator valued measure
$\hat{\mathcal{G}}$	Hermitian generator of dynamics
$\hat{\mathcal{H}}$	Hamiltonian
$\mathcal{H}$	Hilbert space associated to the considered physical system
$\mathcal{H}_A \otimes \mathcal{H}_B$	Tensor product of Hilbert spaces $\mathcal{H}_A$ and $\mathcal{H}_B$
$\mathbb{I}$	Identity operator on the relevant Hilbert space
$\sigma(N)$	The permutation group of dimension N
$\boldsymbol{\mathcal{I}}^{\mathrm{C}}$	The classical Fisher information matrix (CFIM)
$\boldsymbol{\mathcal{I}}^{\mathrm{Q}}$	The quantum Fisher information matrix (QFIM)
s_i	The standard deviation of a Gaussian state associated with particle i
N	The number of physical resources used (e.g. photons)
$\boldsymbol{\mathcal{L}}$	The symmetric logarithmic derivative (SLD)
$\boldsymbol{\mathcal{L}}^{(R)}$	The right logarithmic derivative (RLD)
$\boldsymbol{\mathcal{L}}^{(L)}$	The symmetric logarithmic derivative (LLD)
n	Number of modes of a bosonic field
$\hat{\boldsymbol{a}}$	Vector of boson operators $\hat{a}_j$, $\hat{a}_j^\dagger$, for $j = 1, 2, \ldots, 2n$
$\hat{\boldsymbol{R}}$	Vector of quadrature operators $\hat{q}_j$, $\hat{p}_j$
$\hat{q}_j$	Quadrature position operator
$\hat{p}_j$	Quadrature momentum operator

σ_α	Pauli matrices for $\alpha = \{\mathbb{1}, x, y, z\}$
$\boldsymbol{H}$	Hessian matrix
r	Correlation coefficient for multi-variate normal distributions
r_ξ	Amplitude of squeezing
ϑ_ξ	Direction of squeezing
$\chi_\rho(\boldsymbol{\zeta})$	Multivariate characteristic function for $\boldsymbol{\zeta} \in \mathbb{R}^{2n}$
$\boldsymbol{S}_\xi$	Symplectic map for a single mode squeezing unitary
$\boldsymbol{R}_\vartheta$	Symplectic map for a phase operator

Abbreviations

BCH	**B**aker-**C**ampbell-**H**ausdorff
CFIM	**C**lassical **F**isher **I**nformation **M**atrix
CRB	**C**ramér-**R**ao **B**ound
GHZ	**G**reenberger-**H**orne-**Z**eilinger $(\|0\rangle^{\otimes M} + \|1\rangle^{\otimes M})/\sqrt{2}$ state
HL	**H**eisenberg **L**imit, $\Delta\vartheta \propto N^{-1}$
HUP	**H**eisenberg **U**ncertainty **P**rinciple
IID	**I**ndependent and **I**dentically **D**istributed
MLE	**M**aximum **L**ikelihood **E**stimation
NOON	Maximal path entangled $(\|N,0\rangle + \|0,N\rangle)/\sqrt{2}$ state
PDF	**P**robability **D**istribution **F**unction
POVM	**P**ositive **O**perator **V**alued Measure
QCRB	**Q**uantum **C**ramér–**R**ao **B**ound
QET	**Q**uantum **E**stimation **T**heory
QFIM	**Q**uantum **F**isher **I**nformation **M**atrix
RLD	**R**ight **L**ogarithmic **D**erivative
SLD	**S**ymmetric **L**ogarithmic **D**erivative
SPE	**S**ingle-**P**hoton **E**mitters
SQL	**S**tandard **Q**uantum **L**imit, $\Delta\vartheta \propto N^{-1/2}$
VEV	**V**acuum-**E**xpectation-**V**alues

List of Tables

List of Figures

Part 1

Introduction and Background

We commit this part of the thesis to introduce the motivation of this work, and to review the necessary theoretical preliminaries that will be used in subsequent parts. By this very nature, none of the material presented in the constituent chapters to this part contain original work. In chapter 1, we contextualise the role quantum metrology has in quantum theory. After a brief highlight of important milestones in the field, we explain the goals and motivations of quantum sensing. Chapter 2 introduces some concepts from quantum optics necessary for understanding the research in later chapters. Finally, in chapter 3, we review methods in quantum estimation theory.

Chapter 1

Introduction

The work in this thesis has been driven by a twofold motivation. First, determining the precision bounds of parameter estimations of unknown physical parameters with resolutions that surpass classical limits, and second, realising practical implementations that saturate these bounds. As we will see, this requires 'quantum resources'. This requirement often makes the practical implementations of these improved estimation resolutions extremely difficult. For this reason, very few experiments have demonstrated the fundamental resolution limits that quantum mechanics predicts. Before detailing the approach to parameter estimations, we first introduce the subject of quantum mechanics and quantum metrology in this chapter. Many clear and pedagogical accounts of the development of quantum physics exist in the literature [Glauber, 2005]. The introduction provided here is brief and intended to summarise some of the achievements in quantum metrology. We conclude by presenting a roadmap of the thesis ahead.

1.1 Foundations of quantum optics

Although the interface between classical and quantum mechanics remains a heavily researched topic [Wetterich, 2009; Jeong et al., 2014], among the first strains to appear in classical electromagnetism was accounting for the observed spectral distribution of blackbody radiation. Averting the so-called '*ultraviolet catastrophe*' required that the energies of harmonic oscillator modes be quantised. This realisation by M. Planck in 1900 was a key departure from classical treatise on light. Together with A. Einstein's theory of the photoelectric effect in 1905, and L. de Broglie's hypothesis of a wave-particle duality in 1924, this paved an alternative quantum mechanical description of light as particles.

In midst of these developments, the study of optics continued its development to maturity without the need for a quantum description of light. Many experiments could be described through application of Maxwell's equations of electromagnetism. For example, interferences of field amplitudes explained Young's two slit experiment, where light is incident on two slits. The catalysis for the development of a full quantum treatment of optics was the R. H. Brown and R. Q. Twiss intensity interferometer [Brown and Twiss, 1956a,b, 1957, 1958a,b] that

measured the correlation in photon number arrivals at two detectors. This intensity correlation revealed information on the two-time beam intensity, and by simply altering the setup, the time separation could be controlled. An enhanced correlation of photons—or *bunching*—from a seemingly uncorrelated thermal source was observed for short time separations[1]. Although the effect could be predicted by treating the intensity fluctuations of the electric field [Brown and Twiss, 1956b; Purcel, 1956], it did little to subside general scepticism surrounding the veracity of the result. This provided the groundwork for the seminal work of R. J. Glauber, whose quantum theory of optical coherence [Glauber, 1963a,b,c] explained the effects of the Hanbury-Brown and Twiss experiment and permitted additional predictions. The first was the possibility of anti-bunching, which describes an increase in the average temporal separation of photon count statistics, or sub-Poissonian statistics [Walls and Milburn, 2008]. The second was the squeezing of quantum fluctuations, which was first observed by Slusher et al. [1985]. Squeezing was also demonstrated in other systems [Wu et al., 1986].

A cascade of research efforts oversaw the maturity of quantum optics. The first theoretical and experimental realisation of non-classical behaviour from a physically accessible system was anti-bunching generated in resonance fluorescence from a two-level atom [Kimble et al., 1977; Carmichael et al., 1980]. Experimental work in the 1960s and 70s lead to improvements in photon counting detectors. These devices could now distinguish between the different photon number statistics from coherent and incoherent light. In tandem, new sources of laser light were being developed. In the 1980s, experimental work by Mukai and Yamamoto [1981], showed that suppressing the pump noise reveals the quantum behaviour of the laser.

Generation of single photon sources were pioneered by Santori et al. [2001] using quantum dots and later through parametric down-conversion (PDC) [Takeuchi et al., 2003]. In PDC, a strong pump photon illuminates a nonlinear crystal and produces two photons with lower energies. The emerging '*down-converted*' photon pairs conserve the total energy and momentum of the pump and are entangled in either frequency, polarisation or momentum. This generates intensity correlations that have demonstrated violations in Bell's inequalities [Aspect et al., 1982; Weihs et al., 1998; Matsukevich et al., 2008; Ansmann et al., 2009], have been used in quantum imaging [Pittman et al., 1995], and continuous variable quantum communication tasks [Porzio et al., 2007; Gehring et al., 2015].

These efforts opened the door to work in quantum information processing. First, the development of squeezed states helped realise applications of quantum information processing [Loudon and Knight, 1987; Braunstein and Kimble, 1998; Braunstein and van Loock, 2005; Andersen et al., 2009], quantum teleportation [Furusawa et al., 1998], continuous variable quantum computing [Menicucci et al., 2006, 2007; Aoki et al., 2009; Yonezawa and Furusawa, 2010], and Einstein-Podolsky-Rosen (EPR) experiments [Reid and Drummond, 1988; Ou et al., 1992]. Second, ion trap technology had been proposed as the foremost method to control single quantum systems. A scalable theoretical scheme proposed by J. I. Cirac and P. Zoller detailed how lasers could be used to process the information stored in the states of trapped ions [Cirac and Zoller, 1995]. Ion trap technology has so far provided the most promising approach to quantum information processing [Knight et al., 2003]. The current record for the maximum number of entangled and individually controllable qubits is 20 [Friis et al., 2018].

The speed of transmission and robustness against decoherence make single photons ideal for quantum information processing [Northup and Blatt, 2014]. However, many quantum information protocols require high-purity single photon sources. This is difficult to realise since

[1]The definition of short timescales is in comparison with the coherence time of the thermal state.

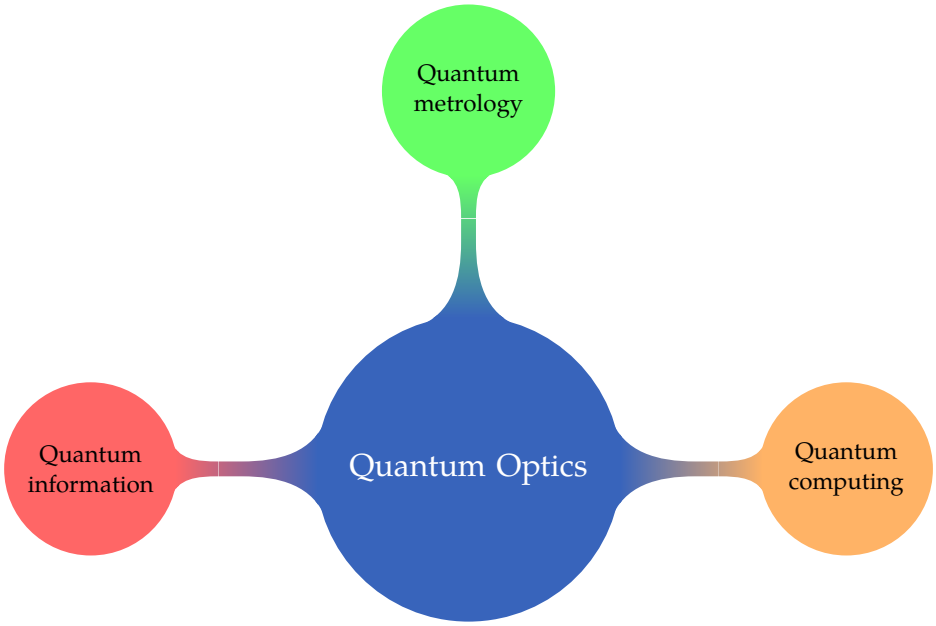

Figure 1.1: *Modern day quantum optics has applications in diverging fields of quantum metrology and sensing, quantum computation and quantum information processing.*

enhancing single-photon efficiency is incompatible with methods to suppress multi-photon emissions. Achieving ultrahigh purity single photon sources is part of an active research by a number of different experimental groups [Shields, 2007; Heinze et al., 2015]. Another difficulty is the very weak optical nonlinearities of optical fields. Quantum computing requires strong entanglement between independent degrees of freedom to realise nonlinear operations in the form of switches when processing information. Despite work on nonlinear optics, generating photon interactions is hard to realise [Chang et al., 2014]. One method to circumvent this difficulty is to use adaptive photon counting measurements, which was proposed by E. Knill, R. Laflamme G. J. Milburn (KLM) in 2001 [Knill et al., 2001]. Experimental demonstrations of simple quantum gates using only linear optical interactions soon followed [Ralph et al., 2002; O'Brien et al., 2003]. The KLM scheme heralded a new era of universal linear-optical quantum computing (LOQC) [Kok et al., 2007; O'Brien, 2007; Kok, 2016].

Modern day quantum optics continues to evolve through different sub-fields (see figure 1.1). An important development for sensing applications is quantum metrology. We will introduce this in the next section.

1.2 Quantum metrology

For many quantities in physics, direct measurements are not possible. This is common in quantum optical experiments, where variables such as entanglement, phase, time, and purity do not have associated quantum observables. In these situations, the value of a parameter—or vector of parameters—must be inferred from a set of measurements of a different but related observable, or set of observables. This procedure is addressed in estimation theory [Kay, 1993], the formalism underlying the study of sensing and metrology, where the objective is to find the fundamental precision bounds of parameter estimates.

1.2.1 Applications of quantum metrology

The astounding potential of metrology has been displayed through a century of creative and fruitful applications. The origin of its application in science can be traced back to the definition of physical units. Since then, modern metrology has been applied to a range of applications including:

Radar: estimate the delay of radar echoes in the presence of noise

Imaging: track the orientation and position of an object

Seismology: estimate size and depth of oil reserves/rock formation

Telecommunications: estimate carrier frequency to demodulate signal.

The push for superior image qualities and better resolutions in imaging devices has seen a sharp increase in the number of pixels used per unit area. This miniaturisation sees each pixel illuminated with minute photon fluxes, down to the detection of single photons. Any performance improvements to optical metrology, sensing, and information is then inherently limited by the microscopic properties of nature itself. These difficulties reflect the 'death march of Moore's law' in manufacturing that has placed physical limits to the lithography industry [Sreenivasan, 2017] and conventional computing [Markov, 2014]. Despite the maturity of metrology, these difficulties naturally gave rise to a new era of *quantum metrology*, which uses the laws of quantum mechanics to surpass classical resolution limits. At the heart is a desire to improve our ability of manipulating the quantum nature of light. Whilst the initial interest in metrology as the science of measurements endures, quantum metrology heralds the possibility of exploring new avenues of research with consequences for both academic ingenuity and technological prowess. Imaging is one clear example of this.

Progress in science has historically leaped forward in tandem with improvements to imaging techniques. Consider early work by G. Galilei who, through improvements to the design of telescopes, presented supporting observations of the heliocentric theory of the Solar System. Progressive improvements of the telescope has culminated in the Hubble space telescope become one of the largest and most versatile imaging devices of space, enabling breakthroughs in astrophysics. In contrast, development of the microscope around 1660 pushed knowledge of science at small scales. This enabled the first observation of the cell by R. Hooke in 1665. Since, progressive efforts have been made to push the resolution of light microscopes past E. K. Abbe's stipulated limit. This culminated in the 2014 Nobel prize in Chemistry awarded "*for the development of super-resolved fluorescence microscopy*" [Betzig et al., 2018]. Other examples of how imaging techniques have been applied include tracking the movement of proteins tagged with fluorescent dyes [Heller et al., 2013] and imaging to search for exoplanets [Macintosh et al., 2014].

The wave nature of light imposes fundamental limits to achievable resolutions of optical imaging devices. One strategy to resolve finer details is to reduce the wavelength of the light. A particular drawback of this method becomes clear when applied to biological samples, since high energy light can be destructive [Wolfgramm et al., 2013]. Breakthroughs in imaging methods that surpass the diffraction limit are expected to follow in tandem with advancements in quantum metrological protocols. This will lead to advancements in all complementary fields of research as well as the development of more precise and intricate imaging devices for the next generation. An immediate and recent exemplification of this can be recognised through

the powerful and breathtaking field of gravitational-wave astronomy; an emerging branch of observational astronomy that uses gravitational waves to collect data about massive galactic objects such as neutron stars and black holes. Exotic states of light, such as squeezed light, are now routinely used to enhance the sensitivities of large interferometers, such as the advanced LIGO for the measurement of gravitational waves [Caron et al., 1995; Abbott et al., 2004; Abadie et al., 2011; Aasi et al., 2013]. Estimations of gravitational wave amplitudes have also been made by considering phonons in Bose-Einstein condensates [Berrada et al., 2013; Sabìn et al., 2014].

1.2.2 Methods in quantum estimation theory

Any measurement scheme is plagued with errors of both systematic and statistical nature. A completely classical approach to reduce the statistical errors of a stochastic nature is to repeat the experiment ν times. The central limit theorem states that the normalised sum of identical and independently distributed (IID) samples of a random variable approximates to a normal distribution as the sample size gets larger[2]. Owing to this, the resulting root mean square error (RMSE) of a repeated experiment scales as $\nu^{-1/2}$. For a single shot experiment ($\nu = 1$), and a given measurement procedure, the best classical scaling is achieved by using an N separable optical probe state, constructed from N unentangled states. This increases the effective resources used and gives rise to the standard quantum limit (SQL), where the error scales as $N^{-1/2}$ [Caves, 1980], which is the best classical scaling achievable through N repeated measurements.

Through meticulous preparation of the measurement scheme, it should be possible to suppress all stochastic noise associated with classical indeterminacy in the probe states. However, this suppression will have no effect on the *quantum vacuum fluctuations* inherent in the state, which fundamentally imposes some minimum quantum optical noise [Gardiner and Zoller, 2004]. For some electromagnetic field with frequency ω, the minimum quantum optical noise is quantified with amplitude [Loudon and Knight, 1987]:

$$\mathscr{E}_0 = \left(\frac{\hbar\omega}{2\epsilon_0 V}\right)^{\frac{1}{2}}, \tag{1.1}$$

for some mode volume V, and ϵ_0 is the permittivity of free space. Notice that it is independent of the field strength, which implies that even in vacuum with no field present, this quantum noise endures. Hence, Eq. (1.1) quantifies the vacuum fluctuations of an optical field of frequency ω.

Despite this, probes endowed with quantum resources, such as entanglement or non-classical correlations, provides opportunity to propel estimation theory past the SQL. Specifically, although quantum mechanics has placed strict limits on the achievable precision of parameter estimates, it can be used to *approach* these limits. In fact, the use of quantum resources is necessary to achieve the fundamental *Heisenberg limit* for error scalings: N^{-1}, where N is the number of probe states used [Braunstein, 1992]. An example of another non-classical resource used is squeezing. Squeezed states reduce the optical noise in one of the field quadratures while increasing the noise in the other. Figure 1.2 illustrates how different types of optical squeezing can be used to engineer precision enhancements. Squeezed states have successfully demonstrated enhanced resolutions that surpass the standard quantum limit in interferometric and imaging applications [Bradshaw et al., 2017; Li et al., 2016; Ruppert et al., 2016], and in

[2]The central limit theorem holds even if the original variables are not normally distributed themselves. One exception to this are Lévy processes. However, under certain conditions the sum of IID samples of a multi-dimensional Lévy process still converges to a multivariate Gaussian distribution [Grabchak, 2013].

Regime	Variance resource scaling	Achievability
Standard quantum limit (SQL)	$1/N$	Remove all classical noise
Heisenberg (HL)	$1/N^2$	Quantum resources

Table 1.1: *Comparison of achieving the different regimes of variance scalings with the resources used in metrology. We will derive a generalisation of these variance scalings for multiple-parameters later in chapter 3 where we also discuss their achievability in further detail.*

quantum metrology [Anisimov et al., 2010; Huang et al., 2015] for phase estimations [Berni et al., 2015] and tracking [Yonezawa et al., 2012]. Realising the Heisenberg limit for parameter estimates is the main attraction of using squeezed light for quantum metrology.

The characterisation of N for any estimation strategy is important. The precision of parameter estimates is bounded by the physical resources, a matter addressed by the query complexity of the quantum network describing the estimation procedure—that is, the number of times a measured system is sampled [Giovannetti et al., 2006; Zwierz et al., 2012b]. The resource count of a physical system is defined by the variance of the generator of translations in the parameter to be estimated. Incorrect characterisation of the resources has suggested so-called '*super Heisenberg-scalings*' [Beltrán and Luis, 2005; Boixo et al., 2007; Roy and Braunstein, 2008]. Reconciliation of the resource count led to consistency with the HL [Zwierz et al., 2010]. Table 1.1 summarises the fundamental precision scalings for classical and quantum metrology.

Quantum metrology is rooted in the theory of quantum parameter estimation, pioneered by Helstrom [1976] and Holevo [2011]. The archetypal schema for general parameter estimations is decomposed into three distinct steps: (I) probe preparation, (II) parameterisation through an interaction with a system that encodes a set of parameters to estimate, and (III) probe readout, with possibility of feedback. For a given interaction, this describes two aspects of control for the experimenter; a suitable choice of probe state that is sensitive to changes in the parameters to assimilate maximal information, and an appropriate measurement that maximises the information extracted from the probe. This is a two-step optimisation problem. A natural figure of merit to quantify the performance of the estimation is the variance between parameter estimates and the true value. The quantum Cramér-Rao bound (QCRB) was introduced to characterise this optimisation procedure, and has become a standard tool in providing a lower bound on the variance of an unbiased estimator that maps measured data from quantum measurements to parameter estimations [Helstrom, 1976]. It provides a fundamental bound to the achievable precision of any estimating strategy and depends only on the uncertainty in the quantum state. An important statistical quantity that determines the QCRB is the quantum Fisher information (QFI), which depends only on the probability distribution from which data is sampled. In information geometry, the QFI is equivalent to the Bures metric, which quantifies the distinguishability of quantum systems [Amari and Nagaoka, 2007; ichi Amari, 2016]. A large information content implies that small changes to the parameter achieve large statistical displacements of the evolved probe in state space [Braunstein and Caves, 1994]. A more complete discussion of statistical distances can be seen in Bengtsson and Zyczkowski

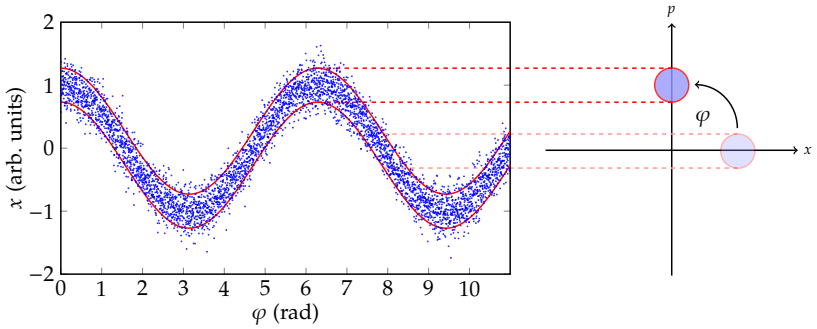

(a) *Laser light or Glauber semi-classical coherent states. Equal noise in both quadratures.*

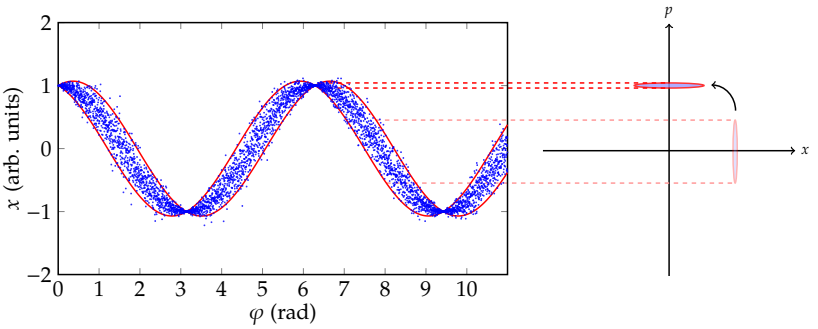

(b) *Enhanced phase noise with concomitant decrease in amplitude fluctuations.*

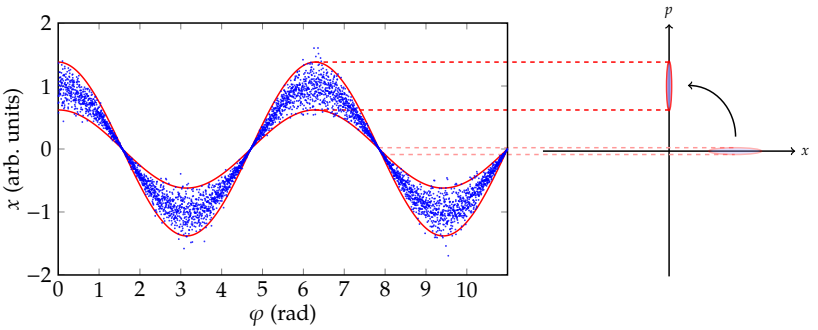

(c) *Enhanced amplitude noise with concomitant decrease in phase fluctuations.*

Figure 1.2: *Illustration of different quadrature x and p noises for optical fields, through simulations of the electric field, as measured through homodyne measurements with varying phases. Fig. 1.2a represents Glauber's semi-classical coherent states. These states have circularly symmetric uncertainty regions in phase space for both the phase and amplitude. A state with no noise would be ideal to achieve extreme sensitivities. However, this is fundamentally not possible since all optical fields retain quantum uncertainties quantified by Heisenberg's uncertainty relation. However, the uncertainty relation lower bounds only the noise product of both quadratures, implying that we can reduce the uncertainty in one quadrature, followed by an equal and concomitant increase in the second. Experimentally, this is realised through 'squeezed sources'. Fig. 1.2b and Fig. 1.2c illustrates a phase squeezed and amplitude squeezed coherent state as input respectively. This illustrates that choosing the direction of squeezing is important in the estimation of phase or amplitude of optical fields.*

[2008]; Kok and Lovett [2010]. The larger the dependence, the more distinguishable the evolved state becomes to its unperturbed state. Since the QCRB is the inverse of the QFI (for a single data sample), this permits an estimate with a lower estimated variance. With the information content being governed entirely by the state space structure, we observe again that minimising the QCRB requires optimising the state choice.

1.3 Previous work in quantum metrology

Quantum mechanics has established physical limitations to precision bounds in myriad applications in parameter estimation. An early example of this is the energy-time uncertainty relation. Its credibility was put to question by A. Einstein, who in 1930 argued that a photon emerging from a box can be prepared with exact energy and emitted at a predictable time [Dieks and Lam, 2008]. This was refuted by N. Bohr who developed the box thought experiment illustrated in figure 1.3.

Approaching the limitations to precision bounds through high precision measurements has seen the development of fundamental theories across science. Quantum enhanced measurements have demonstrated performance improvements in a wide variety of applications that have implications for technology and science. Examples include atomic clocks, remote sensing, navigation, and thermometry [Tóth and Apellaniz, 2014; Degen et al., 2017; Pearce et al., 2017]. We start this section by detailing specific problems in quantum metrology that have attracted considerable research effort, before reviewing more general frameworks in estimation theory.

1.3.1 Single parameter phase-like estimations

Early work in this field predominantly focused on single parameter estimations of unitary, multiplicative parameters. Specifically, for some parameter ϕ to estimate, the probe evolution is governed by the unitary $\hat{U} = \exp[-\phi\hat{\mathcal{H}}]$, where $\hat{\mathcal{H}}$ is a Hermitian generator. Examples of parameter estimations that come under this category are phase and time [Leibfried et al., 2004; Giovannetti et al., 2011; Tóth and Apellaniz, 2014]. The quantum enhanced limit for this has been shown to always be attainable [Paris, 2009]. Further examples include estimates of the profile of time-varying fields [Tsang et al., 2011; Magesan et al., 2013] and gradient magnetometry [Urizar-Lanz et al., 2013]. These problems are categorised by *phase-shift Hamiltonians*; a special case where the parameter to estimate multiplies a parameter-independent Hermitian generator [Holevo, 1978; Braunstein et al., 1996]. An immediate example of this is single phase estimations. A Mach-Zehnder interferometer illustrated in figure 1.4 makes high precision measurements of a relative phase difference between two beams of light derived from some input state $|\psi_{\text{in}}\rangle$. This phase referenced method has become a standard tool in estimation theory and has received considerable attention given its applications in enhanced phase estimations in optical interferometry [Demkowicz-Dobrzanski et al., 2009; Pezzé and Smerzi, 2014], frequency measurements [Bollinger et al., 1996; Huelga et al., 1997], and biosensors [Luff et al., 1998; Yang et al., 2001].

Phase-shift Hamiltonians have attracted significantly more attention since a large proportion of metrological protocols can be reduced to that of phase estimation [Giovannetti et al., 2004]. This has proven particularly important in quantum enhanced Hamiltonian tomography, where unknown multiplicative coefficients of the Hamiltonian are estimated after a suitable decomposition [Yurke et al., 1986; Sanders and Milburn, 1995; Dorner et al., 2009; Skotiniotis et al., 2015].

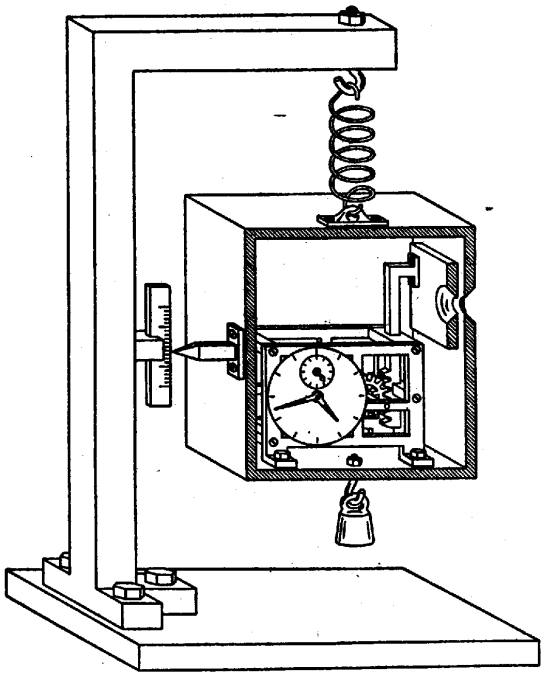

Figure 1.3: *Einstein-Bohr photon box [Dieks and Lam, 2008]. Bohr's arguments upheld the uncertainty relation between the energy and emission time of a photon emission.*

It has long been known that quantum resources are required to improve the estimation precision of a single phase parameter in optical interferometry [Caves, 1981]. For Mach-Zehnder interferometers, the highly entangled NOON states provide a quadratic improvement to give the Heisenberg scaling for phase estimates [Lee et al., 2002]. In general however, the type of resource used needs to be tailored specifically for the estimation protocol. This makes a universally applicable optimal sensing device difficult to realise. Typically though, the Greenberger-Horne-Zeilinger (GHZ) states are suited for local phase estimations. Practically, the entanglement generation of these states and measurement readout times must be lower than some threshold to observe an advantage over separable states [Dooley et al., 2016]. Alternatively, highly squeezed non-classical states have been reported to provide a quadratic advantage when estimating certain Gaussian transformations [Friis et al., 2015]. These resources have also been exploited in quantum imaging to drive resolution capabilities past the Abbe-Rayleigh criterion [Abbe, 1873; Rayleigh, 1879; Fei et al., 1997; Boto et al., 2000; Abouraddy et al., 2001; Thiel et al., 2007; Kolobov, 2007; Lloyd, 2008; Oppel et al., 2012; Pearce et al., 2015]. For single parameter phase-shift Hamiltonians, the optimal probe resource was addressed by Giovannetti et al. [2006]. The optimal state that maximises the QFI is constructed from an equal superposition of eigenstates corresponding to the minimum and maximum eigenvalues of the Hamiltonian [Giovannetti et al., 2006, 2011].

1.3.2 Arbitrary Hamiltonian parameters and multiple parameters

Quantum metrology has been applied to more general scenarios than single multiplicative parameters of generators evolving under unitary dynamics. These generalisations include:

Arbitrary Hamiltonian parameterisations: i.e. estimating parameters that appear as non mul-

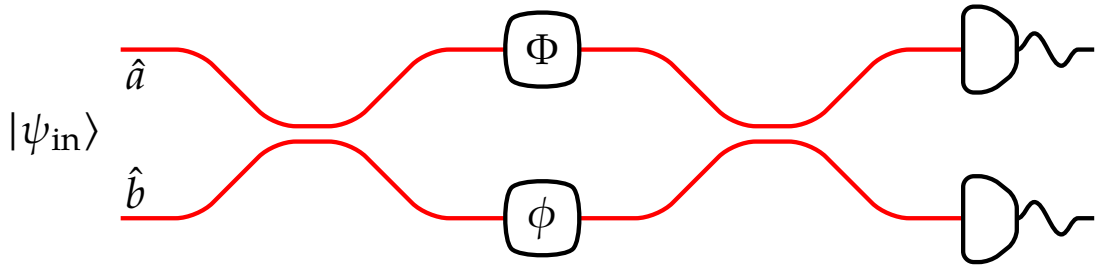

Figure 1.4: *Illustration of a Mach-Zehnder interferometer, as proposed by L. Mach and L. Zehnder in 1891. An optical path difference between both arms of the interferometer results in a relative phase difference. High precision measurements of this phase difference have found many applications. Here, $\hat{a}$ and $\hat{b}$ define two input modes. The objective is to estimate the unknown phase Φ by controlling the phase ϕ and measuring the photon intensities at the output. This is represented by the detectors on the right.*

tiplicative factors to the Hamiltonian.

Multiple parameters: Simultaneous or separable estimates of multiple parameters.

Non-unitary probe evolutions: Estimates of parameters evolving under decoherences.

Continuous variable systems: Metrology with Gaussian probe states.

First, arbitrary Hamiltonian parameterisations would allow application of quantum metrology to a wider variety of quantum systems. This has been considered only recently by a few authors [Brody and Graefe, 2013; Pang and Brun, 2014, 2016; Seveso and Paris, 2017; Fraïsse and Braun, 2017]. A second generalisation is multiple parameter estimation. This has direct practical applications since many applications, such as microscopy, optical, electromagnetic, and gravitational field imaging, demand knowledge of multiple parameters. Further, it has been shown that simultaneous estimation of parameters can achieve better precision than estimating them individually for equivalent resources and under certain conditions [Humphreys et al., 2013; Baumgratz and Datta, 2016]. This has seen a surge of recent work focused on yielding quantum enhanced sensing from simultaneous estimation of multiple parameters [Fujiwara, 1994; Matsumoto, 2002; Monras and Illuminati, 2011; Genoni et al., 2013; Crowley et al., 2014; Vidrighin et al., 2014; Yao et al., 2014; Yue et al., 2014; Knott et al., 2016; Kok et al., 2017]. Multi-parameter quantum enhanced sensing has also provided a novel paradigm for investigating the information processing capabilities of multipartite or multimode quantum correlated states and measurements. Bounding the covariance of multi-parameter estimates through the Ziv-Zakai bound was considered by several authors [Zhang and Fan, 2014; Berry et al., 2015]. Finally, a well researched application of quantum metrology is the class of pure states and unitary transformations. A more realistic model accounts for mixed states evolving under decoherent evolutions. We briefly review this in the next subsection.

1.3.3 Estimation of parameters with non-unitary dynamics

Practical applications of quantum metrology must include a description of the interaction of a system with its environment. Unfortunately, noise degrades the optimal quadratic enhancement

of precision estimates to one that is a constant improvement over classical methods [Demkowicz-Dobrzański et al., 2012]. To specifically quantify this impact, an estimate of the decoherence parameter(s) is necessary. To address this, a general method to calculate parameter precision bounds in the presence of noise was developed by Chin et al. [2012]; Kołodyński and Demkowicz-Dobrzański [2013]. This was extended to many-body open systems in [Beau and del Campo, 2017]

Despite the reduced precision enhancement, all hope is not lost. Entanglement and passive external ancillas can be used to improve the precision in open quantum metrology [Demkowicz-Dobrzański and Maccone, 2014]. Interestingly, quantum illumination is the only application of quantum metrology that retains its advantage over classical methods, even when decoherence effects completely destroy the entanglement [Tan et al., 2008].

1.3.4 Parameter estimation with continuous variables

We described previously that calculating the QFI is central to any quantum metrological protocol. However, doing so is not always an easy task. All of the work described in the previous subsection relies on knowledge of the density matrix to find the QFI. This approach is much less convenient for Gaussian states. These states are heavily used in continuous-variable quantum information. We defer specific details to the forthcoming chapters and suffice to say that Gaussian states can be completely characterised through only the first and second moments of the quadrature operators. The evolution of Gaussian states is then conveniently addressed in the phase-space formalism [Adesso et al., 2014]. By mapping transformations of the state to transformations of the moments, the theory for estimation using Gaussian states is more conveniently done through the phase-space formalism.

The first work in this direction was completed by Pinel et al. [2012] who derived the expression for the ultimate limit to parameter estimations using pure Gaussian states of arbitrarily many modes. This was shortly followed by a generalisation of the quantum fidelity to mixed and pure Gaussian states [Spedalieri et al., 2013]. Marian and T. A. Marian developed on this work by analysing the fidelity of a pair of multimode Gaussian states [Marian and Marian, 2012]. The general result is difficult to solve if the number of modes is greater than two, unless the Gaussian states commute or at least one of them is pure. For one and two mode Gaussian states, they derived an analytic result of the fidelity. This allowed for the derivation of the general formula for single mode Gaussian states [Pinel et al., 2013]. An alternative approach to finding the QFI and the symmetric logarithmic derivative (SLD) is through the mean displacement and covariance matrix of the Gaussian state. This approach has been taken by a number of authors. The first result in this direction was by A. Monras in 2013 who derived the form of the SLD for general Gaussian states evolving under Gaussian unitaries [Monras, 2013]. By taking an SLD ansatz that is quadratic in the quadrature operators, the SLD and QFI is written as an infinite series solution to the Stein-equation. A similar approach by Z. Jiang confirmed Monras' result and gave the SLD for states in exponential form in terms of the generator and its moments [Jiang, 2014]. Y. Gao and H. Lee followed an alternative method to derive the SLD and the QFI for multi-mode Gaussian states. The necessity of inverting relatively large matrices is a drawback of this method [Gao and Lee, 2014]. A recent attempt to unify these results for multi-mode Gaussian states was reported in [Šafránek et al., 2015].

1.3.5 Optimal implementation

Once the fundamental limits to the precision of parameter estimations have been determined, a natural question that arises is the following: *given that all classical noise have been eliminated, how can we identify the measurement(s) that practically saturate these bounds?* A key term that describes the optimal measurement in the so-called symmetric logarithmic derivative (SLD) [Braunstein et al., 1996]. Specifically, an optimal measurement is constructed from the eigenstates of the SLD [Paris, 2009]. In almost all cases, determining the measurement that corresponds to this theoretical description is difficult on two accounts. First, it generally depends on the parameters that we would like to estimate. Adaptive strategies have been suggested to circumvent this [Berry and Wiseman, 2000, 2002]. The second difficulty is in the context of multiple-parameter estimations. If the SLDs for each parameter are mutually compatible—that is they all commute with one another—then a simultaneous, optimal estimate for all of the parameters can be made in their common eigenbases. Generally, optimal measurements may not commute. In this case, a compromise between the convenience of a simultaneous measurement and the attainable estimation precision for each parameter must be addressed. To illustrate this, a tradeoff between simultaneous phase and loss estimation in interferometry was addressed by Vidrighin et al. [2014]; Crowley et al. [2014]. The conditions for when the information content from simultaneous estimation of multiple parameters matches or exceeds that from separable measurements for pure and mixed states was analysed by Ragy et al. [2016].

Even for single parameters, determining the measurements from the SLD is difficult. Because of this, few works in the literature have managed to discuss how to perform quantum optimal estimates. Specifically for thermometry, photon number counting and classical post-processing of the data has been proposed as an optimal measurement [Helstrom, 1968; Nair and Tsang, 2015]. An alternative method that estimates the temperature with close to optimal precision and without the need for adaptive strategies was proposed by Pearce et al. [2017]. This is exactly the Mach-Zehnder interferometer scheme illustrated in figure 1.4 but with a random variable phase shift. As this shows, any accessible measurement scheme should decompose the SLD in terms of linear optics and additional classical post-processing.

1.4 Research outline of this thesis

In this thesis, we extend previous work by considering different applications of quantum estimation theory. We present a general framework for the detection and estimation of deformations applied to a grid of sources. This makes progress towards multi-parameter quantum estimation theory and addresses two commonly visited problems in quantum metrology: source optimisation and source localisation. We find general results, while also reconciling previous work. Specifically, entanglement between different probe states must be carefully chosen to deliver precision enhancements over classical strategies.

This thesis is structured as follows. In chapters 2 and 3, we review some background theory on quantum optics and quantum estimation theory respectively. Our research will follow this. In chapter 4, we estimate the distances d between neighbouring light sources along a one-dimensional array. We evaluate how changing the nature of the light sources attached effects the estimation precision. Our formalism uses the Hamiltonian formulation of the quantum Fisher information matrix (QFIM) as the figure of merit to quantify the amount of information we have on d as the array is stretched. We compare the performance of single photon emitters, coherent, thermal, and entangled sources of single photon emitters on the estimation of d. For

some number of sources, the optimal probe state is determined. This work provides a method to identify an array stretching by maximising the sensitivity of the QFI by selecting different sources. An immediate application of this would be to detect stresses and strains exerted on materials that are sensitive to deformations. This would allow for corrective measures to prevent possible fractures.

In chapter 5, we consider a source localisation problem to detect any deformations applied to a grid of sources. Localising each source in the grid with better accuracy depends on our ability to engineer grids that maximise the sensitivity of the QFIM. In this chapter, we derive the generators of local translations of unitary evolutions that describe any general grid deformation, and show that our result is a simple multi-parameter extension of other results in the literature. We obtain a general result for the QFIM through these generators for any grid deformation and explore the set of affine spatial maps, including composite stretches, shears, and, rotations. We explore how changing the configuration of emitters in the grid enhances our estimation sensitivity of the applied grid deformation. Our work in this chapter provides a cross disciplinary utility. It is well suited for quantum process tomography, to reconstruct the master equation of optical systems. Our work here also makes progress towards multi-parameter quantum estimation with arbitrarily parameterised unitary evolutions with generally non-commuting Hermitian generators. However, the application of our formalism to grid metrology does not encounter non-commutative generators. To take full advantage of this theory and address optimal measurements for non-compatible observables, we consider a separate application in the next chapter.

In chapter 6, we estimate the amplitude and direction of complex squeezing. The characterisation of generated squeezed light is necessary on multiple accounts. First, it is important to ensure the generated states match the level of squeezing required to realise specific quantum technologies. Second, since optical losses destroy the nonclassical properties of squeezed states and generally decompose them to approximate coherent sources, characterising the squeezed state exactly can define these losses. Finally, experiments that incorporate nonlinear optics such as in condensed matter systems, the Wigner function can exhibit non-trivial dynamics such as the highly non-Gaussian '*banana*' states that exhibit amplitude-dependent phase shifts [Stobińska et al., 2008]. Knowledge of both the quadrature squeezing in addition to the quadratures can help to better characterise the transformed state. Motivated by this, we address the joint estimation of the two defining parameters of a squeezing operation in phase space. We derive the Cramér-Rao bound, providing the theoretical benchmark on the bi-variate estimation precision for general single mode Gaussian probe fields. We find the quantum optimal estimators of complex squeezing. This is a true multi-parameter quantum estimation of incompatible observables.

We conclude the thesis with a summary of the main results and potential future work in chapter 7. Appendices are provided to supplement the text.

CHAPTER 2

QUANTUM OPTICS

The quantisation of radiation energies by M. Planck in 1900 ignited the birth of quantum mechanics. However, it was not until H. Brown and R. Q. Twiss performed experiments on their intensity interferometer, that a rigorous application of quantised fields became necessary. Modern day quantum optics remains an active area of research with developments branching to quantum information, quantum communication and quantum sensing. Central to these applications are the development and use of exotic quantum states of light, and their interaction with matter. In this chapter, we provide a summary of quantum mechanics and present a quantised description of the electromagnetic field. This work will be essential for the research presented in Part II of this thesis.

2.1 A brief introduction to quantum mechanics

J. von Neumann unified E. Schrödinger's wave formulation of quantum mechanics with the matrix formulation pioneered by W. Heisenberg, M. Born, and P. Jordan in 1932 to form the basis of modern quantum mechanics. In this section we review key concepts of non-relativistic quantum mechanics that we will make use of in this thesis. A relativistic extension of quantum mechanics was first made by P. Dirac in 1928 [Dirac and Bohr, 1927]. This was generalised by S. Tomonaga, J. Schwinger, and R. Feynman who developed the modern theory of quantum electrodynamics [Dyson, 1949]. For a complete exposition of quantum mechanics, the reader is encouraged to read texts by von Neumann [1996]; Dirac [1988].

2.1.1 The postulates of quantum mechanics

The postulates of quantum mechanics describes how physical quantities and measurements map to their mathematical structure in vector spaces. A self contained exposition of vector spaces has been provided in appendix A. We follow Kok [2018] to list the postulates:

Postulate 1: *At any time t, the state of a physical system S is represented by a normalised ray $|\psi\rangle_s$ in the Hilbert space $\mathcal{H}_s$ of the system.* ■

Postulate 2: *All observable attributes $\hat{O}_S$ of S correspond to Hermitian operators that: (I) act on $|\psi\rangle_s$, and (II) are described by real eigenvalues and eigenvectors that form a complete basis.*

We reserve the carot $\hat{O}_s$ for operators. The properties of Hermitian operators summarised in this postulate follow from the spectral theorem. Consider some Hermitian operator $\hat{O}_s$ defined on some space $\mathcal{V}$. For some eigenvector $|\psi_j\rangle_s \in \mathcal{V}$ and eigenvalues $\psi_j \in \mathbb{C}$:

$$\hat{O}_S \, |\psi_j\rangle_s = \psi_j \, |\psi_j\rangle_s \, , \tag{2.1}$$

then (omitting the subscript S)

$$\left\langle \psi_j \left| \hat{O} \right| \psi_k \right\rangle = \left\langle \psi_k \left| \hat{O}^\dagger \right| \psi_j \right\rangle \quad \Longrightarrow \quad \psi_j = \psi_j^* . \tag{2.2}$$

The orthogonality of the eigenvectors follows by applying this result to the inner product $\langle \psi_j | \hat{O} | \psi_k \rangle$:

$$\left(\psi_j - \psi_k \right) \left\langle \psi_j \left| \hat{O} \right| \psi_k \right\rangle = 0. \tag{2.3}$$

For $\psi_j \neq \psi_k$, $j \neq k$, the eigenvectors have a zero inner product if and only if they are orthogonal. Since the eigenvectors are also normalised, we say it is *orthonormal*. This property implies that any state can be written in terms of this basis. Hence we are able to write any state of a quantum system as a superposition of these eigenstates:

$$|\Psi\rangle = \sum_j \alpha(\psi_j) \left| \psi_j \right\rangle , \quad \text{such that} \quad \sum_j \left| \alpha(\psi_j) \right|^2 = 1, \tag{2.4}$$

where the amplitudes $\alpha(\psi_j)$ are governed by postulate 3. ■

Postulate 3: *A measurement of the observable $\hat{O}$ made on some general state $|\Psi\rangle$ generates the eigenvalues ψ_j as outcomes with probability $p(\psi_j)$.*

The probability of obtaining any outcome from a measurement is distributed according to Born's rule:

$$p(\psi_j) = \left| \alpha(\psi_j) \right|^2 = \left| \left\langle \psi_j \middle| \Psi \right\rangle \right|^2 . \tag{2.5}$$

This is simply Fourier theory. For an m-fold degeneracy in the eigenvalues, the probability is the sum over m-fold degenerate subspace. For continuous systems, we can write the spectral decomposition of $\hat{O}$ as

$$\hat{O} = \int \mathrm{d}x \, f(x) \, |x\rangle \, \langle x| \, . \tag{2.6}$$

We can then introduce the average value of $\hat{O}$ with respect to the state $|\Psi\rangle$:

$$\left\langle \hat{O} \right\rangle = \langle \Psi | \, \hat{O} \, | \Psi \rangle = \int \mathrm{d}x \, f(x) \, |\Psi(x)|^2 \, , \tag{2.7}$$

where we have defined the wave function $\Psi(x) = \langle x | \Psi \rangle$. Its absolute value is interpreted as the probability density. ■

Postulate 4: *Dynamics of (closed) quantum systems is governed by unitary transformations $\hat{U}$, satisfying $\hat{U}\hat{U}^\dagger = \hat{U}^\dagger\hat{U} = \mathbb{1}$. For the state of a quantum system described by $|\psi(t_0)\rangle$ at time t_0, the state at time $t > t_0$ reads*

$$|\Psi(t)\rangle = \hat{U}(t, t_0)\,|\Psi(t_0)\rangle\,. \tag{2.8}$$

The conservation of probability ensures the norm of the state $|\Psi(t)\rangle$ is preserved as it evolves. The wavefunction $\Psi(x)$ introduced in the previous postulate helps address the time evolution of a general wave packet $|\Psi\rangle$ under the action of some Hermitian operator. We propagate the wavefunction in time through the time-evolution operator $\hat{U}$, which is generated by some Hamiltonian operator $\hat{\mathcal{H}}$ [Kok, 2018]:

$$\hat{U} = \exp\left[-\frac{i}{\hbar}\hat{\mathcal{H}}\,\mathrm{d}t\right]. \tag{2.9}$$

Using this and Eq. (2.8), we have:

$$|\Psi(t+\mathrm{d}t)\rangle = \exp\left[-i\hat{\mathcal{H}}\,\mathrm{d}t/\hbar\right]|\Psi(t)\rangle = \left(\mathbb{1} - i\hat{\mathcal{H}}\,\mathrm{d}t/\hbar + \ldots\right)|\Psi(t)\rangle\,, \tag{2.10}$$

$$= |\Psi(t)\rangle + \mathrm{d}t\frac{\partial}{\partial t}|\Psi(t)\rangle + \ldots\,, \tag{2.11}$$

where the second line is a Taylor expansion of $|\Psi(t+\mathrm{d}t)\rangle$ to first order in $\mathrm{d}t$. By comparing both lines, we have the *Schrödinger's equation*:

$$i\hbar\frac{\partial}{\partial t}|\Psi(t)\rangle = \hat{\mathcal{H}}\,|\Psi(t)\rangle\,. \tag{2.12}$$

The Schrödinger's equation governs dynamics of the state with time. From the exponential term in Eq. (2.10), we see that the Hermitian operator $\hat{\mathcal{H}}$ has the same dimensions as energy. We refer to it as the *Hamiltonian operator*, which describes the total energy of the system: $\hat{\mathcal{H}}\,|\Psi(t)\rangle = E\,|\Psi(t)\rangle$. ■

Postulate 5: *For a measurement of $\hat{O}$ that yields ψ_j as the outcome, the state immediately after the measurement collapses to the normalised eigenstate $|\psi_j\rangle$.*

Post measurement, the state of a system is projected to the eigenstate corresponding to the measured outcome. This process is modelled by the projector $\hat{P}_j = |\psi_j\rangle\langle\psi_j|$ that exists on the subspace spanned by the eigenvector(s) associated with measurement outcome ψ_j. It is easy to verify some defining properties of the projector: $\langle\hat{P}_j\rangle = p(\psi_j)$, $\sum_j \hat{P}_j = \mathbb{1}$, and $\hat{P}_j^2 = \hat{P}_j = \hat{P}_j^\dagger$. The measurement can then be described by

$$|\Psi\rangle \to \frac{\hat{P}_j\,|\Psi\rangle}{\left\|\hat{P}_j\,|\Psi\rangle\right\|^2}. \tag{2.13}$$

Note that the first measurement statistically distributes the collapse of the state according to Born's rule. However, a second immediate measurement on the collapsed state will result in the same outcome. ■

2.1.2 Mixed states and the density matrix

Pure states describe isolated systems. However, when a system interacts with its environment, it becomes entangled and can no longer be described by state vectors $|\Psi\rangle$. Density operators generalise the description of pure states to statistical mixtures of states, and is written as the convex sum of pure state density matrices:

$$\rho = \sum_j p_j \rho_j^{\text{pure}} = \sum_j p_j \left|p_j\right\rangle \left\langle p_j\right|, \tag{2.14}$$

where we have defined the density matrix for a pure state as the projector $\rho_j^{\text{pure}} = |p_j\rangle \langle p_j|$. The density operator must satisfy the following criteria for physical systems:

1. $\rho^\dagger = \rho$, (*Hermiticity*)
2. $\text{Tr}[\rho] = 1$, (*Normalisation*)
3. $\rho \geq 0$, (*Positivity*)

where $\text{Tr}[\boldsymbol{A}]$ is the trace of any matrix $\boldsymbol{A}$. Note that the purity $\gamma = \text{Tr}[\rho^2] = \sum_j p_j^2 \leq 1$ can be used as a signature of mixed states, with equality holding only for pure states. The uncertainty in the state is evident from the statistical uncertainty in the expectation value of some observable $\hat{O}$:

$$\langle \hat{O} \rangle = \sum_{j=1} p_j \text{Tr}\left[\hat{O}\left|\psi_j\right\rangle\left\langle\psi_j\right|\right] = \text{Tr}\left[\sum_{j=1} p_j \left|\psi_j\right\rangle\left\langle\psi_j\right|\hat{O}\right] = \text{Tr}\left[\rho\hat{O}\right]. \tag{2.15}$$

The *Bloch sphere* illustrated in figure 2.1 provides a visualisation of density matrices. To understand how, we introduce the quantum counterpart of the binary classical bit—the quantum bit or *qubit*. We write any general qubit state in terms of the basis vectors $|\mathbf{0}\rangle = (1,0)^\top$, $|\mathbf{1}\rangle = (0,1)^\top \in \hat{\mathbb{C}}^2$[1] as

$$|\Psi\rangle = \cos\left[\frac{\vartheta}{2}\right]|\mathbf{0}\rangle + \exp\left[j\varphi\right]\sin\left[\frac{\vartheta}{2}\right]|\mathbf{1}\rangle\,. \tag{2.16}$$

From this, it is clear to identify the north (south) pole as the vector $|\mathbf{0}\rangle$ ($|\mathbf{1}\rangle$). The Bloch representation for the density matrix of qubits is a 2×2 matrix. A suitable basis for this is the identity and the orthogonal, Hermitian, unitary, and traceless Pauli matrices:

$$\sigma_x(\sigma_1) = \begin{pmatrix} 0 & 1 \\ 1 & 0 \end{pmatrix}, \quad \sigma_y(\sigma_2) = \begin{pmatrix} 0 & -i \\ i & 0 \end{pmatrix}, \quad \sigma_z(\sigma_3) = \begin{pmatrix} 1 & 0 \\ 0 & -1 \end{pmatrix}. \tag{2.17}$$

Defining $\boldsymbol{\sigma} = (\sigma_x, \sigma_y, \sigma_z)^\top$ and $\boldsymbol{r} = (r_x, r_y, r_z)$ is the *Bloch vector*, then the density matrix is written

$$\rho = \frac{1}{2}(\mathbb{1} + \boldsymbol{r}\boldsymbol{\sigma}) = \frac{1}{2}\begin{pmatrix} 1+r_z & r_x - ir_y \\ r_x + ir_y & 1-r_z \end{pmatrix}, \tag{2.18}$$

with eigenvalues $(1 \pm |\boldsymbol{r}|)/2$. From the positivity of the density matrices, we are required to have $|\boldsymbol{r}|^2 \leq 1$. Since pure states have unit purity, $\text{Tr}[\rho^2] = (1 + |\boldsymbol{r}|^2)/2 = 1$, then we see that the surface of the Bloch-sphere represents pure states, and mixed states the interior.

[1] Equivalently, the Bloch vector in $\mathbb{C}^2$ forms a complex projective line $\mathbb{C}P^1$.

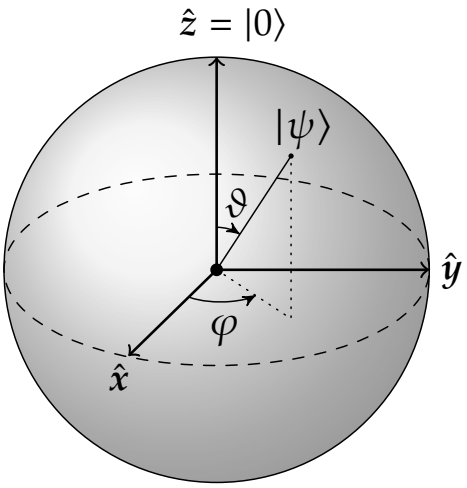

Figure 2.1: *Bloch sphere representation of density matrices in a unit 2-sphere. The poles represents classical bits and qubits the whole sphere. Pure states occupy the surface of the sphere, with the interior occupied by mixed states. The maximally mixed state is the origin of the sphere.*

A measurement of the Pauli σ_z matrix collapses the qubit to either of the poles, with a probability that is a function of ϑ (see postulate 5). The Bloch sphere makes this intuitive: the closer the vector is to a certain pole, the more likely it becomes that the state collapses to it. A phase change of the state (achieved by changing φ through a rotation about the z-axis) does not affect this collapse. More generally, any measurement of the qubit collapses its state to antipodal positions along the measurement axes. We will revisit the Bloch sphere to provide a geometric picture of quantum operations in chapter 3.

2.1.3 Heisenberg and interaction pictures

How does a state evolve with time? There are three possible answers to this question [Dirac, 2003]. We saw in subsection 2.1.1 that the operators remain constant while the wavefunction dynamically evolves according to Schrödinger's equation. This is known as the *Schrödinger picture*. Alternatively, the time evolution can be tracked in the *Heisenberg picture*, where operators change in time while the states remain constant. We can relate both by comparing the expectation values of operators, which should be invariant of the description used. Hence, we write

$$\begin{aligned}\left\langle \hat{O} \right\rangle &= \mathrm{Tr}\left[|\Psi_S(t)\rangle \langle \Psi_S(t)| \hat{O}_S \right] = \mathrm{Tr}\left[\hat{U}(t) |\Psi_S(0)\rangle \langle \Psi_S(0)| \hat{U}^\dagger(t) \hat{O}_S \right] \\ &= \mathrm{Tr}\left[|\Psi_H\rangle \langle \Psi_H| \hat{O}_H(t) \right],\end{aligned} \tag{2.19}$$

where the subscript 'S' and 'H' defined the operators and states in the Schrödinger picture and Heisenberg picture respectively, and we defined time-independent states and time-varying operators:

$$|\Psi_H\rangle = |\Psi_S(0)\rangle\,, \tag{2.20}$$

$$\hat{O}_H(t) = \hat{U}^\dagger(t) \hat{O}_S \hat{U}(t) \tag{2.21}$$

Equivalent to the Schrödinger equation for time evolution for states, we want to find the corresponding *Heisenberg equation* for time evolution for operators. From the derivative of the

expectation value of $\hat{O}$:

$$\begin{aligned}
\frac{\mathrm{d}}{\mathrm{d}t}\left\langle \Psi_{\mathrm{S}}(t)\middle|\hat{O}\middle|\Psi_{\mathrm{S}}(t)\right\rangle &= \frac{\mathrm{d}}{\mathrm{d}t}\left\langle \Psi_{\mathrm{S}}(0)\middle|\hat{U}^{\dagger}(t)\hat{O}_{\mathrm{S}}\hat{U}(t)\middle|\Psi_{\mathrm{S}}(t)\right\rangle \\
&= \langle\Psi_{\mathrm{S}}(0)|\left[\dot{\hat{U}}^{\dagger}(t)\hat{O}_{\mathrm{S}}\hat{U}(t)+\hat{U}^{\dagger}(t)\dot{\hat{O}}_{\mathrm{S}}\hat{U}(t)+\hat{U}^{\dagger}(t)\hat{O}_{\mathrm{S}}\dot{\hat{U}}(t)\right]|\Psi_{\mathrm{S}}(t)\rangle \\
&= \langle\Psi_{\mathrm{H}}|\left[\frac{i}{\hbar}\hat{\mathcal{H}}\hat{O}_{\mathrm{H}}(t)-\frac{i}{\hbar}\hat{O}_{\mathrm{H}}(t)\hat{\mathcal{H}}+\frac{\partial\hat{O}_{\mathrm{H}}(t)}{\partial t}\right]|\Psi_{\mathrm{S}}(t)\rangle \qquad (2.22)\\
&= \langle\Psi_{\mathrm{H}}|\frac{\mathrm{d}\hat{O}_{\mathrm{H}}(t)}{\mathrm{d}t}|\Psi_{\mathrm{H}}\rangle\,, \qquad (2.23)
\end{aligned}$$

where we obtained Eq. (2.22) by using the definition of the unitary in Eq. (2.10) and where we defined

$$\frac{\mathrm{d}\hat{O}_{\mathrm{H}}(t)}{\mathrm{d}t}=\frac{i}{\hbar}\left[\hat{\mathcal{H}},\hat{O}_{\mathrm{H}}(t)\right]+\frac{\partial\hat{O}_{\mathrm{H}}(t)}{\partial t}, \qquad (2.24)$$

which is the Heisenberg equation. The partial derivative is a function of the explicit time dependence of the operator.

For completeness, we detail a third representation—the interaction (or Dirac) picture—for the time dependence of states and operators. This representation can be considered as an intermediary between the Schrödinger and Heisenberg pictures since both the states and operators carry time dependence. This is particularly suited to quantum field theory where operators can act on the state at different times, which was pioneered by F. Dyson in the the 1950's [Peskin and Schroeder, 1995]. In this picture, state are similarly defined as transformations of Schrödinger's states. Consider some Hamiltonian in the Schrödinger picture that can be separated into a free and an interaction term [Griffiths, 2016]

$$\hat{\mathcal{H}}=\hat{\mathcal{H}}_0+\hat{\mathcal{H}}_I, \qquad (2.25)$$

where $\hat{\mathcal{H}}_0$ and $\hat{\mathcal{H}}_I$ are referred to as the *free* and *interaction Hamiltonians* respectively, with $[\hat{\mathcal{H}}_0,\hat{\mathcal{H}}_I]\neq 0$ in general. This split is arbitrary and can be exploited for convenience, though typically $\hat{\mathcal{H}}_I$ is chosen to be weak in strength compared with $\hat{\mathcal{H}}_0$ (in field theory, $\hat{\mathcal{H}}_0$ is chosen to be quadratic in the fields, with terms of higher order associated with the interaction Hamiltonian). We start by introducing a time dependence for the states *and* the operators such that

$$\left\langle\hat{O}(t)\right\rangle=\mathrm{Tr}\left[\hat{O}(t)\rho(t)\right] \qquad (2.26)$$

which motivates the interaction-picture form of the states and operators

$$\hat{O}_I(t)=\exp\left[\frac{i}{\hbar}\hat{\mathcal{H}}_0t\right]\hat{O}(t)\exp\left[-\frac{i}{\hbar}\hat{\mathcal{H}}_0t\right], \qquad (2.27)$$

$$\begin{aligned}
\rho_I(t) &= \exp\left[\frac{i}{\hbar}\hat{\mathcal{H}}_0t\right]\rho(t)\exp\left[-\frac{i}{\hbar}\hat{\mathcal{H}}_0t\right] \\
&= \exp\left[\frac{i}{\hbar}\hat{\mathcal{H}}_0t\right]\exp\left[-\frac{i}{\hbar}\hat{\mathcal{H}}t\right]\rho(0)\exp\left[\frac{i}{\hbar}\hat{\mathcal{H}}t\right]\exp\left[-\frac{i}{\hbar}\hat{\mathcal{H}}_0t\right], \qquad (2.28)
\end{aligned}$$

Representation	State	Operators
Schrödinger	$\rho_{\mathrm{S}}(t) = \exp[-i\hat{\mathcal{H}}]\rho_{\mathrm{S}}(0)\exp[i\hat{\mathcal{H}}]$	-
Heisenberg	-	$\hat{O}_{\mathrm{H}}(t) = \exp[i\hat{\mathcal{H}}]\hat{O}_{\mathrm{S}}\exp[-i\hat{\mathcal{H}}]$
Dirac	$\rho_{\mathrm{I}}(t) = \exp[i\hat{\mathcal{H}}_0]\rho_{\mathrm{S}}(t)\exp[-i\hat{\mathcal{H}}_0]$	$\hat{O}_{\mathrm{I}}(t) = \exp[i\hat{\mathcal{H}}_0]\hat{O}_{\mathrm{S}}(t)\exp[-i\hat{\mathcal{H}}_0]$

Table 2.1: *Comparison between the Schrödinger, Heisenberg, and Dirac pictures for time evolutions of quantum systems ($\hbar = 1$).*

which ensures the expectation values remain invariant of the representation chosen. By taking its derivative, we can find the appropriate evolution for the state:

$$\frac{\mathrm{d}\rho_I(t)}{\mathrm{d}t} = \frac{i}{\hbar}\left[\hat{\mathcal{H}}_0, \rho_I(t)\right] + \exp\left[\frac{i}{\hbar}\hat{\mathcal{H}}_0 t\right]\left(\frac{\mathrm{d}\rho(t)}{\mathrm{d}t}\right)\exp\left[-\frac{i}{\hbar}\hat{\mathcal{H}}_0 t\right], \tag{2.29}$$

$$\overset{(2.25)}{=} \frac{i}{\hbar}\left[\hat{\mathcal{H}}_0, \rho_I(t)\right] - \frac{i}{\hbar}\exp\left[\frac{i}{\hbar}\hat{\mathcal{H}}_0 t\right]\left[\hat{\mathcal{H}}_0 + \hat{\mathcal{H}}_I, \rho(t)\right]\exp\left[-\frac{i}{\hbar}\hat{\mathcal{H}}_0 t\right], \tag{2.30}$$

$$\overset{(2.28)}{=} -\frac{i}{\hbar}\left[\hat{\mathcal{H}}_I, \rho_I(t)\right]. \tag{2.31}$$

This is the *interaction-picture Liouville-von Neumann equation*, which is analogous to the von Neumann, but with the interaction Hamiltonian instead of the full Hamiltonian. Similarly, from the definition of the interaction-picture operators, we have the differential equation

$$\frac{\mathrm{d}\hat{O}_I(t)}{\mathrm{d}t} = \frac{i}{\hbar}\left[\hat{\mathcal{H}}_0, \hat{O}_I(t)\right] + \frac{\partial\hat{O}_I(t)}{\partial t}, \tag{2.32}$$

which is a Heisenberg-like equation for the observable but with the total Hamiltonian replaced by the free Hamiltonian. Table 2.1 summarises the main features of all three representations.

2.2 The quantised electromagnetic field

We now move on to the quantisation of the electromagnetic field. We follow the approach by Gerry and Knight, [2004, p. 10–29]; Walls and Milburn, [2008, p. 7–10]. The electromagnetic field (EM) is described in terms of the two perpendicular vector fields: the electric field $\boldsymbol{E}(\boldsymbol{r}, t)$ and the magnetic field $\boldsymbol{B}(\boldsymbol{r}, t)$. Both of these fields can themselves be written in terms of a time dependent vector potential $\boldsymbol{A}(\boldsymbol{r}, t)$ and a time dependent scalar potential $\phi(\boldsymbol{r}, t)$. Only the fields ($\boldsymbol{E}$ and $\boldsymbol{B}$) are physical, not the potential fields. As we will show, the potentials ($\boldsymbol{A}$ and ϕ) are functions whose derivatives give the fields. Their introduction often makes electromagnetic calculations easier than working with the fields. To show how the fields can be written in terms

of the potentials, we start from Maxwell's equations in vacuum (source free) [Jackson, 1998]:

$$\nabla \cdot \boldsymbol{B} = 0, \tag{2.33}$$
$$\nabla \times \boldsymbol{E} = -\partial_t \boldsymbol{B}, \tag{2.34}$$
$$\nabla \cdot \boldsymbol{E} = 0, \tag{2.35}$$
$$\nabla \times \boldsymbol{B} = \mu_0 \epsilon_0 \partial_t \boldsymbol{E}. \tag{2.36}$$

We want to express the Maxwell equations in terms of the vector potential $\boldsymbol{A}$ and find its wave equation. Using vector calculus identities, we write

$$\boldsymbol{B} = \nabla \times \boldsymbol{A}, \tag{2.37}$$

with the Coulomb gauge,

$$\nabla \cdot \boldsymbol{A} = 0, \tag{2.38}$$

to determine the vector potential uniquely. We similarly express the electric field in terms of $\boldsymbol{A}$, through Faraday's law of induction, to find $\boldsymbol{E} = \nabla\phi - \partial_t \boldsymbol{A}$. Taking the divergence, and using Gauss' law, and the Coulomb gauge, we find:

$$\nabla^2 \phi = \Delta\phi = 0, \tag{2.39}$$

where $\nabla^2 f = \Delta f = \left(\frac{\partial^2}{\partial x^2} + \frac{\partial^2}{\partial y^2} + \frac{\partial^2}{\partial z^2}\right) f$ is the Laplace operator on some function f. For some well-defined, and twice continuously differentiable scalar field ϕ defined on some region $V \subset \boldsymbol{R}^d$, Green's identity maps a volume integral to a surface integral according to [Strauss, 2008]:

$$\iiint_V \mathrm{d}V \, \left(\phi\Delta\phi - (\nabla\phi)^2\right) = \oiint_{S(V)} \mathrm{d}S \, \phi \, (\nabla\phi \cdot \boldsymbol{n}) = \oiint_{S(V)} \phi \nabla\phi \cdot \mathrm{d}\boldsymbol{S}, \tag{2.40}$$

where $S(V)$ denotes the boundary surface of some volume V, $\mathrm{d}\boldsymbol{S}$ is a surface vector element, and $\boldsymbol{n}$ defines a unit vector pointing outwards of the volume that is normal to the surface element $\mathrm{d}S$. Due to Eq. (2.35), the scalar potential is required to be scalar, and so we choose $\phi(\boldsymbol{r}, t) = 0$. Imposing this criteria on Green's identity and using Eq. (2.39), we obtain

$$\iiint_V \mathrm{d}V \, (\nabla\phi)^2 = 0. \tag{2.41}$$

Since the integrand is always positive, this implies that the derivatives of the scalar potential are zero: $\nabla\phi = 0$ (constant scalar field everywhere). From Eq. (2.34), we then have the following for the electric field:

$$\boldsymbol{E} = -\partial_t \boldsymbol{A}. \tag{2.42}$$

The wave equation that determines the vector potential is recovered by combining Eq. (2.42) with Eq. (2.36) to obtain:

$$\Delta\boldsymbol{A} - \frac{1}{c^2}\partial_t^2 \boldsymbol{A} = 0, \tag{2.43}$$

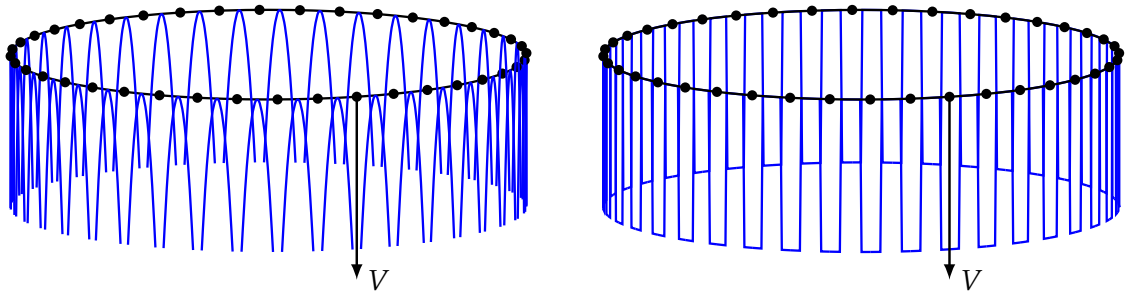

(a) *Periodic quadratic potential.*

(b) *Periodic square potential.*

Figure 2.2: *Any material with many positive ions and electrons (depicted here in black) is a quantum-mechanical many-body system. Fortunately, many features of the system may be understood through the simplified model depicted in figure 2.2a: ions are assumed to be stationary and spaced with distance L_x along the array. They provide a periodic potential satisfying $V(x + L_x) = V(x)$ through which the electrons (where x runs along the ion ring). Figure 2.2b shows an idealised square Kronig Penny potential [de L. Kronig and Penney, 1931], which simplifies the treatment.*

where $c = (\mu_0 \epsilon_0)^{-1/2}$. A similar approach can be taken to obtain the wave equation for ϕ under the Coulomb gauge. To solve the wave equation for $\boldsymbol{A}$, we must specify the boundary conditions of the cavity. For a cavity with well-defined edges, the electric field amplitude must be zero at the boundaries and will take the form of a standing wave. This constrains the existence of the field to specific vibrational modes within a volume—referred to as the *modes of the volume*. For periodic boundary conditions, such as that illustrated in figure 2.2, the field is a travelling wave. Hence, similar to finite volume problems [Eymard et al., 2000], the mode expansion of $\boldsymbol{A}$ can be decomposed in terms of the discrete Fourier components:

$$\boldsymbol{A}(\boldsymbol{r}, t) = \boldsymbol{A}^{(+)}(\boldsymbol{r}, t) + \boldsymbol{A}^{(-)}(\boldsymbol{r}, t), \tag{2.44}$$

where

$$\boldsymbol{A}^{(+)}(\boldsymbol{r}, t) = \sum_{k=0}^{\infty} \boldsymbol{\mathcal{E}}_k a_k u_k(\boldsymbol{r}) \exp\left[-i\omega_k t\right], \tag{2.45}$$

$\boldsymbol{A}^{(-)}(\boldsymbol{r}, t) = [\boldsymbol{A}^{(+)}(\boldsymbol{r}, t)]^*$, $\omega_k = c|\boldsymbol{k}| > 0$, where the sum is over the wavevector $\boldsymbol{k}$, with components defined through

$$\boldsymbol{k}_s = \frac{2\pi n_s}{L_s}, \tag{2.46}$$

where n_s label the modes in the perpendicular directions $s \in \{x, y, z\}$ with periodic length L_s, and $u_k(\boldsymbol{r})$ are mode functions for the cavity weighted by complex amplitudes a_k. The real vector $\boldsymbol{\mathcal{E}}_k$ reflects the vectorial nature of the field and are chosen to ensure the amplitudes a_k

are dimensionless. The physical fields $\boldsymbol{E}$ and $\boldsymbol{B}$ can now be written as [Griffiths, 1998]

$$\boldsymbol{E}(\boldsymbol{r},t) = i\sum_{k=0}^{\infty} \boldsymbol{\mathcal{E}}_k \left(a_k u_k(\boldsymbol{r}) \exp\left[-i\omega_k t\right] - a_k^* u_k^*(\boldsymbol{r}) \exp\left[i\omega_k t\right]\right), \tag{2.47}$$

$$\boldsymbol{B}(\boldsymbol{r},t) = i\sum_{k=0}^{\infty} \frac{1}{\omega_k}\boldsymbol{\mathcal{E}}'_k \left(a_k u_k(\boldsymbol{r}) \exp\left[-i\omega_k t\right] - a_k^* u_k^*(\boldsymbol{r}) \exp\left[i\omega_k t\right]\right), \tag{2.48}$$

where $\boldsymbol{\mathcal{E}}'_k = \boldsymbol{k}\times\boldsymbol{\mathcal{E}}_k$. Combining Eq. (2.44) with Eq. (2.43), we see that the wave equation for $\boldsymbol{A}$ transforms into an eigenvalue equation for the mode function $u_k(\boldsymbol{r})$

$$\Delta u_k(\boldsymbol{r}) - \frac{\omega_k^2}{c^2}u_k(\boldsymbol{r}) = 0. \tag{2.49}$$

For a cavity of volume $V = L_x L_y L_z$, the boundary conditions for the vector potential require

$$\boldsymbol{A}(x + n_x L_x, y + n_y L_y, z + n_z L_z) = \boldsymbol{A}(x,y,z). \tag{2.50}$$

The mode functions are then written [Walls and Milburn, 2008]:

$$u_k(\boldsymbol{r}) = \frac{1}{\sqrt{V}}\exp\left[i(\boldsymbol{k}\cdot\boldsymbol{r})\right], \tag{2.51}$$

which are plane waves. Since the Laplace operator is Hermitian, these cavity modes form the complete orthonormal set:

$$\iiint_V \mathrm{d}V\, u_k^*(\boldsymbol{r}) u_{k'}(\boldsymbol{r}) = \delta_{k,k'}, \tag{2.52}$$

where $\mathrm{d}V = \mathrm{d}^3\boldsymbol{r}$. Despite this property, these modes extend over all space for an infinite cavity ($L_x, L_y, L_z \to \infty$), which does not provide a suitable description for physical state. A localised *wave packet* in space provides a better description and is constructed from a superposition of different cavity modes.

The resulting EM fields are classical vector fields that by construction obey Maxwell's equations and the wave equation in vacuum, and are illustrated in figure 2.3. The total energy of the EM field is given by the Hamiltonian [Kok and Lovett, 2010]

$$\mathcal{H} = \iiint_V \mathrm{d}^3\boldsymbol{r}\left(\frac{\epsilon_0}{2}\boldsymbol{E}^2 + \frac{1}{2\mu_0}\boldsymbol{B}^2\right). \tag{2.53}$$

We are now ready to quantise these classical vector fields using the *canonical quantisation* procedure. First, introduce the canonical position and momentum variables

$$q_k(t) = \sqrt{\frac{\hbar}{2\omega_k}}\left(a_k \exp\left[-i\omega_k t\right] + a_k^* \exp\left[i\omega_k t\right]\right), \tag{2.54}$$

$$p_k(t) = -i\sqrt{\frac{\hbar\omega_k}{2}}\left(a_k \exp\left[-i\omega_k t\right] - a_k^* \exp\left[i\omega_k t\right]\right). \tag{2.55}$$

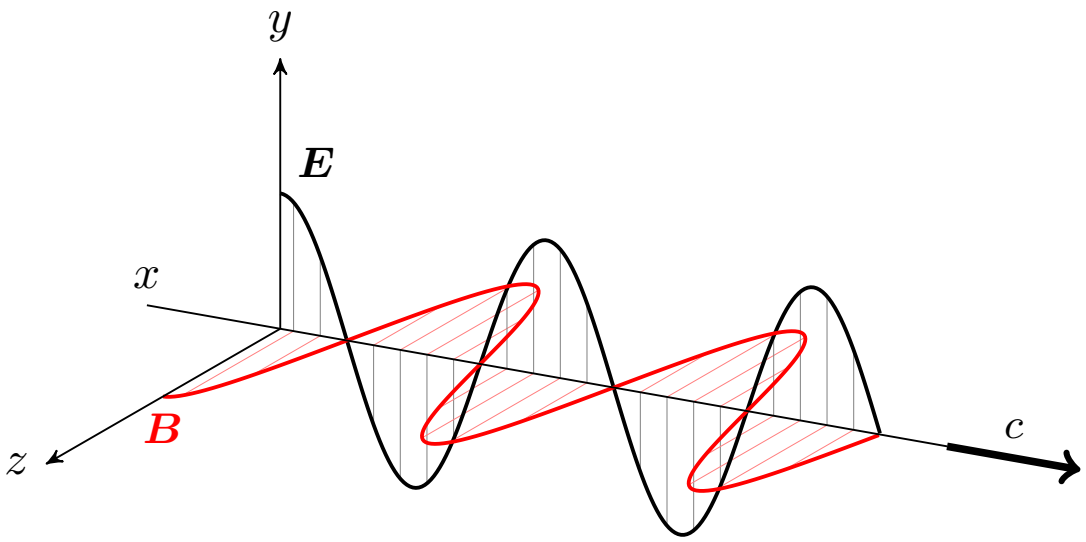

Figure 2.3: *Electric and magnetic field propagation.*

In classical optics, these describe the field quadratures, or coordinates of a system with energy $\mathcal{H}(q_j, p_j; t)$. In the classical Hamiltonian formulation, system dynamics are fully described through

$$\frac{\mathrm{d}q_j}{\mathrm{d}t} = \frac{\partial \mathcal{H}}{\partial p_j}, \quad \frac{\mathrm{d}p_j}{\mathrm{d}t} = -\frac{\partial \mathcal{H}}{\partial q_j}. \tag{2.56}$$

To generalise this to the quantum mechanical position and momentum operators, the complex mode operators a_k in Eq. (2.55) are 'promoted' to operators $\hat{a}_k$. Then, we impose the canonical commutation relations,

$$[\hat{q}_k, \hat{p}_{k'}] = i\hbar\delta_{k,k'}, \tag{2.57}$$

and

$$[\hat{q}_k, \hat{q}_{k'}] = [\hat{p}_k, \hat{p}_{k'}] = 0, \tag{2.58}$$

where $[\hat{A}, \hat{B}] = \hat{A}\hat{B} - \hat{B}\hat{A}$ is the commutator of $\hat{A}$ and $\hat{B}$. This implies that the mode operators, $\hat{a}_k$, of the EM field obey the bosonic commutation relations [Loudon, 2000]

$$\left[\hat{a}_k, \hat{a}^\dagger_{k'}\right] = \delta_{k,k'}, \tag{2.59}$$

and

$$[\hat{a}_k, \hat{a}_{k'}] = \left[\hat{a}^\dagger_k, \hat{a}^\dagger_{k'}\right] = 0, \tag{2.60}$$

where $\hat{a}^\dagger_k$ is the Hermitian conjugate of $\hat{a}_k$. The zero commutators are associated with operators corresponding to different modes of the EM field since these are decoupled. The quantised electric field then reads

$$\hat{\boldsymbol{E}}(\boldsymbol{r}, t) = \hat{\boldsymbol{E}}^{(+)}(\boldsymbol{r}, t) + \hat{\boldsymbol{E}}^{(-)}(\boldsymbol{r}, t), \tag{2.61}$$

where we have defined

$$\hat{\boldsymbol{E}}^{(+)}(\boldsymbol{r},t) = i\sum_{k=0}^{\infty} \boldsymbol{\mathcal{E}}_k \hat{a}_k u_k(\boldsymbol{r}) \exp\left[-i\omega_k t\right], \tag{2.62}$$

with $\hat{\boldsymbol{E}}^{(-)}$ defined as the Hermitian conjugate of $\hat{\boldsymbol{E}}^{(+)}$. This shows a decomposition of the field into non-Hermitian positive and negative frequency terms. Physically, the term $\hat{\boldsymbol{E}}^{(+)}$ is responsible for the absorption of photons and $\hat{\boldsymbol{E}}^{(-)}$ their emission. The magnetic field can be similarly decomposed. The total energy of this field, or the Hamiltonian operator becomes [Grynberg et al., 2010]

$$\hat{\mathcal{H}} = \iiint_V \mathrm{d}^3\boldsymbol{r}\left(\frac{\epsilon_0}{2}\hat{\boldsymbol{E}}^2 + \frac{1}{2\mu_0}\hat{\boldsymbol{B}}^2\right) = \sum_k \left(\frac{\hat{p}_k^2}{2} + \frac{\omega_k^2 \hat{q}_k^2}{2}\right) = \sum_k \hbar\omega_k\left(\hat{a}_k^\dagger \hat{a}_k + \frac{1}{2}\right), \tag{2.63}$$

with

$$\hat{q}_k = \frac{1}{\sqrt{2}}\left(\hat{a}_k + \hat{a}_k^\dagger\right), \tag{2.64}$$

$$\hat{p}_k = -\frac{i}{\sqrt{2}}\left(\hat{a}_k - \hat{a}_k^\dagger\right). \tag{2.65}$$

The final equality in Eq. (2.63) *resembles* a sum over harmonic oscillators for the conjugate pair q_k and p_k. The EM field is then *formally analogous* to an infinite collection of harmonic oscillators (in the absence of sources), with the total energy of the field interpreted as the sum of energies of decoupled harmonic oscillators with positions q_k, momenta p_k, and frequencies ω_k. We also observe that canonical quantisation discretises the energy of the field. The finite energy changes are referred to as the *quanta* of the field. For the EM field, this quanta corresponds to a photon. To elucidate energy quantisation and understand the role of the mode operators $\hat{a}_k$, and $\hat{a}_k^\dagger$, we introduce the Fock (or number) basis, and some other commonly used bases to describe the EM field in the following section.

2.3 Quantised radiation states

The quantum properties of physical systems are described by two things [Peskin and Schroeder, 1995]: (I) Hermitian operators associated with an observable satisfying well defined commutation relations with its canonical conjugate operators, and (II) state vectors that belong to some Hilbert space $\hat{\mathcal{H}}$, which describes specific states of the system. In the previous section, we recalled how to find the quantum Hamiltonian of the quantised radiation field. We now want to introduce quantum states of this field. This will provide some commonly used bases that describe the EM field. Any complete basis can be used to expand the state of a system. We will see that the certain bases are better suited to certain problems.

2.3.1 Fock states

Since the radiation in the Hamiltonian formalism is analogous to an ensemble of independent material harmonic oscillators, eigenstates of $\hat{\mathcal{H}}$ are the usual states of the harmonic oscillator,

labelled the Fock states such that $\hat{\mathcal{H}} |\boldsymbol{n}\rangle = E |\boldsymbol{n}\rangle$. To understand the role of the mode operators, consider

$$\begin{aligned}
\hat{\mathcal{H}} \hat{a}^\dagger_{\boldsymbol{k}'} |\boldsymbol{n}\rangle &= \sum_{\boldsymbol{k}} \hbar\omega_{\boldsymbol{k}} \left(\hat{a}^\dagger_{\boldsymbol{k}} \hat{a}_{\boldsymbol{k}} + \frac{1}{2} \right) \hat{a}^\dagger_{\boldsymbol{k}'} |\boldsymbol{n}\rangle \,, \\
&= \sum_{\boldsymbol{k}} \hbar\omega_{\boldsymbol{k}} \left[\hat{a}^\dagger_{\boldsymbol{k}} \left(\delta_{\boldsymbol{k},\boldsymbol{k}'} + \hat{a}^\dagger_{\boldsymbol{k}'} \hat{a}_{\boldsymbol{k}} \right) + \frac{\hat{a}^\dagger_{\boldsymbol{k}'}}{2} \right] |\boldsymbol{n}\rangle \,, \\
&= \hat{a}^\dagger_{\boldsymbol{k}'} \left[\hbar\omega_{\boldsymbol{k}'} + \sum_{\boldsymbol{k}} \hbar\omega_{\boldsymbol{k}} \left(\hat{a}^\dagger_{\boldsymbol{k}} \hat{a}_{\boldsymbol{k}} + \frac{1}{2} \right) \right] |\boldsymbol{n}\rangle \,, \\
&= (\hbar\omega_{\boldsymbol{k}'} + E_n) \, \hat{a}^\dagger_{\boldsymbol{k}'} |\boldsymbol{n}\rangle \,,
\end{aligned} \tag{2.66}$$

where $|\boldsymbol{n}\rangle = |n_{k_1}\rangle \otimes |n_{k_1}\rangle \otimes \ldots = |n_{k_1}, n_{k_2}, \ldots\rangle$ spans the Hilbert space associated with all the modes. We see that $\hat{a}^\dagger_{\boldsymbol{k}'} |n\rangle$ is also an eigenstate of the Hamiltonian with energy $E_n + \hbar\omega_{\boldsymbol{k}'}$. Since the mode energy increases by a single quantum of amount $\Delta E = \hbar\omega_{\boldsymbol{k}'}$, the operator $\hat{a}^\dagger_{\boldsymbol{k}'}$ is called the *creation operator* of mode $\boldsymbol{k}'$. Similarly, $\hat{a}_{\boldsymbol{k}'} |n\rangle$ is called the *annihilation operator* since it decreases the mode energy by ΔE. We have now established the operators associated with the emission and absorption of single photons. This is central to the quantum theory of light

Observables associated with the quantised radiation state are represented through operators composed from Hermitian combinations of the creation and annihilation operators. We already wrote the quadrature operators as such a combination. Another important combination is their product:

$$\hat{n}_k = \hat{a}^\dagger_k \hat{a}_k, \tag{2.67}$$

which is the *number operator*, so called since it has the number states as its eigenstates,

$$\hat{n}_k |n_k\rangle = n_k |n_k\rangle \,. \tag{2.68}$$

where n_k is the number of photons in mode k. Combining Eq. (2.67) with the Hamiltonian (2.63), we observe that the energy of single mode is proportional to the number of photons in that mode. The eigenstates $|n_k\rangle$ form a complete orthonormal set

$$\langle n_k | m_k \rangle = \delta_{n_k, m_k}, \tag{2.69}$$

with the *resolution of the identity* (consult appendix A):

$$\sum_k |n_k\rangle \langle n_k| = \mathbb{1}. \tag{2.70}$$

We can now determine the action of the creation and annihilation operators on the Fock states. Since the creation operator creates a photon, its action on some number state can be written as [Barnett and Radmore, 2005]

$$\hat{a}^\dagger_k |n_k\rangle = p_{n_k} |n_k + 1\rangle \,, \tag{2.71}$$

where p_{n_k} is potentially complex since $\hat{a}^\dagger$ is non-Hermitian. To determine the constant of proportionality, consider the amplitude of Eq. (2.71):

$$\left(\hat{a}^\dagger_k |n_k\rangle \right)^\dagger \hat{a}^\dagger_k |n_k\rangle = \langle n_k | \hat{a}_k \hat{a}^\dagger_k |n_k\rangle = \langle n_k | \left(\hat{a}^\dagger_k \hat{a}_k + 1 \right) |n_k\rangle = (n_k + 1) = |p_{n_k}|^2. \tag{2.72}$$

Conventionally, the phase is chosen such that $p_{n_k} = \sqrt{n_k + 1}$. Then, we can easily show that

$$\begin{aligned} \hat{a}_k^\dagger |n_k\rangle &= \sqrt{n_k + 1}\, |n_k + 1\rangle , \\ \hat{a}_k |n_k\rangle &= \sqrt{n_k}\, |n_k - 1\rangle . \end{aligned} \tag{2.73}$$

Note that it is not possible to have negative photon numbers. This is implicit in the above definitions and can also be seen from $\langle n_k | \hat{a}_k^\dagger \hat{a}_k |n_k\rangle = n_k$, which requires the expectation value of the number operator to be positive. Any number state can be generated by repeated use of the creation operator, giving

$$|n_k\rangle = \frac{\left(\hat{a}_k^\dagger\right)^{n_k}}{\sqrt{n_k!}} |0\rangle , \tag{2.74}$$

with $|0\rangle$ the *vacuum state*.

Any pure state can be written as the complex superposition of Fock states:

$$|\psi\rangle = \sum_{n=0}^{\infty} c_n |n\rangle , \quad \text{with} \quad \sum_{n=0}^{\infty} |c_n|^2 = 1. \tag{2.75}$$

Then, an n-photon Fock state is the state $|\psi\rangle$ with $c_j = 0$ for all $j \neq n$.

2.3.2 Coherent states

Coherent states, written $|\alpha\rangle$, describe the output of a laser operating above threshold [Barnett and Radmore, 2005]. In the following, to ease the notation, we consider only a single mode. This allows us to consider a fixed wavevector and omit the sum. Since coherent states are semi-classical states, we expand it as a superposition of the number states for any given mode:

$$|\alpha\rangle = \exp\left[-\frac{1}{2}|\alpha|^2\right] \sum_{n=0}^{\infty} \frac{\alpha^n}{\sqrt{n!}} |n\rangle , \tag{2.76}$$

where α can be any complex number. Coherent states are generated by operating with the *displacement operator* on the vacuum state alone: $|\alpha\rangle = \hat{D}(\alpha) |0\rangle$ with

$$\hat{D}(\eta) = \exp\left[\eta \hat{a}^\dagger - \eta^* \hat{a}\right] , \tag{2.77}$$

with η some arbitrary complex number. The operational meaning of the displacement operator will become clear when we introduce the phase space formalism of quantum optics.

From the expansion in Eq. (2.76), a number of properties can be attributed to coherent states. First, we see that coherent states are *right eigenstates* of the annihilation operator with eigenvalue α:

$$\begin{aligned} \hat{a} |\alpha\rangle &= \exp\left[-|\alpha|^2/2\right] \sum_{n=0}^{\infty} \frac{\alpha^n}{\sqrt{n!}} \hat{a} |n\rangle , \\ &= \exp\left[-|\alpha|^2/2\right] \sum_{n=0}^{\infty} \frac{\alpha^n}{\sqrt{n!}} \sqrt{n}\, |n-1\rangle , \\ &= \exp\left[-|\alpha|^2/2\right] \sum_{n=0}^{\infty} \frac{\alpha^n}{\sqrt{(n-1)!}} |n-1\rangle , \\ &= \alpha |\alpha\rangle . \end{aligned} \tag{2.78}$$

Since $\hat{a}^\dagger$ does not commute with $\hat{a}$, the coherent states are not right eigenstates of the creation operator. Instead, from a similar reasoning to the above, the coherent states are *left eigenstates* of the creation operator with eigenvalue α^*. Second, coherent states do not have defined photon numbers. Photon number measurements will be distributed with Poissonian statistics with average $|\alpha|^2$. A third feature of the coherent states is that unlike the number states, they are not mutually orthogonal:

$$\langle\alpha|\beta\rangle = \exp\left[-\frac{1}{2}\left(|\alpha|^2 + |\beta|^2 - 2\alpha^*\beta\right)\right], \tag{2.79}$$

such that

$$|\langle\alpha|\beta\rangle|^2 = \exp\left[-|\alpha-\beta|^2\right]. \tag{2.80}$$

Despite this, they form an over-complete set. We might expect that the generalisation of the completeness relation to the continuous variable to be $\int \mathrm{d}^2\alpha\, |\alpha\rangle\langle\alpha| = \mathbb{1}$ where the integration is over the complex plane. However, because of the non-orthogonality of the states $|\alpha\rangle$ this requires modification [Barnett and Radmore, 2005]. Writing $\alpha = r\exp[i\phi]$ and using the expansion of coherent state in the Fock basis, we find

$$\begin{aligned}
\iint \mathrm{d}^2\alpha\, |\alpha\rangle\langle\alpha| &= \sum_{n,m=0}^{\infty} \int_0^\infty \mathrm{d}r\, r \exp\left[r^2\right] r^{n+m} \int_0^{2\pi} \mathrm{d}\phi \frac{\exp[i\phi(n-m)]}{\sqrt{n!m!}} |n\rangle\langle m|, \\
&= \sum_{n,m=0}^{\infty} \int_0^\infty \mathrm{d}r\, r \exp\left[r^2\right] r^{n+m} \frac{\delta_{n,m}}{\sqrt{n!m!}} |n\rangle\langle m|, \\
&= \sum_{n=0}^{\infty} \int_0^\infty \mathrm{d}r\, r \exp\left[r^2\right] \frac{r^{2n}}{n!} |n\rangle\langle n|, \\
&= \pi \sum_{n=0}^{\infty} |n\rangle\langle n|, \\
&= \pi\, \mathbb{1},
\end{aligned} \tag{2.81}$$

where we used the standard integral $\int_0^\infty \mathrm{d}r\, \exp[-ar^2] r^n = p!/(2a^{p+1}), n = 2p+1, p \in \mathbb{Z}, a > 0$. This modification follows since there are more than sufficient coherent states to expand any state.

2.4 Representations of the electromagnetic field

From the description of the electromagnetic field and its states in the preceding sections, we now describe the quantum statistics of the field. This is essential to describe how values of a given physical property of the field are distributed. We start by introducing different Hilbert-space bases that can be used to write the quantum mechanical state of light. Then, we introduce the characteristic function and quasi-probability distributions that allow for a more complete statistical description of the field.

2.4.1 Expansion in number states

We described how the number states form a complete set in section 2.3.1. Hence any density operator may be expanded in the Fock basis as

$$\rho = \sum_{j,k=0}^{\infty} c_{j,k} \left|j\right\rangle \left\langle k\right| \tag{2.82}$$

This expansion generally contains nonzero off-diagonal terms. The number state representation is particularly suited to problems where knowledge of the photon number distribution is required. A notable example which uses the number representation is the thermal state, with density operator [Fano, 1957]

$$\rho = \frac{\exp\left[-\beta\hat{\mathcal{H}}\right]}{\mathrm{Tr}\left[\exp\left[-\beta\hat{\mathcal{H}}\right]\right]}, \tag{2.83}$$

where $\beta = 1/k_B T$, k_B is Boltzmann's constant, and T the temperature. Using the form of the Hamiltonian in Eq. (2.63), we find

$$\rho = \frac{\exp\left[-\sum_k \beta\hbar\omega_k \left(\hat{n}_k + \frac{1}{2}\right)\right]}{\mathrm{Tr}\left[\exp\left[-\sum_{k'} \beta\hbar\omega_{k'} \left(\hat{n}_{k'} + \frac{1}{2}\right)\right]\right]} = \frac{\exp\left[-\sum_k \beta\hbar\omega_k \hat{n}_k\right]}{\mathrm{Tr}\left[\exp\left[-\sum_{k'} \beta\hbar\omega_{k'} \hat{n}_{k'}\right]\right]}. \tag{2.84}$$

From the properties of the number operator, $\langle j|f(\hat{n})|k\rangle = f(k)\delta_{k,j}$. Hence, any operator function of the number operator has a diagonal form in the number basis. This motivates the expansion of the thermal state in the number basis. We start by evaluating the denominator—known as the *partition function*, $\mathcal{Z}$—which is the normalisation of the state [Gerry and Knight, 2004]:

$$\begin{aligned}
\mathcal{Z} = \mathrm{Tr}\left[\exp\left[-\sum_{k'} \beta\hbar\omega_{k'}\hat{n}_{k'}\right]\right] &= \prod_k \sum_{n_k} \left\langle n_k\right| \exp\left[-\sum_{k'} \beta\hbar\omega_{k'}\hat{n}_{k'}\right] \left|n_k\right\rangle, \\
&= \prod_k \sum_{n_k} \left\langle n_k\right| \prod_{k'} \exp\left[-\beta\hbar\omega_{k'}\hat{n}_{k'}\right] \left|n_k\right\rangle, \\
&= \prod_k \sum_{n_k} \exp\left[-\beta\hbar\omega_k n_k\right], \\
&= \prod_k \frac{1}{1-\exp\left[-\beta\hbar\omega_k\right]},
\end{aligned} \tag{2.85}$$

where we used $\langle m|g(\hat{n})|n\rangle = g(n)\delta_{nm}$ for the second equality. To find the average photon number, we define $\alpha_k = \beta\hbar\omega_k$ and determine the expectation of the number operator:

$$\begin{aligned}
\langle\hat{n}_k\rangle = \frac{1}{\mathcal{Z}} \sum_k n_k \exp\left[-\alpha_k n_k\right] &= -\frac{1}{\mathcal{Z}} \partial_{\alpha_k} \left(\sum_k \exp\left[-\alpha_k n_k\right]\right), \\
&= -\frac{1}{\mathcal{Z}} \partial_{\alpha_k} \left(\frac{1}{1-\exp\left[-\alpha_k\right]}\right), \\
&= \frac{1}{\exp\left[\beta\hbar\omega_k\right] - 1}.
\end{aligned} \tag{2.86}$$

Now, we write the thermal state in the number basis and use Eq. (2.85) and Eq. (2.86) to obtain [Leonhardt, 2010]:

$$\begin{aligned}\rho &= \frac{\bigotimes_k \exp\left[-\beta\hbar\omega_k \hat{n}_k\right]}{\prod_{k'}(1-\exp\left[-\beta\hbar\omega_{k'}\right])^{-1}}, \\ &= \bigotimes_k \sum_{n_k} \left(1-\exp\left[-\beta\hbar\omega_k\right]\right) \exp\left[-\beta\hbar\omega_k \hat{n}_k\right] |n_k\rangle \langle n_k| , \\ &= \bigotimes_k \sum_{n_k} \frac{\langle \hat{n}_k \rangle^{n_k}}{(1+\langle \hat{n}_k \rangle)^{1+n_k}} |n_k\rangle \langle n_k| .\end{aligned} \tag{2.87}$$

Since each mode is described in its independent Hilbert space, the total multi-mode field is simply constructed from the product of the distribution functions for each mode. The state in Eq. (2.87) is the *black-body radiation* state. To maintain ease in notation, we consider single mode states without loss of generality hereafter (strictly this is true for only temporal states).

2.4.2 Expansion in coherent states—P representation

The over-completeness property of coherent states implies that any traceable, Hermitian operator $\hat{O}$ can be written diagonal in the coherent state basis [Jordan, 1964]. That is, if the diagonal coherent state matrix elements $\langle\alpha|\hat{O}|\alpha\rangle$ are known, all the matrix elements in the number basis can be deduced. To see this, consider the following weighted coherent state expectation value of $\hat{O}$:

$$\exp\left[|\alpha|^2\right] \left\langle \alpha \middle| \hat{O} \middle| \alpha \right\rangle = \sum_{j,k} \left\langle j \middle| \hat{O} \middle| k \right\rangle \frac{(\alpha^*)^j \alpha^k}{\sqrt{j!k!}}, \tag{2.88}$$

where we used the definition of the coherent states introduced in Eq. (2.76). Hence

$$\left\langle j \middle| \hat{O} \middle| k \right\rangle = \frac{1}{\sqrt{j!k!}} \partial^j_{\alpha^*} \partial^k_{\alpha} \left[\exp\left[|\alpha|^2\right] \left\langle \alpha \middle| \hat{O} \middle| \alpha \right\rangle\right]\Big|_{\alpha=0}. \tag{2.89}$$

Thus, for well defined diagonal elements $\langle\alpha|\hat{O}|\alpha\rangle$ for all α, all of the matrix elements $\langle j|\hat{O}|k\rangle$ in the number basis can be determined. The density operator can always be chosen to be diagonal in the coherent-state basis [Gerry and Knight, 2004]:

$$\rho = \iint \mathrm{d}^2\alpha \; P(\alpha) |\alpha\rangle \langle\alpha| , \tag{2.90}$$

where $P(\alpha)$ is a representation of the phase space distribution. This is known as the diagonal coherent state representation or the *P-representation*. The non-orthogonality of the coherent states enables the state to be written in this diagonal expansion, which is generally not true for the number states, whose orthogonality requires off-diagonal elements for a complete description of the state. Note that the distribution $P(\alpha)$ is analogous to a classical probability distribution since it is normalised

$$\iint \mathrm{d}^2\alpha \; P(\alpha) = \iint \mathrm{d}^2\alpha \; \langle\alpha|\alpha\rangle P(\alpha) = \mathrm{Tr}\left[\iint \mathrm{d}^2\alpha \; P(\alpha) |\alpha\rangle \langle\alpha|\right] = \mathrm{Tr}[\rho] = 1. \tag{2.91}$$

However, from the diagonal elements in the coherent basis

$$\langle \delta | \rho | \delta \rangle = \iint \mathrm{d}^2\alpha \; P(\alpha) \exp\left[- |\alpha - \delta|^2 \right], \tag{2.92}$$

where we used the overlap between two coherent states as defined in Eq. (2.80), the distribution is not required to be positive. This relaxes the positivity criterion of probability distributions. We naturally describe the P-distribution as a quasi-probability distribution. For P-distributions of different states, the reader is referred to common quantum optics texts, such as Loudon [2000]; Walls and Milburn [2008].

This representation is useful since it expands the density matrix in terms of the classical coherent states. It also provides an equivalence of expectation values of normally ordered operators (see appendix B for details of operator ordering) to their classical counterparts. This is the *optical equivalence theorem*, which can be demonstrated by considering the expectation value of some function $g = \sum_{n,m} c_{n,m} (\hat{a}^\dagger)^n \hat{a}^m$:

$$\begin{aligned} \langle g(\hat{a}^\dagger, \hat{a}) \rangle &= \mathrm{Tr}\left[\rho \sum_{n,m} c_{n,m} (\hat{a}^\dagger)^n \hat{a}^m \right] \\ &= \iint \mathrm{d}^2\alpha \; P(\alpha) \sum_{n,m} c_{n,m} \langle \alpha | \, (\hat{a}^\dagger)^n \hat{a}^m \, | \alpha \rangle \\ &= \iint \mathrm{d}^2\alpha \; P(\alpha) \sum_{n,m} c_{n,m} (\alpha^*)^n \alpha^m \\ &= \iint \mathrm{d}^2\alpha \; P(\alpha) g(\alpha^*, \alpha). \end{aligned} \tag{2.93}$$

Hence the expectation value of any operator function in Hilbert space is equivalent to the expectation value of the corresponding function of complex numbers with respect to the P-distribution. We generalise this in the following subsection.

2.4.3 Characteristic functions

The P-distribution introduced in the former subsection is formally defined as the Fourier transform of normally-ordered *characteristic functions* $\chi_P(\eta)$. In this subsection, we introduce this function and its properties. Alternative distributions naturally arise through different choices of characteristic functions. The *Wigner representation (W)* and the *Husimi representation (Q)* are two popular representations that are defined in terms of a characteristic function that gives operators averages in symmetric (or Weyl) order, and in antinormal order respectively [Carmichael, 2002]. We focus on only these operator orderings, but for completeness we draw attention to the work of Agarwal and Wolf [1970], who introduced phase space calculus methods to define different representations.

Together with the P-distribution, all of the distributions can be written in terms of the s-ordered characteristic function defined through [Barnett and Radmore, 2005]

$$\chi(\eta, s) = \mathrm{Tr}\left[\rho \hat{D}(\eta) \right] \exp\left[\frac{s \, |\eta|^2}{2} \right] \tag{2.94}$$

for some density operator ρ, $\eta \in \mathbb{C}$, $\hat{D}(\eta)$ the displacement operator as defined in Eq. (2.77), and s corresponds to specific ordering of the creation and annihilation operators in the characteristic

function. Specifically, for $s = 1, 0, -1$, we have the normal, symmetric, and anti-normal ordered characteristic functions respectively:

$$\chi(\eta, 1) = \chi_P(\eta) = \mathrm{Tr}\left[\rho \exp\left[\eta\hat{a}^\dagger\right] \exp\left[-\eta^*\hat{a}\right]\right] \tag{2.95}$$

$$\chi(\eta, 0) = \chi_W(\eta) = \mathrm{Tr}\left[\rho \exp\left[\eta\hat{a}^\dagger - \eta^*\hat{a}\right]\right] \tag{2.96}$$

$$\chi(\eta, -1) = \chi_Q(\eta) = \mathrm{Tr}\left[\rho \exp\left[-\eta^*\hat{a}\right] \exp\left[\eta\hat{a}^\dagger\right]\right], \tag{2.97}$$

where we used the operator identities in appendix C. The subscript P, W, Q associates each distribution to specific operator orderings. Note that the characteristic function is generally complex and at $\eta = 0$, we have $\chi(0, s) = \mathrm{Tr}[\rho] = 1$ independent of the operator ordering. The characteristic function contains all the information necessary to describe the density matrix of the state and the s-ordered operator expectation values [Barnett and Radmore, 2005, p. 107]:

$$\left\langle \hat{a}^{\dagger p}\hat{a}^q \right\rangle_s = \left(\frac{\partial}{\partial\eta}\right)^p \left(-\frac{\partial}{\partial\eta^*}\right)^q \chi(\eta, s)\bigg|_{\eta=0}. \tag{2.98}$$

Since the distributions are defined as Fourier transforms of $\chi(\eta)$, it is clear that they too satisfy these requirements. We detail these in the next subsections.

2.4.4 Other quasi-probability distributions

In the remaining subsections we define and describe properties of the Wigner and Husimi quasi-probability distributions in phase space. First, they are real-valued and normalised in contrast to the characteristic function. Additionally, the expectation value of operator functions of $\hat{a}$ and $\hat{a}^\dagger$ can be determined from weighted integrals of these distributions. These three properties reflect general features of probability distributions. However, as we saw in subsection 2.4.2, these distributions can have regions of negative probability which violates the non-negative Kolmogorov axiom.

The s-ordered quasi-probability distribution is the Fourier transform of the s-ordered characteristic function [Carmichael, 2002]:

$$P_s(\eta) = \frac{1}{\pi^2}\iint \mathrm{d}^2\alpha\ \chi(\alpha, s) \exp\left[\alpha\eta^* - \alpha^*\eta\right]. \tag{2.99}$$

We can define the inverse relationship to write the s-ordered characteristic function in terms of its associated quasi-probability distribution. Combining with Eq. (2.98), we can re-write the s-ordered operator averages via

$$\left\langle \hat{a}^{\dagger p}\hat{a}^q \right\rangle_s = \iint_{-\infty}^{\infty} \mathrm{d}^2\eta\ P_s(\eta)\eta^{*p}\eta^q, \tag{2.100}$$

which could have been expected since differential operations in real space become multiplicative operations in Fourier space. This statement generalises the optical equivalence theorem to different operator orderings. The nomenclature for each distribution is the following convention: $P_1(\eta) = P(\eta)$, $P_0(\eta) = W(\eta)$, and $P_{-1}(\eta) = Q(\eta)$. We conclude these properties by mentioning that each distribution can be mutually related through a convolution with a Gaussian [Scully and Zubairy, 1997, p. 83–86; Barnett and Radmore, 2005, p. 116].

The Wigner function is well suited for visualising quantum states in phase space, which we describe in the following section.

2.5 Quantum optics in phase space

A Gaussian state is fully characterised by its first two moments and has a Gaussian Wigner functions [Schumaker, 1986]. The phase space representation is well suited to providing a theoretical description of Gaussian states and their evolutions. This is since the Gaussian signature of states are preserved during dynamics from *Gaussian channels*, albeit with transformed first and second moments. In this section, we review the Gaussian state formalism and establish the notation that will be useful for our applications to quantum estimation. We will also review the generation and manipulation of Gaussian states by describing common unitary evolutions in quantum optics to suitable symplectic transformations of the state. We set $\hbar = 1$ in the following.

2.5.1 Bosonic systems

Consider a system $\mathcal{S}$ comprised of n modes of a bosonic field. The Hilbert space of $\mathcal{S}$ can be written as the tensor product $\mathcal{H} = \otimes_{j=1}^{n} \mathcal{H}_j$, where $\mathcal{H}_j$ is the infinite dimensional Fock space of mode j. Each individual Hilbert space is spanned by the number basis $\{|m\rangle_j\}$, $m \in \mathbb{N}$. In the phase space formalism it is convenient to arrange these boson operators in a vectorial operator $\hat{\boldsymbol{a}} := (\hat{a}_1, \hat{a}_1^\dagger, \ldots, \hat{a}_n, \hat{a}_n^\dagger)^\top$. The vector $\hat{\boldsymbol{a}} \in \mathbb{R}^{2n}$ satisfies the compact commutation relation [Weedbrook et al., 2012]

$$\left[\hat{\boldsymbol{a}}_j, \hat{\boldsymbol{a}}_k\right] = \boldsymbol{\Omega}_{jk} \quad \text{for} \quad j, k \in \{1, 2, \ldots, 2n\}, \tag{2.101}$$

where the symplectic matrix

$$\boldsymbol{\Omega} = \bigoplus_{j=1}^{n} i\sigma_y = \bigoplus_{j=1}^{n} \begin{pmatrix} 0 & 1 \\ -1 & 0 \end{pmatrix} \tag{2.102}$$

satisfies $\boldsymbol{\Omega}^\top = -\boldsymbol{\Omega} = \boldsymbol{\Omega}^{-1}$, and σ_y is the Pauli y matrix. The bosonic commutation relation in Eq. (2.101) is the multimode form of the commutation relation we found earlier in Eq. (2.59).

All bosonic systems may be equivalently described through the quadrature field operators, introduced earlier in Eq. (2.65), since they are proportional to the bosonic operators. For mode j, we write them again for convenience

$$\hat{q}_j = \frac{1}{\sqrt{2}}\left(\hat{a}_j + \hat{a}_j^\dagger\right), \quad \text{and} \quad \hat{p}_j = \frac{i}{\sqrt{2}}\left(\hat{a}_j^\dagger - \hat{a}_j\right). \tag{2.103}$$

These canonical operators are the dimensionless. They act as the position and momentum operators of the quantum harmonic oscillator, and satisfy the canonical commutation relations $[\hat{q}_j, \hat{p}_k] = i\delta_{j,k}$ in natural units ($\hbar = 1$). We similarly introduce the vector of canonical operators $\hat{\boldsymbol{R}} = (\hat{q}_1, \hat{p}_1, \ldots, \hat{q}_n, \hat{p}_n)^\top$ so that we can re-write these canonical commutation relations in the compact form

$$\left[\hat{\boldsymbol{R}}_j, \hat{\boldsymbol{R}}_k\right] = i\boldsymbol{\Omega}_{jk}. \tag{2.104}$$

This form is suited for a phase space representation of the state.

Property	**Hilbert space, $\mathcal{H}$**	**Phase space, Γ**
Description	ρ	$\boldsymbol{d}, \boldsymbol{\Sigma}$
Dimension	∞	$2n$
Space structure	$\bigotimes$	$\bigoplus$
State kinematics	$\hat{U} \mid \hat{U}^\dagger \hat{U} = \mathbb{1}$, $\rho' \to \hat{U}\rho\hat{U}^\dagger$	$\boldsymbol{S} \mid \boldsymbol{S\Omega S}^\top = \boldsymbol{\Omega}$, $\boldsymbol{d}' \to \boldsymbol{Sd}, \boldsymbol{\Sigma}' \to \boldsymbol{S\Sigma S}^\top$

Table 2.2: *Comparison of properties of the Hilbert space and phase space representations for an N-mode Gaussian state. The unitary operations $\hat{U}$ are assumed to be quadratic in the field operators as described by Eq. (2.107). Table summary adapted from [Adesso et al., 2014].*

2.5.2 Evolution of Gaussian states

An n-mode state described by the density matrix ρ is a Gaussian state if its characteristic function

$$\chi(\boldsymbol{\zeta}) = \exp\left[\frac{1}{2}\boldsymbol{\zeta}^\top(\boldsymbol{\Omega\Sigma\Omega}^\top)\boldsymbol{\zeta} - i(\boldsymbol{\Omega\lambda}^\top\boldsymbol{\zeta})\right], \tag{2.105}$$

is Gaussian. Here $\boldsymbol{\zeta} = (\zeta_1, \zeta_1^*, \ldots, \zeta_n, \zeta_n^*)^\top \in \mathbb{R}^{2n}$. Further, a Gaussian unitary is one that preserves the Gaussian nature of the characteristic function. Specifically, the characteristic function for a Gaussian state is entirely characterised by the first (mean) and second (covariance) moments of the quantum state defined by

$$\boldsymbol{\lambda} = \mathrm{Tr}\left[\rho\hat{\boldsymbol{a}}\right], \quad \boldsymbol{\Sigma}_{jk} = \left\langle\left\{\hat{\tilde{a}}_j, \hat{\tilde{a}}_k\right\}\right\rangle, \tag{2.106}$$

where $\hat{\tilde{a}}_j = \hat{a}_j - \langle\hat{a}_j\rangle$ and $\{\hat{A}, \hat{B}\} = \hat{A}\hat{B} + \hat{B}\hat{A}$ is the anticommutator of operators $\hat{A}$ and $\hat{B}$.

A Gaussian evolution is any trace preserving quantum channel Φ: $\rho \to \Phi[\rho]$ that transforms Gaussian states to Gaussian states. This requires that Gaussian unitaries have Hamiltonian linear or bilinear in the field operators [Schumaker, 1986; Weedbrook et al., 2012] of the form

$$\hat{\mathcal{H}} = i(\boldsymbol{\alpha}\hat{\boldsymbol{b}}^\dagger + \hat{\boldsymbol{b}}^\dagger\boldsymbol{F}\hat{\boldsymbol{b}} + \hat{\boldsymbol{b}}^\dagger\boldsymbol{G}\hat{\boldsymbol{b}}^{\dagger\top}) + \mathrm{H.c.}, \tag{2.107}$$

where $\hat{\boldsymbol{b}} = (\hat{a}_1, \ldots, \hat{a}_n)^\top$, $\hat{\boldsymbol{b}}^\dagger = (\hat{a}_1^\dagger, \ldots, \hat{a}_n^\dagger)$, $\boldsymbol{\alpha} \in \mathbb{C}^n$ and $\boldsymbol{F}$, $\boldsymbol{G}$ are $n \times n$ Hermitian matrices. These interaction Hamiltonians are exponentiated to generate the unitary evolution of a system $\hat{U} = \exp[-i\hat{\mathcal{H}}t]$. In the Heisenberg picture, these unitaries corresponds to a linear unitary Bogoliubov transformation

$$\hat{\boldsymbol{b}}' = \hat{U}^\dagger\hat{\boldsymbol{b}}\hat{U} = \boldsymbol{A}\hat{\boldsymbol{b}} + \boldsymbol{B}\hat{\boldsymbol{b}}^\dagger + \boldsymbol{\alpha}, \tag{2.108}$$

where the $n \times n$ complex matrices $\boldsymbol{A}$ and $\boldsymbol{B}$ satisfy $\boldsymbol{AB}^\top = \boldsymbol{BA}^\top$ and $\boldsymbol{AA}^\top = \boldsymbol{BB}^\top + \mathbb{1}$ to ensure continuity of the commutation relations in Eq. (2.101). Using Eq. (2.103), we can see how Bogoliubov transformations affect the quadrature operators. In the Heisenberg picture, Gaussian

unitaries of the form Eq. (2.107) describe affine maps of the quadrature operators: $\hat{\boldsymbol{x}}' = \boldsymbol{S}\hat{\boldsymbol{x}} + \boldsymbol{d}$, for some $\boldsymbol{d} \in \mathbb{R}^{2n}$ and some real $2n \times 2n$ matrix $\boldsymbol{S}$. This is true regardless of whether the input state is Gaussian or not. Preservation of commutation relation requires that $\boldsymbol{S}\boldsymbol{\Omega}\boldsymbol{S}^\top = \boldsymbol{\Omega}$—which requires $\boldsymbol{S}$ to be symplectic. Since the eigenvalues of the quadrature operators must follow the same transformation rule, the action of Gaussian unitaries correspond to affine symplectic transformations. Kinematics of Gaussian states in the phase space is then conveniently tracked through the states moments

$$\boldsymbol{\lambda}' = \boldsymbol{S}\boldsymbol{\lambda} + \boldsymbol{d}, \quad \boldsymbol{\Sigma}' = \boldsymbol{S}\boldsymbol{\Sigma}\boldsymbol{S}^\top. \tag{2.109}$$

The converse is also true: symplectic transformations of the moments described by Eq. (2.109) are generated by a unitary transformation induced by interaction Hamiltonians of the form Eq. (2.107) [Simon et al., 1988; Schleich, 2001]. We summarise the equivalence between the Hilbert space formalism and the phase space formalism in table 2.2.

To motivate the next subsection on physical implementations of bilinear and quadratic Hamiltonians, we note that any symplectic transformation $\boldsymbol{S}$ may be decomposed as

$$\boldsymbol{S} = \boldsymbol{O}\begin{pmatrix} \boldsymbol{D} & \boldsymbol{0} \\ \boldsymbol{0} & \boldsymbol{D}^{-1} \end{pmatrix}\boldsymbol{O}', \tag{2.110}$$

where the positive diagonal matrix $\boldsymbol{D}$ describes a single-mode squeezer, and the orthogonal, symplectic matrices $\boldsymbol{O}$ and $\boldsymbol{O}'$ describe *passive devices* [Braunstein, 2005]. This is the *Bloch-Messiah* decomposition and has physical implication for the experimental realisation of Hamiltonians of the form written in Eq. (2.107) [Kok and Lovett, 2010].

2.5.3 Bilinear and quadratic Hamiltonians

In the previous subsection, we saw that Gaussian unitaries have the form $\hat{U} = \exp[-i\hat{\mathcal{H}}](\hbar = 1)$, with $\hat{\mathcal{H}}$ the interaction Hamiltonian described in Eq. (2.107). In this subsection, we will see how these unitary evolutions describe different physical devices in quantum optics. We start by observing that the interaction Hamiltonian has terms that can be categorised into two important classes for many problems in quantum optics: the *bilinear* and *quadratic* forms in the creation and annihilation operators. For the vector of creation and annihilation operators introduced in the previous subsection and some Hermitian matrix $\boldsymbol{F} \in \mathbb{C}^{2n}$, we write the bilinear contribution to the Hamiltonian as

$$\hat{\phi}(\hat{\boldsymbol{b}}) = \hat{\boldsymbol{b}}^\top \boldsymbol{F}\hat{\boldsymbol{b}}, \tag{2.111}$$

and the quadratic contributions as

$$\hat{\phi}(\hat{\boldsymbol{b}}^\dagger, \hat{\boldsymbol{b}}) = \hat{\boldsymbol{b}}^{\dagger\top} \boldsymbol{F}\hat{\boldsymbol{b}}. \tag{2.112}$$

Both contributions describe specific physical systems. The term in Eq. (2.111) is written as a product of equal numbers of creation and annihilation operators. They describe *passive devices* that preserve the total number of photons and include beam-splitters, phase-shifters, half/quarter wave plates, and polarisation rotators. The lowest order Gaussian Hamiltonian that satisfies this hence termed bilinear. Alternatively, *active devices* such as squeezers and down-converters do not preserve the total number of photons. These terms are quadratic in the creation and annihilation operators.

2.5.3.1 Displacement operator

The first term in the Hamiltonian (2.107) is linear in the field operators and has the form $\boldsymbol{\alpha}\hat{\boldsymbol{b}}^\dagger - \hat{\boldsymbol{b}}\boldsymbol{\alpha}^\dagger$. This corresponds to the action of the multi-mode displacement operator written

$$\hat{D}(\boldsymbol{\eta}) = \bigotimes_{j=1}^{n} \hat{D}_j(\eta_j), \tag{2.113}$$

for $\hat{D}_j(\eta_j)$ defined in Eq. (2.77). In the Heisenberg picture, this unitary corresponds to the following mode transformations:

$$\hat{D}^\dagger(\eta)\hat{b}\hat{D}(\eta) = \hat{b} + \eta. \tag{2.114}$$

Hence, the displacement operator, as the name suggests, only shifts the first moment and leaves the second moment unchanged.

2.5.3.2 Phase operator and the beamsplitter

The second term in the Hamiltonian (2.107) describes bilinear contributions from devices such as phase-shifters and beam-splitters. To show this, we write

$$\hat{\boldsymbol{b}}^\dagger \boldsymbol{F} \hat{\boldsymbol{b}} = \sum_j F_{jj}\hat{b}_j^\dagger \hat{b}_j + \sum_{k,l} F_{kl}\hat{b}_k^\dagger \hat{b}_l \tag{2.115}$$

The first term in (2.115) corresponds to the action of phase-shifter $\hat{U}(\vartheta) = \exp[-i\vartheta\hat{b}_j^\dagger\hat{b}_j]$ for $F_{jj} = \vartheta$. The Heisenberg evolution of modes are then written:

$$\hat{U}^\dagger(\vartheta)\hat{a}_j\hat{U}(\vartheta) = \exp[-i\vartheta]\hat{a}_j. \tag{2.116}$$

This implements a phase shift and is commonly used in interferometric set-ups. For single modes, it generates no change which can be seen in the interaction picture. This transformation does not affect the first-moment of the state but changes the second moment with the symplectic matrix

$$\boldsymbol{R}_\vartheta = \begin{pmatrix} \cos[\vartheta] & \sin[\vartheta] \\ -\sin[\vartheta] & \cos[\vartheta] \end{pmatrix}. \tag{2.117}$$

The second bilinear contributions comes from from the cross terms $F_{jk}\hat{b}_j^\dagger\hat{b}_k$. A common linear device that takes this form is the beam splitter unitary

$$\hat{U}(\chi) = \exp\left[\chi\hat{a}^\dagger\hat{b} - \chi^*\hat{a}\hat{b}^\dagger\right], \tag{2.118}$$

for some coupling $\chi = \varphi\exp[i\vartheta] \in \mathbb{C}$, and where we relabelled the mode operators. In the Heisenberg picture, this unitary corresponds to the following mode transformations:

$$\hat{U}^\dagger(\chi)\hat{a}\hat{U}(\chi) = \cos[\varphi]\hat{a} + \exp[i\vartheta]\sin[\varphi]\hat{b}, \tag{2.119}$$

$$\hat{U}^\dagger(\chi)\hat{b}\hat{U}(\chi) = \cos[\varphi]\hat{b} + \exp[-i\vartheta]\sin[\varphi]\hat{a}, \tag{2.120}$$

respectively, and the corresponding symplectic matrix transformation is

$$\boldsymbol{S}_\chi = \begin{pmatrix} \cos[\varphi]\mathbb{1}_2 & \sin[\varphi]\boldsymbol{R}_\vartheta \\ -\sin[\varphi]\boldsymbol{R}_\vartheta^\top & \cos[\varphi]\mathbb{1}_2 \end{pmatrix}, \tag{2.121}$$

where $\boldsymbol{R}_\vartheta$ is the symplectic rotation matrix (2.117). Similar to phase-shifters, beam-splitters change only the second moments of a state.

2.5.3.3 Single mode squeezing

The final term in the Hamiltonian (2.107), $\hat{\boldsymbol{b}}^\dagger \boldsymbol{G} \hat{\boldsymbol{b}}^{\dagger\top}$, describes quadratic contributions generated from nonlinear interactions of photons. For example, a photon incident on a non-linear crystal can generate a pair of photons that conserve both energy and momentum. By phase-matching the emitted photons, we have a single-mode squeezing transformation described by the unitary

$$\hat{S}(\xi) = \exp\left[\frac{1}{2}\left(\xi(\hat{a}^\dagger)^2 - \xi^*(\hat{a})^2\right)\right], \tag{2.122}$$

where $\xi = r\exp[i\psi]$. The Heisenberg mode evolution is

$$\hat{S}^\dagger(\xi)\hat{a}\hat{S}(\xi) = \cosh[r]\hat{a} + \exp[i\psi]\sinh[r]\hat{a}^\dagger, \tag{2.123}$$

with the corresponding symplectic matrix transformation

$$\boldsymbol{\Sigma}_\xi = \cosh[r]\mathbb{1}_2 - \sinh[r]\begin{pmatrix}\cos[\psi] & \sin[\psi] \\ \sin[\psi] & -\cos[\psi]\end{pmatrix}. \tag{2.124}$$

The symplectic matrix transformations for different optical systems will be used in chapter 6 to determine evolved state covariance matrices.

Chapter 3

Quantum estimation theory

In this chapter we review some key concepts in estimation theory that will be useful in our work later. Principally, we are concerned with estimating some parameters from a set of experimental data. A completely classical approach, introduced independently by H. Cramér and C. R. Rao in the 1940s, constrains the variance of parameter estimates by a quantity that entirely depends on the statistical nature of the data [Cramér, 1999]. This statistical nature accounts for any experimental uncertainties. Removing uncertainties associated with specific measurements leads to the quantum analogue of estimation theory. This was first addressed by C. Helstrom in 1967. Central to both formalisms is the Fisher information quantity. We present the derivation of this quantity and describe its relevance in parameter estimations protocols.

3.1 Classical bounds on precision measurements

Experimental science is primarily concerned with making high precision measurements. Commonly however, direct measurements may not be possible, either due to experimental impediments, or due to more fundamental reasons. This is particularly true in experimental quantum optics, where quantities such as phase and purity do not have associated measurable observables. In such situations an indirect approach may be adopted where the value of the quantities of interest are inferred through data-processing of data coming from measurements of a different, but related, observable. The problem of estimating the value of a vector of parameters $\boldsymbol{\varphi} = (\varphi_1, \ldots, \varphi_D)^\top$ from a set of observed data $\boldsymbol{x} = (x_1, \ldots, x_\mathcal{D})^\top$ is formally addressed in parameter estimation theory. Owing to experimental uncertainties and errors, the inference of parameters is related to the measurement outcomes through some conditional probability distribution $p(\boldsymbol{\varphi}|\boldsymbol{x})$. Any general parameter estimation strategy can be described through the following main procedures:

1. State preparation of a suitable probe state $\rho(\mathbf{0})$ of a system S,

2. Evolution (parameterisation) of the probe to the state: $\rho(\boldsymbol{\varphi}) = \Lambda[\rho(\mathbf{0})](\boldsymbol{\varphi})$, and

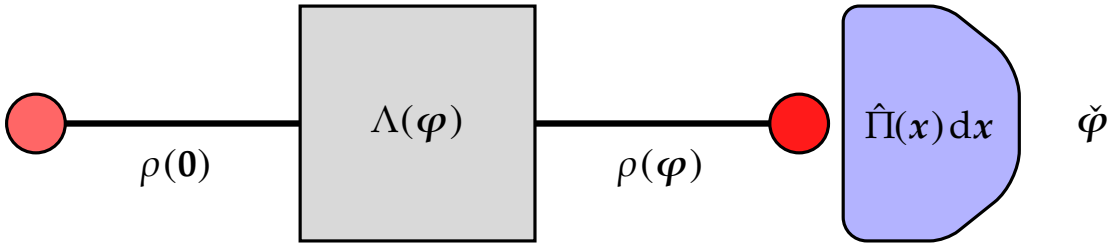

Figure 3.1: *General channel parameter estimation scheme. The quantum channel $\Lambda(\boldsymbol{\varphi})$ parameterises an input probe state with the vector of parameters that we wish to estimate. The probe is measured by an operator of the form $\hat{\Pi}(\boldsymbol{x})d\boldsymbol{x}$ and distributed estimates according to Born's rule. By data processing the measurement outcomes, we obtain our estimate $\check{\boldsymbol{\varphi}}$. The goal of quantum metrology is in finding both the optimal probe state and observable that minimises the covariance matrix of unbiased estimates.*

3. The evolved probe is measured by some complete, self-adjoint observable $\hat{X} = \int \mathrm{d}\boldsymbol{x}\, \boldsymbol{x}\hat{\Pi}(\boldsymbol{x})$ to achieve an estimation of $\boldsymbol{\varphi}$.

This archetypal schema is illustrated in figure 3.1. It can be modelled by describing the evolved state of the system through $\rho(\boldsymbol{\varphi})$, and by associating a positive operator valued measure (POVM), $\hat{\Pi}(\boldsymbol{x})\,\mathrm{d}\boldsymbol{x}$, to the measurement outcome $\boldsymbol{x}$. The probability distribution $p(\boldsymbol{x}|\boldsymbol{\varphi})$ is then given by Born's rule

$$p(\boldsymbol{x}|\boldsymbol{\varphi})\,\mathrm{d}\boldsymbol{x} = \mathrm{Tr}\left[\hat{\Pi}(\boldsymbol{x})\rho(\boldsymbol{\varphi})\right]\mathrm{d}\boldsymbol{x}, \tag{3.1}$$

where $\rho(\boldsymbol{\varphi})$ is the evolved probe state; parameterised by the vector of parameters we want to estimate, and $\int \mathrm{d}\boldsymbol{x}\,\hat{\Pi}(\boldsymbol{x}) = \hat{\mathbb{I}}$. Born's rule gives the probability distribution function (PDF) that distributes the measurement outcomes $\boldsymbol{x}$, given the parameterisation $\boldsymbol{\varphi}$. The evolved state captures uncertainties associated with the state-preparation procedure, while the POVM captures those associated with the measurement stage. Together with Born's rule, they model the probabilistic nature of the measurement data.

Given that the PDF of the data $p(\boldsymbol{x}|\boldsymbol{\varphi})$ is known (i.e. we have a model of the physical process), we now detail how an estimate of the set of parameters $\boldsymbol{\varphi} = (\varphi_1, \ldots, \varphi_D)^\top$ may be extracted from a set of observation data $\boldsymbol{x} = (x_1, \ldots, x_\mathcal{D})^\top$, with D not necessarily equal to $\mathcal{D}$. We follow the derivation of Braunstein and Caves [1994], who introduce the estimator $\check{\boldsymbol{\varphi}}$, which is a function of the observed data and provides estimates of the parameters. Specifically

$$\check{\boldsymbol{\varphi}} = f(\boldsymbol{x}), \tag{3.2}$$

where the notation $\check{\cdot}$ is reserved for estimators to avoid confusion with the carot $\hat{\cdot}$ reserved for quantum mechanical operators. The true value of $\boldsymbol{\varphi}$ is in general a tuple of numbers. In contrast, its estimates are random variables. This is a subtle difference that is rooted in the probabilistic nature of the data; two runs of an experiment with equal parameters $\boldsymbol{\varphi}_1 = \boldsymbol{\varphi}_2$ will not generate equal data due to statistical fluctuations: $\boldsymbol{x}_1 \neq \boldsymbol{x}_2$. Hence the estimates for both runs will differ from the actual values, and not be equal to each other. Any estimator that generates the true value of $\boldsymbol{\varphi}$ from the measurement data is referred to as a *perfect estimator*. Unfortunately, since this is unrealistic, we require a method to characterise the performance of estimators. A natural choice is the *variance* of the estimator [Helstrom, 1973; Cramér, 1999]. Our objective is then to find an estimator that has the smallest variance in parameter estimates.

For the remainder of this chapter, we can safely assume that the measured data $\boldsymbol{x}$ is continuous without any loss of generality.

3.1.1 The classical multi-parameter Cramér-Rao bound

We start by recounting classical data processing. We note that finding the exact form for the variance of our estimator is generally not possible. Hence we search for a lower bound that constrains the variance instead. Various methods to achieve this exist, but we follow the method introduced by H. Cramér and C. R. Rao [Cramér, 1999]. For a multi-parameter estimation of $\boldsymbol{\varphi}$, we start by defining the variation in the estimates of $\boldsymbol{\varphi}$ as

$$\delta\check{\boldsymbol{\varphi}} = \check{\boldsymbol{\varphi}} - \langle\check{\boldsymbol{\varphi}}\rangle, \tag{3.3}$$

where $\langle\check{\boldsymbol{\varphi}}\rangle$ is the average value of the estimator:

$$\langle\check{\boldsymbol{\varphi}}\rangle = \int \mathrm{d}\boldsymbol{x}\, p(\boldsymbol{x}|\boldsymbol{\varphi})\check{\boldsymbol{\varphi}}. \tag{3.4}$$

We define the error in the parameter φ_j as $\Delta\check{\varphi}_j = \check{\varphi}_j - \varphi_j$. Notice that the estimators variance is not the same as its mean square error:

$$\left\langle(\Delta\check{\varphi}_j)^2\right\rangle = \left\langle(\check{\varphi}_j - \varphi_j)^2\right\rangle = \mathrm{Var}[\check{\varphi}_j] + \mathrm{B}[\check{\varphi}_j]^2, \tag{3.5}$$

where $\mathrm{Var}[\check{\varphi}_j] = \langle\check{\varphi}_j^2\rangle - \langle\check{\varphi}_j\rangle^2$ and $\mathrm{B}[\check{\varphi}_j] = \langle\check{\varphi}_j\rangle - \varphi_j$ is the bias of the estimator. We see that the mean square error is equal to the variance if and only if we have an *unbiased estimator*: $\mathrm{B}[\check{\varphi}_j] = 0$. Unbiased estimators ensure that the average of the estimates converge to the true value of the parameter: $\langle\check{\boldsymbol{\varphi}}\rangle = \boldsymbol{\varphi}$. Since for any estimator $\langle\delta\check{\boldsymbol{\varphi}}\rangle = \mathbf{0}$, then for ν separable measurements with measurement outcomes $\boldsymbol{x_1}, \ldots, \boldsymbol{x_\nu}$ [Helstrom, 1976]

$$\int \mathrm{d}\boldsymbol{x}_1 \cdots \int \mathrm{d}\boldsymbol{x}_\nu\, p(x_1|\boldsymbol{\varphi}) \cdots p(\boldsymbol{x}_\nu|\boldsymbol{\varphi})\delta\check{\varphi}_j = 0. \tag{3.6}$$

To understand how this varies with φ_k, we differentiate Eq. (3.6) with respect to the parameter φ_k and use the definition of the estimate variation in Eq. (3.3) to obtain

$$\int \mathrm{d}\boldsymbol{x}_1 \cdots \int \mathrm{d}\boldsymbol{x}_\nu\, p(\boldsymbol{x}_1|\boldsymbol{\varphi}) \cdots p(\boldsymbol{x}_\nu|\boldsymbol{\varphi}) \left(\sum_{l=1}^{\nu} \frac{\partial \ln[p(\boldsymbol{x}_l|\boldsymbol{\varphi})]}{\partial\varphi_k}\right)\delta\check{\varphi}_j - \left\langle\frac{\mathrm{d}\langle\check{\varphi}_j\rangle}{\mathrm{d}\varphi_k}\right\rangle = 0, \tag{3.7}$$

where we used $\mathrm{d}\delta\check{\varphi}_k/\,\mathrm{d}\varphi_k = -\,\mathrm{d}\langle\check{\varphi}_k\rangle/\,\mathrm{d}\varphi_k$ since $\check{\varphi}_k$ is an estimator and does not depend on the $\boldsymbol{\varphi}$. More generally, we can write Eq. (3.7) in vectorial form

$$\int \mathrm{d}\boldsymbol{x}_1 \cdots \int \mathrm{d}\boldsymbol{x}_\nu\, p(\boldsymbol{x}_1|\boldsymbol{\varphi}) \cdots p(\boldsymbol{x}_\nu|\boldsymbol{\varphi}) \left(\sum_{l=1}^{\nu} \boldsymbol{a}^\top \frac{\partial \ln[p(\boldsymbol{x}_l|\boldsymbol{\varphi})]}{\partial\boldsymbol{\varphi}}\right)\delta\check{\boldsymbol{\varphi}}^\top \boldsymbol{b} = \boldsymbol{a}^\top \frac{\mathrm{d}\langle\check{\boldsymbol{\varphi}}\rangle}{\mathrm{d}\boldsymbol{\varphi}}\boldsymbol{b}, \tag{3.8}$$

where we used the fact that $\mathrm{d}\langle\check{\boldsymbol{\varphi}}\rangle/\,\mathrm{d}\boldsymbol{\varphi}$ is independent of $\boldsymbol{x}_1, \ldots, \boldsymbol{x}_\nu$, and multiplied by $\boldsymbol{a}^\top$ on the left and by $\boldsymbol{b}$ on the right, with $\boldsymbol{a}$ and $\boldsymbol{b}$ being arbitrary D-dimensional vectors. We now use the Cauchy-Schwarz inequality for two general functions g and h (consult appendix A),

$$|\langle g, h\rangle|^2 \leq \langle g, g\rangle \cdot \langle h, h\rangle \equiv \|g\|^2 \cdot \|h\|^2, \tag{3.9}$$

with $\|g\|$ defined as the 2-norm of g, to re-write the left hand side of Eq. (3.8). We substitute

$$\begin{aligned} g &= \sum_{l=1}^{\nu} \boldsymbol{a}^\top \frac{\partial \ln[p(\boldsymbol{x}_l|\boldsymbol{\varphi})]}{\partial \boldsymbol{\varphi}}, \\ h &= (\delta\check{\boldsymbol{\varphi}})^\top \boldsymbol{b}, \end{aligned} \tag{3.10}$$

to obtain

$$\begin{aligned} &\boldsymbol{a}^\top \int \mathrm{d}\boldsymbol{x}_1 \cdots \int \mathrm{d}\boldsymbol{x}_\nu \prod_{j=1}^{\nu} p(\boldsymbol{x}_j|\boldsymbol{\varphi}) \left(\sum_{k=1}^{\nu} \frac{\partial \ln[p(\boldsymbol{x}_k|\boldsymbol{\varphi})]}{\partial \boldsymbol{\varphi}}\right)\left(\sum_{l=1}^{\nu} \frac{\partial \ln[p(\boldsymbol{x}_l|\boldsymbol{\varphi})]}{\partial \boldsymbol{\varphi}}\right)^\top \boldsymbol{a} \\ &\times \boldsymbol{b}^\top \int \mathrm{d}\boldsymbol{x}_1 \cdots \int \mathrm{d}\boldsymbol{x}_\nu \prod_{j'=1}^{\nu} p(\boldsymbol{x}_{j'}|\boldsymbol{\varphi})(\delta\check{\boldsymbol{\varphi}})(\delta\check{\boldsymbol{\varphi}})^\top \boldsymbol{b} \geq \left|\boldsymbol{a}^\top \frac{\mathrm{d}\langle\check{\boldsymbol{\varphi}}\rangle}{\mathrm{d}\boldsymbol{\varphi}} \boldsymbol{b}\right|^2. \end{aligned} \tag{3.11}$$

Elements of the first term evaluate to zero unless $k = l$. Further, we can simplify this expression by defining the classical Fisher information (CFI):

$$\begin{aligned} \mathcal{I}^{\mathrm{C}}(\boldsymbol{\varphi}) &= \int \mathrm{d}\boldsymbol{x}\, p(\boldsymbol{x}|\boldsymbol{\varphi}) \left(\frac{\partial \ln[p(\boldsymbol{x}|\boldsymbol{\varphi})]}{\partial \boldsymbol{\varphi}}\right)\left(\frac{\partial \ln[p(\boldsymbol{x}|\boldsymbol{\varphi})]}{\partial \boldsymbol{\varphi}}\right)^\top, \\ &= \int \mathrm{d}\boldsymbol{x}\, \frac{1}{p(\boldsymbol{x}|\boldsymbol{\varphi})} \left(\frac{\partial p(\boldsymbol{x}|\boldsymbol{\varphi})}{\partial \boldsymbol{\varphi}}\right)\left(\frac{\partial p(\boldsymbol{x}|\boldsymbol{\varphi})}{\partial \boldsymbol{\varphi}}\right)^\top. \end{aligned} \tag{3.12}$$

This quantity is at the root of estimation theory. It quantifies the average information for the estimation variables $\boldsymbol{\varphi}$ obtainable through some physical measurement that distributes output data according to Born's rule $p(\boldsymbol{x}|\boldsymbol{\varphi})$. It can be observed from Eq. (3.12) that the multi-parameter classical Fisher information matrix (CFIM) is symmetric: $\mathcal{I}^{\mathrm{C}}(\boldsymbol{\varphi})^\top = \mathcal{I}^{\mathrm{C}}(\boldsymbol{\varphi})$. Since it is also positive-definite, its inverse exists. Since for an invertible matrix, the transpose and inverse operations commute, we see that

$$\left(\mathcal{I}^{\mathrm{C}}(\boldsymbol{\varphi})^{-1}\right)^\top = \left(\mathcal{I}^{\mathrm{C}}(\boldsymbol{\varphi})^\top\right)^{-1} = \mathcal{I}^{\mathrm{C}}(\boldsymbol{\varphi})^{-1}, \tag{3.13}$$

which proves that its inverse is also symmetric. The inequality in Eq. (3.11) becomes

$$\nu \boldsymbol{a}^\top \mathcal{I}^{\mathrm{C}}(\boldsymbol{\varphi}) \boldsymbol{a} \boldsymbol{b}^\top \langle(\delta\check{\boldsymbol{\varphi}})(\delta\check{\boldsymbol{\varphi}})^\top\rangle \boldsymbol{b} \geq \left|\boldsymbol{a}^\top \frac{\mathrm{d}\langle\check{\boldsymbol{\varphi}}\rangle}{\mathrm{d}\boldsymbol{\varphi}} \boldsymbol{b}\right|^2. \tag{3.14}$$

Note that the multiplicative factor ν arises since the CFI has an additive property for independent measurements. Collectively, the positive definite and additive properties make the Fisher information a suitable physical measure of information. With these properties, since $\boldsymbol{a}$ is arbitrary, we are permitted to take

$$\boldsymbol{a} = \left(\mathcal{I}^{\mathrm{C}}(\boldsymbol{\varphi})^{-1}\right)^\top \frac{\mathrm{d}\langle\check{\boldsymbol{\varphi}}\rangle}{\mathrm{d}\boldsymbol{\varphi}} \boldsymbol{b}. \tag{3.15}$$

Upon substitution into Eq. (3.14), we get after some simplification

$$\nu \langle(\delta\check{\boldsymbol{\varphi}})(\delta\check{\boldsymbol{\varphi}})^\top\rangle \geq \left(\frac{\mathrm{d}\langle\check{\boldsymbol{\varphi}}\rangle}{\mathrm{d}\boldsymbol{\varphi}}\right)^\top \mathcal{I}^{\mathrm{C}}(\boldsymbol{\varphi})^{-1} \frac{\mathrm{d}\langle\check{\boldsymbol{\varphi}}\rangle}{\mathrm{d}\boldsymbol{\varphi}}. \tag{3.16}$$

Writing $\langle(\delta\check{\boldsymbol{\varphi}})(\delta\check{\boldsymbol{\varphi}})^\top\rangle$ as the covariance matrix between the estimators $\check{\varphi}_1, \ldots, \check{\varphi}_\nu$, we see its elements are lower bounded by the classical Fisher information via the *classical Cramér-Rao bound* (CCRB) [Cramér, 1999]

$$\mathrm{Cov}\left[\check{\varphi}_j, \check{\varphi}_k\right] \geq \frac{1}{\nu}\left(\frac{\mathrm{d}\langle\check{\varphi}_k\rangle}{\mathrm{d}\varphi_j}\frac{\mathrm{d}\langle\check{\varphi}_j\rangle}{\mathrm{d}\varphi_k}\right)\left[\mathcal{I}^{\mathrm{C}}(\boldsymbol{\varphi})^{-1}\right]_{jk}. \tag{3.17}$$

This places a minimum value to the covariances of an estimator. It is a consequence of the statistical nature of the data, which only permits an inference of the parameters. The coefficient derivatives ensure dimensional consistency by accounting for differences in units between $\check{\varphi}_j$ and φ_j. Saturating the CCRB for all values of $\boldsymbol{\varphi}$ requires finding an *efficient estimator*. However, there is no guarantee that an estimator exists that attains the bound. Also, since the Cramér-Rao bound generally depends on the parameters $\boldsymbol{\varphi}$, the choice of an estimator must be taken subjectively for any experiment.

Instead of relating the CFI to the average error in the estimators, we can relate it to the average error in the actual value of the parameters $\boldsymbol{\varphi}$. The former is determined by the measurement data, the estimator, and the calculated probability distribution $p(\boldsymbol{x}|\boldsymbol{\varphi})$, whereas the latter depends only on the actual value of $\boldsymbol{\varphi}$. Re-writing the CCRB requires relating the variances of the estimator and the actual value of the parameters. To this end, we use standard error propagation formulae to write the error $\delta\varphi_j$ in the parameter φ_j for a single data point $\boldsymbol{x}$ in terms of the estimator $\check{\varphi}$:

$$\delta\varphi_j = \frac{\check{\varphi}_j}{\mathrm{d}\langle\varphi_j\rangle/\,\mathrm{d}\varphi_j} - \varphi_j. \tag{3.18}$$

Combining this with Eq. (3.3), we relate the error $\delta\varphi_j$ to the error in the estimator. We find

$$\langle(\delta\check{\varphi}_j)^2\rangle = \left|\frac{\mathrm{d}\langle\varphi_j\rangle}{\mathrm{d}\varphi_j}\right|\left(\left\langle(\delta\varphi_j)^2\right\rangle - \left\langle\delta\varphi_j\right\rangle^2\right). \tag{3.19}$$

We then combine Eq. (3.19) with the estimator bound in Eq. (3.17), to arrive at a second form of the CCRB:

$$\mathrm{Cov}\left[\varphi_j, \varphi_k\right] \geq \frac{1}{\nu}\left[\mathcal{I}^{\mathrm{C}}(\boldsymbol{\varphi})^{-1}\right]_{jk} + \langle\delta\varphi_j\rangle\langle\delta\varphi_k\rangle \geq \frac{1}{\nu}\left[\mathcal{I}^{\mathrm{C}}(\boldsymbol{\varphi})^{-1}\right]_{jk}. \tag{3.20}$$

This places a theoretical minimum value on the error in the parameters $\boldsymbol{\varphi}$. For any classical or quantum experiment that makes ν independent samples of the probe, the covariances must be larger than ν times the inverse of the CFI. This is expected; the more information that we have, the greater the precision with which we can estimate $\boldsymbol{\varphi}$. Hence, we must choose a suitable estimator, which generates the conditional measurement outcome probabilities $p(\boldsymbol{x}|\boldsymbol{\varphi})$ that maximises the CFI. This provides a dual degree of freedom: one of constructing suitable states of the system $\rho(\boldsymbol{\varphi})$ and choosing the POVM $\hat{\Pi}(\boldsymbol{x})$.

An important case of the CCRB arises when the CFI is constant. The precision of estimates then increases with the number of experimental repeats ν according to:

$$\mathrm{Cov}\left[\varphi_j, \varphi_k\right] \sim \frac{1}{\nu}. \tag{3.21}$$

This scaling is referred to as the standard quantum limit (SQL), and is purely due to ν independent runs of the experiment. In the next section, we will explore how using quantum resources can improve this scaling, to achieve a tighter bound.

3.2 Quantum estimation theory

We have seen how uncertainties associated with the probe preparation and the measurement stages allows us to make only statistical inferences of parameters of interest. If we remove uncertainties related with specific measurements, any further statistical uncertainties in the data will result entirely from quantum noise inherent in the probe state. Assuming that we can measure any self-adjoint operator, then operationally, the quantum Fisher information matrix (QFIM) is the maximisation of the classical Fisher information over all measurement strategies:

$$\mathrm{Cov}\left[\varphi_j, \varphi_k\right] \geq \frac{1}{\nu}\left[\left\{\max_{\hat{\Pi}(\boldsymbol{x})} \mathcal{I}^{\mathrm{C}}(\boldsymbol{\varphi})\right\}^{-1}\right]_{jk} = \frac{1}{\nu}\left[\mathcal{I}^{\mathrm{Q}}(\boldsymbol{\varphi})^{-1}\right]_{jk}, \tag{3.22}$$

where $\mathcal{I}^{\mathrm{Q}}$ is the QFIM associated with the POVM that achieves the inequality. The QFIM can then be understood as an optimisation of the CFIM. What we see is that the bound in Eq. (3.22) holds for all possible POVMs. Since we still have the $1/\sqrt{\nu}$ scaling for the estimation error, no quantum entangling strategies at the measurement stage can introduce enhancements past the SQL regime. With the QFIM a function of only the state of the system, any improvements to the precision scaling must originate from a suitable choice of the initial probe state $\rho(\mathbf{0})$ (see figure 3.1). Specifically, we want to find the result

$$\mathrm{Cov}\left[\varphi_j, \varphi_k\right] \geq \frac{1}{\nu}\left[\left\{\max_{\rho(\mathbf{0})} \mathcal{I}^{\mathrm{Q}}(\boldsymbol{\varphi})\right\}^{-1}\right]_{jk}. \tag{3.23}$$

In this section, we follow the approach of Braunstein and Caves [1994] who demonstrated that the QFIM arises as a solution to both these maximisation procedures. We will find the functional dependence of the QFIM on the probe state. In analogy with classical metrology, we will then write the quantum version of the CCRB.

3.2.1 The quantum Fisher information

Recall from Eq. (3.1) that Born's rule gives the probability distribution function that describes how measurement outcomes are distributed,

$$p(\boldsymbol{x}|\boldsymbol{\varphi}) = \mathrm{Tr}\left[\hat{\Pi}(\boldsymbol{x})\rho(\boldsymbol{\varphi})\right]. \tag{3.24}$$

We start by finding the CFIM first. From Eq. (3.12) we see that this requires taking the derivative with respect to the parameter φ_j

$$\partial_j p(\boldsymbol{x}|\boldsymbol{\varphi}) = \mathrm{Tr}\left[\hat{\Pi}(\boldsymbol{x})\partial_j\rho(\boldsymbol{\varphi})\right], \tag{3.25}$$

where we defined $\partial_j = \partial/\partial\boldsymbol{\varphi}_j$ for brevity. To help define the derivative of the state, we introduce the symmetric logarithmic derivative (SLD), $\boldsymbol{\mathcal{L}} = (\mathcal{L}_1, \mathcal{L}_2, \ldots, \mathcal{L}_D)^\top$, as the self-adjoint operator that satisfies the equation:

$$\partial_j\rho(\boldsymbol{\varphi}) = \frac{1}{2}\left\{\rho(\boldsymbol{\varphi}), \mathcal{L}_j\right\}. \tag{3.26}$$

There are alternative state derivative descriptions, which are the right logarithmic derivative (RLD) [Belavkin, 1976; Genoni et al., 2013] and left logarithmic derivative (LLD) defined through

$$\partial_j \rho(\boldsymbol{\varphi}) = \rho(\boldsymbol{\varphi}) \mathcal{L}_j^{(R)}, \tag{3.27}$$

$$\partial_j \rho(\boldsymbol{\varphi}) = \mathcal{L}_j^{(L)} \rho(\boldsymbol{\varphi}), \tag{3.28}$$

respectively. These relax the symmetric definition of the logarithmic derivative. However, these descriptions have not attracted as much attention as the SLD in quantum estimation theory for two reasons. First, the precision of single parameter estimates derived from the SLD is tighter than the corresponding bound derived from the RLD [Helstrom, 1976]. Second, the single parameter SLD bound is asymptotically attainable with the number of experimental runs. This is not true for multi-parameter estimates, since bounds derived from all logarithmic derivatives are generally not attainable [Monras and Illuminati, 2011]. Finally, the RLD and LLD are generally not Hermitian. Consequently, the optimal estimator derived from these two quantities may not correspond to a physical POVM. Despite this, the use of non-self adjoint operators have been demonstrated to saturate the multi-parameter QCRB [Yuen and Lax, 1973; Hayashi, 2005, p. 113–125]. In the remainder of this thesis, we will consider only precision bounds based on the Hermitian symmetric logarithmic derivative.

From the definition in Eq. (3.26), we can see that the SLD has vanishing trace: $\mathrm{Tr}[\rho(\boldsymbol{\varphi})\mathcal{L}] = 0$. Substituting Eq. (3.26) into Eq. (3.25) gives

$$\begin{aligned} \partial_j p(\boldsymbol{x}|\boldsymbol{\varphi}) &= \frac{1}{2}\mathrm{Tr}\left[\rho(\boldsymbol{\varphi})\hat{\Pi}(\boldsymbol{x})\mathcal{L}_j\right] + \frac{1}{2}\mathrm{Tr}\left[\rho(\boldsymbol{\varphi})\mathcal{L}_j\hat{\Pi}(\boldsymbol{x})\right], \\ &= \mathrm{Re}\left\{\mathrm{Tr}\left[\rho(\boldsymbol{\varphi})\hat{\Pi}(\boldsymbol{x})\mathcal{L}_j\right]\right\}. \end{aligned} \tag{3.29}$$

where we used the property that for Hermitian operators $\hat{A}$, $\hat{B}$, and $\hat{C}$: $\mathrm{Tr}[\hat{A}\hat{B}\hat{C}] = (\mathrm{Tr}[\hat{A}\hat{C}\hat{B}])^*$. The CFIM from Eq. (3.12) can then be re-written as

$$\mathcal{I}^{\mathrm{C}}(\boldsymbol{\varphi}) = \int \mathrm{d}\boldsymbol{x}\, \frac{\left(\mathrm{Re}\left\{\mathrm{Tr}\left[\rho(\boldsymbol{\varphi})\hat{\Pi}(\boldsymbol{x})\mathcal{L}\right]\right\}\right)\left(\mathrm{Re}\left\{\mathrm{Tr}\left[\rho(\boldsymbol{\varphi})\hat{\Pi}(\boldsymbol{x})\mathcal{L}^{\top}\right]\right\}\right)}{\mathrm{Tr}\left[\hat{\Pi}(\boldsymbol{x})\rho(\boldsymbol{\varphi})\right]}. \tag{3.30}$$

Armed with the classical Fisher information, we now maximise it over the POVMs $\hat{\Pi}(\boldsymbol{x})$, as discussed earlier for Eq. (3.22). The result will be the measurement independent QFIM. Since for some complex vectors $\boldsymbol{\alpha}, \boldsymbol{\beta} \in \mathbb{C}^2$, $\mathrm{Re}[\boldsymbol{\alpha}]\mathrm{Re}[\boldsymbol{\beta}] \leq \|\boldsymbol{\alpha}\boldsymbol{\beta}\|$, we develop Eq. (3.30) [Paris, 2009]:

$$\begin{aligned} \mathcal{I}^{\mathrm{C}}(\boldsymbol{\varphi}) &\leq \int \mathrm{d}\boldsymbol{x} \left\| \frac{\mathrm{Tr}\left[\rho(\boldsymbol{\varphi})\hat{\Pi}(\boldsymbol{x})\mathcal{L}\right]}{\sqrt{\mathrm{Tr}\left[\hat{\Pi}(\boldsymbol{x})\rho(\boldsymbol{\varphi})\right]}} \right\|^2, \\ &= \int \mathrm{d}\boldsymbol{x} \left\| \mathrm{Tr}\left[\frac{\sqrt{\rho(\boldsymbol{\varphi})}\sqrt{\hat{\Pi}(\boldsymbol{x})}}{\sqrt{\mathrm{Tr}\left[\hat{\Pi}(\boldsymbol{x})\rho(\boldsymbol{\varphi})\right]}} \sqrt{\hat{\Pi}(\boldsymbol{x})}\, \mathcal{L} \sqrt{\rho(\boldsymbol{\varphi})} \right] \right\|^2, \end{aligned} \tag{3.31}$$

where equality holds if and only if $\mathrm{Im}[\mathrm{Tr}[\rho(\boldsymbol{\varphi})\hat{\Pi}(\boldsymbol{x})\mathcal{L}]] = 0$, i.e. if the vectors lie in the real space $\mathbb{R}^2$, which requires the SLD to be Hermitian. Introducing $(\Delta\mathcal{L})^2$ as the variance of the SLD,

we use the Cauchy-Schwartz inequality defined earlier in Eq. (3.9) to obtain:

$$\begin{aligned}\mathcal{I}^{\mathrm{C}}(\boldsymbol{\varphi}) &\leq \int \mathrm{d}\boldsymbol{x}\,\mathrm{Tr}\left[\sqrt{\hat{\Pi}(\boldsymbol{x})}\,\boldsymbol{\mathcal{L}}\sqrt{\rho(\boldsymbol{\varphi})}\left(\sqrt{\hat{\Pi}(\boldsymbol{x})}\,\boldsymbol{\mathcal{L}}\sqrt{\rho(\boldsymbol{\varphi})}\right)^{\dagger}\right],\\ &= \int \mathrm{d}\boldsymbol{x}\,\mathrm{Tr}\left[\rho(\boldsymbol{\varphi})\boldsymbol{\mathcal{L}}\hat{\Pi}(\boldsymbol{x})\boldsymbol{\mathcal{L}}^{\top}\right],\\ &= \mathrm{Tr}\left[\rho(\boldsymbol{\varphi})\boldsymbol{\mathcal{L}}\boldsymbol{\mathcal{L}}^{\top}\right],\\ &= \mathrm{Tr}\left[\rho(\boldsymbol{\varphi})(\Delta\boldsymbol{\mathcal{L}})^{2}\right],\end{aligned} \tag{3.32}$$

where the final equality used the vanishing trace property of the SLD. This completes the maximisation of the CFIM over all possible measurements. It shows that the classical Fisher information for any measurement is upper bounded by the quantum Fisher information matrix (QFIM) $\mathcal{I}^{\mathrm{Q}}(\boldsymbol{\varphi})$.

$$\mathcal{I}^{\mathrm{C}}(\boldsymbol{\varphi}) \leq \mathcal{I}^{\mathrm{Q}}(\boldsymbol{\varphi}) = \mathrm{Tr}\left[\rho(\boldsymbol{\varphi})\boldsymbol{\mathcal{L}}\boldsymbol{\mathcal{L}}^{\top}\right]. \tag{3.33}$$

Elements of the QFIM are then written $[\mathcal{I}^{\mathrm{Q}}]_{jk} = \mathrm{Tr}[\rho(\boldsymbol{\varphi})\{\boldsymbol{\mathcal{L}}_j, \boldsymbol{\mathcal{L}}_k\}]/2$ with the anticommutator of operators $\hat{A}$ and $\hat{B}$ defined as $\{\hat{A}, \hat{B}\} = \hat{A}\hat{B} + \hat{B}\hat{A}$. We see that the QFIM is independent of the POVM and is a function of only the state. The calculation of the QFIM for any physical system is at the heart of quantum metrology and is typically a difficult task. Determining the QFIM using the SLD operator is particularly suited to unitary quantum metrology. It is less suited for noisy processes, where the calculation involves complex optimisation procedures [Sarovar and Milburn, 2006; Escher et al., 2011a]. To address this, an extended Hilbert space approach may be taken where information about the parameter is obtained by observing both the system and its environment [Escher et al., 2012]. This method prescribes the QFIM in terms of the state evolving Hamiltonian, and is well suited to many physical implementations of parameter estimations, including open quantum systems [Chin et al., 2012; Kołodyński and Demkowicz-Dobrzański, 2013; Alipour et al., 2014; Demkowicz-Dobrzański and Maccone, 2014].

Analogous to the method in the preceding section, the variance of any estimator of $\boldsymbol{\varphi}$ can now be lower bounded by the *quantum Cramér-Rao bound* (QCRB)

$$\mathrm{Cov}\left[\check{\varphi}_j, \check{\varphi}_k\right] \geq \frac{1}{\nu}\left(\frac{\mathrm{d}\langle\check{\varphi}_k\rangle}{\mathrm{d}\varphi_j}\frac{\mathrm{d}\langle\check{\varphi}_j\rangle}{\mathrm{d}\varphi_k}\right)\left[\mathcal{I}^{\mathrm{Q}}(\boldsymbol{\varphi})^{-1}\right]_{jk}. \tag{3.34}$$

In information theory, the QCRB is interpreted as a distinguishability measure for two probability distributions that describes the initial and evolved probe state [Braunstein and Caves, 1994; Braunstein et al., 1996; Bengtsson and Zyczkowski, 2008]. The QFI is then equal to the Bures metric, which characterises the difference between two probability distributions, through their *statistical distance* in the state space of the quantum probe states (see appendix D for further details). This metric then tracks dynamics in the distance with changes to the probe state. A large QFI implies that a small change in $\boldsymbol{\varphi}$ corresponds to a large displacement of the state, and hence becomes more distinguishable from the initial state. This implies that the initial probe state may be chosen for optimised measurements of $\boldsymbol{\varphi}$. However, if no flexibility on the choice of the state can be afforded, the best estimation precision possible requires searching for the measurement that minimises the variance via Eq. (3.34).

We may equivalently re-write the QCRB to show its dependence on the average error in the true value of the parameters:

$$\mathrm{Cov}\left[\varphi_j, \varphi_k\right] \geq \frac{1}{\nu}\left[\mathcal{I}^{\mathrm{Q}}(\boldsymbol{\varphi})^{-1}\right]_{jk}. \tag{3.35}$$

The factor ν, which is the number of repeat measurements, represents the classical improvement to precision scaling. In the following, we examine how quantum resources can improve the estimation precision (for a single experimental run $\nu = 1$). Any optimal estimator for the estimation of $\boldsymbol{\varphi}$ corresponds to the POVM, which equates the CFIM with the QFIM. This happens when both of the inequalities in Eq. (3.31) and Eq. (3.32) are saturated. The first is satisfied when the SLD is Hermitian and so corresponds to a proper quantum mechanical observable. The second equality requires the following be satisfied for all $\boldsymbol{\varphi}$ [Paris, 2009]

$$\frac{\sqrt{\hat{\Pi}(\boldsymbol{x})}\sqrt{\rho(\boldsymbol{\varphi})}}{\mathrm{Tr}\left[\rho(\boldsymbol{\varphi})\hat{\Pi}(\boldsymbol{x})\right]} = \frac{\sqrt{\hat{\Pi}(\boldsymbol{x})}\,\boldsymbol{\mathcal{L}}\sqrt{\rho(\boldsymbol{\varphi})}}{\mathrm{Tr}\left[\rho(\boldsymbol{\varphi})\hat{\Pi}(\boldsymbol{x})\boldsymbol{\mathcal{L}}\right]}. \tag{3.36}$$

This requires the POVM $\hat{\Pi}(\boldsymbol{x})$ to be constructed by the complete set of eigenstates describing the SLD, $\boldsymbol{\mathcal{L}}$ [Braunstein et al., 1996]. Eq. (3.36) represents purely classical post-processing of data that saturates the bound in Eq. (3.33), such that $\mathcal{I}^{\mathrm{C}}(\boldsymbol{\varphi}) = \mathcal{I}^{\mathrm{Q}}(\boldsymbol{\varphi})$. For single parameters the QCRB provides an ultimate bound for unbiased estimators, and can be asymptotically saturated through maximum likelihood estimation [Geyer, 2013]. This estimator has found widespread uses owing to the fact that a finite sample size affords satisfactory performance [Braunstein, 1992]. This can be realised by local operations and classical communications LOCC [Hayashi, 2005; Giovannetti et al., 2011]. For multiple parameters, the QCRB is generally not attainable for simultaneous measurements of each parameter if the SLDs associated with the parameters do not commute. It is important to note that the SLD may not correspond to the optimal observable to be measured. Instead, an explicit form of the optimal quantum estimator that saturates the QCRB was first written by Paris [2009], and takes the form

$$\hat{O}(\boldsymbol{\varphi}) = \boldsymbol{\varphi}\mathbb{1} + \mathcal{I}^{\mathrm{Q}}(\boldsymbol{\varphi})^{-1}\boldsymbol{\mathcal{L}}, \tag{3.37}$$

which is a projective measurement onto the eigenstates of the SLD [Paris, 2009]. This estimator is suitably unbiased ($\langle\hat{O}(\boldsymbol{\varphi})\rangle = \boldsymbol{\varphi}$) and saturates the QCRB. The first term represents the average estimate and the second the smallest covariance of the optimal measurement. Determining the measurement $\hat{O}(\boldsymbol{\varphi})$ is generally a difficult task since it depends on the vector of parameters to be estimated, $\boldsymbol{\varphi}$. To overcome this difficulty, adaptive measurements have been suggested [Berry and Wiseman, 2000, 2002]. This adds another layer of difficulty in finding the optimal measurement of multiple parameters with non-commuting SLDs. Therefore, the multivariate QCRB is generally non-saturable. However, even for incompatible SLD operators, the multiparameter SLD QCRB remains asymptotically attainable if and only if [Monras and Illuminati, 2011; Ragy et al., 2016]

$$\mathrm{Tr}\left[\rho(\boldsymbol{\varphi})[\boldsymbol{\mathcal{L}}_j, \boldsymbol{\mathcal{L}}_k]\right] = 0. \tag{3.38}$$

Additionally, if this condition holds, the information content from a simultaneous measurement of all parameters may match that obtained from separate measurements of each parameter.

The condition in Eq. (3.38) is necessary and sufficient for unitary evolutions on pure states Matsumoto [2002], which is equivalent to requiring the existence of commuting generators that generate the evolution of the probe. For mixed states, the demands to realise optimal simultaneous estimation are more involved. Specifically, we require the existence of a single probe state that maximises the QFI for all values of $\boldsymbol{\varphi}$, a compatible measurement that ensures saturability of the QCRB, and a diagonal QFIM, which would allow independent estimations of each parameter [Ragy et al., 2016]. Alternative methods to provide better precision bounds may involve collective measurements over many independent copies of the system, which is experimentally challenging.

From the above discussion we see that the SLD operator plays a pivotal role in quantum estimation theory. For a multi-parameter estimation problem, finding the SLD for each parameter in $\boldsymbol{\varphi}$ is sufficient to inform whether a simultaneous, efficient estimation can be performed. It also prescribes the optimal estimator that saturates the QCRB; the fundamental limit to estimation precisions allowed by quantum mechanics. We therefore turn our attention to find a functional form for the SLD.

The SLD was implicitly defined in Eq. (3.26). This is a basis-independent Lyapunov matrix equation that has the general solution for the SLD elements [Paris, 2009]

$$\boldsymbol{\mathcal{L}}_j = 2\int_0^\infty \mathrm{d}t\ \exp\left[-\rho(\boldsymbol{\varphi})t\right]\partial_j\rho(\boldsymbol{\varphi})\exp\left[-\rho(\boldsymbol{\varphi})t\right]. \tag{3.39}$$

The Lyapunov representation proves to be very useful for scenarios in which a periodic nature is observed for the anti-commutator of the density matrix and its partial derivative [Liu et al., 2016]. If this is not true, we can introduce a basis dependency by considering the spectral decomposition of the state (the density matrix is positive semidefinite so can be diagonalised)

$$\rho(\boldsymbol{\varphi}) = \sum_{j=1}^{s} p_j(\boldsymbol{\varphi})\,|\varrho_j(\boldsymbol{\varphi})\rangle\,\langle\varrho_j(\boldsymbol{\varphi})|\,, \tag{3.40}$$

where $s = \dim[\mathrm{supp}(\rho(\boldsymbol{\varphi}))]$ is the dimension of the support set of $\rho(\boldsymbol{\varphi})$ [Liu et al., 2014]. Note that both the eigenvalues and eigenvectors depend on the parameters $\boldsymbol{\varphi}$. For ease of notation, we will drop this dependence. By use of this decomposition, then we find from Eq. (3.26) that

$$\langle\varrho_k|\partial_j\rho(\boldsymbol{\varphi})|\varrho_l\rangle = \frac{1}{2}(p_l + p_k)[\boldsymbol{\mathcal{L}}_j]_{kl}, \tag{3.41}$$

with $[\boldsymbol{\mathcal{L}}_j]_{kl} := \langle\varrho_k|\boldsymbol{\mathcal{L}}_j|\varrho_l\rangle$. Since generally both the eigenvalues and eigenstates of $\rho(\boldsymbol{\varphi})$ in Eq. (3.40) depend on the parameter $\boldsymbol{\varphi}$, the matrix element observed on the LHS of Eq. (3.41) becomes

$$[\partial_j\rho(\boldsymbol{\varphi})]_{kl} = (\partial_j p_k)\delta_{kl} + p_l\langle\varrho_k|\partial_j\varrho_l\rangle + p_k\langle\partial_j\varrho_k|\varrho_l\rangle = (\partial_j p_k)\delta_{kl} + (p_l - p_k)\langle\varrho_k|\partial_j\varrho_l\rangle, \tag{3.42}$$

and which yields, from Eq. (3.41), the final form for the SLD operator

$$\boldsymbol{\mathcal{L}}_j = \sum_{k=1}^{s}\frac{(\partial_j p_k)}{p_k}\,|\varrho_k\rangle\,\langle\varrho_k| + \sum_{k,l=1}^{s}\frac{2(p_k - p_l)\langle\partial_j\varrho_k|\varrho_l\rangle}{p_k + p_l}\,|\varrho_k\rangle\,\langle\varrho_l|\,, \tag{3.43}$$

which is valid for all $p_k + p_l \neq 0$, and is Hermitian. From Eq. (3.43) it is clear that the SLD takes arbitrary values for $k, l > s$. However, since the spectral decomposition of the state is not

defined outside the support set s, we take $[\boldsymbol{\mathcal{L}}]_{kl} = 0$ for all $\{k, l\} > s$. Hence the SLD exists only on the support set of the state. Note that Eq. (3.43) is not defined for pure states. However a simple form exists if we write any general family of pure states as $\rho(\boldsymbol{\varphi}) = |\psi(\boldsymbol{\varphi})\rangle\langle\psi(\boldsymbol{\varphi})|$. Using $\rho(\boldsymbol{\varphi})^2 = \rho(\boldsymbol{\varphi})$ for pure states, then differentiating with respect to the parameters $\boldsymbol{\varphi}$ and comparing with the implicit definition Eq. (3.26) we arrive at

$$\boldsymbol{\mathcal{L}} = 2\partial_{\boldsymbol{\varphi}}\rho(\boldsymbol{\varphi}), \quad \rho(\boldsymbol{\varphi}) \text{ pure.} \tag{3.44}$$

The SLD for pure states is now well-defined. However, for mixed states, the SLD often requires diagonalising the density matrix. For arbitrarily large s-dimensional states, this becomes increasingly difficult. To address this difficulty, alternative methods at determining $\boldsymbol{\mathcal{L}}$ have been developed. For example, it has been shown that evaluating $\boldsymbol{\mathcal{L}}$ is isomorphic to solving a set of linear algebraic equations [Ercolessi and Schiavina, 2013]. Additionally, since the SLD describes the dynamics of the system, the Hamiltonian formalism can be alternatively used to determine the QCRB and the optimal measurements. We detail this formalism next.

3.2.2 Hamiltonian formalism of the quantum Fisher information

Consider some unitary process where the state parameterisation is introduced through the unitary $\hat{U}(\boldsymbol{\varphi})$, then $\rho(\boldsymbol{\varphi}) = \hat{U}(\boldsymbol{\varphi})\rho(0)\hat{U}^\dagger(\boldsymbol{\varphi})$ with $\hat{U}(\boldsymbol{\varphi})^\dagger$ the transposed complex conjugate of $\hat{U}(\boldsymbol{\varphi})$. For some generator of dynamics in the vector of parameters $\boldsymbol{\varphi}$, $\hat{\boldsymbol{\mathcal{F}}}$, we have

$$\hat{U}(\boldsymbol{\varphi}) = \exp\left[-i\hat{\boldsymbol{\mathcal{F}}}\boldsymbol{\varphi}\right]. \tag{3.45}$$

The operator $\hat{\boldsymbol{\mathcal{F}}}$ is a local generator which characterises the sensitivity of the system state $\rho(\boldsymbol{\varphi})$ on changes in $\boldsymbol{\varphi}$ after unitary evolutions. If the unitary for the physical process governing the parameterisation is known, the generator of changes in φ_j is defined by [Pang and Brun, 2014]

$$\hat{\mathcal{F}}_j = i\hat{U}^\dagger(\boldsymbol{\varphi})\partial_j\hat{U}(\boldsymbol{\varphi}), \tag{3.46}$$

which is Hermitian since $\hat{U}^\dagger(\partial_j\hat{U}) = -(\partial_j\hat{U}^\dagger)\hat{U}$ and can be easily demonstrated by Taylor expanding $\rho(\boldsymbol{\varphi})$. We want to re-express the QFIM in Eq. (3.33) in terms of the generator $\hat{\mathcal{F}}$.

Consider elements of the QFIM, written again for convenience:

$$\left[\boldsymbol{\mathcal{I}}^{\mathrm{Q}}\right]_{jk} = \frac{1}{2}\mathrm{Tr}\left[\rho(\boldsymbol{\varphi})\{\boldsymbol{\mathcal{L}}_j, \boldsymbol{\mathcal{L}}_k\}\right]. \tag{3.47}$$

We use the same spectral decomposition in Eq. (3.40) for the evolved probe state and the identity $\sum_{j=1}^{\mathfrak{R}} |\varrho_j\rangle\langle\varrho_j| = \mathbb{1}$, where $\mathfrak{R} = \mathrm{rank}[\rho(\boldsymbol{\varphi})]$ the rank of the state. Note that for $s \neq \mathfrak{R}, \mathfrak{R} > s$ we have a non-full rank density matrix. We then write the elements of the QFIM as

$$\left[\boldsymbol{\mathcal{I}}^{\mathrm{Q}}\right]_{jk} = \frac{1}{2}\sum_{l=1}^{s}\sum_{m=1}^{\mathfrak{R}} p_l\left([\boldsymbol{\mathcal{L}}_j]_{lm}[\boldsymbol{\mathcal{L}}_k]_{ml} + [\boldsymbol{\mathcal{L}}_k]_{lm}[\boldsymbol{\mathcal{L}}_j]_{ml}\right), \tag{3.48}$$

where we have defined $[\boldsymbol{\mathcal{L}}_j]_{lm} = \langle\varrho_l|\boldsymbol{\mathcal{L}}_j|\varrho_m\rangle$, and for clarity we recall $j, k \in \{1, 2, \ldots, D\}$, and $s = \dim[\mathrm{supp}(\rho(\boldsymbol{\varphi}))]$ is less than the dimension of the system, $\mathfrak{R}$. We can now substitute the expression for the SLDs we obtained in Eq. (3.43), which after simplification yields

$$\left[\boldsymbol{\mathcal{I}}^{\mathrm{Q}}\right]_{jk} = \sum_{l=1}^{s}\frac{(\partial_j p_l)(\partial_k p_l)}{p_l} + \sum_{l=1}^{s}\sum_{m=1}^{\mathfrak{R}}\frac{2p_l(p_l - p_m)^2}{(p_l + p_m)^2}\left[\langle\partial_j\varrho_l|\varrho_m\rangle\langle\varrho_m|\partial_k\varrho_l\rangle + \langle\partial_k\varrho_l|\varrho_m\rangle\langle\varrho_m|\partial_j\varrho_l\rangle\right]. \tag{3.49}$$

We split the last terms F_1 and F_2 using $\sum_{j=1}^{\Re} = \sum_{j=1}^{s} + \sum_{j=s+1}^{\Re}$, where

$$F_1 = \sum_{l,m=1}^{s} \frac{2p_l(p_l - p_m)^2}{(p_l + p_m)^2} \left[\langle \partial_j \varrho_l | \varrho_m \rangle \langle \varrho_m | \partial_k \varrho_l \rangle + \langle \partial_k \varrho_l | \varrho_m \rangle \langle \varrho_m | \partial_j \varrho_l \rangle \right], \tag{3.50}$$

$$F_2 = \sum_{l=1}^{s} \sum_{m=s+1}^{\Re} 2p_l \left[\langle \partial_j \varrho_l | \varrho_m \rangle \langle \varrho_m | \partial_k \varrho_l \rangle + \langle \partial_k \varrho_l | \varrho_m \rangle \langle \varrho_m | \partial_j \varrho_l \rangle \right]. \tag{3.51}$$

Since $\sum_{j=s+1}^{\Re} |\varrho_j\rangle \langle \varrho_j| = \mathbb{1} - \sum_{j=1}^{s} |\varrho_j\rangle \langle \varrho_j|$, we can re-express term F_2. Also since unitary dynamics are generally governed by the von Neumann equation

$$\partial_j \rho(\boldsymbol{\varphi}) = i \left[\rho(\boldsymbol{\varphi}), \hat{\mathcal{F}}_j \right], \tag{3.52}$$

we write the QFIM elements in terms of the generator according to [Sidhu and Kok, 2017]

$$\begin{aligned} \left[\mathcal{I}^{\mathrm{Q}} \right]_{jk} = &\sum_{l=1}^{s} \frac{(\partial_j p_l)(\partial_k p_l)}{p_l} + \sum_{l=1}^{s} 4p_l \left[\mathrm{Cov}\left(\hat{\mathcal{F}}_j, \hat{\mathcal{F}}_k \right) \right]_l \\ &- \sum_{l \neq m}^{s} \frac{8p_l p_m}{(p_l + p_m)} \left\langle \varrho_l \left| \hat{\mathcal{F}}_j \right| \varrho_m \right\rangle \left\langle \varrho_m \left| \hat{\mathcal{F}}_k \right| \varrho_l \right\rangle, \end{aligned} \tag{3.53}$$

where we recall that $s = \dim[\mathrm{supp}(\rho(\boldsymbol{\varphi}))]$ is the dimension of the support set of $\rho(\boldsymbol{\varphi})$ and $\{l, m \in \mathbb{Z} | 1 \leq l, m \leq s\}$ define the elements of the QFIM matrix elements. This expression holds for any evolution of the probe. For unitary evolutions, the eigenvalue spectrum remains invariant such that the first term of Eq. (3.53) evaluates to zero. The covariance matrix of the generators on the jth-eigenstate of the initial state in Eq. (3.53) is defined as

$$\left[\mathrm{Cov}\left(\hat{\mathcal{F}}_j, \hat{\mathcal{F}}_k \right) \right]_l = \frac{1}{2} \left\langle \varrho_l \left| \left\{ \hat{\mathcal{F}}_j, \hat{\mathcal{F}}_k \right\} \right| \varrho_l \right\rangle - \left\langle \varrho_l \left| \hat{\mathcal{F}}_j \right| \varrho_l \right\rangle \left\langle \varrho_l \left| \hat{\mathcal{F}}_k \right| \varrho_l \right\rangle. \tag{3.54}$$

This generalises the result by Liu et al. [2014] to multi-parameter estimations. In the literature, Eq. (3.53) is often written in the following compact form [Braunstein and Caves, 1994; Liu et al., 2015]

$$\left[\mathcal{I}^{\mathrm{Q}} \right]_{jk} \leq 4 \left[\mathrm{Cov}\left(\hat{\mathcal{F}}_j, \hat{\mathcal{F}}_k \right) \right]_{\mathrm{input}}, \tag{3.55}$$

where the subscript 'input' describes the initial input state. The equality is strictly limited to pure states under unitary evolutions and the inequality applies to all other quantum states. Explicitly for single parameter quantum estimation protocols using pure states, it is easy to see that the QFIM reduces to a constant equal to the variance of the generator of translations for $\boldsymbol{\varphi}$. We summarise some subtleties that arise from the unitary transformation formulation of the QFIM. First, the generator captures the dynamics of the parameterisation process of the state and is basis-independent. Second, the QFIM depends only on the generator and the initial states. The form in Eq. (3.55) provides an easily computable upper bound on the QFI for different quantum states. A zero generator variance results when the state is invariant under unitary dynamics of the type described by Eq. (3.45). Third, entanglement between specific eigenstates of the generator can be used to construct an optimal state which maximises the QFIM [Giovannetti

Formalism	Main quantity & advantages	Thesis chapter
Hamiltonian	$\hat{\mathcal{H}}$; Basis-independent, optimal source	4, 5 and 6
SLD	$\mathcal{L}$; Optimal measurement	4 and 6
Kraus	$\hat{\mathcal{K}}$; Noisy quantum metrology	3

Table 3.1: *Different formalisms of quantum estimation theory, and the relevant chapters in this thesis.*

et al., 2006, 2011]. Finally, comparing the implicit definition of the SLD with the von Neumann equation yeids [Tóth and Apellaniz, 2014]

$$\mathcal{L}_j = 2i \sum_{k,l=1}^{s} \frac{[\hat{\mathcal{F}}_j]_{k,l}(p_k - p_l)}{p_k + p_l} |\psi_k\rangle \langle\psi_l| \tag{3.56}$$

where $[\hat{\mathcal{F}}_j]_{k,l}$ defines the matrix elements of the generator encountered in Eq. (3.46).

We have covered two common formalisms to calculate the QFI for parameter estimations. A third, which we mention for completeness, is the *Kraus formalism*. This description has uses for practical quantum parameter estimations in open, noisy systems [Sarovar and Milburn, 2006; Kołodyński and Demkowicz-Dobrzański, 2013; Falaye et al., 2017]. This is since it is suited to describing the effects of various types of noise. We will revisit how in subsection 3.2.3. Table 3.1 provides a comparative summary of each of the formalisms.

3.2.3 Entanglement assisted quantum metrology

We saw from subsection 3.2.1 that estimating the vector of parameters encoded in a probe state has the standard quantum limit scaling for the RMSE, $\nu^{-1/2}$, where ν is the number of repeat measurements. To understand how 'quantum resources' improve estimation precisions, we note that multiple parameters can generally be estimated sequentially or in parallel. For parallel estimation strategies, there are four possible configurations of employing quantum entanglement as a resource at the probe preparation and measurement stage. These configurations are compactly written CC, CQ, QC, QQ, where C (Q) indicates classical (quantum) resources [Giovannetti et al., 2006] and are illustrated in figure 3.2. Since the bound generated in Eq. (3.35) holds for all possible POVM, no quantum entangling strategies at the measurement stage can introduce enhancements past the SQL regime. As a result of this, the CC and CQ strategies will always yield at best the SQL [Giovannetti et al., 2011]. Any resolution enhancements must then be sourced from the other controllable stage of the general estimation protocol illustrated in figure 3.1: the probe preparation. In this subsection, we consider how entangling strategies at the probe stage can push the precision of estimations past the classical limit.

Consider a single parameter nuclear spin example, where some initial probe evolves through a unitary channel: $\rho(\boldsymbol{\varphi}) = \hat{U}(\boldsymbol{\varphi})\rho(\mathbf{0})\hat{U}^{\dagger}(\boldsymbol{\varphi})$ with $\hat{U}(\boldsymbol{\varphi}) = \exp[i\varphi\hat{\sigma}_z/2]$, where $\hat{\sigma}_z$ is the Pauli spin-flip gate. Then for some initial quibit state written in the computational basis

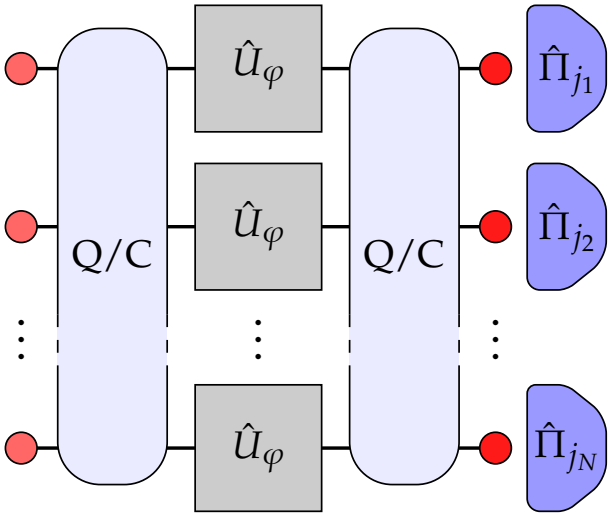

Figure 3.2: *General parallel parameter estimation strategies. The initial probe states, $\rho(\mathbf{0})$ are represented by the light red circles on the left. Each probe state passes through a evolving channel, illustrated by the grey central squares, and emerges parameterised with $\boldsymbol{\varphi}$. Application of a local measurement $\hat{\Pi}_j$ is represented by the blue polygons on the right. Entanglement between the initial and final states of the probe can be utilised in four combinations, represented by the light blue rectangles. Figure adapted from reference [Giovannetti et al., 2006].*

$|\psi(0)\rangle = |+\rangle = (|0\rangle + |1\rangle)/\sqrt{2}$, the unitary maps $|0\rangle \to \exp[i\varphi/2]\,|0\rangle$ and $|1\rangle \to \exp[-i\varphi/2]\,|1\rangle$. Writing the evolved probe state as $|\psi(\varphi)\rangle$ and its derivative as $\partial_\varphi\,|\psi(\varphi)\rangle = |\psi'(\varphi)\rangle$, then since the qubit state is pure, the quantum Fisher information is readily obtained from Eq. (3.53)

$$\mathcal{I}^{\mathrm{Q}}(\varphi) = \langle\psi'(\varphi)|\psi'(\varphi)\rangle - |\langle\psi'(\varphi)|\psi(\varphi)\rangle|^2\,. \tag{3.57}$$

Table 3.2 summarises the QFIM and the achievable precision scalings for different probe states. The results in this table have been illustrated in figure 3.3. The precision improvement provided by using N separable qubits (N here quantifies the resources used),

$$|\psi(0)\rangle = \left[\frac{(|0\rangle + |1\rangle)}{\sqrt{2}}\right]^{\otimes N}, \tag{3.58}$$

is equivalent to a classical advantage. The linearity of the probe reproduces the same effect of repeating the same estimation protocol N-times. This is since the QFIM is additive for independent probe states: $\boldsymbol{\mathcal{I}}^{\mathrm{Q}}[\rho(\boldsymbol{\varphi})^{\otimes N}] = N\boldsymbol{\mathcal{I}}^{\mathrm{Q}}[\rho(\boldsymbol{\varphi})]$. To improve this performance we must consider non-linear probe states. Consider using the entangled N-qubit Greenberger-Horne-Zeilinger (GHZ) state

$$|\psi(0)\rangle = \frac{|0\rangle^{\otimes N} + |1\rangle^{\otimes N}}{\sqrt{2}}, \tag{3.59}$$

which has the same resource count as Eq. (3.58). From the QCRB, we obtain the following RMS scaling: $\delta\varphi \geq 1/N$. This is the *Heisenberg scaling*[1]. Realising this quadratic improvement over the

[1]The Heisenberg limit bears no relation to the Heisenberg uncertainty principle that the name may suggest.

Probe state ($\rho(\mathbf{0})$)	**Quantum Fisher information** ($\mathcal{I}^{\mathrm{Q}}$)	**Quantum precision scaling** ($\delta\varphi$)
Qubit state	1	1
N seperable qubits	N	$1/\sqrt{N}$—(SQL)
N–qubit GHZ state	N^2	$1/N$—(HL)

Table 3.2: *Comparison of achievable quantum precision scalings using different probe states. The precision of estimating the spin of a nuclear ensemble can be improved by using different resources. We may choose the resource to be N separable copies of the qubit state. The quantum contribution to the precision scaling then has the same effect of repeating the estimation N times independently. This is the standard quantum limit (SQL). Alternatively, entangled sources can achieve Heisenberg-limited (HL) scaling.*

standard quantum limit is one of the main objects of quantum metrology and estimation theory. When the number of physical resources is known and correctly accounted for, the Heisenberg limit maintains its optimality as the fundamental limit to precision experiments [Zwierz et al., 2012a] (we will briefly revisit this in the next subsection).

Achieving the HL is state dependent. However, the probe state chosen should be tailored to achieve the best practical precision for a specific parameter. For example, squeezed light is routinely used for phase estimations [Aasi et al., 2013]. A natural question that arises is: *what is the optimal probe state that maximises the QFIM for a parameter estimation protocol?* This was answered by Giovannetti et al. [2006]: the probe state constructed from the superposition of eigenstates corresponding the minimum and maximum eigenvalues of the generator $\hat{\mathcal{G}}$ is optimal. Specifically, writing $\hat{\mathcal{G}}\,|\psi\rangle_{\max} = g_{\max}\,|\psi\rangle_{\max}$, then the state that maximises the QFIM is:

$$|\Psi\rangle_{\mathrm{Opt}} = \frac{|\psi\rangle_{\max} + |\psi\rangle_{\min}}{\sqrt{2}}. \tag{3.60}$$

Only a few experiments have reported a HL scaling for parameter estimates [Higgins et al., 2007, 2009]. This is generally due to two factors. First, achieving the SQL is practically difficult since it requires eliminating non-intrinsic system noises. Second, state entanglement of multipartite systems is challenging to realise due to their increasing susceptibility to environmental losses with increasing particle number. For example, the path-entangled NOON states defined

$$|\varphi_{\mathrm{NOON}}\rangle = \frac{1}{\sqrt{2}}\left(|N\rangle_1|0\rangle_2 + |0\rangle_1|N\rangle_2\right) \tag{3.61}$$

can be shown to achieve the HL resolution scaling for phase measurements in optical interferometers [Kok and Lovett, 2010]. However, as with number states, for $N \geq 2$, these states become plagued with decoherences. Even small Markovian noise reduces the HL scaling achievable by highly entangled states to scalings proportional to the SQL [Huelga et al., 1997; Kołodyński and Demkowicz-Dobrzański, 2010; Escher et al., 2011b]. Common decoherences include depolarisation, dephasing and amplitude damping. Generally, the dynamics of a system that interacts

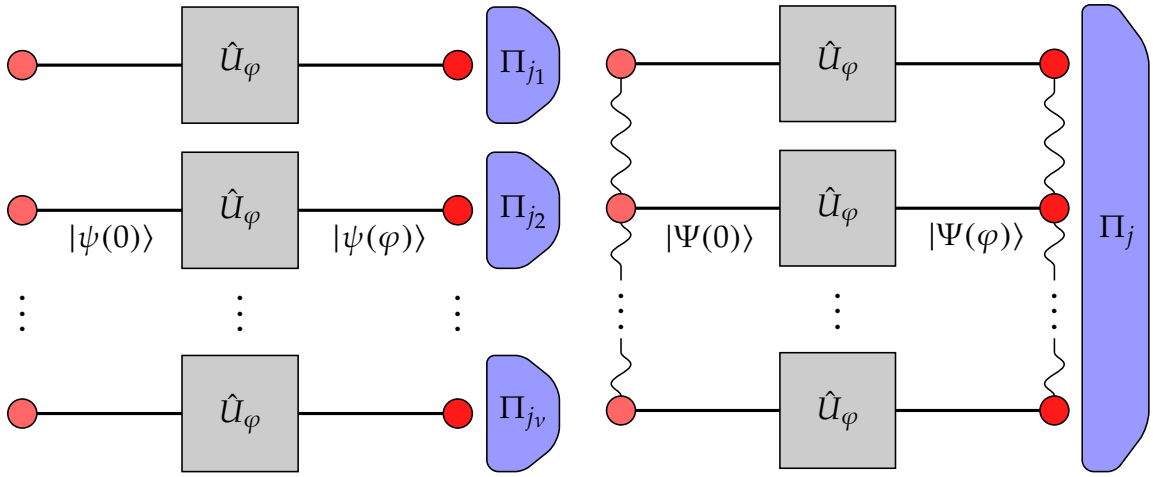

(a) *Separable/independent probe states.* (b) *Entangled probe with same resources.*

Figure 3.3: *Demonstration of parameter estimate precision scalings with classical and quantum probe states, using parallel estimation. Figure 3.3a illustrates the use of parallel estimation strategy using N independent probe states. The uncertainty in the parameter φ then scales as $1/\sqrt{N}$. Alternatively, entangling the N input probe states, and performing a collective measurement, as illustrated in figure 3.3b, achieves a scaling $1/N$.*

with its environment can be described as the quantum channel [Breuer and Petruccione, 2002]

$$\rho' = \mathcal{E}(\rho) = \mathrm{Tr}_E\left[\hat{U}(\rho \otimes \rho_E)\hat{U}^\dagger\right], \tag{3.62}$$

where $\mathcal{E}$ is the quantum operation, and $\mathrm{Tr}_E[\cdot]$ the partial trace over the environment. Note that the bi-partite system $\rho \otimes \rho_E$ evolves according to some unitary. However the evolved state can not be written as a unitary evolution of ρ. Let $\{|e\rangle_j\}$ be an orthonormal basis that spans the environment state space, then the *operator-sum representation* writes the final state of the system in terms of the operators $\hat{S}$, which act on the system alone [Nielsen and Chuang, 2010]. Specifically,

$$\rho' = \mathcal{E}(\rho) = \sum_j \left\langle e_j \middle| \hat{U}\left(\rho \otimes |e_0\rangle\langle e_0|\right)\hat{U}^\dagger \middle| e_j \right\rangle = \sum_j \hat{S}_j \rho \hat{S}_j^\dagger, \tag{3.63}$$

where $\hat{S}_j = \langle e_j|\hat{U}|e_0\rangle$ are the *Kraus operators* or *operation elements* of $\mathcal{E}$[2]. Since $\mathrm{Tr}[\mathcal{E}(\rho)] = 1$, we have the completeness relation of the Kraus operators $\sum_j \hat{S}_j^\dagger \hat{S}_j$, and that the quantum operation $\mathcal{E}$ must be trace-preserving. The Bloch-representation of the density matrix ρ (Eq. (2.18)) requires $\mathcal{E}$ to be an affine map. The Bloch vector then transforms according to $\boldsymbol{r}' = \boldsymbol{A}\boldsymbol{r} + \boldsymbol{b}$, with $\boldsymbol{A}$ a 3×3 real matrix and $\boldsymbol{b}$ some real vector. The Kraus operators describing this can be expanded using the Pauli matrices $P = \{\mathbb{1}, \sigma_x, \sigma_y, \sigma_z\}$: $\hat{S}_j = c_j\mathbb{1} + \sum_{k=1}^3 d_{jk}\sigma_k$, and can be used to describe certain decoherences. Figure 3.4 illustrates the effect of common decoherences on the Bloch sphere.

[2]For an environmental bath with infinite degrees of freedom, the unitary that evolves the bipartite system can be easily specified. Specifically, for a Hilbert space of dimension d, the environment can be modelled in a Hilbert space of dimensions $d_E \leq d^2$ [Nielsen and Chuang, 2010]. Also, the bath can suitably be described as a pure state initially under a *purification* operation.

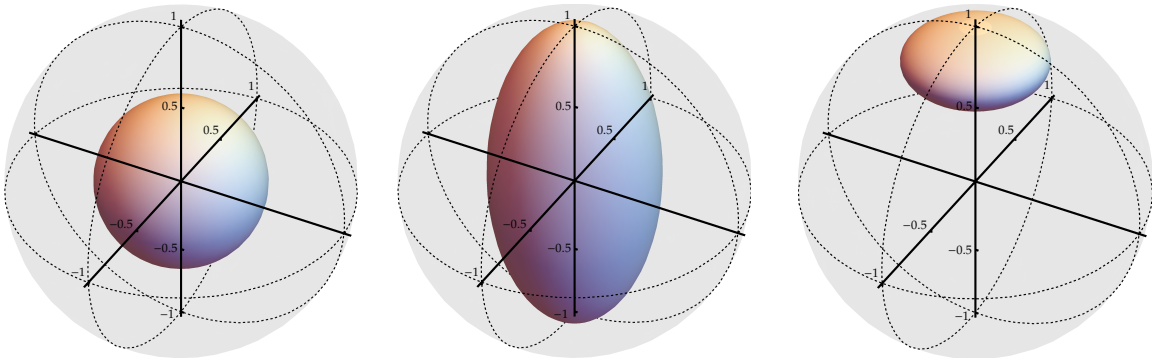

(a) *Depolarising noise.* (b) *Dephasing noise.* (c) *Spontaneous Emmission.*

Figure 3.4: *Geometric effect of decoherences on the Bloch sphere: the shaded region represents the initial Bloch sphere with unit radius, and coloured regions the evolution of vectors in the presence of various types of noise. In figure 3.4a, the effect of a depolarising channel shrinks the Bloch sphere towards the centre (maximally-mixed point). Dephasing noise describes the loss of coherence in a system, and is illustrated in Figure 3.4b. The effects of a phase flip operation, which is described by the Pauli-Z matrix—so-called due to it's effect on the Bloch vector—results in a contraction of the sphere about the Z-direction. Figure 3.4c describes amplitude damping where the system relaxes to the ground state.*

The use of quantum entanglement to achieve better resolutions than classical counterparts was first shown by Caves in 1981 [Caves, 1981]. However, owing to the difficulty and stabilisation of highly entangled states, alternative approaches to achieve quantum enhanced measurements have been investigated [Braun et al., 2018]. These methods rely on the use of quantum correlations, and identical particles. To this end, we note that entanglement is necessary but not sufficient for enhanced precision scalings.

3.2.4 Resource count

It is clear from the last subsection that the use of different probe states leads to different scalings of the estimation precision. We need to characterise and quantify the type of resources that establish the precision bounds allowed theoretically. To appreciate why, a series of proposals reported *super-Heisenberg* scalings [Beltrán and Luis, 2005; Boixo et al., 2007; Roy and Braunstein, 2008], which surpassed the HL. In these cases, the precision scaled with the number of resources used, and the variance of estimates was unbounded. By reconciling the definition of the resources used in a parameter estimation protocol, the Heisenberg limit is found to be generally optimal [Zwierz et al., 2010]. The physical resource should be defined as the expectation value of the generator of translations in φ. For common optical phase estimations, the resource count should be the average photon number used in the probe state. By re-addressing the scaling of the Fisher information, the reported super-Heisenberg scalings were found not to supersede the HL scaling.

Part 2

Research

In this part of the thesis, we detail the research performed over the course of the PhD. In chapter 4, we apply estimation theory to address the source optimisation problem. We provide a cross-utility platform that can be used for many applications. Chapter 5 develops on this work, and extends the treatment to multi-parameter estimations of parameters that appear as arbitrary factors in a Hamiltonian. In chapter 6, we consider the optimal estimation of complex squeezing in phase space. This addresses the limitations and practical implementations that saturate the theoretic fundamental bounds.

Chapter 4

Probe optimisation for estimation of source separations

In this chapter we introduce analysis of spatial deformations to an array of light sources and study how the estimation precision of the interspacing distance d changes with the sources of light used. The quantum Fisher information (QFI) is used as the figure of merit in this work to quantify the amount of information we have on the estimation parameter. We derive the generator of translations $\hat{\mathcal{G}}$ in d due to an arbitrary homogeneous deformation applied to the array. We show how the variance of the generator can be used to easily consider how different deformations and light sources can effect the estimation precision. The single parameter estimation problem is applied to the array and we report on the optimal state that maximises the QFI for d. Contrary to what may have been expected, the higher average mode occupancies of the classical states performs better in estimating d when compared with single photon emitters. The optimal entangled state is constructed from the eigenvectors of the generator and found to outperform all these states. We also find the existence of multiple optimal estimators for the measurement of d. Our results find applications in evaluating stresses and strains, fracture prevention in materials expressing great sensitivities to deformations, and selecting frequency distinguished quantum sources from an array of reference sources.

In Sec. 4.1 we derive the form of the generator of translations in the source separation distance d of a stationary array of arbitrary sources due to some general applied homogeneous deformation matrix Ξ. We apply the generator in Sec. 4.2 to capture the dynamics of the state parameterisation after a stationary 1-dimensional array of classical and quantum light sources undergoes a stretching deformation $\Xi \to \xi_s$. The parameterisation arises from the pairings of different sources along the array. We calculate the QFI to compare the performance of arrays of single photon emitters (SPEs), coherent, thermal, and entangled sources of light on the estimation of d. In contrast to what may have been expected from earlier work [Thiel et al., 2007; Oppel et al., 2012], we find that the higher mode occupancies of classical coherent and thermal states affords better estimation precisions when compared with the SPEs. This would be favourable since generating classical states may be less resource-expensive to create. However a quantum enhancement is observed when entanglement is employed. In agreement with separate work, the optimal state is that which entangles the eigenstates corresponding to the maximum and minimum difference eigenvalues of the generator. We demonstrate that entanglement as a

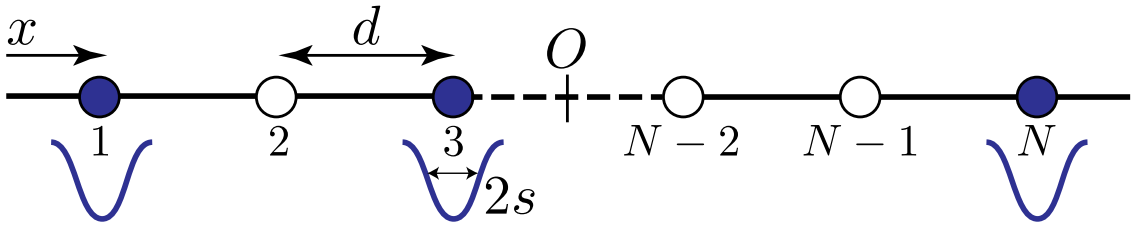

Figure 4.1: *Array of identical, stationary, and equidistant emitters, each with an intrinsic spatial Gaussian uncertainty s (blue envelopes). The continuous variable x runs along the source plane, d is the source separation, and O defines the midpoint of the array of N sources. For a source operation efficiency, η, filled sources are understood to emit a photon whereas the unfilled sources do not. In this work, all sources will be assumed to operate with efficiency $\eta = 1$.*

resource must be carefully used to provide precision enhancements. This insight is reminiscent of previous studies where entanglement was concluded a necessary but insufficient resource for quantum metrology [Gottesman, 1997; Tsang, 2008; Tilma et al., 2010; Braun et al., 2018]. In all these studies, rarely are the optimal measurement strategies considered. To address this, we discuss the optimal estimator for SPES in Sec. 4.3.

4.1 Generator of translations

We consider a 1D array of N identical, stationary, and equidistant emitters, each with an intrinsic spatial Gaussian uncertainty s. This has been illustrated in figure 4.1 and has been experimentally realised to some extent for near-identical, pure, heralded single photon emitters (SPES) [Spring et al., 2017]. We estimate the source separation distance d after the array is subjected to a general homogeneous deformation. This amounts to a single parameter estimation which would help determine the deformation $\boldsymbol{\Xi}$ and the nature of the sources required to maximise the QFI. Let $\boldsymbol{r}$ define the initial coordinates of a source. After some applied deformation the final source coordinates can be written

$$\tilde{\boldsymbol{r}} = \boldsymbol{\Xi}\boldsymbol{r}, \tag{4.1}$$

with the displacement being $\boldsymbol{\varepsilon} = (\boldsymbol{\Xi} - 1)\boldsymbol{r} = \tilde{\boldsymbol{r}} - \boldsymbol{r}$. The deformations considered in this work leave the spatial distribution (and hence the variance) of each source invariant and only shift the expected source positions μ_j, $j \in S_N$ where S_N denotes the set of positive integers $\{1, 2, \ldots, N\}$. Cases where the source distribution change would suggest the unlikely scenario where the nature of the sources change with the deformation. Figure 4.2 illustrates the differing effects of both types of deformations. Before calculating the QFI, we first derive the generator of translations in the estimating parameter d due to a homogenous deformation.

Without loss of generality, we first consider an array of N sources, each with a general spatial profile $f(x_j, \mu_j)$ for the jth-source, where x_j defines the general coordinate along the array for source j and μ_j is the central position of source j. In what follows, we reserve bold

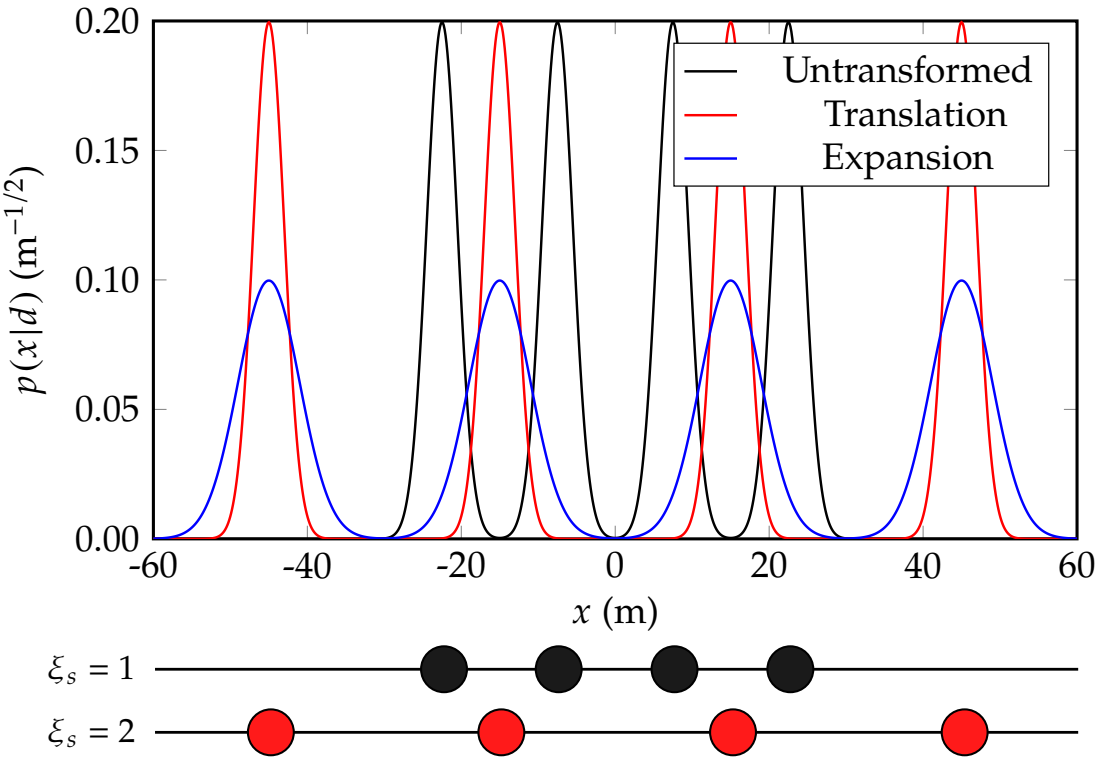

Figure 4.2: *Consider the undeformed array of $N = 4$ Gaussian spatially profiled sources with a standard deviation of $s = 2$ and a source separation distance $d = 15$ shown in solid black. For a simple homogeneous stretching of a 1D array, $\Xi_s \to \xi_s = 2$, the red distribution illustrates the intended behaviour of the generator on the source probability distribution. The expected source positions shift without changing the shape of the probability distribution. The blue distribution represents the unwanted result where the probability distribution is changed implying the nature of the sources changes according the type of transformation considered.*

typesetting for tuples. The state may be written

$$\begin{aligned} |\Psi(d)\rangle &= \bigotimes_{j=1}^{N} \int \mathrm{d}x_j \; f(x_j, \mu_j) \hat{a}_j^\dagger(x_j) \, |0\rangle_j \,, \\ &= \int \mathrm{d}\boldsymbol{x} \; f(\boldsymbol{x}, \boldsymbol{\mu}) \hat{a}^\dagger(\boldsymbol{x}) \, |\boldsymbol{0}\rangle \,, \end{aligned} \tag{4.2}$$

where $f(\boldsymbol{x}, \boldsymbol{\mu}) = \prod_{j=1}^{N} f(x_j, \mu_j)$, $\hat{a}^\dagger(\boldsymbol{x}) = \prod_{j=1}^{N} \hat{a}_j^\dagger(x_j)$, $\mathrm{d}\boldsymbol{x} = \prod_{j=1}^{N} \mathrm{d}x_j$, and $|\boldsymbol{0}\rangle = |0\rangle^{\otimes N}$ is the multimode vacuum. The jth-source position vector is chosen to be symmetric about the array centre O (see figure 4.1) such that

$$\mu_j = \left[j - \frac{(N+1)}{2} \right] d. \tag{4.3}$$

For now we assume that each source is mutually independent such that they can be described by separate Hilbert spaces. Hence the mode operators obey the commutation relations

$[\hat{a}_j(x), \hat{a}_k^\dagger(y)] = \delta_{jk}\delta(x-y)$ and all other combinations are zero. We later relax this assumption to allow for source overlapping.

We search for the unitary that generates the new probability distribution after a deformation is applied. Describing the deforming matrix $\boldsymbol{\Xi}$ in 1D as ξ, we search for the unitary transformation $\hat{U}(\xi)$ that specifically performs the following operation:

$$\hat{U}(\xi)\,|\Psi(d)\rangle = \int \mathrm{d}\boldsymbol{x}\; f(\boldsymbol{x}, \tilde{\boldsymbol{\mu}}(\xi))\hat{a}^\dagger(\boldsymbol{x})\,|\boldsymbol{0}\rangle\,, \tag{4.4}$$

where

$$\tilde{\mu}_j(\xi) = \mu_j + \varepsilon_j(\xi) = \xi\mu_j. \tag{4.5}$$

This changes the expected mean positions of the sources but does not change the source variances. By substituting the state Eq. (4.2) into Eq. (4.4), Fourier transforming the creation operators, and rearranging terms, we find

$$\hat{U}(\xi)\hat{a}^\dagger(\boldsymbol{k})\hat{U}^\dagger(\xi) = \exp\left[i(\xi-1)\sum_{j=1}^{N} k_j\mu_j\right]\hat{a}^\dagger(\boldsymbol{k}). \tag{4.6}$$

This corresponds to a linear unitary Bogoliubov transformation of the mode operators in the Heisenberg picture. To find the unitary that performs of this operation, we write the exponent of the exponential in Eq. (4.6) as $i\varphi$, such that $\hat{U}(\xi) = \exp[i\varphi\hat{A}]$. For small φ, $\hat{U}(\xi) = \mathbb{1} + i\varphi\hat{A}$, we require the operator $\hat{A}$ to be Hermitian to ensure unitarity at lowest order in φ. Using this to expand Eq. (4.6) to lowest order in φ, we find the condition

$$\left[\hat{A}, \hat{a}\right] = \hat{a}, \tag{4.7}$$

which is satisfied when $\hat{A}$ is the number operator. The operation in Eq. (4.6) is then achieved by the following form of the unitary

$$\hat{U}(\xi) = \exp\left[i\,(\xi-1)\sum_{j=1}^{N}\mu_j\int \mathrm{d}k_j\; k_j\,\hat{n}_j(k_j)\right], \tag{4.8}$$

which may be verified by means of the Baker-Campbell-Hausdorff (BCH) identity, and where $\hat{n}_j(k_j) = \hat{a}_j^\dagger(k_j)\hat{a}_j(k_j)$ is the number operator of the jth source in mode k_j. Writing the total unitary as the product $\hat{U}(\xi) = \otimes_{j=1}^{N}\hat{U}_j(\xi)$, where $\hat{U}_j(\xi)$ is the unitary that performs translations in source j by ε_j. From Eq. (3.46), the generator of changes in d due to ξ can be written as

$$\hat{\mathcal{G}}(\xi) = i\hat{U}^\dagger(\xi)\partial_d\hat{U}(\xi). \tag{4.9}$$

Combining with Eq. (4.8) provides the final form of our generator,

$$\hat{\mathcal{G}}(\xi) = -(\xi-1)\sum_{j=1}^{N}\mu_j'\int \mathrm{d}k_j\; k_j\,\hat{n}_j(k_j), \tag{4.10}$$

where $\mu_j' = \partial_d\mu_j = j - (N+1)/2 = \mu_j/d$. This generator characterises the dynamical property of the parameterisation process of the state on ξ due to homogenous deformations, and its

Hermiticity follows from the properties of the number operator. It has units of momentum, which is expected since the array sources undergo individual spatial translations according to some homogeneous expansion by factor ξ. The unitary in Eq. (4.8) may then be rewritten as

$$\hat{U}(\xi) = \exp\left[-id\hat{\mathcal{G}}(\xi)\right]. \tag{4.11}$$

This unitary describes the shift in expected source positions along an array, governed by some homogeneous transformations of the array, without modifying their spatial profile. It is related to the momentum translation operator. To observe this, recall Lagrange's translation operator,

$$\exp\left[b\frac{\partial}{\partial x}\right] f(x) = f(x+b). \tag{4.12}$$

By change of variables, we can describe a dilation operation through

$$y \equiv \exp[x], \implies x = \ln[y]. \tag{4.13}$$

Defining $g(y) = g(\exp[x]) \equiv f(x)$, then

$$\exp\left[by\frac{\partial}{\partial y}\right] g(y) = g(\exp[b+x]) = g(\exp[b]\, y). \tag{4.14}$$

This dilates the coordinate y by a factor of $\exp[b]$; a stretching of factor 2 requires $b = \ln 2$. In terms of quantum mechanical position and momentum operators, the dilation operator is $\exp[ib\hat{y}\hat{p_y}]$: a rotation in phase space. To recognise the generator in Eq. (4.10) as a form of Lagrange's dilation operator, recall the commutation relations satisfied by the mode operators:

$$\left[\hat{a}_j, \hat{a}_k^\dagger\right] = \delta_{jk}, \tag{4.15}$$

which are combinatorially isomorphic to (the so-called Bargmann representation)

$$\left[\frac{\partial}{\partial y}, y\right] = 1, \tag{4.16}$$

such that

$$\exp\left[it\omega\hat{a}^\dagger\hat{a}\right] g(\hat{a}^\dagger) = g\left(\exp[it\omega]\,\hat{a}^\dagger\right). \tag{4.17}$$

The form of the unitary in Eq. (4.11) implies that the *change* in the QFI as a result of the array deformation may be determined from the variance of the generator [Braunstein et al., 1996]. The QFI of the deformed array is instead computed from the variance of the generator $\hat{\mathcal{G}}(\xi)$ with the factor $(\xi - 1)$ in Eq. (4.10) replaced by ξ. This is a consequence of having derived the unitary by considering the shift in expected source positions, $\varepsilon_j = (\xi - 1)\mu_j$, resulting from a homogenous deformation, ξ. In this representation, the QFI is determined entirely by $\hat{\mathcal{G}}$ and the initial state of the undeformed array. In the next section, we evaluate the variance of the generator for arrays of well-defined classical and quantum states of light.

4.2 Classical and quantum light sources

We consider stretching deformations of the array with a factor ξ_s. From the variance of the generator, we calculate the QFI for the array of identical, stationary, and equidistant emitters shown in figure 4.1. We compare the performance of different sources of light on the estimation precision of d. This will identify whether difficult-to-prepare states for enhanced precision measurements is a useful and feasible tradeoff. We choose to work in the near-field regime over the far field. These define different regions of the electromagnetic field around the sources and allow the use of intensity measurements in the near field to estimate d as opposed to higher-order correlation measurements in the far field [Oppel et al., 2012; Pearce et al., 2015]. For complete state detection, the QFI remains invariant of the regime considered. To demonstrate this, consider complete state detection and the parameter-independent unitary, $\hat{U}_{\text{FF}}$, which propagates the near-field pure state to the far field: $|\Psi_{\text{FF}}\rangle = \hat{U}_{\text{FF}} |\Psi_{\text{NF}}\rangle$. For a parameter-independent unitary,

$$|\Psi'_{\text{FF}}\rangle = \partial_d |\Psi_{\text{FF}}\rangle = \hat{U}_{\text{FF}} \partial_d |\Psi_{\text{NF}}\rangle \,, \tag{4.18}$$

we find $\mathcal{I}^{\text{Q}}_{\text{FF}} = \mathcal{I}^{\text{Q}}_{\text{NF}}$. Hence, for complete detection of the state, parameter estimation in both regimes yields the same precision. This equivalence cannot be extended to the case of incomplete detection of the state. Such an occurrence may be modelled by considering a near-field calculation comprised of source efficiencies $\eta < 1$.

4.2.1 Single photon emitters

We start by considering N independent sources. Each is assumed to be generated deterministically with efficiency $\eta = 1$. A photon is generated by the jth source if $|1\rangle_j = \hat{b}^\dagger_j |0\rangle_j$, where $\hat{b}^\dagger_j$ is the mode operator describing a photon with a Gaussian spatial profile with centre μ_j and standard deviation s[1]. This requires the following form for the creation operator:

$$\hat{b}^\dagger_j = \frac{1}{(2\pi s^2)^{1/4}} \int \mathrm{d}x_j \exp\left[-(x_j - \mu_j)^2/4s^2\right] \hat{a}^\dagger_j(x_j). \tag{4.19}$$

We initially assume the limit of clear separation, $d \gg s$, where each source may be considered mutually independent. The pure state describing the jth-source $|\psi\rangle_j = \hat{b}^\dagger_j |0\rangle_j$ is then described by its own Hilbert space $\mathcal{H}_j$. Defining the total Hilbert space by $\mathcal{H} = \otimes_{j=1}^N \mathcal{H}_j$, then the state of the whole array shown in figure 4.1 may be written as the product state

$$|\Psi(d)\rangle = \bigotimes_{j=1}^{N} |\psi\rangle_j \tag{4.20}$$

where $|\Psi(d)\rangle \in \mathcal{H}$. Since the generator of translations in d is defined in Fourier space, we are required to Fourier transform the state to compute the variance $(\Delta\hat{\mathcal{G}})^2$. Using

$$\hat{a}^\dagger_j(x_j) = \frac{1}{\sqrt{2\pi}} \int \mathrm{d}k_j \hat{a}^\dagger_j(k_j) \exp\left[i x_j k_j\right] \tag{4.21}$$

[1] We denote the Gaussian standard deviation of the sources as s. This distinguishes it from the permutation element σ used in appendix E.

and combining with Eq. (4.19), the complete state of N sources in Fourier space may be written as

$$|\Psi(d)\rangle = \left(\frac{2s^2}{\pi}\right)^{\frac{N}{4}} \int \mathrm{d}\boldsymbol{k}\, \exp\left[i\boldsymbol{k}\cdot\boldsymbol{\mu} - s^2\boldsymbol{k}\cdot\boldsymbol{k}\right]\, \hat{a}^\dagger(\boldsymbol{k})\, |\boldsymbol{0}\rangle\,, \tag{4.22}$$

where the d dependence arises in the tuple $\boldsymbol{\mu}$ since $\mu_{j+1} - \mu_j = d$. After an applied stretching of the array about the centre O, the QFI of the deformed array of sources is determined from the variance of the 1D generator. The expectation of the generator is zero, which is a consequence of an odd parity integral. Physically, this is since the stretching is performed about the centre of the array and the array does not move as a whole. This is reminiscent of the average momentum of a particle trapped in a harmonic potential well. Hence the QFI is given by $4\langle\hat{\mathcal{G}}^2(\xi_s)\rangle$:

$$\begin{aligned}\langle\hat{\mathcal{G}}^2(\xi_s)\rangle = \left(\frac{2s^2}{\pi}\right)^{\frac{N}{2}} \sum_{j=1}^{N} \mu_j^2 \int \mathrm{d}\boldsymbol{k}\, \mathrm{d}\boldsymbol{k}'\, \mathrm{d}k_j''\, \mathrm{d}k_j'''\, k_j''\, k_j''' \\ \times \exp\left[i(\boldsymbol{k}-\boldsymbol{k}')\cdot\boldsymbol{\mu} - s^2(\boldsymbol{k}\cdot\boldsymbol{k} + \boldsymbol{k}'\cdot\boldsymbol{k}')\right] \nu(\boldsymbol{k}', k_j'', k_j''', \boldsymbol{k}),\end{aligned} \tag{4.23}$$

where

$$\nu(\boldsymbol{k}', k_j'', k_j''', \boldsymbol{k}) = \langle\boldsymbol{0}|\, \hat{a}(\boldsymbol{k}')\hat{n}_j(k_j'')\hat{n}_j(k_j''')\hat{a}^\dagger(\boldsymbol{k})\, |\boldsymbol{0}\rangle\,. \tag{4.24}$$

The vacuum expectation value $\nu(\boldsymbol{k}', k_j'', k_j''', \boldsymbol{k})$ for arbitrary N may be written

$$\nu(\boldsymbol{k}', k_j'', k_j''', \boldsymbol{k}) = \delta(k_j'' - k_j''')\delta(k_j''' - k_j)\delta(k_j' - k_j'') \prod_{\substack{i=1,\\ i\neq j}}^{N} \delta(k_i' - k_i). \tag{4.25}$$

Substituting Eq. (4.25) into Eq. (4.23), we obtain the QFI for an array of SPEs stretched by factor ξ_s:

$$\mathcal{I}_{\mathrm{SPE}}^{\mathrm{Q}} = 4(\Delta\hat{\mathcal{G}})^2 = \frac{\xi_s^2}{s^2}\sum_{j=1}^{N}\mu_j'^2 = \frac{\xi_s^2 N(N^2-1)}{12s^2}, \tag{4.26}$$

where we recall $\mu_j' = \partial_d\mu_j$. The first equality holds since the generator is independent of d, the second from the variance of the generator. The third equality is from the explicit summation of μ_j' which was defined earlier. We note that the QFI is independent of the separation distance d, which is welcoming since the parameter to be estimated is often outside the control of the experimenter. A better estimate of d can be achieved by increasing the number of sources N and the stretching factor ξ_s, and decreasing the intrinsic Gaussian emission uncertainty s, as expected. The cubic dependence on N may preliminarily suggest a precision scaling which surpasses the Heisenberg limit. However, the resource count of this physical system is defined by the variance of the generator of translations in d [Giovannetti et al., 2006; Zwierz et al., 2010, 2012b], which is not the number of photons. The physical interpretation of the resource is difficult to characterise. Since the QFI depends on the number of sources used and their placement along the array, we conjecture that the resource measure is proportional to the number of source pairings, which scales quadratically.

4.2.2 Single photon emitters from a single Hilbert space

If we drop the requirement that $d \gg s$, then neighbouring source distributions may overlap. The resulting QFI is expected to vary with the source separation distance. To understand this dependence, we drop the assumption that each source can be described by a different Hilbert space. This requires different commutations relations to those used earlier, where it was assumed that each source was mutually independent. Specifically, we have $[\hat{a}(x), \hat{a}^\dagger(y)] = \delta(x-y)$ with all other combinations being zero. The Kronecker δ is dropped since we now associate all of the sources with the same Hilbert space $\mathcal{H}$, which can no longer be decomposed in a tensor product structure. These updated commutation relations allow for different source distributions to overlap and will help determine how the QFI varies with the source separation distance. This demonstration will be made for the array of SPE emitters without loss of generality. For distinction with the QFI derived through use of the former commutation relations, we define the QFI calculated with these updated commutation relations as $\mathfrak{I}^{Q}_{\text{SPE}}$.

We start by considering a stretched array of N sources, each emitting photons deterministically with a Gaussian spatial profile. The stretching factor about the array centre is ξ_s and transforms the mean jth source position to

$$\tilde{\mu}_j = \left[j - \left(\frac{N+1}{2} \right) \right] \xi_s d. \tag{4.27}$$

The state describing the N sources in the near field is written

$$|\Psi\rangle = \frac{1}{\mathcal{N}} \int_{-\infty}^{\infty} \mathrm{d}\boldsymbol{x} \ \exp\left[\sum_{j=1}^{N} \frac{-(x_j - \tilde{\mu}_j)^2}{4s^2} \right] \hat{a}^\dagger(\boldsymbol{x}) \, |0\rangle, \tag{4.28}$$

where $\hat{a}^\dagger(\boldsymbol{x}) = \hat{a}^\dagger(x_1) \cdots \hat{a}^\dagger(x_N)$ and $\mathcal{N}$ is the normalisation constant. We note the subtle change to the notation used for the vacuum state and the mode operators which now span the entire Hilbert space $\mathcal{H}$. This is in contrast to Eq. (4.22), where mode operators corresponding to the jth source acted only on its associated Hilbert space. Defining

$$g_\alpha^\beta = \exp\left[-\frac{1}{2s^2} \sum_{k=\alpha}^{\beta} x_k^2 - x_k(\tilde{\mu}_k + \tilde{\mu}_{\sigma(k)}) \right] \tag{4.29}$$

then

$$|\mathcal{N}|^2 = \exp\left[\frac{-d^2 \mathcal{I}^{\text{Q}}_{\text{SPE}}}{2} \right] \sum_{\sigma} \int_{-\infty}^{\infty} \mathrm{d}\boldsymbol{x} \ g_1^N, \tag{4.30}$$

where we recall the definition of $\mathcal{I}^{\text{Q}}_{\text{SPE}}$ from Eq. (4.26) in the main section and σ denotes all of the possible permutations associated with the number of sources, N. Since Eq. (4.28) is a pure state the QFI may be determined from

$$\mathfrak{I}^{Q}_{\text{SPE}} = 4 \left\{ \langle \Psi' | \Psi' \rangle - |\langle \Psi | \Psi' \rangle|^2 \right\}, \tag{4.31}$$

where $|\Psi'\rangle = \partial_d |\Psi\rangle$. We later realise this method provides the same result for the QFI as that determined from the variance of the generator $\hat{\mathcal{G}}(\xi_s)$, providing a convincing verification.

Noting that the normalisation constant has no dependence on the integration variable, then by use of the following vacuum expectation value

$$\langle 0|\prod_{j=1}^{N}\hat{b}(x_j)\prod_{j=1}^{N}\hat{b}^{\dagger}(x'_j)|0\rangle = \sum_{\sigma}\prod_{j=1}^{N}\delta\left(x_j - x'_{\sigma(j)}\right), \tag{4.32}$$

and the permutation group identities summarised in Appendix E, we find

$$\begin{aligned}\langle\Psi|\Psi'\rangle &= \gamma + \frac{e^{-d^2\mathcal{I}^{\mathrm{Q}}_{\mathrm{SPE}}/2}}{2s^2|\mathscr{N}|^2}\sum_{\sigma}\int_{-\infty}^{\infty}\mathrm{d}\boldsymbol{x}\left(\sum_{j=1}^{N}\tilde{\mu}'_j x_j - ds^2\mathcal{I}^{\mathrm{Q}}_{\mathrm{SPE}}\right)g_1^N,\\ &= \gamma - \frac{d\mathcal{I}^{\mathrm{Q}}_{\mathrm{SPE}}}{2} + \frac{e^{-d^2\mathcal{I}^{\mathrm{Q}}_{\mathrm{SPE}}/2}}{2s^2|\mathscr{N}|^2}\sum_{\sigma}\left[\sum_{j=1}^{N}\tilde{\mu}'_j\int_{-\infty}^{\infty}\mathrm{d}\boldsymbol{x}\,x_j\,g_1^N\right],\end{aligned} \tag{4.33}$$

where we define the constant $\gamma = \gamma(d,N) = \partial_d\left[\ln\left(\frac{1}{\mathscr{N}}\right)\right]$. The second line used the definition of the normalisation constant Eq. (4.30). To ease the notation, we denote the last term in Eq. (4.33) as $\mathscr{B}$. Similarly,

$$\begin{aligned}\langle\Psi'|\Psi'\rangle = \gamma\left(\gamma + 2\mathscr{B} - d\mathcal{I}^{\mathrm{Q}}_{\mathrm{SPE}}\right) + \frac{d^2(\mathcal{I}^{\mathrm{Q}}_{\mathrm{SPE}})^2}{4} - \mathscr{B}d\mathcal{I}^{\mathrm{Q}}_{\mathrm{SPE}}\\ + \frac{e^{-d^2\mathcal{I}^{\mathrm{Q}}_{\mathrm{SPE}}/2}}{4s^4|\mathscr{N}|^2}\sum_{\sigma}\left[\sum_{j,k=1}^{N}\tilde{\mu}'_{\sigma(j)}\tilde{\mu}'_k\int_{-\infty}^{\infty}\mathrm{d}\boldsymbol{x}\,x_j x_k\,g_1^N\right].\end{aligned} \tag{4.34}$$

We define $\mathscr{C}$ to be the last term in Eq. (4.34). From Eq. (4.31) we get the following for the QFI

$$\mathfrak{I}^{\mathrm{Q}}_{\mathrm{SPE}} = 4\left(\mathscr{C} - |\mathscr{B}|^2\right). \tag{4.35}$$

Despite this simplicity, the evaluation of the QFI for particular values of d can only be addressed through a numerical approach due to the sum over all permutations associated with the two expressions involved. It has no dependence on γ, which is expected since the normalisation constant trivially has no physical contribution to the information in the system. On the numerical front, the simplicity of Eq. (4.35) provides a two-fold advantage. First, there are fewer terms to evaluate. Second, this term dominates the value of all other terms which contributes the QFI. This domination sees the resulting difference between $\langle\Psi'|\Psi'\rangle$ and $\langle\Psi'|\Psi\rangle$ to be zero. A solution to overcome this would be to increase the working precision of the numerical analysis at the expense of greater computational time. Identifying the cancellation of terms avoids unnecessarily large computation times. We note that the evaluation of the QFI is reduced to that of two terms only: $\mathscr{B}$ and $\mathscr{C}$. However, both terms contain multidimensional integrals over all possible permutations for any given N. The computation time to evaluate this using a brute-force method increases rapidly with N, rendering this unsuitable. We address this by taking a functional approach to the problem. This is possible since both terms $\mathscr{B}$ and $\mathscr{C}$ are comprised of repeat integrals, differing only in the index of the source positions. For convenience, both

terms are written here

$$\mathscr{B} = \frac{e^{-d^2 \mathcal{I}^{\mathrm{Q}}_{\mathrm{SPE}}/2}}{2s^2|\mathscr{N}|^2} \sum_{\sigma} \left(\sum_{j=1}^{N} \tilde{\mu}'_j \int_{-\infty}^{\infty} \mathrm{d}\boldsymbol{x}\, x_j\, g_1^N \right), \tag{4.36}$$

$$\mathscr{C} = \frac{e^{-d^2 \mathcal{I}^{\mathrm{Q}}_{\mathrm{SPE}}/2}}{4s^4|\mathscr{N}|^2} \sum_{\sigma} \left(\sum_{j,k=1}^{N} \tilde{\mu}'_{\sigma(j)} \tilde{\mu}'_k \int_{-\infty}^{\infty} \mathrm{d}\boldsymbol{x}\, x_j x_k\, g_1^N \right). \tag{4.37}$$

Both contain repeating Gaussian integrals of the type $h_n = \int_{-\infty}^{\infty} \mathrm{d}x_j\, x_j^n\, g_j^j$. By analytically solving and defining

$$\begin{aligned} h_0 &= \sqrt{2\pi s^2} \exp\left[\frac{(\tilde{\mu}_j + \tilde{\mu}_{\sigma(j)})^2}{8s^2} \right], \\ h_1 &= \sqrt{\frac{\pi s^2}{2}} \left(\tilde{\mu}_j + \tilde{\mu}_{\sigma(j)} \right) \exp\left[\frac{(\tilde{\mu}_j + \tilde{\mu}_{\sigma(j)})^2}{8s^2} \right], \\ h_2 &= \sqrt{\frac{\pi s^2}{8}} \left[\left(\tilde{\mu}_j + \tilde{\mu}_{\sigma(j)} \right)^2 + 4s^2 \right] \exp\left[\frac{(\tilde{\mu}_j + \tilde{\mu}_{\sigma(j)})^2}{8s^2} \right]. \end{aligned} \tag{4.38}$$

we rewrite the terms $\mathscr{B}$ and $\mathscr{C}$. Simplifying, we find that

$$\mathscr{B} = \frac{\sum_{\sigma} \left\{ \sum_{j=1}^{N} \left[\tilde{\mu}'_j (\tilde{\mu}_j + \tilde{\mu}_{\sigma(j)}) \right] \exp\left[\sum_{k=1}^{N} \frac{\tilde{\mu}_k \tilde{\mu}_{\sigma(k)}}{4s^2} \right] \right\}}{4s^2 \sum_{\sigma} \exp\left[\sum_{l=1}^{N} \frac{\tilde{\mu}_l \tilde{\mu}_{\sigma(l)}}{4s^2} \right]}, \tag{4.39a}$$

$$\mathscr{C} = \frac{\sum_{\sigma} \left(\left\{ \sum_{j=1}^{N} \tilde{\mu}'_j \tilde{\mu}'_{\sigma(j)} \left[(\tilde{\mu}_j + \tilde{\mu}_{\sigma(j)})^2 + 4s^2 \right] + \sum_{\substack{j,k=1, \\ j \neq k}} \tilde{\mu}'_{\sigma(j)} \tilde{\mu}'_k (\tilde{\mu}_j + \tilde{\mu}_{\sigma(j)})(\tilde{\mu}_k + \tilde{\mu}_{\sigma(k)}) \right\} \exp\left[\sum_{l=1}^{N} \frac{\tilde{\mu}_l \tilde{\mu}_{\sigma(l)}}{4s^2} \right] \right)}{16s^4 \sum_{\sigma} \exp\left[\sum_{l=1}^{N} \frac{\tilde{\mu}_l \tilde{\mu}_{\sigma(l)}}{4s^2} \right]}. \tag{4.39b}$$

The same result is reached if the calculation was repeated using instead the variance of the generator. We find that the QFI from Eq. (4.35) depends only on the properties of the source positions. This is a property of the QFI which depends only on the state. Since it contains a sum over all possible permutations of source overlaps, a reduced analytic form is not possible and a numerical approach is taken. The simulation results are illustrated in figure 4.3 and indeed show a dependence with d. As expected, for small separation distances the estimation precision increases with increasing d. For larger source separations where neighbouring sources are spatially distinct, the QFI converges to the value governed by Eq. (4.26). This mutual independence was assumed to hold for $d \gg s$. However, we observe from figure 4.3 that this regime is in fact satisfied when $d \geq 2s$ for all N for a unit (untransformed) stretching factor. Between these two regimes, a small bump is observed between $d \sim (0.2 - 1.5)s$. This nearest-neighbour effect persists for arbitrarily large number of sources N on the array. The observed protuberance in figure 4.3 appears to suggest that light sources with a higher average mode occupancy may be preferential for the estimation of d. To test this, we will next determine the precision scalings achievable with an array of coherent and thermal states. If this proposition is found to be true, the use of coherent and thermal states over single photon emitters in this context would give a better estimate of d. In what follows, we shall assume each source to be mutually independent.

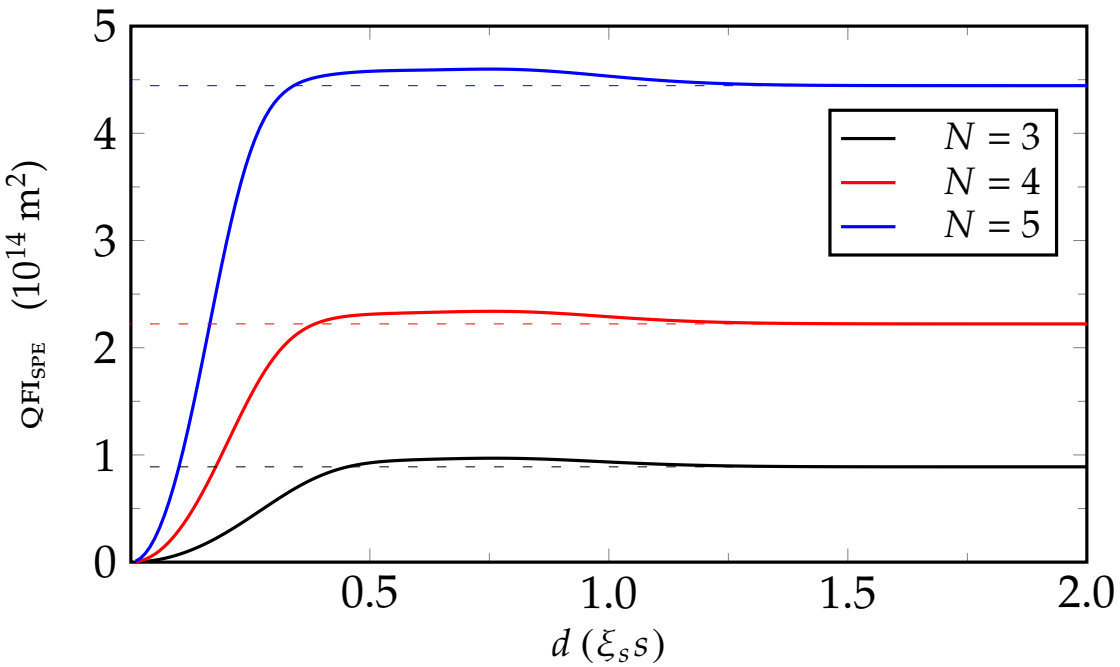

Figure 4.3: *The QFI with varying d in units of s, where $s = 300$ nm—typical of photons from quantum dots—and $\xi_s = 2$. Photon bunching is allowed and we note that the QFI approaches the value determined by Eq. (4.26) for $d \sim 2\xi_s s$. The observed bump preceding the limit of clear separation is a consequence of photon interference arising due to all the permutations of achieving the same detection.*

4.2.3 Coherent sources

The semi-classical single-mode coherent state is defined as

$$|\alpha_j\rangle = \exp\left[\frac{-|\alpha_j|^2}{2}\right] \sum_n \frac{\alpha_j^n \hat{b}_j^{\dagger n}}{n!} |0\rangle, \tag{4.40}$$

where $\alpha_j = r_j \exp[i\varphi_j]$ is the amplitude associated with the source mode $j \in S_N$ and $b_j^\dagger$ is the creation operator for that mode. To encode the source separation distance d into Eq. (4.40), we use the same mode creation operator $\hat{b}_j = \int dx_j f(x_j, \mu_j) \hat{a}_j^\dagger(x)$ as defined for the single photon emitters, where the function $f(x_j, \mu_j)$ defines the spatial Gaussian profile. Assuming negligible overlap between different sources, the N–mode coherent state, $|\Psi\rangle_\mathrm{c} = \otimes_{j=1}^N |\alpha_j\rangle$, is written

$$\begin{aligned} |\Psi\rangle_\mathrm{c} &= \exp\left[-\frac{N|\alpha|^2}{2}\right] \frac{1}{\mathscr{N}_\mathrm{c}} \sum_{n_1=0}^{\infty} \cdots \sum_{n_N=0}^{\infty} \left[\prod_{j=1}^{N} \frac{\left(r \exp[i\varphi_j] \int \mathrm{d}x_j\ f(x_j)\ \hat{a}_j^\dagger(x_j)\right)^{n_j}}{n_j!}\right] |\mathbf{0}\rangle, \\ &= \exp\left[-\frac{N|\alpha|^2}{2}\right] \frac{1}{\mathscr{N}_\mathrm{c}} \sum_{\{\boldsymbol{n}\}\geq 0} \mathscr{A}(\boldsymbol{n}) \int \mathrm{d}\boldsymbol{x}^{\boldsymbol{n}}\ f(\boldsymbol{x})^{\boldsymbol{n}}\ \hat{a}^{\dagger \boldsymbol{n}}(\boldsymbol{x})\ |\mathbf{0}\rangle, \end{aligned} \tag{4.41}$$

where $\boldsymbol{n}! = n_1! n_2! \cdots n_N!$, $\boldsymbol{\alpha}(\boldsymbol{x})^{\boldsymbol{n}} = \prod_{j=1}^N \alpha_j(x_j)^{n_j}$, $\hat{a}^{\dagger \boldsymbol{n}}(\boldsymbol{x}) = \prod_{j=1}^N \hat{a}_j^{\dagger n_j}(x_j)$, $\mathscr{N}_\mathrm{c} = {}_\mathrm{c}\langle\Psi|\Psi\rangle_\mathrm{c}$ is the normalisation constant and $\mathscr{A}(\boldsymbol{n}) = \prod_{j=1}^N r^{n_j} \exp[i\varphi_j n_j]/n_j!$. Applying a stretching with factor

ξ_s, we can calculate the QFI of the new state from the variance of the generator yielding

$$\mathcal{I}^{\mathrm{Q}}_{\mathrm{Coherent}} = \frac{\xi_s^2 \exp[-Nr^2]}{s^2} \sum_{\{\boldsymbol{n}\}\geq 0} \prod_{j=1}^{N} \left(\frac{r^{2n_j}}{n_j!}\right) \sum_{k=1}^{N} \mu_k'^2 n_k^2. \tag{4.42}$$

We immediately observe that the QFI is independent of the phase φ_j of the coherent states. Although the QFI is a function of the state alone, this independence may be understood by considering the phase difference of any two sources, $\Delta\varphi$, at any region of space along the near-field plane. A change to the phase difference $\Delta\varphi \mapsto \Delta\varphi + \varphi_0$ only occurs if any one of the two sources contributing the phase difference shifts along the array. However, since

$$\frac{\partial}{\partial x}(\Delta\varphi + \varphi_0) = \frac{\partial \Delta\varphi}{\partial x}, \tag{4.43}$$

any changes to the phase of each source do not contribute to the overall QFI. Any information change is encoded in the separation distance.

A meaningful comparison with the SPES requires a unit average photon number in the N-coherent state, such that $\langle \hat{n} \rangle = |\alpha|^2 = r^2 = 1$. For the limiting value $n_j \to \infty \;\forall\; j \in S_N$, Eq. (4.42) takes a similar form to $\mathcal{I}^{\mathrm{Q}}_{\mathrm{SPE}}$ as follows

$$\mathcal{I}^{\mathrm{Q}}_{\mathrm{Coherent}} = \frac{\xi_s^2 N(N^2-1)}{6s^2}. \tag{4.44}$$

We note that the scaling with resources is similar to that of the SPES, and the constant factor of 2 improvement results from the increased mode occupancy of the coherent states.

4.2.4 Thermal sources

Another class of widely occurring states in nature are the thermal states. In this section, we replace the array of single photon sources for the classical thermal states. This would address a comparative performance on the estimation on the source separation distance d. A thermal state emits at all frequencies with an intensity determined by the Planck distribution. This distribution can be considered an infinite number of independent spectral modes [Barnett and Radmore, 2005; Walls and Milburn, 2008]. The N-mode blackbody distribution is defined by

$$\rho_{\mathrm{Bb}} = \bigotimes_{j=1}^{N} \rho^{j}_{\mathrm{Th}} = \sum_{\{\boldsymbol{n}\}\geq 0} \frac{c_{\boldsymbol{n}}}{\boldsymbol{n!}} \hat{b}_{\boldsymbol{k}}^{\dagger \boldsymbol{n}} |\mathbf{0}\rangle\langle\mathbf{0}| \hat{b}_{\boldsymbol{k}}^{\boldsymbol{n}}, \tag{4.45}$$

where the total spectral mode creation operator

$$\hat{b}_{\boldsymbol{k}}^{\dagger \boldsymbol{n}} = \bigotimes_{j=1}^{N} \hat{b}_{k_j}^{\dagger n_j} \tag{4.46}$$

is composed from the tensor product over the jth source mode operator and $\boldsymbol{n!} = \prod_{j=1}^{N} n_j!$. The photon-counting distribution or occupancy number $c_{\boldsymbol{n}}$ is determined from the Bose-Einstein probability distribution and has the form

$$c_{\boldsymbol{n}} = \prod_{j=1}^{N} \frac{\overline{n}_j^{n_j}}{(1+\overline{n}_j)^{1+n_j}}, \tag{4.47}$$

where

$$\overline{n}_j = \left\langle \hat{n}_j \right\rangle = \mathrm{Tr}\left[\rho_{\mathrm{Bb}} \hat{n}_j\right] \tag{4.48}$$

is the mean photon number for the jth source. The creation operator $\hat{b}_j^\dagger$ defines the same inherent Gaussian uncertainty in the position basis as that used for the coherent states. Since the blackbody distribution is defined in the Fourier space, we are required to use the Fourier transform of the field operator in Eq. (4.19) for a single mode. This yields

$$\hat{b}_j^\dagger = \left(\frac{2s^2}{\pi}\right)^{1/4} \int \mathrm{d}k_j \; \hat{a}_j^\dagger(k_j) \exp\left[k_j(-k_j s^2 + i\mu_j)\right], \tag{4.49}$$

which upon substitution into Eq. (4.45) yields the final form of the array of thermal states ρ_{Bb}. It describes thermal states produced at positions μ_j, each with an average number of photons $\overline{n}_j$. It runs along the continuous variable k, in contrast to Eq. (4.45), which describes a discrete combination over the different Hilbert spaces associated with each source.

The QFI for multimode states becomes additive such that for the blackbody state in Eq. (4.45) we can write

$$\mathcal{I}^{\mathrm{Q}}_{\mathrm{Bb}} = \sum_{j=1}^{N} \left[\mathcal{I}^{\mathrm{Q}}_{\mathrm{Th}}\right]_j, \tag{4.50}$$

where the sum is over the thermal modes. Since the thermal states are mixed states, the variance of the generator provides only an upper bound to the QFI. Hence, using the full form of the QFI in Eq. (3.53) for an arbitrary thermal state we have

$$\mathcal{I}^{\mathrm{Q}}_{\mathrm{Th}} = 4 \sum_{k=0}^{\infty} p_k \left(\Delta \hat{\mathcal{G}}^2\right)_k - \sum_{\substack{k,l=0,\\ k\neq l}}^{\infty} \frac{8 p_k p_l}{p_k + p_l} \left|\left\langle \varrho_k \left| \hat{\mathcal{G}} \right| \varrho_l \right\rangle\right|^2, \tag{4.51}$$

where the probabilities and eigenstates of the jth-mode thermal state ρ^j_{Th} are given by

$$p_k = \frac{c_{n_k}}{n_k!}, \qquad |\varrho_k\rangle_j = \hat{b}_j^{\dagger n_k} |0\rangle_j . \tag{4.52}$$

As expected, we find that the expectation of the generator is zero since a stretching of the array does not produce a net shift of the sources about the origin O. We then find

$$\begin{aligned} \mathcal{I}^{\mathrm{Q}}_{\mathrm{Bb}} &= \frac{\xi_s^2}{s^2} \sum_{j=1}^{N} \mu_j'^2 \sum_{n_j=0}^{\infty} \frac{n_j^2 \overline{n}_j^{n_j}}{(1+\overline{n}_j)^{1+n_j}}, \\ &= \frac{\xi_s^2}{s^2} \sum_{j=1}^{N} \mu_j'^2 \overline{n}_j (1 + 2\overline{n}_j), \end{aligned} \tag{4.53}$$

where the second equality made use of the infinite summation identity $\sum_k k^2 a^k = a(1+a)/(1-a)^3$, since $|\overline{n}_j/1+\overline{n}_j| < 1$. For a meaningful comparison with single photon emitters we take a unit average photon number, requiring $\langle \hat{n}_j \rangle = \overline{n}_j = 1$. This gives

$$\mathcal{I}^{\mathrm{Q}}_{\mathrm{Bb}} = \frac{\xi_s^2 N(N^2-1)}{4s^2}. \tag{4.54}$$

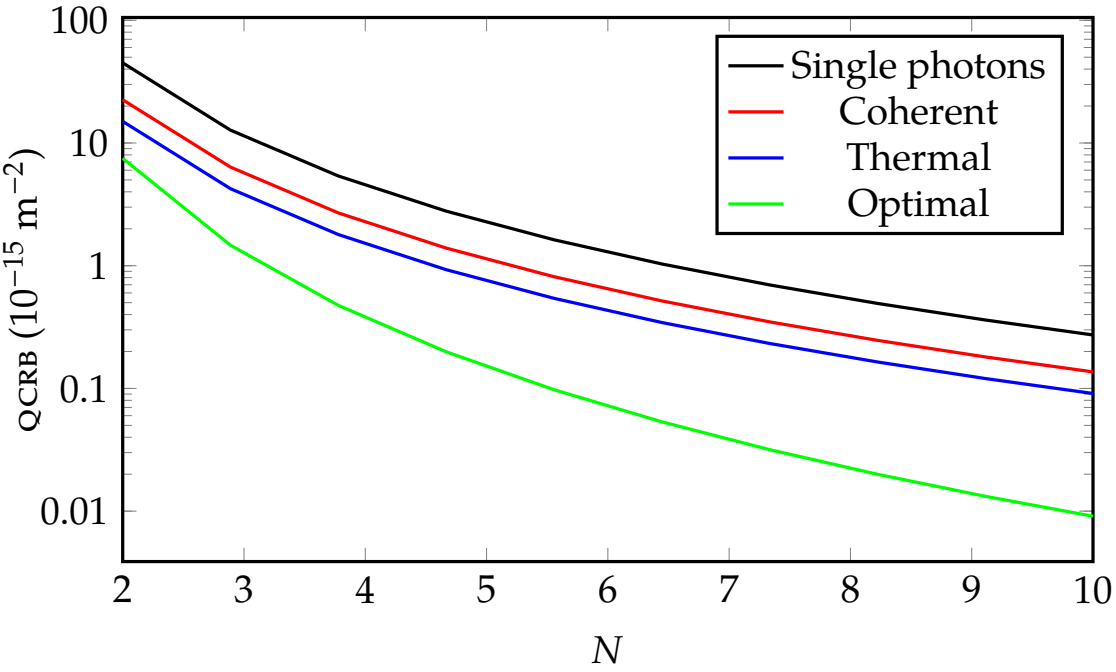

Figure 4.4: *QCRB scaling with N for single photon emitters, coherent, thermal states, and the optimally entangled state Eq.* (4.59) *with* $s = 300$ *nm and* $\xi_s = 2$. *The higher mode occupancy of thermal states permits better estimation performance when compared with the quantum single photon emitters. However, the optimal state remains the entangled state constructed from the eigenvectors corresponding to the minimum and maximum eigenvalues of the generator* $\hat{\mathcal{G}}$.

Figure 4.4 illustrates this scaling with the number of thermal sources N along the array. Earlier studies have shown that with data post processing, higher-order correlations of independent sources yield more information than thermal light sources [Oppel et al., 2012]. Here, we find that thermal states provide a better estimate of the source separation distance for a single-shot experiment ($\nu = 1$) in the absence of any post-processing techniques.

The relative performance of the different states as illustrated in figure 4.4, holds if we consider arbitrary photon number emissions by each source. This is straight forward to see for the single photon emitters and the thermal state. In subsection 4.2.3 we derived the QFI for a coherent state with a photon number distribution collapsed to have unit average photon emission. We lift this limitation by considering an arbitrary number r^2 of photons emitted by each coherent source along the array. In Eq. (4.42) we had

$$\mathcal{I}^{\mathrm{Q}}_{\mathrm{Coherent}}(\hat{n}) = \frac{\xi_s^2 \exp[-Nr^2]}{s^2} \sum_{\{\boldsymbol{n}\}\geq 0} \prod_{j=1}^{N} \left(\frac{r^{2n_j}}{n_j!}\right) \sum_{k=1}^{N} \mu_k'^2 n_k^2. \tag{4.55}$$

where $r^2 = \langle \hat{n} \rangle$ is the average number of photons emitted by each source. This is numerically difficult to compute due to the infinite summation, but we can analytically obtain an expression.

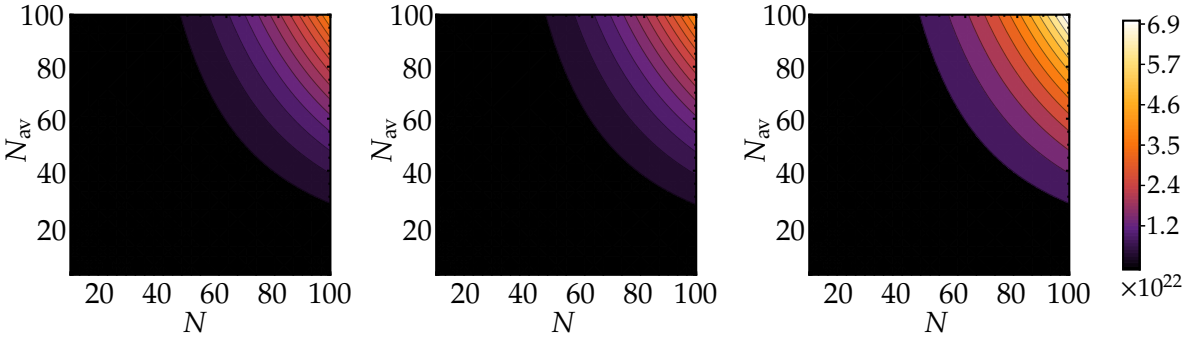

(a) *Single photon emitters.* (b) *Coherent states.* (c) *Thermal states.*

Figure 4.5: *Contour plot of the QFI for N N_{av}-Fock states, coherent states and thermal states. Here we allow the average photon emitted by each source to vary. Note that the thermal states still perform best.*

Defining the summation as

$$S(\langle\hat{n}\rangle) = \sum_{n_1,n_2,\ldots,n_S=0}^{\infty}\left[\left(\prod_{j=1}^{N}\frac{\langle\hat{n}\rangle^{n_j}}{n_j!}\right)\sum_{k=1}^{N}\mu_k'^2 n_k^2\right], \tag{4.56}$$

then we can re-write $S(\langle\hat{n}\rangle)$

$$\begin{aligned}
S(\langle\hat{n}\rangle) &= \sum_{j=1}^{N}\left[\sum_{n_j=0}^{\infty}\left(\frac{\langle\hat{n}\rangle^{n_j}}{n_j!}\mu_j'^2 n_j^2\right)\prod_{\substack{k=0,\\k\neq j}}^{N}\sum_{n_k=0}^{\infty}\frac{\langle\hat{n}\rangle^{n_k}}{n_k!}\right],\\
&= \sum_{j=1}^{N}\left[\sum_{n_j=0}^{\infty}\left(\frac{\langle\hat{n}\rangle^{n_j}}{n_j!}\mu_j'^2 n_j^2\right)\prod_{\substack{k=0,\\k\neq j}}^{N}\exp\left[\langle\hat{n}\rangle\right]\right],\\
&= \exp\left[(N-1)\langle\hat{n}\rangle\right]\sum_{j=1}^{N}\mu_j'^2\sum_{n_j=0}^{\infty}\frac{\langle\hat{n}\rangle^{n_j}}{n_j!}n_j^2,\\
&= \exp\left[(N-1)\langle\hat{n}\rangle\right]\sum_{j=1}^{N}\mu_j'^2\left(\langle\hat{n}\rangle+\langle\hat{n}\rangle^2\right)\exp\left[\langle\hat{n}\rangle\right],
\end{aligned} \tag{4.57}$$

where we used the identity $\sum_j^\infty j^2\alpha^j/j! = (\alpha+\alpha^2)\exp[\alpha]$, which is in fact the *second moment of the Poisson distribution* of the coherent states. Using the definition of the source expected positions and combining with Eq. (4.55), then we have a general form of the QFI for coherent states

$$\mathcal{I}^{\mathrm{Q}}_{\mathrm{Coherent}}(\hat{n}) = \frac{\xi_s^2(\langle\hat{n}\rangle+\langle\hat{n}\rangle^2)N(N^2-1)}{12s^2}. \tag{4.58}$$

The relative comparison with arbitrary photon expectations is illustrated in figure 4.5.

4.2.5 Entangled states of single photon emitters and the optimal state

In this section we consider how entanglement can be used as a resource to improve the estimation precision for detection of spatial deformations. Since the QFI is a property of the quantum state alone and does not depend on a particular measurement scheme, the estimation precision is limited only by the uncertainty in the state. The optimal state defines the statistical properties of the probe state which saturates the QCRB. However, it does not address the optimal measurement strategy that should be employed to achieve this bound. We defer a discussion of this to the next section.

Giovannetti *et al.* showed the optimal state to be that which entangles the states corresponding to the maximum and minimum eigenvectors of the generator $\hat{\mathcal{G}}$ [Giovannetti et al., 2011]. Specifically, we consider

$$|\Psi\rangle_{\text{Opt}} = \frac{|\psi\rangle_{\max} + |\psi\rangle_{\min}}{\sqrt{2}}, \tag{4.59}$$

where $|\psi\rangle_{\max}$ is the state corresponding to the maximum eigenvalue of the generator such that $\hat{\mathcal{G}}\,|\psi\rangle_{\max} = g_{\max}\,|\psi\rangle_{\max}$ and similarly for the state $|\psi\rangle_{\min}$. Then, from the variance of the generator we have

$$\mathcal{I}^{\text{Q}}_{\text{Opt}} = 4\Delta\hat{\mathcal{G}}^2 = (g_{\max} - g_{\min})^2\,. \tag{4.60}$$

From the matrix elements of the generator in the momentum Fock-basis

$$\langle n_\alpha(k_\alpha)|\hat{\mathcal{G}}|n_\beta(k_\beta)\rangle = \xi_s \mu'_\beta k_\alpha n_\beta(k_\beta)\delta_{\alpha\beta}, \tag{4.61}$$

where $\alpha, \beta \in S_N$, we see that the generator is diagonal with eigenvalues given when $\alpha = \beta$. Given the definition of the source positions in Eq. (4.3), the maximum eigenvalue corresponds to $\alpha = N$ and the minimum to $\alpha = 1$ when $n_1(k_1) = n_N(k_N) = N$. This finding could have been consistently anticipated from the results obtained in the preceding sections. For the same resource count, all of the calculations for the QFI for the different sources considered contained the term $\sum_j \mu'^2_j$. Hence the optimal state—that which maximises the QFI—would have all N-photons emitting from the most extremal positions about the array centre O. From this, we construct the optimally entangled state in Eq. (4.59) by identifying

$$\begin{aligned} |\psi\rangle_{\max} &= \int \mathrm{d}x^N f(x,\mu_N)^N \frac{\hat{a}^\dagger_N(x)^N}{\sqrt{N!}}\,|\mathbf{0}\rangle \\ |\psi\rangle_{\min} &= \int \mathrm{d}x^N f(x,\mu_1)^N \frac{\hat{a}^\dagger_1(x)^N}{\sqrt{N!}}\,|\mathbf{0}\rangle \end{aligned} \tag{4.62}$$

Then from the variance of the generator we obtain

$$\mathcal{I}^{\text{Q}}_{\text{Opt}} = \frac{\xi_s^2 N^2 (N-1)^2}{4s^2}. \tag{4.63}$$

The scaling of the QCRB with N has been illustrated in figure 4.4. As expected, it outperforms the SPES, coherent and thermal states. We note that not all entangled states reproduce a better

performance than the classical states. To demonstrate this, consider the following simple entangled state of SPEs:

$$|\psi(d)\rangle = \sqrt{p}\,|\psi(d)\rangle_{\text{odd}} + \sqrt{1-p}\,|\psi(d)\rangle_{\text{even}}\,, \tag{4.64}$$

which emits single photons from either the odd sources along the array, $|\psi(d)\rangle_{\text{odd}}$, or the even sources, $|\psi(d)\rangle_{\text{even}}$. From the variance of the generator we obtain

$$\mathcal{I}^{\text{Q}}_{\text{E-SPE}} = \frac{\xi_s^2}{s^2}\left[p\sum_{\substack{j=1,\\ j=\text{odd}}}^{N}\mu_j'^2 + (1-p)\sum_{\substack{j=2,\\ j=\text{even}}}^{N}\mu_j'^2\right]. \tag{4.65}$$

Figure 4.6 illustrates the scaling of the QFI with N for different values of p. For $p = 0$ ($p = 1$), it is preferred to have an odd (even) number of sources to maximise the QFI. The difference observed for varying p becomes negligible for large N. A precision enhancement with entangled states is better achieved if the state is prepared such that the N-photons are distributed with maximal distance.Specifically, we note that for a maximally entangled state $p = 1/2$, Eq. (4.65) reduces to

$$\mathcal{I}^{\text{Q}}_{\text{E-SPE}} = \frac{1}{2}\mathcal{I}^{\text{Q}}_{\text{SPE}}. \tag{4.66}$$

Hence, entanglement as a resource does not necessarily always provide precision enhancements. This is reminiscent of separate studies in both optical imaging and quantum computing where entanglement was necessary but insufficient in providing performance enhancements [Gottesman, 1997; Tsang, 2008]. While the entangled state introduced by Giovannetti *et al.* remains optimal, it is constructive to acknowledge the increasing number of researchers who consider entanglement unnecessary to achieve resolutions beyond the diffraction limit [Tilma et al., 2010; Braun et al., 2018].

4.3 Optimal estimator

An optimal estimator is one that saturates the QCRB in the asymptotic limit of large samples. From chapter 3 we saw that it corresponds to a minimisation of the covariance of the estimator. We first consider intensity measurements. If found to be optimal, we expect the classical Fisher information (CFI) for photon number counting to become identical to its corresponding QFI.

We start by finding the CFI for the stretched array of N independent SPEs with $\eta = 1$. The detector is placed in the near field and is discretised into M pixels, which covers the entire spatial extent of the array. For some state $\rho(d)$ incident on the detector, the measurement is generally described by a positive operator-valued measure POVM. Intensity measurements of the state are most common in imaging and can often be described by operators which are diagonal in the Fock basis. Hence we write the probability distribution of number counting at each pixel as

$$\begin{aligned} p(n_1,\ldots,n_M) &= \text{Tr}\left[\rho(d)\,|n_1\rangle\langle n_1|\otimes\cdots\otimes|n_M\rangle\langle n_M|\right], \\ &= \text{Tr}\left[\rho(d)\,|\vec{n}\rangle\langle\vec{n}|\right], \\ &= |\langle\vec{n}|\psi(d)\rangle|^2\,, \end{aligned} \tag{4.67}$$

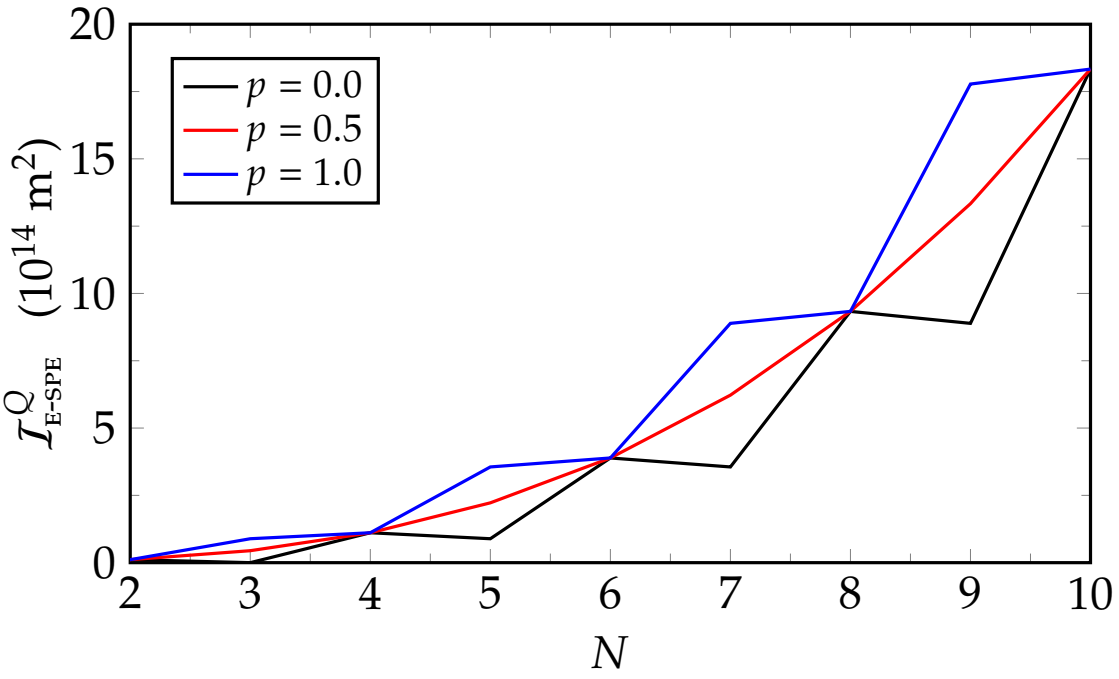

Figure 4.6: *Scaling of the QFI with N for the entangled single photon emitter state (4.64) for different p and s = 300 nm. This demonstrates that entanglement does not generally provide enhancements to parameter estimates.*

where we use the notation $\vec{n}$ to define vectors spanning the Hilbert space of the detector. We note that the form of the probability distribution in Eq. (4.67) is motivated by photon counting and the separable form of the single photon emitter state. Since we assume the sources to be well separated, then in the near field it is unlikely that more than one photon is detected at the same pixel. This truncates the Fock basis of each of the sources to values in the set $n_k \in \{0, 1\}$ for all $k \in S_M$. Hence we find that

$$p(\vec{n}|d) = \prod_{j=1}^{N} \left| f(x_j, \tilde{\mu}_j) \right|^2, \tag{4.68}$$

where $f(x_j, \tilde{\mu}_j)$ defines a normalised Gaussian centred on $\tilde{\mu}_j$ and standard deviation s. We then obtain

$$\mathcal{I}^C_{\text{SPE}} = \int \mathrm{d}\boldsymbol{x} \frac{1}{p(\vec{n}|d)} \left(\frac{\partial p(\vec{n}|d)}{\partial d} \right)^2 = \frac{\xi_s^2 N(N^2-1)}{12 s^2} \tag{4.69}$$

for the near-field CFI. We find that the CFI is equal to the QFI, since the probability distribution in Eq. (4.68) is the same as that describing the state $\rho(d)$ of the array of SPEs. This equivalence implies that photon-number counting in the near field is the optimal measurement strategy which saturates the QCRB. To examine this statement further, we recall that the optimal observable is given by the eigenbasis of the SLD for single-parameter estimations. Since for pure states $\rho(d) = \rho(d)^2$, then from the implicit definition of the SLD, we have [Fujiwara and Nagaoka,

1995]

$$\hat{\mathscr{L}}(d) = 2\partial_d \rho(d). \tag{4.70}$$

The optimal estimator then becomes

$$\hat{O}(d) = d1 + \frac{12}{\xi_s^2 N(N^2-1)} \sum_{j=1}^{N} \mu_j' \int_{-\infty}^{\infty} \mathrm{d}\boldsymbol{x}\, \mathrm{d}\boldsymbol{x}' f(\boldsymbol{x}) f(\boldsymbol{x}') \left(x_j + x_j' - 2\mu_j\right) \hat{a}^\dagger(\boldsymbol{x}) \left|\boldsymbol{0}\right\rangle \left\langle \boldsymbol{0}\right| \hat{a}(\boldsymbol{x}'). \tag{4.71}$$

To check the optimality of the estimator, we confirm that its variance reproduces the inverse of the QFI for a single-shot experiment $\nu = 1$. For shorthand, we redefine Eq. (4.71) as $\hat{O}(d) = d1 + \hat{Q}$, where the first term ensures that the estimator is unbiased since $\mathrm{Tr}[\hat{O}(d)\rho(d)] = d$. From

$$\hat{O}(d)^2 = d(\check{O}(d) + \hat{Q}) + \hat{Q}^2 \tag{4.72}$$

and since the expectation of the SLD is zero, we have

$$\langle \hat{O}(d)^2 \rangle = d^2 + \left\langle \hat{Q}^2 \right\rangle. \tag{4.73}$$

From this we find the characteristic condition for any optimal estimator: $\Delta\hat{O}(d)^2 = 1/\mathcal{I}^{\mathrm{Q}}_{\mathrm{SPE}}$. We also observe that the SLD is a function of the source distribution and describes interference effects between different sources along the array. Surprisingly, the form of the estimator in Eq. (4.71) has off-diagonal elements in the number basis, which suggests that intensity measurements along the near field are not the only optimal strategy. The existence of a second optimal estimator that is not photon number counting motivates an open question into the uniqueness of optimal measurements. A possible cause for this may be the degeneracy of the eigenstates of the generator.

4.4 Discussion and summary

In this chapter, we applied the theory of quantum estimation to an array of identical, stationary and equidistant emitters each with an intrinsic spatial Gaussian uncertainty profile. The quantum Fisher information (QFI) has been used as the figure of merit for the estimation of the source separation distance d in the near field. We compare the estimation performance of different classical and quantum light sources. In order to efficiently report this comparison, we derive the generator $\hat{\mathcal{G}}$ responsible for changes in d due to a general spatially homogeneous deformation ξ applied to the array. These deformations change the expected mean positions of the sources, leaving the source variances invariant. Each source was assumed to be mutually independent and was treated in its individual Hilbert space.

First, to quantify when the mutual independency of sources is valid and observe the dependence of the QFI on d, we allow for source overlaps. Calculating the QFI for an array of SPEs, we found that a numerical approach is necessary to find the QFI. The QFI was observed to initially increase with d until $d \sim \xi_s s/4$ after which it settles to the value consistent with those determined for $d \gg s$. In between these two regimes, we find that the QFI peaks slightly above that predicted when $d > 2s$. This is a nearest-neighbour effect and remains for arbitrary

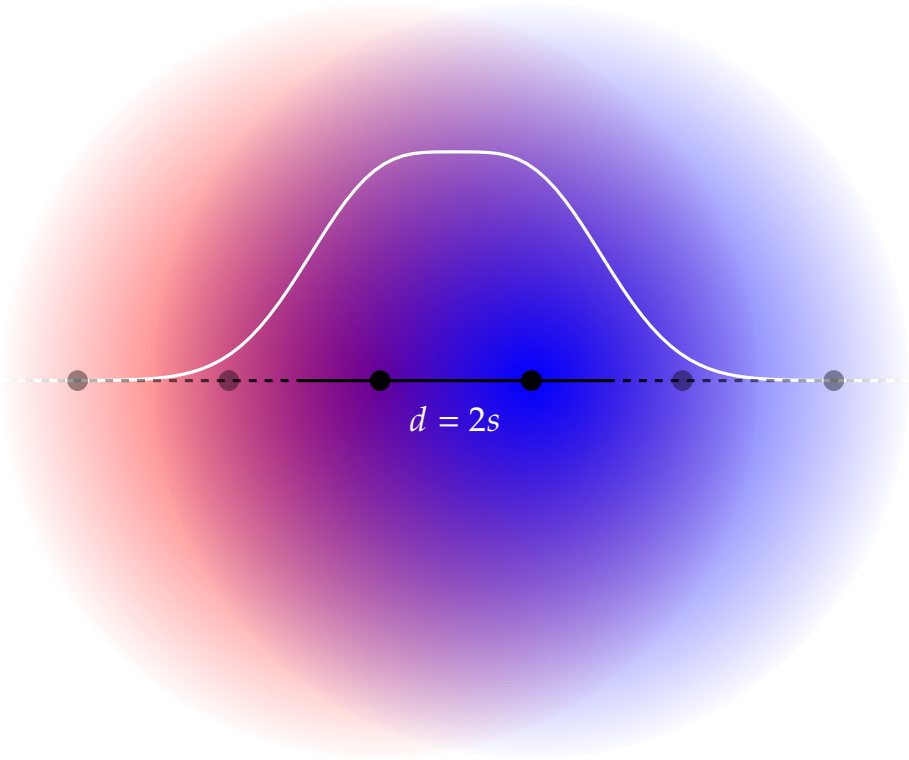

Figure 4.7: *Illustration of separation distance required for mutually independent sources. The white distribution is the joint spatial probability distribution.*

N. Figure 4.7 illustrates the total spatial distribution from two neighbouring sources that are considered well-separated by a distance $d = 2s$. These results gave an indication that a source with higher average mode occupancy is favoured in this context for the estimation of d. With this insight, we explored the estimation performance of different classical and quantum states with the assumption of mutual independency.

We considered arrays of single photon emitters as well as coherent, thermal, and entangled light sources and conveniently summarise the following results:

$$\mathcal{I}^{\mathrm{Q}}_{\mathrm{Bb}} = \frac{\xi_s^2 N(N^2-1)}{4s^2} = \frac{3}{2}\mathcal{I}^{\mathrm{Q}}_{\mathrm{Coh}} = 3\mathcal{I}^{\mathrm{Q}}_{\mathrm{SPE}} = 6\mathcal{I}^{\mathrm{Q}}_{\mathrm{E\text{-}SPE}}. \tag{4.74}$$

The photon number distributions for the blackbody and coherent states were set to one for fair comparison with the single photon emitters. Interestingly, we find that higher mode occupancies of the classical sources provide better estimates of d than single photon emitters. This is contrary to what may have been expected from earlier work, where higher-order correlations of single photon sources yield more information than thermal light sources. However, unlike this previous work, no post selection of data was used here. The scalings determined here are based on the maximal information content in the state. We demonstrated that the relative performance of different states, summarised in Eq. (4.74), holds if we consider arbitrary photon number emissions by each source.

The preference of classical sources in this context was found to be misleading. By using the entanglement resource between the sources carefully, we find that it provides a precision

enhancement. By constructing the optimal state which entangles the eigenstates corresponding to the maximum and minimum eigenvectors of the generator $\hat{\mathcal{G}}$, we found

$$\mathcal{I}^{\mathrm{Q}}_{\mathrm{Opt}} = \frac{\xi_s^2 N^2 (N-1)^2}{4s^2}. \tag{4.75}$$

Physically the optimal state is found to be an extension of the NOON state. It is a superposition of all N photons emitted from the most extremal positions about the array centre O.

To address the optimal measurement scheme that saturates the QCRB, we first considered calculating the classical Fisher information for intensity measurements. Since we found it is equivalent to the QFI, photon number counting is found to be optimal. From the eigenbasis of the symmetric logarithmic derivative, we find the existence of a second optimal estimator, which is not photon counting. To support our claim of its optimality, we confirm that it is unbiased and bounded by the quantum Fisher information. The existence of multiple optimal estimators motivates an open question into the uniqueness of optimal measurements.

The work in this chapter permits the precise evaluation of deformed coordinates of the quantum emitters and allows for corrective measures to negate their effects. This would find applications in evaluating stresses and strains and fracture prevention in materials expressing great sensitivities to deformations, and in selecting a particular quantum source distinguished by its frequency from an array of references or differing sources. Further research will consider the effect of incomplete detection of the state on the estimation precision, treatment of source efficiencies, temporal jitters, non homogeneous deformations in higher dimensions, and far-field detection.

Chapter 5

Multi-parameter estimations with arbitrary Hamiltonians

In this chapter we present a framework for the detection and estimation of deformations applied to a grid of sources. Quantum metrology for grid deformations provides an ideal testbed to examine multi-parameter estimations for arbitrarily parameterised channel evolutions with generally non-commuting Hermitian generators. We generalise the local generator of translations for deformation parameters to multi-parameter estimations and use it to explore how well different deformations can be detected and corrected for. This approach holds for any deformation. We explore the application of our theory to the set of affine geometry maps. Both the configuration of the grid and the properties of the sources help to maximise the sensitivity of the QFIM to changes in the deformation parameters. For the non-multiplicative Hamiltonian parameterisations resulting from grid rotations about any chosen axis, the QFI can be made independent of the rotation angle, ϑ, for specific source properties and grid configurations. The quantum Cramér-Rao bound is then attainable without the use of adaptive strategies.

5.1 Generator formalism for quantum metrology

In this section we review the generator formalism of the QCRB. We find that the QFIM and hence the QCRB depends on only the initial probe states through the generator of translations in the parameters $\boldsymbol{\varphi}$. A natural question that arises concerns the form of the generator. Hamiltonians which are parameterised by simple multiplicative factors have received much of the attention in this field [Braunstein and Caves, 1994; Kolenderski and Demkowicz-Dobrzański, 2008; Holevo, 2011; Vaneph et al., 2013]. In this case, the generator of translations are parameter independent and are just the Hamiltonian. In this work, we consider more general forms of parameter-dependent generators due to its wider applicability in quantum parameter estimations. This arises when the parameters appear as different orders in the eigenvalues and/or eigenvectors decomposition of the Hamiltonian. This scenario is less developed, with a few authors considering general parameterisations of Hamiltonians. With this motivation, in subsection 5.1.1 we generalise the approach developed by Pang and Brun [Pang and Brun, 2014], and Wilcox [Wilcox, 1967] to derive the form of the generator for arbitrary Hamiltonian pa-

rameterisations for multi-parameter estimations. Once the form of the generator is established, we are able to determine the multi-parameter QFIM. How this is achieved is summarised in subsection 5.1.4.

5.1.1 Multiparameter generators for arbitrary parameterisations

Consider evolving a quantum state $\rho(\mathbf{0})$ by some system Hamiltonian, $\hat{\mathcal{H}}(\boldsymbol{\varphi})$. For the archetypal quantum estimation channel, the input probe state evolves according to

$$\Lambda[\rho(\mathbf{0})] = \hat{U}(\boldsymbol{\varphi})\rho(\mathbf{0})\hat{U}^{\dagger}(\boldsymbol{\varphi}) \tag{5.1}$$

with

$$\hat{U}(\boldsymbol{\varphi}) = \exp\left[-i\hat{\mathcal{H}}(\boldsymbol{\varphi})\right] \approx \exp\left[-i\hat{\boldsymbol{G}}\delta\boldsymbol{\varphi}^{\top} + O(\boldsymbol{\varphi}^2)\right], \tag{5.2}$$

where we assume that we can linearise the unitary in $\boldsymbol{\varphi}$[1]. Our objective is to find the form of the generator $\hat{\boldsymbol{G}}$ such that the unitary can be written approximately in the form shown in Eq. (5.2). The initial probe state is chosen so as to maximise its sensitivity to changes in $\boldsymbol{\varphi}$. Under infinitesimal changes to the parameterisation, this sensitivity may be characterised by the following Taylor expansion to second order of the evolving unitary

$$\hat{U}(\boldsymbol{\varphi}+\delta\boldsymbol{\varphi}) \approx \hat{U}(\boldsymbol{\varphi}) + \nabla_{\boldsymbol{\varphi}}\hat{U}(\boldsymbol{\varphi})\delta\boldsymbol{\varphi}^{\top} + \frac{1}{2}\delta\boldsymbol{\varphi}\boldsymbol{H}\delta\boldsymbol{\varphi}^{\top}, \tag{5.3}$$

where the parameter derivative vector, $\boldsymbol{\nabla}_{\boldsymbol{\varphi}}$, and Hessian matrix, $\boldsymbol{H}$, have the elements

$$\begin{aligned}\left[\nabla_{\boldsymbol{\varphi}}\hat{U}(\boldsymbol{\varphi})\right]_j &= \partial_j\hat{U},\\ \left[\boldsymbol{H}(\boldsymbol{\varphi})\right]_{jk} &= \partial_j\left[\nabla\hat{U}(\boldsymbol{\varphi})\right]_k = \partial^2_{jk}\hat{U}(\boldsymbol{\varphi}),\end{aligned} \tag{5.4}$$

with $\partial_j = \partial/\partial\varphi_j$ and $\partial^2_{jk} = \partial^2/\partial\varphi_j\partial\varphi_k$. The parameter derivative vector, $\boldsymbol{\nabla}_{\boldsymbol{\varphi}}$, differentiates the unitary matrix with respect to each element of $\boldsymbol{\varphi}$, which may generally correspond to different physical observables. This is a subtle, but important distinction with the gradient vector that differentiates a function with respect to different elements of $\boldsymbol{\nabla}$, which correspond to the *same* observable. To maintain full generality, we do not specify $\boldsymbol{\varphi}$ at this stage. Hence, we are unable to define the inner product of the operators in Eq. (5.4) to determine their Hermitian conjugate. Hence, we write

$$\hat{U}(\boldsymbol{\varphi}+\delta\boldsymbol{\varphi})^{\dagger} \approx \hat{U}^{\dagger}(\boldsymbol{\varphi}) + \left(\nabla_{\boldsymbol{\varphi}}\hat{U}(\boldsymbol{\varphi})\right)^{\dagger}\delta\boldsymbol{\varphi}^{\top} + \frac{1}{2}\delta\boldsymbol{\varphi}\boldsymbol{H}^{\dagger}\delta\boldsymbol{\varphi}^{\top}, \tag{5.5}$$

For unbiased estimators, the average of the estimated data will yield the true value $\boldsymbol{\varphi}$ in the asymptotic limit. The general objective of finding a measurement and estimator with highest sensitivity to small variations in $\boldsymbol{\varphi}$ then justifies taking the approximation $\|\boldsymbol{R}\delta\boldsymbol{\varphi}\| \ll 1$, where the risk matrix $\boldsymbol{R}$ ensures dimensional consistency. This implies that we may make the approximation $\delta\boldsymbol{\varphi}\boldsymbol{H}\delta\boldsymbol{\varphi}^{\top} \approx 0$, such that the unitary in Eq. (5.3) and Eq. (5.5) may be truncated to first order in $\delta\boldsymbol{\varphi}$. By considering the sensitivities of the initial probe state to infinitesimal changes in $\boldsymbol{\varphi}$, we are able to find the generator of translations in $\boldsymbol{\varphi}$. Hence,

$$\begin{aligned}\rho(\boldsymbol{\varphi}+\delta\boldsymbol{\varphi}) &= \left(\mathbb{1} + \nabla\hat{U}\delta\boldsymbol{\varphi}^{\top}\hat{U}^{\dagger}\right)\rho(\boldsymbol{\varphi})\left(\mathbb{1} + \hat{U}\nabla\hat{U}\delta\boldsymbol{\varphi}^{\top}\right),\\ &\approx \exp\left[-i\hat{\boldsymbol{G}}\delta\boldsymbol{\varphi}^{\top}\right]\rho(\boldsymbol{\varphi})\exp\left[i\hat{\boldsymbol{G}}^{\dagger}\delta\boldsymbol{\varphi}^{\top}\right],\end{aligned} \tag{5.6}$$

[1] The assumption of linearising the unitary transformation, $\hat{U}$, in $\boldsymbol{\varphi}$ can always be realised.

where elements of the local generator of parameter translations $\hat{\boldsymbol{G}}$ are given by

$$\left[\hat{\boldsymbol{G}}(\boldsymbol{\varphi})\right]_j = \hat{G}_j = i[\partial_j \hat{U}(\boldsymbol{\varphi})]\hat{U}^\dagger(\boldsymbol{\varphi}). \tag{5.7}$$

The derivative of the exponential operator $\hat{U}$ is given by Duhamel's formula [Wilcox, 1967]

$$\begin{aligned}\partial_j \hat{U} &= -i\int_0^1 \mathrm{d}\alpha \exp\left[-i(1-\alpha)\hat{\mathcal{H}}\right]\partial_j\hat{\mathcal{H}}\exp\left[-i\alpha\hat{\mathcal{H}}\right], \\ &= -i\hat{U}\hat{A}_j = -i\hat{A}_j\hat{U},\end{aligned} \tag{5.8}$$

where $\hat{A}_j(\boldsymbol{\varphi})$ is a Hermitian operator defined by the integral equation determined from Eq. (5.8). By combining Eq. (5.8) with Eq. (5.7), we find an integral equation representation for the generator of translations

$$\hat{G}_j = \hat{A}_j = \int_0^1 \mathrm{d}\alpha \exp\left[-i\alpha\hat{\mathcal{H}}\right]\left(\partial_j\hat{\mathcal{H}}\right)\exp\left[i\alpha\hat{\mathcal{H}}\right]. \tag{5.9}$$

A number of properties of the local generator immediately follow from this. First, its Hermicity can be confirmed from Eq. (5.9) which is demanded for the state evolution expressed in Eq. (5.6) to remain valid. To show this, we require knowledge of $(\partial_j\hat{\mathcal{H}})^\dagger$. Since $\hat{G}_j$ governs *local* dynamics in φ_j we write

$$i\partial_j|\psi\rangle = \hat{G}_j|\psi\rangle. \tag{5.10}$$

Spectrally decomposing $\hat{\mathcal{H}}$ using the complete orthonormal basis $\{p_j, |\psi_j\rangle\}$, differentiating with respect to φ_j and using Eq. (5.10) we recover the Von Neumann equation

$$\frac{\mathrm{d}\hat{\mathcal{H}}}{\mathrm{d}\varphi_j} = \partial_j\hat{\mathcal{H}} - i\left[\hat{G}_j, \hat{\mathcal{H}}\right]. \tag{5.11}$$

The first term is the eigenvalue dependence on the parameter and is Hermitian. Since we have $(\partial_j\hat{\mathcal{H}})^\dagger = \partial_j\hat{\mathcal{H}}$ then the Hermicity follows. Second, we notice that $\hat{\mathcal{H}}$ is not necessarily equivalent to $\hat{\boldsymbol{G}}\boldsymbol{\varphi}^\top$ in general as expected. An equality is only valid when the Hamiltonian has multiplicative dependence on the parameters $\boldsymbol{\varphi}$. Specifically, for Hamiltonian tomography $\hat{\mathcal{H}}(\boldsymbol{\varphi}) = \sum_j \varphi_j\hat{\mathcal{H}}_j$, we recover $\hat{G}_j = \hat{\mathcal{H}}_j$. Third, despite our second observation, it is clear from Eq. (5.8) that the generator of translations in φ_j commutes with the unitary describing the channel evolution, $[\hat{G}_j, \hat{U}] = 0$. This maintains conservation of the physical observable corresponding to the generator. Further, the generators of different parameters do not commute in general.

5.1.2 Solving the integral equation for the generator

In this subsection, we want to solve the integral operator Eq. (5.9) to find a solution for $\hat{G}_j$. Doing so will yield the generator for arbitrary Hamiltonian parameters and will allow the calculation of the QFI. Our approach to solving the integral operator equation for $\hat{G}_j$, is to use the Baker Campbell Hausdorff (BCH) identity on the integrand. This will represent the solution as an infinite series of nested commutators between the Hamiltonian $\hat{\mathcal{H}}$ and its derivative $\partial_j\hat{\mathcal{H}}$.

Note that this approach is generally better suited for perturbative solutions for infinite series. The BCH for a Hermitian operator $\hat{B}$ and arbitrary operator $\hat{A}$ reads

$$\begin{aligned} \exp\left[\mu\hat{B}\right]\hat{A}\exp\left[-\mu\hat{B}\right] &= \hat{A} + \mu\left[\hat{B},\hat{A}\right] + \frac{\mu^2}{2!}\left[\hat{B},\left[\hat{B},\hat{A}\right]\right] + \ldots, \\ &= \sum_{n=0}^{\infty}\frac{\mu^n}{n!}C_{\hat{B}}^{(n)}(\hat{A}), \end{aligned} \tag{5.12}$$

for some $\mu \in \mathbb{C}$ and where we have defined $C_{\hat{B}}^{(n)}(\hat{A})$ as the nth–order nested commutator of $\hat{A}$ and $\hat{B}$ (note the subscript n *does not* refer to a power). Using Eq. (5.12) to re-express the integrand of Eq. (5.9) and performing the integration, we obtain

$$\begin{aligned} \hat{G}_j &= \hat{\mathcal{H}}_j - \frac{i}{2!}\left[\hat{\mathcal{H}},\hat{\mathcal{H}}_j\right] - \frac{1}{3!}\left[\hat{\mathcal{H}},\left[\hat{\mathcal{H}},\hat{\mathcal{H}}_j\right]\right] + \ldots, \\ &= \sum_{n=0}^{\infty}\frac{(-i)^n}{(n+1)!}C_{\hat{\mathcal{H}}}^{(n)}\left(\hat{\mathcal{H}}_j\right), \\ &= g\left[-iC_{\hat{\mathcal{H}}}\right]\left(\hat{\mathcal{H}}_j\right), \end{aligned} \tag{5.13}$$

where $\hat{\mathcal{H}}_j = \partial_j\hat{\mathcal{H}}$ and where we defined the generating function of the expansion coefficients in Eq. (5.13) as

$$g[t] = \frac{\exp[t]-1}{t}. \tag{5.14}$$

Eq. (5.13) is a series solution for the local generator of translations for the parameter $[\boldsymbol{\varphi}]_j$. It reproduces the adjoint action series of Duhamel's formula in Eq. (5.8). Operationally, since it depends only on the operator $\hat{\mathcal{H}}$, we should expect to be able to write the generator in terms of the eigenvalues and eigenvectors of $\hat{\mathcal{H}}$. Hence, we consider the following spectral decomposition of the Hamiltonian: assume that $\hat{\mathcal{H}}$ has n_g unique eigenvalues, each with value E_j, $j \in \{1,2,\ldots,n_g\}$ and degeneracy d_j such that the corresponding eigenvectors are $|E_j^{(k)}\rangle$, $k \in \{1,2,\ldots,d_j\}$ satisfying $\langle E_\alpha^{(\beta)}|E_\gamma^{(\delta)}\rangle = \delta_{\alpha\gamma}\delta_{\beta\delta}$. The Hamiltonian is then diagonal in this basis, and we write

$$\hat{\mathcal{H}}(\boldsymbol{\varphi}) = \sum_{j=1}^{n_g}\sum_{k=1}^{d_j}E_j(\boldsymbol{\varphi})\left|E_j^{(k)}(\boldsymbol{\varphi})\right\rangle\left\langle E_j^{(k)}(\boldsymbol{\varphi})\right|, \tag{5.15}$$

where we allow both the eigenvalues and eigenvectors to depend on $\boldsymbol{\varphi}$. Then, from its derivative, we have

$$\hat{\mathcal{H}}_j = \sum_{k=1}^{n_g}\sum_{l=1}^{d_j}\left[\partial_j E_k\left|E_k^{(l)}\right\rangle\left\langle E_k^{(l)}\right| + E_k\partial_j\left(\left|E_k^{(l)}\right\rangle\left\langle E_k^{(l)}\right|\right)\right]. \tag{5.16}$$

Using the resolution of the identity and the orthonormality criterion of the projectors of the Hamiltonian, the nth–order nested commutator of $\hat{\mathcal{H}}$ and $\hat{\mathcal{H}}_j$ becomes

$$\begin{aligned} C_{\hat{\mathcal{H}}}^{(n)} &= -\sum_{a,b,c,d}(E_a - E_c)^{n+1}\left|E_a^{(b)}\right\rangle\left\langle E_a^{(b)}\middle|\partial_j E_c^{(d)}\right\rangle\left\langle E_c^{(d)}\right|, \\ &= -\sum_{a,b,c,d}(E_a - E_c)^{n+1}\hat{\mathcal{A}}_{a,b,c,d}, \end{aligned} \tag{5.17}$$

for $n \geq 1$, where we have collected all summations under the same sign for brevity, although they are paired such that a, c sum over distinct eigenvalues and b, d sum over the eigenvector degeneracies for eigenvalues E_a, E_c respectively, and, where we introduce the weighted projector

$$\hat{\mathcal{A}}_{a,b,c,d} = \left\langle E_a^{(b)} \middle| \partial_j E_c^{(d)} \right\rangle \hat{\Gamma}_{ac}^{(bd)}, \tag{5.18}$$

for brevity. Clearly then the nth-order nested commutators captures the dynamics resulting from the eigenvectors dependence on $\boldsymbol{\varphi}$. The zeroth-order nested commutator is, by definition, the derivative of the Hamiltonian, written in Eq. (5.16). By inspection the first term of $\hat{\mathcal{H}}_j$ reproduces the eigenvalue contribution to the local generator of translations $\hat{G}_j$ written in the main body of the text. By use of the resolution of the identity, the eigenvector dependence of $\hat{\mathcal{H}}_j$ (second term) is in fact the result obtained by $C^{(0)}_{\hat{\mathcal{H}}}$, such that

$$\hat{\mathcal{H}}_j = \sum_{k=1}^{n_g} \partial_j E_k \hat{P}_k + C^{(0)}_{\hat{\mathcal{H}}}, \tag{5.19}$$

where we introduced the projector $\hat{P}_k = \sum_j |E_k^{(j)}\rangle \langle E_k^{(j)}|$ onto the E_k-eigenspace of $\hat{\mathcal{H}}(\boldsymbol{\varphi})$. Our task now is to generate an expression for the eigenvector dependence of the generator (the sum over nth-order nested commutators), so we temporarily omit the first term of $\hat{\mathcal{H}}_j$. Then, combining the result of the nth-order nested commutators in Eq. (5.17) and Eq. (5.19) with the series solution of the generator in Eq. (5.13), we have

$$\begin{aligned} \hat{G}_j(\boldsymbol{\varphi}) &= \sum_{k=1}^{n_g} \partial_j E_k \hat{P}_k + i \sum_{a,b,c,d} \left(\sum_{n=0}^{\infty} \frac{[-i(E_a - E_c)]^n}{n!} - 1 \right) \mathcal{A}_{a,b,c,d}, \\ &= \sum_{k=1}^{n_g} \partial_j E_k \hat{P}_k + i \sum_{a,b,c,d} \left(\exp[-i(E_a - E_c)] - 1 \right) \mathcal{A}_{a,b,c,d}, \end{aligned} \tag{5.20}$$

where we write the proportionality to indicate our omission of the term with eigenvalue dependence. By use of the identity

$$\exp[-i(E_a - E_c)] - 1 = -2i \exp\left[-\frac{i(E_a - E_c)}{2} \right] \sin\left[\frac{(E_a - E_c)}{2} \right], \tag{5.21}$$

and including the eigenvalue dependence, we arrive at the following form of the local generator of translations:

$$\begin{aligned} \hat{G}_j(\boldsymbol{\varphi}) = \sum_{k=1}^{n_g} \partial_j E_k \hat{P}_k + 2 \sum_{k \neq l} \sum_{m=1}^{d_k} \sum_{n=1}^{d_l} &\exp\left[-i(E_k - E_l)/2\right] \\ &\times \sin\left[\frac{E_k - E_l}{2} \right] \left\langle E_l^{(n)} \middle| \partial_j E_k^{(m)} \right\rangle \left| E_k^{(m)} \right\rangle \left\langle E_l^{(n)} \right|. \end{aligned} \tag{5.22}$$

This is a generalisation of the result obtained by Pang and Brun [2014] to multiple parameters. We will review the method they used to show this in the next subsection. Checking for consistency, we verify that for phase-like Hamiltonians we obtain the expected multiplicative factors of the parameters $\hat{G}(\varphi) = \varphi \sum_k E_k \hat{P}_k = \varphi \hat{\mathcal{H}}$, and, that the generator is Hermitian. This circumvents common methods, such as restricting the domain of the parameters $\boldsymbol{\varphi}$, or multiplying by the imaginary unit, to ensure Hermiticity or self-adjointness of operators. Further, we

observe that the generator has two distinct parts. The first part is due to the dependence of the eigenvalues on φ_j and the second due to the dependence of the eigenstates on φ_j. We expect the QFI to exhibit this same feature. Increasing the channel QFI can be achieved by enhancing the sensitivity of the generator through additional terms in the Hamiltonian $\hat{\mathcal{H}}$ [Fraïsse and Braun, 2017]. Specifically, for time evolutions with parameter independent eigenvalues, Eq. (5.15) exhibits a periodic time dependence of the channel QFI [Pang and Brun, 2014]. Generally, this alone does not saturate the Heisenberg limit precision, but has been shown to with use of feedback controls [Yuan and Fung, 2015; Yuan, 2016]. A key difficulty of finding the generator can be observed from Eq. (5.15), which requires the spectral decomposition $\{E_j, |E_j^{(k)}\rangle\}$ of the Hamiltonian $\hat{\mathcal{H}}$. For large dimensional systems, obtaining this spectrum is in general a difficult problem. This in general can not be circumvented as we will see in the next subsection. This difficulty in fact plagues the calculation of the QFI in any chosen formalism.

5.1.3 Alternative approach

In this subsection, we look at an alternative method to solve the integral operator equation for the local generator of translations in φ_j, which achieves the the same result as the previous subsection. We follow the method first proposed in [Wilcox, 1967; Pang and Brun, 2014] to show it agrees with our result for multi-parameter estimation. This method recasts the integrand $Y(\alpha)$ of Eq. (5.9) as a first order differential equation and introduces the super-operator $\hat{\mathscr{H}}[Y(\alpha)] = [\hat{\mathcal{H}}, Y(\alpha)]$.

Defining the integrand as $\hat{Y}_m(\beta)$, then we have the first order differential equation

$$\partial_\beta \hat{Y}_m(\beta) = -i\left[\hat{\mathcal{H}}, \hat{Y}_m(\beta)\right] = -i\hat{\mathscr{H}}\left[\hat{Y}_m(\beta)\right], \tag{5.23}$$

where $\hat{\mathscr{H}}$ is the Hermitian superoperator of $\hat{\mathcal{H}}$ defined by $\hat{\mathscr{H}}[\hat{O}] = [\hat{\mathcal{H}}, \hat{O}]$, and the initial condition is $\hat{Y}_m(0) = \partial_m \hat{\mathcal{H}}$. To recover our result from the previous section, we consider the same spectral decomposition of the Hamiltonian to solve Duhamel's formula. In Eq. (5.15), we defined the Hamiltonian $\hat{\mathcal{H}}$ to have n_g unique eigenvalues E_j, $j \in \{1, 2, \ldots, n_g\}$, with degeneracies d_j, and corresponding eigenvectors $|E_j^{(k)}\rangle$, $k \in \{1, 2, \ldots, d_j\}$. Hence, we write the superoperator $\hat{\mathscr{H}}$ as

$$\hat{\mathscr{H}}(\boldsymbol{\varphi}) = \sum_{k,l=1}^{n_g} \sum_{i=1}^{d_k} \sum_{j=1}^{d_l} \lambda_{kl}^{(ij)}(\boldsymbol{\varphi}) \hat{\Gamma}_{kl}^{(ij)}(\boldsymbol{\varphi}), \tag{5.24}$$

with

$$\lambda_{kl}^{(ij)}(\boldsymbol{\varphi}) = E_k(\boldsymbol{\varphi}) - E_l(\boldsymbol{\varphi}), \quad \hat{\Gamma}_{kl}^{(ij)}(\boldsymbol{\varphi}) = \left|E_k^{(i)}(\boldsymbol{\varphi})\right\rangle\left\langle E_l^{(j)}(\boldsymbol{\varphi})\right|, \tag{5.25}$$

and where the projectors satisfy $\hat{\Gamma}_{kl}^{(\alpha\beta)}\hat{\Gamma}_{mn}^{(\gamma\delta)} = \delta_{lm}\delta_{\beta\gamma}\hat{\Gamma}_{kn}^{(\alpha\delta)}$. We can now solve the first order operator differential Eq. (5.23) in this basis by writing $\hat{\mathscr{H}}[\hat{Y}_m(\beta)] = \lambda_{kl}^{(ij)}\hat{Y}_m(\beta)$ and using the initial condition

$$\hat{Y}_m(0) = \partial_m \hat{\mathcal{H}} = \sum_{k,l}^{n_g} \sum_{i}^{d_k} \sum_{j}^{d_l} \mathrm{Tr}\left[\hat{\Gamma}_{kl}^{(ij)\dagger} \partial_m \hat{\mathcal{H}}\right] \hat{\Gamma}_{kl}^{(ij)}, \tag{5.26}$$

to obtain

$$\hat{Y}_m(\beta) = \sum_{k,l}^{n_g} \sum_{i}^{d_k} \sum_{j}^{d_l} \mathrm{Tr}\left[\hat{\Gamma}_{kl}^{(ij)\dagger} \partial_m \hat{\mathcal{H}}\right] \hat{\Gamma}_{kl}^{(ij)} \exp\left[-i\lambda_{kl}^{(ij)}\beta\right]. \tag{5.27}$$

Note that the zero eigenvalues of the superoperator occur when $k = l$ with degeneracy $r = \sum_j d_j^2$. From the definition of $\hat{\mathcal{H}}$ in Eq. (5.15) and the properties of the projectors $\hat{\Gamma}_{kl}^{(ij)}$,

$$\mathrm{Tr}\left[\hat{\Gamma}_{kl}^{(ij)\dagger} \partial_m \hat{\mathcal{H}}\right] = \begin{cases} (\partial_m E_k)\delta_{ij} & \text{for } k = l \\ (E_k - E_l)\langle E_l^{(j)} | \partial_m E_k^{(i)} \rangle & \text{for } k \neq l \end{cases}. \tag{5.28}$$

Substituting Eq. (5.27) for the integrand of Eq (5.9) and conducting the integration, we obtain the form of the local generator:

$$\begin{aligned} \hat{G}_j(\boldsymbol{\varphi}) = \sum_{k=1}^{n_g} \partial_j E_k \hat{P}_k + 2 \sum_{k\neq l} \sum_{m=1}^{d_k} \sum_{n=1}^{d_l} \exp\left[-i(E_k - E_l)/2\right] \\ \times \sin\left[\frac{E_k - E_l}{2}\right] \left\langle E_l^{(n)} \middle| \partial_j E_k^{(m)} \right\rangle \left| E_k^{(m)} \right\rangle \left\langle E_l^{(n)} \right|, \end{aligned} \tag{5.29}$$

where we recall that $\hat{P}_k = \sum_j |E_k^{(j)}\rangle \langle E_k^{(j)}|$. This is in exact agreement with the result obtained in the previous subsection.

5.1.4 Quantum Fisher information matrix

In this subsection, we summarise the form of the QFIM required for multi-parameter estimations with generalised Hamiltonian evolutions. We will then be able to use these results for what follows. We start by considering the spectral decomposition of the evolved probe state

$$\rho(\boldsymbol{\varphi}) = \sum_{j=1}^{D} \varrho_j(\boldsymbol{\varphi}) \left|\varrho_j(\boldsymbol{\varphi})\right\rangle \left\langle \varrho_j(\boldsymbol{\varphi})\right|, \tag{5.30}$$

where $D = \dim[\mathrm{supp}(\rho(\boldsymbol{\varphi}))]$ is the dimension of the support of $\rho(\boldsymbol{\varphi})$. We generalise the result for the QFI in [Liu et al., 2014] to multiple parameters

$$\left[\mathcal{I}^{\mathrm{Q}}\right]_{mn} = \sum_{j=1}^{D} 4\varrho_j \left[\mathrm{Cov}\left(\overleftarrow{\partial}_m, \vec{\partial}_n\right)\right]_j - \sum_{j\neq k}^{D} \frac{8\varrho_j\varrho_k}{(\varrho_j + \varrho_k)} \left\langle \varrho_j \middle| \overleftarrow{\partial}_m \middle| \varrho_k \right\rangle \left\langle \varrho_k \middle| \vec{\partial}_n \middle| \varrho_j \right\rangle, \tag{5.31}$$

where $\{m, n \in \mathbb{Z} | 1 \leq m, n \leq D\}$ define the elements of the QFI matrix elements, the arrows above the derivatives indicate the direction of operation, such that $(\vec{\partial}_j |\varrho_k\rangle)^\dagger = \langle \varrho_k | \overleftarrow{\partial}_j$, and the covariance matrix of the generators on the jth-eigenstate of the initial state in Eq. (5.31) is defined as

$$\left[\mathrm{Cov}\left(\overleftarrow{\partial}_m, \vec{\partial}_n\right)\right]_j = \frac{1}{2}\left\langle \varrho_j \middle| \left(\overleftarrow{\partial}_m \vec{\partial}_n + \overleftarrow{\partial}_n \vec{\partial}_m\right) \middle| \varrho_j \right\rangle - \left\langle \varrho_j \middle| \overleftarrow{\partial}_m \middle| \varrho_j \right\rangle \left\langle \varrho_j \middle| \vec{\partial}_n \middle| \varrho_j \right\rangle. \tag{5.32}$$

Despite unitary evolution of the probe, the QFIM may depend on the parameters $\boldsymbol{\varphi}$, $\mathcal{I}^{\mathrm{Q}} = \mathcal{I}^{\mathrm{Q}}(\boldsymbol{\varphi})$. We can easily re-write the QFIM in terms of the generator by realising that

$$|\partial_j \varrho(\boldsymbol{\varphi})\rangle := \partial_j \hat{U}(\boldsymbol{\varphi}) |\varrho(\mathbf{0})\rangle = -i\hat{G}_j |\varrho(\boldsymbol{\varphi})\rangle. \tag{5.33}$$

Given the Hermicity of the generators, it suffices to replace both $\overleftarrow{\partial}_j$ and $\vec{\partial}_j$ with $\hat{G}_j$ in Eq. (5.31) to obtain a general QFIM for arbitrary unitary channel evolutions. This is the form of the QFIM used in this work. We also observe that only for pure states, the QFIM can be written as the covariance matrix of the generators

$$\left[\mathcal{I}^{\mathrm{Q}}\right]_{mn} = 4\mathrm{Re}\left[\langle\varrho|\hat{G}_m\hat{G}_n|\varrho\rangle - \langle\varrho|\hat{G}_m|\varrho\rangle\langle\varrho|\hat{G}_n|\varrho\rangle\right]. \tag{5.34}$$

Note that although the form of the QFIM in Eq. (5.31) holds for probe states of arbitrary ranks, diagonalising a Hamiltonian of increasing rank is generally increasingly difficult.

Recall from chapter 3 that we can intuitively relate the Hamiltonian formalism of the QFIM written in Eq. (5.31) to the SLD formalism. We note from the implicit definition of the SLD that it describes dynamics of the system $\rho(\boldsymbol{\varphi})$. Unitary dynamics are generally given by the von-Neumann equation

$$[\partial_j\rho(\boldsymbol{\varphi})]_{kl} = (\partial_j\varrho_k)\delta_{kl} + (\varrho_l - \varrho_k)\langle\varrho_k|\partial_j\varrho_l\rangle. \tag{5.35}$$

where we defined $[\partial_j\rho(\boldsymbol{\varphi})]_{jk} \coloneqq \langle\varrho_j|\partial_j\rho(\boldsymbol{\varphi})|\varrho_k\rangle$, used the fact that $\partial_j\langle\varrho_k|\varrho_l\rangle = 0$, and where we have dropped explicit dependence on $\boldsymbol{\varphi}$ on the RHS. Similarly, by decomposing the implicit definition of $\mathcal{L}$ in the eigenbasis of the state and combining with Eq. (5.35), we obtain

$$[\mathcal{L}_j]_{kl} = \frac{2(\partial_j\varrho_k)\delta_{kl}}{\varrho_k + \varrho_l} + \frac{2(\varrho_k - \varrho_l)\langle\partial_j\varrho_k|\varrho_l\rangle}{\varrho_k + \varrho_l}, \tag{5.36}$$

where $|\partial_j\varrho(\boldsymbol{\varphi})\rangle \coloneqq \partial_j\hat{U}(\boldsymbol{\varphi})|\varrho(\mathbf{0})\rangle$.

To conclude this section, we have provided a generalisation of the generator for multiparameter estimations. With this, the QFIM can be used as a figure of merit from in Eq. (5.31) and the SLD in Eq. (5.36) to determine the optimal observables. In the next section, we address how the grid configuration can be chosen to enhance the sensitivity of the QFIM.

5.2 Quantum metrology of grid deformations

In this section, we apply the Hamiltonian formalism introduced in the previous section to determine how well different spatial deformations of grids of photon emitters may be detected. One method of gauging how well deformations may be detected is to estimate the change in source positions by tracking changes to the emitted signature of the grid. We use the QCRB as the metric that describes the performance of our ability to estimate different deformations introduced to the grid and to define the ultimate theoretical precision bounds. This problem is isomorphic to source localisation which has been of considerable interest in the literature [Moerner, 2007; Fairhurst, 2011; Tsang, 2015; Sidhu and Kok, 2017]. In the following, we work in the near-field regime, which defines the region of the electromagnetic field adjacent to the sources. This omits the need to propagate the emitted field to an alternative far-field region, allowing us to better concentrate on the source localisation problem.

Consider a two dimensional grid of N_t photon emitters arranged in a $N \times M$ configuration with N (M) the number of sources along the x (y) direction. This grid configuration is illustrated in figure 5.1 for $N = 3$ and $M = 2$. Homogenous deformations introduced to the grid of sources will affect the expected mean positions of each source, not their covariances. By tracking these changes, we aim to estimate the type of deformation the grid has been subjected to. The expected

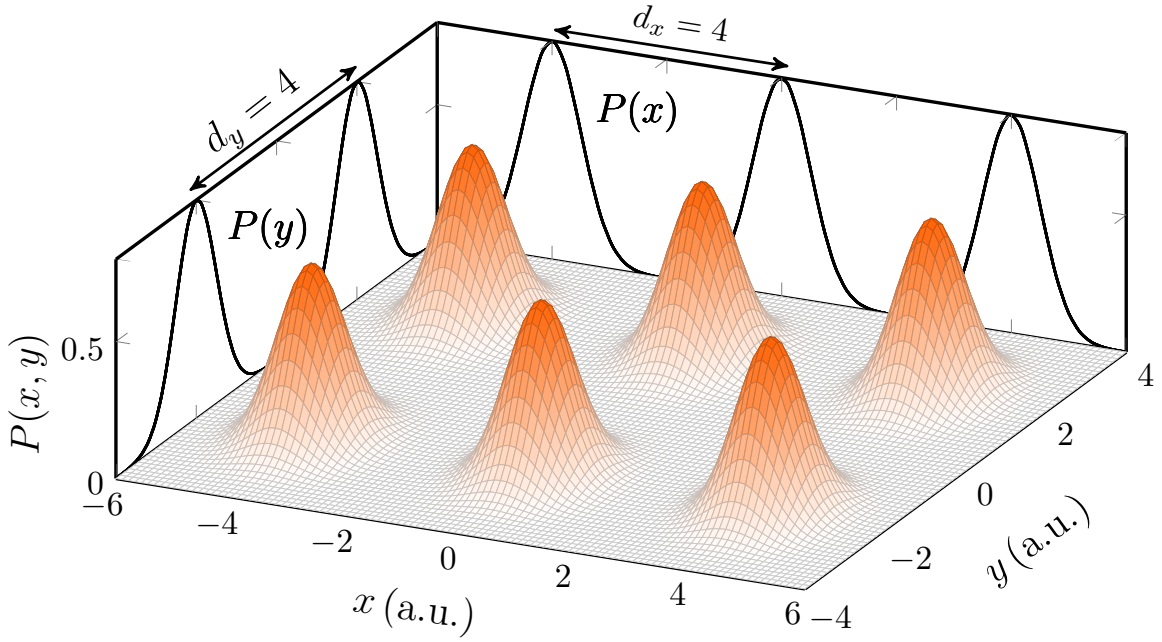

Figure 5.1: *A grid of $N_t = 6$ sources distributed in a 3×2 configuration, each with bi-variate Gaussian spatial profiles and source separation distances $d_x = 4, d_y = 4$ (arbitrary units). The projected probability distributions onto the xz and yz planes are illustrated by $P(x)$ and $P(y)$ respectively. We assume that the sources are independent and identically distributed (IID) such that covariance matrix of the emitted light in the near field is diagonal in the chosen basis. Any deformations introduced to this grid affects only the expected positions of the emitters whilst preserving the source covariances. This is demanded since any deformations should not change the emitters nature.*

position of the jth source, $\boldsymbol{\mu}_j = (\mu_{j_x}, \mu_{j_y})^\top$, $j \in \{1, 2, \ldots, N_t\}$, is chosen to be symmetric about the grid centre O such that

$$\begin{aligned} \mu_{j_x} &= \left[\text{Mod}\left[j-1, N\right] - \left(\frac{N-1}{2}\right)\right] d_x, \\ \mu_{j_y} &= \left[\left\lceil \frac{j}{N} \right\rceil - \left(\frac{M+1}{2}\right)\right] d_y, \end{aligned} \tag{5.37}$$

where $\text{Mod}[a, b]$, $\{a, b\} \in \mathbb{R}$, defines the modulo operation that returns remainder of the division a/b, $\lceil a \rceil = \text{Ceiling}[a]$ returns the smallest integer that is greater than or equal to a, d_x and d_y define the source separation distance in the x and y direction respectively. The convention chosen for labelling emitters j is from bottom left to top right, with increasing j running along the rows. We now assume that the jth-source emits n_j photons, each with a bi-normal spatial distribution with mean position $\boldsymbol{\mu}_j$ and covariance matrix $\boldsymbol{\Sigma}_j$. In what follows, we reserve bold typesetting for tuples. Then, the distribution of each emitted photon may be

described by the first and second moments according to

$$f(\boldsymbol{r}_j, \boldsymbol{\mu}_j) = \frac{1}{2\pi|\boldsymbol{\Sigma}_j|^{1/2}} \exp\left[-\frac{1}{2}(\boldsymbol{r}_j - \boldsymbol{\mu}_j)^\top \boldsymbol{\Sigma}_j (\boldsymbol{r}_j - \boldsymbol{\mu}_j)\right], \tag{5.38}$$

where

$$\boldsymbol{\Sigma}_j = \begin{pmatrix} s_{j_x}^2 & r s_{j_x} s_{j_y} \\ r s_{j_x} s_{j_y} & s_{j_y}^2 \end{pmatrix}, \quad \boldsymbol{\mu}_j = \left(\mu_{j_x}, \mu_{j_y}\right)^\top, \tag{5.39}$$

and r is the correlation coefficient between x and y. The pure state describing the emitted light from the initial undeformed grid of N_t IID sources in the near field may then be written as

$$|\Psi(\boldsymbol{0})\rangle = \int \mathrm{d}\boldsymbol{R}^{\boldsymbol{n}}\ f(\boldsymbol{R}, \boldsymbol{M})^{\boldsymbol{n}/2} \hat{a}^\dagger(\boldsymbol{R})^{\boldsymbol{n}} |\boldsymbol{0}\rangle, \tag{5.40}$$

where $\mathrm{d}\boldsymbol{R} = \prod_{j=1}^{N_t} \mathrm{d}\boldsymbol{r}_j^{n_j}$, $f(\boldsymbol{R}, \boldsymbol{M})^{\boldsymbol{n}} = \prod_{j=1}^{N_t} f(\boldsymbol{r}_j, \boldsymbol{\mu}_j)^{n_j}$ is the mode function with which the state is normalised, $|\boldsymbol{0}\rangle = |0\rangle^{\otimes N_t}$ is the global vacuum state (i.e., no excitations in any mode), and, $\hat{a}^{\dagger \boldsymbol{n}}(\boldsymbol{R}) = \prod_{j=1}^{N_t} \hat{a}_j^{\dagger n_j}(\boldsymbol{r}_j)$ is the multimode creation operator composed of tensor products of creation operator on the Fock space of the jth source, $\hat{a}_j^\dagger(\boldsymbol{r}_j)$. These creation operators do not have explicit time dependence. From its Heisenberg equation of motion, we may write the position dependent creation operator as

$$\hat{b}_j^\dagger(\boldsymbol{r}_j) = \int \mathrm{d}\boldsymbol{k}_j\ \hat{a}_j^\dagger(\boldsymbol{k}_j) \exp\left[i \boldsymbol{r}_j \boldsymbol{k}_j\right]. \tag{5.41}$$

Substituting Eq. (5.41) into Eq. (5.40) and using the definition of the mode function f, we write the state in the Fourier domain as

$$|\Psi(\boldsymbol{0})\rangle = \int \mathrm{d}\boldsymbol{K}^{\boldsymbol{n}}\ g(\boldsymbol{K})^{\boldsymbol{n}/2} \hat{a}^\dagger(\boldsymbol{K})^{\boldsymbol{n}} |\boldsymbol{0}\rangle, \tag{5.42}$$

where the Fourier-space mode profile function g is

$$g(\boldsymbol{k}_j) = \sqrt{\frac{2 s_{j_x}^2 s_{j_y}^2}{\pi}} (1 - r)^{1/4} \exp\left[i \boldsymbol{k}_j^\top \boldsymbol{\mu}_j - \boldsymbol{k}_j^\top \boldsymbol{\Sigma}_j \boldsymbol{k}_j\right], \tag{5.43}$$

which differs from the characteristic function of f owing to the square root of the binormal Gaussian distribution in the state definition in Eq. (5.40). Grid deformations will have the effect of parameterising the initial probe state $\rho(\boldsymbol{0})$ by changing the expected source positions $\boldsymbol{\mu}_j$ to $\tilde{\boldsymbol{\mu}}_j$.

The complexity of the calculation depends on how the grid deformation, $\boldsymbol{F}$, parameterises the generator. The case for multiplicative factors such as grid stretching, was considered in the previous chapter. There, the QFI was used to estimate the source separation distance $\boldsymbol{d} = (d_x, d_y)$. The generator for $\boldsymbol{d}$ used there was

$$\hat{\boldsymbol{G}} = -\sum_j \int \mathrm{d}\boldsymbol{k}_j \boldsymbol{\Lambda}_j \boldsymbol{V}_j^\top \hat{n}(\boldsymbol{k}_j), \tag{5.44}$$

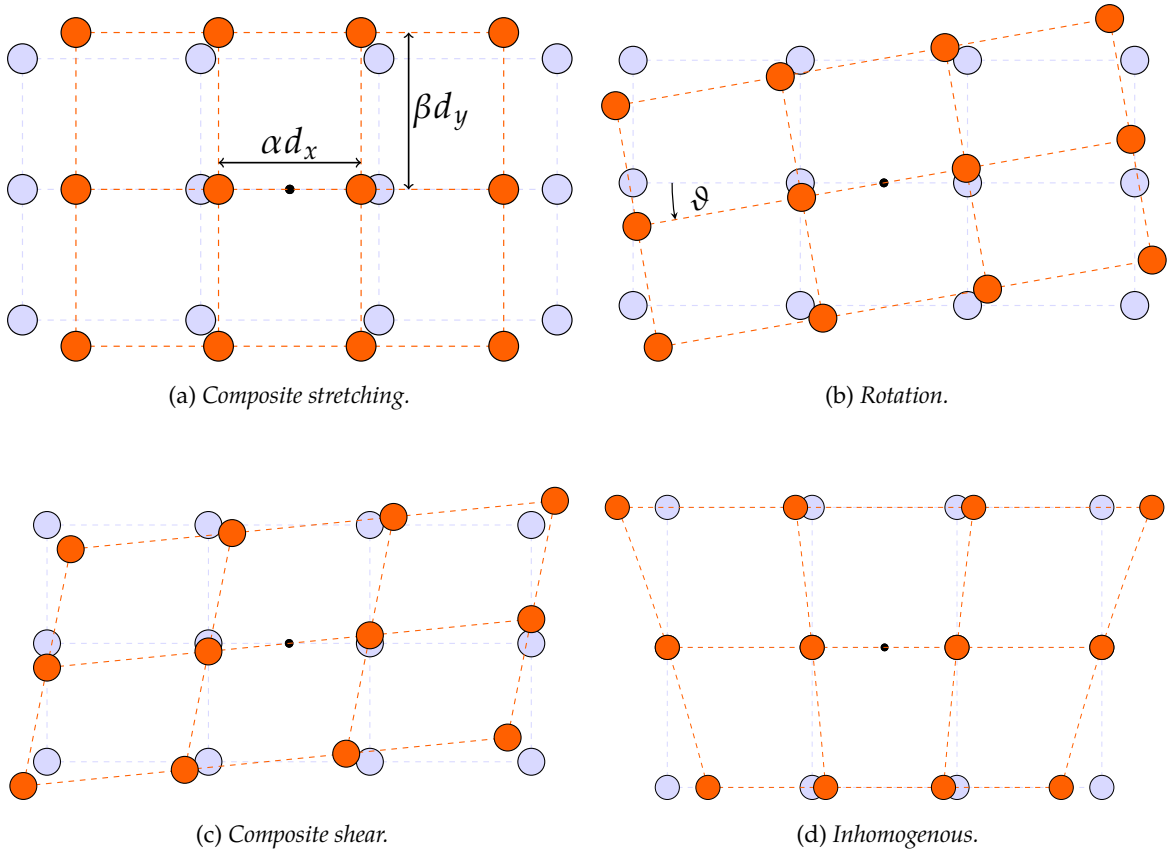

(a) *Composite stretching.*

(b) *Rotation.*

(c) *Composite shear.*

(d) *Inhomogenous.*

Figure 5.2: *This figure illustrates different deformations of the grid of Gaussian distributed sources shown in figure 5.1. The deformed grids are shown with orange sources, and compared with the original-undeformed grid shown with blue sources. The central black dot defines the grid centre O. In figure 5.2a we consider a composite stretching which provides a platform for multiparameter estimation of the unitless multiplicative factors α and β. In figure 5.2b we consider rotations about the grid centre O. Whilst this is a single parameter estimation, it is not a simple multiplicative factor. Figure 5.2c represents a grid shear, and in figure 5.2d we consider a position dependent inhomogeneous (non-linear) deformation, where the x-coordinates are transformed to $x' = x\exp(y/\gamma)$ for $\gamma \in \mathbb{R}$.*

with $\mathbf{\Lambda}_j = \text{diag}(\mu_{j_x}, \mu_{j_y})$, $\boldsymbol{V}_j = (\boldsymbol{F}^\top - 1)\boldsymbol{k}_j^\top$, $\hat{n}$ is the number operator, and, $\hat{\boldsymbol{G}} = (\hat{G}_{d_x}, \hat{G}_{d_y})^\top$ generates dynamics in the source separation distances. We note that this is a self-adjoint operator. For an array of equidistant sources, the generator becomes $\hat{G} = \xi \sum_{j=1}^{N} \mu_j' \int \mathrm{d}k_j\, k_j\, \hat{n}_j(k_j)$ and this system has been explored metrologically in chapter 4. In this work, we consider applying a wider range of homogeneous and inhomogeneous deformations to a two dimensional grid of sources and evaluating their impact on the QFI. By determining how the QFI changes with different deformations, we can track changes to the source coordinates in the grid and apply corrective measures to negate the effects of the deformation. This would also enable evaluation of stresses and strains in materials when deformed. Figure 5.2 illustrates the types of grid deformations that we would like to consider in this section.

Recall that the form of the unitary that parameterises the position of a grid of N_t sources in terms of some deformation is

$$\hat{U}(\boldsymbol{\varphi}) = \exp\left[-i\hat{\mathcal{H}}(\boldsymbol{\varphi})\right], \tag{5.45}$$

where,

$$\hat{\mathcal{H}}(\boldsymbol{\varphi}) = -\sum_{j=1}^{N_t} \int \mathrm{d}\boldsymbol{k}_j \left(\boldsymbol{k}_j \boldsymbol{u}_j^{\top}(\boldsymbol{\varphi})\right) \hat{n}_j(\boldsymbol{k}_j). \tag{5.46}$$

By inspection of this generator, the Fock-basis is suitable to span this operator. Defining the eigenvectors as

$$|\boldsymbol{n}\rangle \equiv |n_1(\boldsymbol{k}_1), \ldots, n_{N_t}(\boldsymbol{k}_{N_t})\rangle, \tag{5.47}$$

then from the eigenvalue problem $\hat{\mathcal{H}}(\boldsymbol{\varphi})|\boldsymbol{n}\rangle = E(\boldsymbol{\varphi})|\boldsymbol{n}\rangle$, we obtain

$$E(\boldsymbol{\varphi}) = -\sum_{j=1}^{N_t} n_j \int \mathrm{d}\boldsymbol{k}_j \left(\boldsymbol{k}_j \boldsymbol{u}_j^{\top}(\boldsymbol{\varphi})\right) \tag{5.48}$$

for the corresponding eigenvalues. Since the eigenvectors have no dependence on the parameter to be estimated, we have that the generator of translations in deformation $[\boldsymbol{\varphi}]_j = \varphi_j$ is

$$\hat{G}_j = \sum_{k=1}^{N_t} \partial_j E_k |\boldsymbol{n}\rangle \langle \boldsymbol{n}|. \tag{5.49}$$

This generator is Hermitian and has units of momentum. This is expected since the grid sources undergoes spatial translations according to some deformation $\boldsymbol{F}$. For any homogenous deformation, there is no net translation of the sources about the grid centre, O (see figure 5.2). This suggests that $\langle \hat{G}_j \rangle = 0$, which can be confirmed through direct calculation. Hence, the QFIM for a pure state becomes

$$\left[\boldsymbol{\mathcal{I}}^{\mathrm{Q}}\right]_{mn} = 2\left\langle \hat{G}_m \hat{G}_n + \hat{G}_n \hat{G}_m \right\rangle = 4\left\langle \hat{G}_m \hat{G}_n \right\rangle. \tag{5.50}$$

The second equality on Eq. (5.50) used a further property of the generators: $[\hat{G}_m, \hat{G}_n] = 0$, which follows directly from Eq. (5.49). Using the definition of the state $|\Psi\rangle$, we can calculate the QFI, which yields

$$\begin{aligned}\left[\boldsymbol{\mathcal{I}}^{\mathrm{Q}}\right]_{mn} = \sum_{j=1}^{N_t} \frac{n_j^2}{(1-r^2)} \Bigg\{ &\frac{(\partial_m u_{j_x})(\partial_n u_{j_x})}{s_{j_x}^2} + \frac{(\partial_m u_{j_y})(\partial_n u_{j_y})}{s_{j_y}^2} \\ &- \frac{r\left[(\partial_m u_{j_x})(\partial_n u_{j_y}) + (\partial_m u_{j_y})(\partial_n u_{j_x})\right]}{s_{j_x} s_{j_y}} \Bigg\}.\end{aligned} \tag{5.51}$$

We note that the QFI depends only on the properties of the probe state and the grid configuration. This suggests that it may be possible to modify both properties to maximise the sensitivity of the QFIM to changes in $\boldsymbol{\varphi}$. We explore this possibility in the following subsections. The result

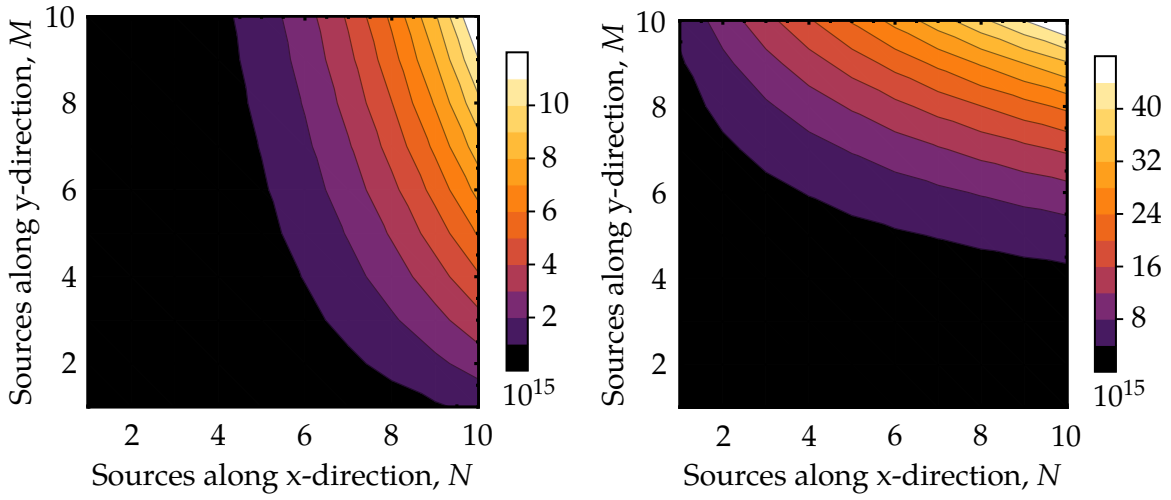

(a) $\mathcal{I}^Q_{\alpha\alpha}$ (b) $\mathcal{I}^Q_{\beta\beta}$.

Figure 5.3: *Diagonal elements of the QFIM for a composite stretching deformation of the grid (illustrated in figure 5.2a) as a function of the grid size N (x-axis) and M (y-axis), with $d_x = 1m$, $d_y = 2m$, $r = 0.5$, and $s_{j_x} = s_{j_y} = s = 300nm$—typical of photons from quantum dots. The zero off-diagonal elements is a consequence of assuming IID sources along the grid. From figure 5.3a we verify that the QFI for the stretching factor α along the x-axis increase as the grid size increases. Increasing the number of emitters along the stretching direction is favoured for this. This recovers the same finding in [Sidhu and Kok, 2017]. Figure 5.3b demonstrates similar conclusions for the QFI for β.*

obtained in Eq. (5.51) is central to the chapter since it completes the metrology approach for grid deformations. It is valid for all possible deformations. For non-homogenous deformations, the deforming matrix will also depend on the source index number j,

$$\boldsymbol{u}_j^\top = \boldsymbol{F}_j \boldsymbol{\mu}_j^\top. \tag{5.52}$$

Site-dependent deformations significantly increase the computation time, so in the remainder of this chapter, we limit our treatment to homogenous deformations. This is the set of affine deformations [Hartshorne, 2010; Kadianakis and Travlopanos, 2016], composed entirely of linear transformations such as rotations, shear, and composite stretches. In this instance, the deformation matrix is the same for all emitters in the grid. To proceed further, we must consider specific parameterisations. In the following sub-sections, we consider different grid deformations and use the Hamiltonian approach to calculate the precision of detecting changes introduced to the grid. We first check that the formalism works for deformations with multiplicative parameterisations of the Hamiltonian, such as grid stretching and shearing, before considering the simplest non-multiplicative parameterisation resulting from grid rotations about any chosen axis.

5.2.1 Grid stretching and shearing deformations

We start by first considering the simplest grid deformation. The stretching shown in figure 5.2a stretches the grid by a factor α in the x-direction and factor β in the y-direction. Each source in

the grid is deformed according to the same deformation matrix described by

$$\boldsymbol{F}_{\text{stretch}} = \begin{pmatrix} \alpha & 0 \\ 0 & \beta \end{pmatrix}, \tag{5.53}$$

This is a multiplicative, bi-variate estimation scheme. We would like to determine how the QFI behaves with changing $\boldsymbol{\varphi} = (\alpha, \beta)$. Using Eq. (5.51) and Eq. (5.52), the 2×2 dimensional QFIM can be written as

$$\left[\mathcal{I}^{\mathrm{Q}}\right]_{kl} = \sum_{j=1}^{N_t} \frac{n_j^2 \mathcal{A}_{kl} \mu_{j_k} \mu_{j_l}}{s_{j_k} s_{j_l}}, \tag{5.54}$$

where we recall that n_j is the number of photons emitted by each source,

$$\mathcal{A}_{kl} = \frac{\delta_{kl}}{(1-r^2)} - (1-\delta_{kl})r \tag{5.55}$$

with $k, l \in \{\alpha, \beta\}$, and where we assumed each source has the same standard deviation in the ordered basis for the grid, $s_{j_x} = s_{j_y} = s$. We note that the only source dependence of the QFIM arises from the expected mean positions of the emitters. All other terms detail the properties of continuous variable Gaussian states for each source, and factorise out of the summation since we assume each source is IID, and are subject to the same deformation $\boldsymbol{F}$. This greatly simplifies the calculation of the QFIM, whose diagonal elements are illustrated in figure 5.3. We observe that the QFIM is independent of $\boldsymbol{\varphi}$, which is entirely a consequence of the multiplicative parameterisation of the Hamiltonian $\hat{\mathcal{H}}$. However, we are still able to maximise the sensitivity of the QFI by adjusting the grid configuration. To understand how, we provide an analytic expression for the diagonal elements

$$\left[\mathcal{I}^{\mathrm{Q}}\right]_{\alpha\alpha} = \frac{d_x^2 N_t (N^2-1)}{12 s^2 (1-r^2)}, \quad \left[\mathcal{I}^{\mathrm{Q}}\right]_{\beta\beta} = \frac{d_y^2 N_t (M^2-1)}{12 s^2 (1-r^2)}. \tag{5.56}$$

It is clear from this that maximising the sensitivity of the QFI is achieved by increasing the number of emitters along the same direction as the grid stretching is performed, for identical number of total sources, N_t. This is in agreement with results obtained in chapter 4. Further, we note that the QFI for α is effectively just the mirror image of the QFI for β, with the mapping $N \leftrightarrow M$, which can also be observed from the contour plots in figure 5.3. The ratio, $\mathscr{R}$, of the diagonal elements

$$\mathscr{R} = \left(\frac{d_x}{d_y}\right)^2 \frac{N^2-1}{M^2-1}, \tag{5.57}$$

provides a clear instructive guide for maximising either the QFI for α or for β, by controlling the grid configuration. To illustrate this, we plot the QCRB along the $N = M$ plane of the contour plots for the stretching deformation in figure 5.4.

The results discussed for composite grid stretching can immediately be applied to grid shearing, since they both parameterise the Hamiltonian with similar multiplicative factors. The composite grid shear illustrated in figure 5.2c, can be described by a shear in the horizontal

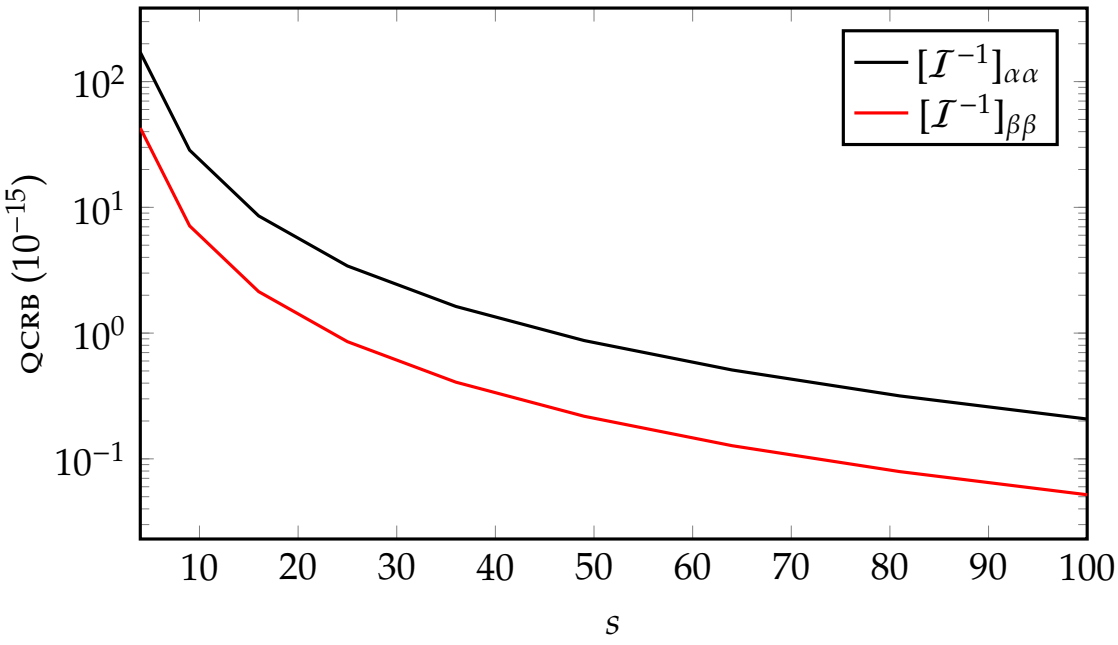

Figure 5.4: *Plot of the QCRB along the $N = M$ slice of the contour plots in figure 5.3. The black solid line illustrates the QCRB for α and the red dashed line for β. For a square grid, $N = M$, the relative difference between the estimate variances is accounted for by the fraction of source separations distances in the x and y directions, according to Eq. (5.57). Along this plane, we choose $d_x = 1$, $d_y = 2$ (and observe a constant factor 4 difference between the two lines).*

direction with factor ι and factor κ in the vertical direction. The deformation matrix for each source along the grid is then described by

$$\boldsymbol{F}_{\text{shear}} = \begin{pmatrix} 1 & \iota \\ \kappa & 1 \end{pmatrix}. \tag{5.58}$$

The generator of translations in $\boldsymbol{\varphi} = (\iota, \kappa)$ has the same form as that for the composite stretching, except for an interchange of basis. The consequence of this is that the QFI for ι is exactly that shown in figure 5.3b. Similarly, the QFI for κ is that shown in figure 5.3a.

5.2.2 Grid rotations

In this subsection, we consider the rotation map illustrated in figure 5.2b. For rotations in the counterclockwise direction, the expected position of each emitter transforms according to the deformation matrix

$$\boldsymbol{F}_{\text{rot}} = \begin{pmatrix} \cos(\vartheta) & -\sin(\vartheta) \\ \sin(\vartheta) & \cos(\vartheta) \end{pmatrix}. \tag{5.59}$$

The transformed expected emitter positions then satisfy the following properties: $\partial_\vartheta \tilde{u}_{j_x} = -u_{j_y}$ and $\partial_\vartheta \tilde{u}_{j_y} = u_{j_x}$. Estimating the rotation angle ϑ is a single parameter estimation protocol, only with a non-multiplicative factor in the Hamiltonian. Our expression for the QFIM written

in Eq. (5.51) accounts for this. From the properties of the transformed source positions, we calculate the QFI to be

$$\left[\mathcal{I}^{\mathcal{Q}}\right]_{\vartheta} = \sum_{j=1}^{N_T} \frac{n_j^2}{(1-r^2)} \left(\frac{u_{j_x}^2}{s_{j_y}^2} + \frac{u_{j_y}^2}{s_{j_x}^2} + \frac{2r u_{j_x} u_{j_y}}{s_{j_x} s_{j_y}} \right). \tag{5.60}$$

For consistency with the preceding subsection, we assume each source has the same standard deviation in the ordered basis of the grid, $s_{j_x} = s_{j_y} = s$. Then using the properties of the ceiling function and the modulo operation, we compute this sum to provide the following, more informative expression of the QFI,

$$\begin{aligned} \left[\mathcal{I}^{\mathcal{Q}}\right]_{\vartheta} = \frac{N_t}{12 s^2 (1-r^2)} \Big\{ & d_x^2 (N^2-1)[1 + r\sin(2\vartheta)] \\ & + d_y^2 (M^2-1)[1 - r\sin(2\vartheta)] \Big\}. \end{aligned} \tag{5.61}$$

From this form, we observe two contributions to the QFI for arbitrarily chosen grid configurations *and* source properties (specifically the correlation coefficient, r, and the covariance matrix). The first provides a constant offset of the QFI and may be enhanced by increasing the number of emitters in the grid in either direction. Alternatively, for the same number of emitters, N_t, the QFI may be enhanced by increasing the mutual source separation distances. The second contribution provides an oscillatory dependence of the QFI on ϑ, which emerges only when the following criteria are met

$$r \neq 0, \quad \text{and,} \quad d_x^2 (N^2-1) \neq d_y^2 (M^2-1). \tag{5.62}$$

The first requirement is on the source properties and the second on the grid configuration. Provided both criteria are met, then from Eq. (5.61) it is clear that the amplitude of the oscillatory behaviour may be enhanced by choosing a grid configuration with $N > M$ for positive r, and $N < M$ for negative r. The interplay between the requirements for a constant QFI can be clearly illustrated by the QCRB. From the inverse of Eq. (5.61), the QCRB is shown in figure 5.5. We note that if the requirements in Eq. (5.62) are not met, the QFI can be made independent of the rotation angle ϑ. The QCRB is then attainable without the use of adaptive strategies.

5.3 Discussions and summary

In this chapter, we have developed a framework for detecting deformations applied to arbitrarily sized grid of sources. This finds many important practical applications in engineering. Our formalism allows the detection of stresses and strains subjected to materials, which provides the ability to prevent fractures before they eventuate. By tracking changes to the expected source positions during an applied deformation, our work is an analogue of the source localisation problem. On the theoretical side, our formalism is the first to estimate the nature of deformations by use of quantum metrology, whilst maintaining full generality for unitary channels evolutions.

Our approach uses the quantum Fisher information as a figure of merit to estimate the type of deformation being administered to the grid. The sources comprising the undeformed grid are taken to be stationary, identical and independently distributed (IID) in a uniform manner with constant x-separation distance d_x, and y-separation d_y between neighbouring emitters. We model the jth source with a bi-normal spatial profile centred on $\boldsymbol{\mu}_j$. Any deformation exacted

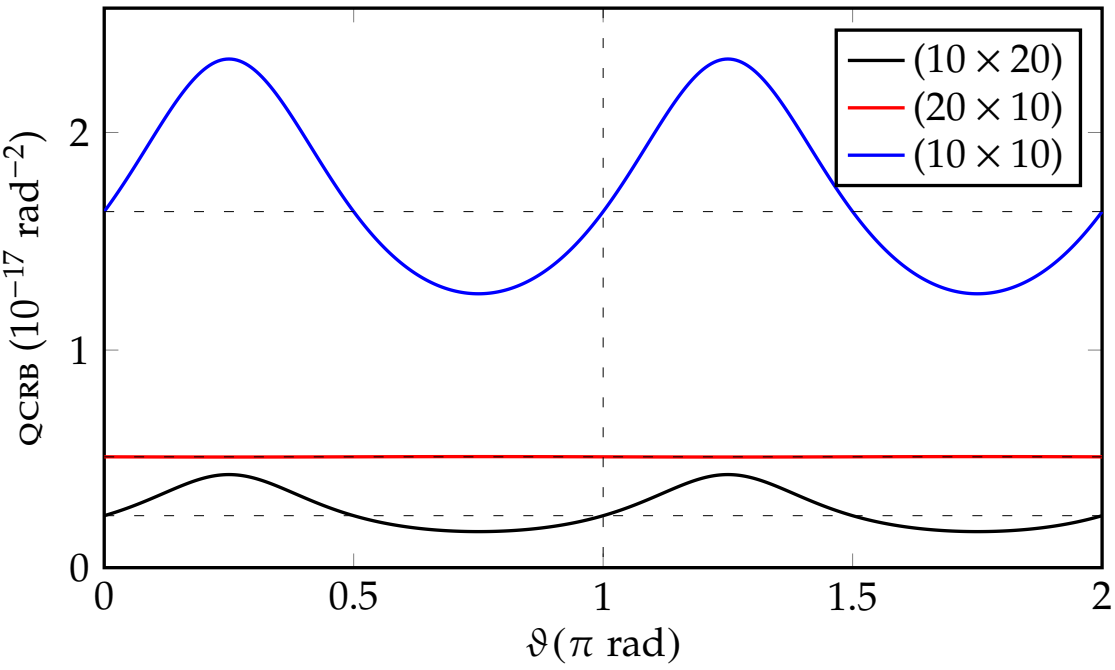

Figure 5.5: *The QCRB for a grid composed of $N_t = NM$ source configuration undergoing a rotation about the centre O, with $d_x = 1m$, $d_y = 2m$, correlation parameter $r = 0.5$, and, $s_{j_x} = s_{j_y} = s = 300nm$. We observe a greater precision of detecting the rotation as the number of sources in the grid increases. The amplitude of the oscillatory behaviour can be made more pronounced by re-arranging sources such that $N > M$ for positive r, and $N < M$ for negative r. Further, we note that since rotations form a homogeneous deformation about the grid centre, a period of π is observed in the variation of the QCRB.*

affects only the expected source positions and not their covariances. This is physically motivated, since the nature of the sources should not be altered in the process. Then, the application of general deformations on the initial grid can be viewed as a unitary process, with grid dynamics described by the Hamiltonian $\hat{\mathcal{H}}$. To ensure full generality, we allow the vector of parameters, $\boldsymbol{\varphi}$, that fully describes the applied deformation, to appear as arbitrary parameterisations of both the eigenvalues and eigenvectors of $\hat{\mathcal{H}}$. We solve for the local generator of translations in $\boldsymbol{\varphi}$, which is a generalisation of the result derived in [Pang and Brun, 2014] to multi-parameter quantum metrology.

For the grid metrology formalism presented here, only the eigenvalues of the Hamiltonian depend on the vector of parameters $\boldsymbol{\varphi}$, encoding information on the applied deformation. The generator describing dynamics in the parameters reduces to the set of commuting operators

$$\hat{G}_j = \sum_{k=1}^{N_t} \partial_j E_k \left|\boldsymbol{n}\right\rangle \left\langle \boldsymbol{n}\right| . \tag{5.63}$$

From this and the IID property of the sources—which permits each source to be treated in its individual Hilbert space—we derive the QFIM from generator co-variances. Our expression of the QFIM holds for any general grid deformation. We provide example applications to homogenous deformations, comprised of linear combinations of rotations, shearing, and, composite stretches.

For composite grid stretches and shears, the deformation parameterises the Hamiltonian with the multiplicative factors (α, β). Since the factor stretch in each direction is independent, the QFIM is diagonal. If a material is understood to be susceptible to fracture due to stretching along a specific direction, the sensitivity of QFI may be maximised by increasing the number of emitters along the direction in which the grid stretching eventuates, for an identical number of total emitters, N_t. The optimal grid configuration then becomes an array of sources, which is in agreement with results obtained in chapter 4, where the source optimisation problem was considered for enhancing estimates of source separation distances in stretched arrays.

We also considered non-multiplicative Hamiltonian parameterisations resulting from grid rotations about any chosen axis. We find that the QFI can be made independent of the rotation angle ϑ, if the following source properties and grid configuration requirements are met: $r = 0$ (zero correlation coefficient of the bi-normal spatial source distributions) and/or $d_x^2(N^2 - 1) = d_y^2(M^2 - 1)$. The QCRB is then attainable without the use of adaptive strategies. If both of the requirements are not met, an oscillatory dependence of the QFI surfaces. Although enhancing the amplitude of oscillations can enhance our estimate of ϑ, adaptive strategies may be required in general.

A natural extension of the work considered here would be to consider the QFI in the far-field. The need for spatially propagating the field was circumvented here by working in the near field of the sources. This would motivate more realistic models and lead to the concept of the quantum Fisher information over a subset in space. Additionally, our formalism provides the machinery for non-commuting generators, multi-parameters, and arbitrary parameterisations of the Hamiltonian. Since, the full extent of this formalism is not taken advantage of with quantum metrology of grid deformations, this would be fruitful future work.

CHAPTER 6

Optimal estimation of complex squeezing

All measurements that use optical fields as probes are subject to fundamental limits in their precision. This is due to the stochastic quantum indeterminacy in the phase and amplitude of the light field. Squeezed states have gained significant attention in quantum optics since they can surpass this precision limit in one quadrature at the expense of a concomitant increased uncertainty to the complementary quadrature. Besides this, squeezed light has become an essential ingredient to realise many other applications in quantum information processing and optical quantum computing. This includes improved detection sensitivities of weak forces such as gravitational waves and enhanced communication rates.

Applications of squeezed light require a certain level of squeezing to demonstrate advantages over classical alternatives. A natural question to ask then is: *given a squeezed probe, how can we be sure that its properties are commensurate with its intended application?* This can be answered by use of quantum state tomography. Alternatively, since we are only interested in the squeezing operations, we apply quantum estimation theory to provide complete characterisation of the amplitude and direction of squeezed states. Previous attempts in the literature to optimally estimate state squeezing have been limited to its magnitude [Chiribella et al., 2006a,b; Gaiba and Paris, 2009; Šafránek et al., 2015; Rigovacca et al., 2017]. However, a complete characterisation requires knowledge of the complex squeezing parameter ξ that parameterises the squeezing Hamiltonian. Few authors have calculated the QFI for complex squeezing [Pinel et al., 2013; Gao and Lee, 2014], but these research efforts did not address the measurements required to attain the fundamental precision bounds for complex squeezing.

In this chapter, we start by deriving the quantum Cramér-Rao bound of ξ for arbitrary single mode Gaussian states. We demonstrate that the optimal observables for both parameters obey a non-commutative nature that prohibits a simultaneous optimal measurement-even in the asymptotic limit. This is a true multi-parameter quantum estimation of incompatible observables, which is the defining contrast from the work completed in the preceding chapter. Within these constraints we find the quantum optimal estimators for individual measurements of both parameters and discuss its physical implementation.

6.1 Single mode Gaussian state model

Gaussian states have found many uses in quantum information processing and quantum metrology. Examples include enhanced resolutions in interferometry, quantum teleportation [Wang et al., 2007], and cryptography [Zhou et al., 2018]. A particularly pleasing feature of Gaussian states is that their description and kinematics can be completely characterised theoretically [Adesso et al., 2014]. Specifically this class of states can be written in terms of Gaussian unitaries operating on some initial Gaussian state ρ_{in}. For pure states $\rho_{\text{in}} = |0\rangle\langle 0|$, while for mixed states it is the thermal state:

$$\rho_{\text{th}} = \sum_{n=0}^{\infty} \frac{\overline{n}^n}{(1+\overline{n})^{1+n}} |n\rangle\langle n| , \tag{6.1}$$

where $\overline{n} = \langle \hat{n} \rangle$ is the expectation of the photon number $\hat{n}$. Thermal radiation exhibits a Gaussian characteristic function with zero mean $\boldsymbol{\lambda}_{\text{th}} = \mathbf{0}$ and covariance matrix $\boldsymbol{\Sigma}_{\text{th}} = (2\overline{n}+1)\mathbb{1}$. For the following discussion we focus on mixed Gaussian probes, though a discussion of pure Gaussian states follows suit.

Any arbitrary single mode Gaussian state can be written in terms of the state [Weedbrook et al., 2012]:

$$\rho_{\text{G}} = \hat{R}_\Theta \hat{S}_\epsilon \hat{D}_\alpha \rho_{\text{th}} \hat{D}_\alpha^\dagger \hat{S}_\epsilon^\dagger \hat{R}_\Theta^\dagger = \hat{U} \rho_{\text{th}} \hat{U}^\dagger, \tag{6.2}$$

where the set Gaussian unitaries

$$\hat{D}_\alpha = \exp\left[\alpha \hat{a}^\dagger - \alpha^* \hat{a}\right], \tag{6.3}$$

$$\hat{S}_\epsilon = \exp\left[\frac{1}{2}(\epsilon^* \hat{a}^2 - \epsilon \hat{a}^{\dagger 2})\right], \tag{6.4}$$

$$\hat{R}_\Theta = \exp\left[-i\Theta\hat{n}\right], \tag{6.5}$$

are defined as the displacement operator, single mode squeezing operator, and phase operator respectively. The identities $\hat{S}_\epsilon^\dagger = \hat{S}_{-\epsilon} = \hat{S}_\epsilon^{-1}$ will prove useful for later. We reiterate that the description of ρ_{G} is completely general, since the ordering of Gaussian unitary operations on the thermal state is a convention. For example, the ordering of a displacement and squeezing operations can be reversed according to

$$\hat{D}_\alpha \hat{S}_\epsilon = \hat{S}_\epsilon \hat{D}_\gamma, \tag{6.6}$$

with $\gamma = \alpha \cosh r_\epsilon - \alpha^* \exp[i\vartheta_\epsilon] \sinh r_\epsilon$. States described by Eq. (6.2) are readily prepared in laboratories and their unitary evolutions realised by use of lasers and atomic ensembles [Ferraro et al., 2005].

For a general Gaussian probe state, we characterise the squeezing operation parameters. This requires estimating the squeezing parameter $\xi = \xi_{\text{I}} + i\xi_{\text{R}} = r\exp[i\vartheta]$, where r indicates the amplitude of squeezing and ϑ the phase. This is a bivariate estimation problem $\boldsymbol{\varphi} = (r, \vartheta)$. We start by considering the following probe state evolution

$$\rho(\boldsymbol{\varphi}) = \hat{S}_\xi \rho_{\text{G}} \hat{S}_\xi^\dagger, \tag{6.7}$$

which is illustrated in figure 6.1. Using this probe description, we determine the fundamental bound to the estimate variance in ξ and determine the measurement strategy that minimises it.

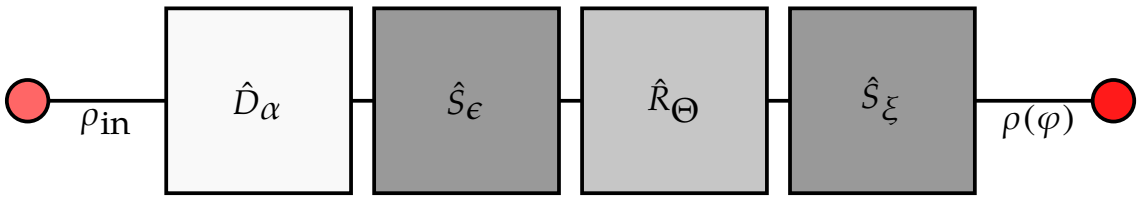

Figure 6.1: *Description of the general Gaussian state in phase space $\rho(\boldsymbol{\varphi})$ used in this work. The final state can be decomposed in terms of the Gaussian unitaries $\hat{V} = \hat{S}_\xi \hat{R}_\Theta \hat{S}_\epsilon \hat{D}_\alpha$, such that $\rho(\boldsymbol{\varphi}) = \hat{V}\rho_{in}\hat{V}^\dagger$. We fully characterise the squeezing ξ of the evolved prove state. Each unitary is represented as a black box in this work. For experimental implementation and applications of each of these Gaussian unitary, we refer the reader to references Carolan et al. [2015]; Andersen et al. [2016]. In this chapter, we consider pure and mixed single mode Gaussian states, which are generated when the input state is the vacuum $|0\rangle\langle 0|$ or the thermal state ρ_{th}, respectively.*

Note that we are not performing state tomography by estimating the squeezing parameter ϵ, but instead we are interested in estimating the applied squeezing ξ.

To calculate the QCRB for $\boldsymbol{\varphi}$ in the Hamiltonian formulation, we require a description of the probe state. Defining

$$\hat{V} = \hat{S}_\xi \hat{R}_\Theta \hat{S}_\epsilon \hat{D}_\alpha, \tag{6.8}$$

such that $\hat{V}^\dagger\hat{V} = \hat{V}\hat{V}^\dagger = \mathbb{1}$, then Eq. (6.7) can be written in the basis $\{p_k, \hat{V}|p_k\rangle\}$ as:

$$\rho(\boldsymbol{\varphi}) = \sum_{n=0}^{\infty} \frac{\overline{n}^n}{(1+\overline{n})^{1+n}} \hat{V}|n\rangle\langle n|\hat{V}^\dagger, \tag{6.9}$$

where $\{p_k, |p_k\rangle\}$ defines the spectral decomposition of the thermal state in the Fock space. This transformation of the probe can be described by a similarity transformation of the thermal state bosonic mode operators $\hat{\boldsymbol{a}}$. In the Heisenberg picture, this corresponds to the linear unitary Bogoliubov transformations of the form

$$\hat{V}^\dagger \hat{a} \hat{V} = \mathcal{A}\hat{a}^\dagger + \mathcal{B}\hat{a} + C \tag{6.10}$$

where the complex numbers $\{\mathcal{A}, \mathcal{B}, C\} \in \mathbb{C}$ are defined by:

$$\begin{aligned}
\mathcal{A} &= -\left(e^{i(\vartheta_\epsilon - \Theta)} \cosh r \sinh r_\epsilon + e^{i(\vartheta+\Theta)} \cosh r_\epsilon \sinh r\right), \\
\mathcal{B} &= e^{-i\Theta} \cosh r \cosh r_\epsilon + e^{i(\vartheta+\Theta-\vartheta_\epsilon)} \sinh r \sinh r_\epsilon, \\
C &= \alpha\mathcal{B} + \alpha^*\mathcal{A},
\end{aligned} \tag{6.11}$$

We can use this similarity transformation to determine the SLD and the QCRB for $\boldsymbol{\varphi}$. However, since Gaussian states are conveniently described using a phase space description, it is also appropriate to describe the state $\rho(\boldsymbol{\varphi})$ in terms of its moments. Unitary transformations on a Hilbert space map to real symplectic transformations of the first and second moments of a state in phase space. Hence, we write the first and second moments of the evolved probe as

$$\boldsymbol{\lambda} = \boldsymbol{S}(\boldsymbol{\lambda}_{\text{th}} + \boldsymbol{d}_\alpha) = \boldsymbol{S}\boldsymbol{d}_\alpha, \tag{6.12}$$

$$\boldsymbol{\Sigma} = \boldsymbol{S}\boldsymbol{\Sigma}_{\text{th}}\boldsymbol{S}^\top = (2\overline{n}+1)\boldsymbol{S}\boldsymbol{S}^\top, \tag{6.13}$$

respectively, where the moments of the thermal state were defined earlier, $\boldsymbol{d}_\alpha = (q, p)^\top$, and where we have defined $\boldsymbol{S} = \boldsymbol{S}_\xi \boldsymbol{R}_\Theta \boldsymbol{S}_\epsilon$ as the total symplectic transformation of the quadrature field operators $\boldsymbol{R}$, with [Weedbrook et al., 2012]

$$\begin{aligned} \boldsymbol{S}_\xi &= \cosh r \mathbb{1} - \sinh r \begin{pmatrix} \cos\vartheta & \sin\vartheta \\ \sin\vartheta & -\cos\vartheta \end{pmatrix}, \\ \boldsymbol{R}_\Theta &= \begin{pmatrix} \cos\Theta & \sin\Theta \\ -\sin\Theta & \cos\Theta \end{pmatrix}. \end{aligned} \tag{6.14}$$

These symplectic matrices transform the operators $\hat{\boldsymbol{R}}$ corresponding to the action of V on the initial thermal state. We will use this formalism to address the optimal measurement strategy that saturates the QCRB in section 6.4.

6.2 Single mode squeezing generators

In this section, we derive the generators of translations for a squeezing operation. These generators will be used to determine the QFI in the next section. Also, this serves as a good exercise since many of the difficulties for optimal measurements can be pre-empted by simply examining the properties of these generators.

Recall from chapter 5 that elements of the generator of translations are given by the following integral equation representation [Wilcox, 1967; Pang and Brun, 2014; Sidhu and Kok, 2018]

$$\hat{\mathcal{G}}_j = \int_0^1 \mathrm{d}\alpha \exp\left[-i\alpha\hat{\mathcal{H}}\right]\left(\partial_j\hat{\mathcal{H}}\right)\exp\left[i\alpha\hat{\mathcal{H}}\right]. \tag{6.15}$$

The Baker-Campbell-Hausdorff (BCH) identity can be used to write the generator $\hat{\mathcal{G}}_j$ as the following infinite series (see Eq. (5.13))

$$\hat{\mathcal{G}}_j = \partial_j\hat{\mathcal{H}} - \frac{i}{2!}\left[\hat{\mathcal{H}}, \partial_j\hat{\mathcal{H}}\right] - \frac{1}{3!}\left[\hat{\mathcal{H}}, \left[\hat{\mathcal{H}}, \partial_j\hat{\mathcal{H}}\right]\right] + \ldots = \sum_{n=0}^{\infty}\frac{(-i)^n}{(n+1)!}C^{(n)}_{\hat{\mathcal{H}}}\left(\partial_j\hat{\mathcal{H}}\right), \tag{6.16}$$

where $C^{(n)}_{\hat{B}}(\hat{A})$ is the nth–order nested commutator of $\hat{A}$ and $\hat{B}$. The action of a single mode squeezer can be analysed as an evolution with the Hamiltonian

$$\begin{aligned} \hat{\mathcal{H}} &= \frac{i}{2}\left(\xi^*\hat{a}^2 - \xi\hat{a}^{\dagger 2}\right) \\ &= r\left[\sin(\vartheta)\left(\hat{q}^2 - \hat{p}^2\right) - \cos(\vartheta)\left\{\hat{q}, \hat{p}\right\}\right], \end{aligned} \tag{6.17}$$

where the second form is parameterised in terms of the canonical position $\hat{q}$ and momentum $\hat{p}$ quadrature operators. From Eq. (6.16) we can find the generator of translations for the squeezing parameters $\boldsymbol{\varphi}$. We find (see appendix F)

$$\hat{\mathcal{G}}_r(\vartheta) = \frac{i}{2}\left(e^{-i\vartheta}\hat{a}^2 - e^{i\vartheta}\hat{a}^{\dagger 2}\right), \tag{6.18}$$

$$\hat{\mathcal{G}}_\vartheta(r, \vartheta) = \alpha\left(\hat{n} + \frac{1}{2}\right) + \frac{\beta}{2}\left(e^{-i\vartheta}\hat{a}^2 + e^{i\vartheta}\hat{a}^{\dagger 2}\right), \tag{6.19}$$

with $\alpha, \beta \in \mathbb{R}$ defined by

$$\begin{aligned} \alpha &= \frac{1}{2}\left(\cosh\left[2r\right] - 1\right), \\ \beta &= \frac{1}{2}\sinh\left[2r\right]. \end{aligned} \tag{6.20}$$

These are real constants that depend only on the magnitude of squeezing. Note that the generator for the squeezing amplitude r could have been readily obtained from $i[\partial_j \hat{U}(\boldsymbol{\varphi})]\hat{U}^\dagger(\boldsymbol{\varphi})$ since it provides a multiplicative factor to the squeezing Hamiltonian. This is not true for the generator for ϑ, since it parameterises the Hamiltonian (6.17) with oscillatory dependence. This explains the indicated dependence of each generator on the parameters in Eq. (6.18) and Eq. (6.19). The generator (6.18) is consistent with the result in Chiribella et al. [2006b] for $\vartheta = 0$. The generator of the directional parameter is interesting; it contains the conjugate number operator as expected, but with an additional squeezing term that specifies the amount and direction of the squeezing. The commutation of both generators,

$$\left[\hat{\mathcal{G}}_r, \hat{\mathcal{G}}_\vartheta\right] = 2i\beta\left(\hat{n} + \frac{1}{2}\right) + i\alpha\left(e^{-i\vartheta}\hat{a}^2 + e^{i\vartheta}\hat{a}^{\dagger 2}\right), \tag{6.21}$$

is zero only in the trivial case of no squeezing. This non-commutativity extends to the SLD, which suggests that for some $\xi \neq 0$, we should anticipate non-commuting SLDs. This implies that there is no common eigenbasis that permits simultaneous optimal measurements of r and ϑ. We will observe this in more detail in subsection 6.4.

6.3 Precision bounds for squeezing in Gaussian probes

In the following section, we turn our attention to finding the fundamental bounds to the precision of estimating $\boldsymbol{\varphi}$. We start by writing the 2×2 QFIM as:

$$\boldsymbol{\mathcal{I}}^{Q}(\boldsymbol{\varphi}) = \begin{pmatrix} \mathcal{I}^{Q}_{rr} & \mathcal{I}^{Q}_{r\vartheta} \\ \mathcal{I}^{Q}_{\vartheta r} & \mathcal{I}^{Q}_{\vartheta\vartheta} \end{pmatrix}. \tag{6.22}$$

This is a symmetric real matrix: $\mathcal{I}^{Q}_{r\vartheta} = \mathcal{I}^{Q}_{\vartheta r}$. Determining the QFIM then reduces to finding three quantities. All these terms can be determined through the Hamiltonian formalism, or equivalently through the SLD formalism. Since we have presented the generators of local translations in $\boldsymbol{\varphi}$ in Eq. (6.18) and Eq. (6.19), we use them to determine the QFIM in this section. We can then define the precision bounds for the amplitude and direction of squeezing in single mode Gaussian probe states described in section 6.1.

The first quantity we want to calculate is the QFI for the real squeezing parameter. For the evolved probe state $\rho(\boldsymbol{\varphi})$ defined in Eq. (6.9), the eigenvalues

$$p_j = \frac{\overline{n}^j}{(\overline{n}+1)^{j+1}}, \tag{6.23}$$

for integer j, do not depend on the estimation parameters $\boldsymbol{\varphi}$. Hence, the only contribution to the QFI comes from the eigenvectors. Combining Eq. (6.19) with the multi-parameter QFI in

Eq. (3.53) from chapter 3, and using the commutator $[\hat{a}, \hat{a}^\dagger] = 1$ to normal order all operator terms, we obtain the following expression for the QFI for the magnitude of squeezing:

$$\begin{aligned}\mathcal{I}^Q_{rr} = &\sum_j p_j \left(2\left\langle \hat{a}^{\dagger 2}\hat{a}^2\right\rangle_{jj} + 4\left\langle \hat{a}^\dagger\hat{a}\right\rangle_{jj} + 2 - e^{-2i\vartheta}\left\langle \hat{a}^4\right\rangle_{jj} - e^{2i\vartheta}\left\langle \hat{a}^{\dagger 4}\right\rangle_{jj}\right) \\ &- \sum_{j,k}\frac{2p_jp_k}{p_j+p_k}\left|e^{-i\vartheta}\left\langle a^2\right\rangle_{jk} - e^{i\vartheta}\left\langle \hat{a}^{\dagger 2}\right\rangle_{jk}\right|^2,\end{aligned} \tag{6.24}$$

with $j, k = 0, 1, 2, \ldots$, and where the expectation values are performed on the eigenspace of the evolved state described by Eq. (6.9). Specifically, the expectation of any arbitrary operator $\hat{A}$ is written $\langle\hat{A}\rangle_{jk} = \langle p_j|\hat{A}|p_k\rangle = \langle n_j|\hat{V}^\dagger\hat{A}\hat{V}|n_k\rangle$. Similarly, we can calculate the remaining elements of the QFIM.

The normally ordered form of the QFI for the direction parameter of squeezing ϑ is written:

$$\begin{aligned}\mathcal{I}^Q_{\vartheta\vartheta} = 4\sum_j p_j\Bigg\{&\left\langle \hat{a}^{\dagger 2}\hat{a}^2\right\rangle_{jj}\left(\alpha^2+\frac{\beta^2}{2}\right) + \left\langle \hat{a}^\dagger\hat{a}\right\rangle_{jj}\left(2\alpha^2+\beta^2\right) + 2\mathrm{Re}\left[\alpha\beta e^{i\vartheta}\left\langle \hat{a}^{\dagger 3}\hat{a}\right\rangle_{jj}\right] \\ &+ 3\mathrm{Re}\left[\alpha\beta e^{i\vartheta}\left\langle \hat{a}^{\dagger 2}\right\rangle_{jj}\right] + \frac{1}{2}\mathrm{Re}\left[\beta^2 e^{2i\vartheta}\left\langle \hat{a}^{\dagger 4}\right\rangle_{jj}\right] + \left(\frac{\alpha^2}{4}+\frac{\beta^2}{2}\right)\Bigg\} \\ &- \sum_{j,k}\frac{8p_jp_k}{p_j+p_k}\left|\alpha\left(\left\langle \hat{a}^\dagger\hat{a}\right\rangle_{jk} + \frac{\delta_{jk}}{2}\right) + \frac{\beta}{2}\left(e^{-i\vartheta}\left\langle \hat{a}^2\right\rangle_{jk} + e^{i\vartheta}\left\langle \hat{a}^{\dagger 2}\right\rangle_{jk}\right)\right|^2,\end{aligned} \tag{6.25}$$

where $2\mathrm{Re}[t] = t + t^*$ defines the real element of any complex number t. For completeness, the normally ordered form for the off-diagonal elements of the QFIM is written

$$\begin{aligned}\mathcal{I}^Q_{r\vartheta} = &4\sum_j p_j\left\{\alpha\mathrm{Im}\left[e^{i\vartheta}\left(\frac{3}{2}\left\langle \hat{a}^{\dagger 2}\right\rangle_{jj} + \left\langle \hat{a}^{\dagger 3}\hat{a}\right\rangle_{jj}\right)\right] + \frac{\beta}{2}\mathrm{Im}\left[e^{2i\vartheta}\left\langle \hat{a}^{\dagger 4}\right\rangle_{jj}\right]\right\} \\ &- i\sum_{j,k}\frac{4p_jp_k}{p_j+p_k}\left(e^{-i\vartheta}\left\langle \hat{a}^2\right\rangle_{jk} - e^{i\vartheta}\left\langle \hat{a}^{\dagger 2}\right\rangle_{jk}\right)\left(\alpha\left[\left\langle \hat{a}^\dagger\hat{a}\right\rangle_{kj} + \frac{\delta_{kj}}{2}\right] + \frac{\beta}{2}\left[e^{-i\vartheta}\left\langle \hat{a}^2\right\rangle_{kj} + e^{i\vartheta}\left\langle \hat{a}^{\dagger 2}\right\rangle_{kj}\right]\right),\end{aligned} \tag{6.26}$$

where $2\mathrm{Im}[t] = t - t^*$. To determine these three information elements, we are required to determine the expectation values of products of normally ordered bosonic mode operators. We evaluate these terms by using the Bogoliubov transformation, which we write again for convenience:

$$\hat{V}^\dagger\hat{a}\hat{V} = \mathcal{A}\hat{a}^\dagger + \mathcal{B}\hat{a} + C, \tag{6.27}$$

with $\{\mathcal{A}, \mathcal{B}, C\} \in \mathbb{C}$ defined in Eq. (6.11), and through repeated use of $\hat{V}^\dagger\hat{V} = \mathbb{1}$. A complete list of all expectation values for this calculation can be see in appendix F. The resulting terms are lengthy and consequently we do not write the QFI elements explicitly.

The QFIM (6.22) is non-singular, implying that we can readily determine the QCRB. Assuming that we have access to the probe state $\rho(\boldsymbol{\varphi})$ (which we assume is known exactly), we are now in a position to define the fundamental precision bound to the estimates of the magnitude and direction of the squeezing applied to this state. In figure 6.2, we plot the diagonal elements of the QCRB as a function of conjugate parameters r and ϑ. Interestingly, we clearly observe white

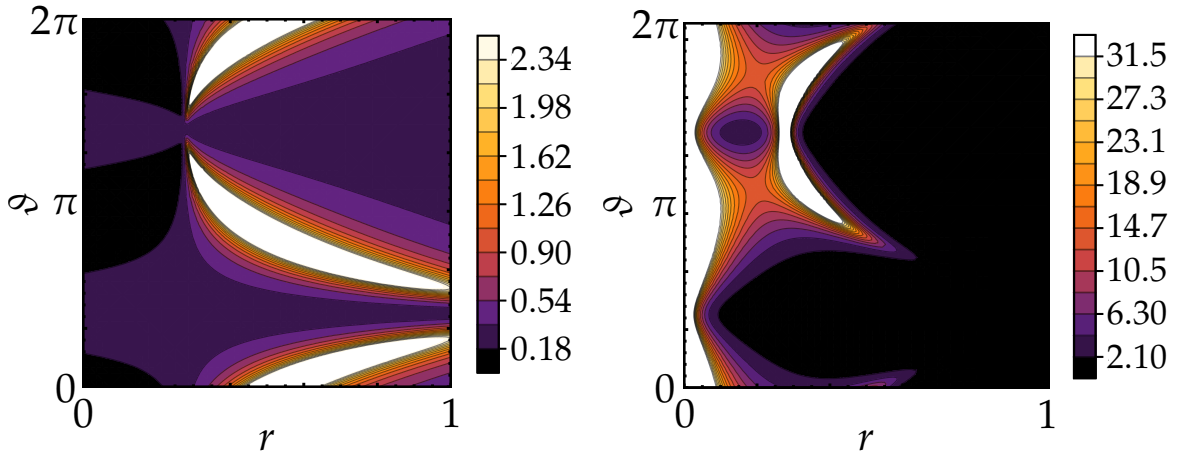

(a) $\mathcal{I}_{rr}^{-1}$ (b) $\mathcal{I}_{\vartheta\vartheta}^{-1}$.

Figure 6.2: *Precision bounds for the estimation of squeezing in the Gaussian probe state $\rho(\boldsymbol{\varphi})$ in phase space, as a function of r (x-axis) and ϑ (y-axis). Figure 6.2a illustrates the QCRB for the amplitude parameter and figure 6.2b for the angle of squeezing. The numerical value of the QCRB exhibits strong dependence on the probe state. For this plot, the free parameters that encode the state are chosen to have the values $r_\epsilon = 0.78, \vartheta_\epsilon = \pi, \alpha = 1, \Theta = 0.8\pi, \overline{n} = 1$. The observed white regions correspond to values of $\boldsymbol{\varphi}$ which generates large variances and should be avoided. Note that saturating the QCRB for the magnitude of squeezing does not require large r. The plot on the right illustrates the minimum squeezing required for optimal directional information on the squeezing.*

regions that correspond to values of ξ that generate large estimate variances. We also note that there is no obvious value of ξ that minimises the estimate variances in both parameters simultaneously. From this feature alone, we expect that simultaneous optimal measurements for both parameters is not possible. We explicitly demonstrate this later. The parameter covariance is not zero and non-negligible, implying that both parameters are correlated. This mutual dependence can be clearly detected in figure 6.2.

For an experimental characterisation of squeezed probe states through an estimation approach, we naturally want the procedure to saturate these precision bounds. Finding the form of these *optimal measurements* is the aim for the next section.

6.4 Optimal measurements of complex squeezing

Optimal estimation of real squeezing was considered by Chiribella et al. [2006b]. The optimal observable requires an optimisation step that depends on the choice of probe. Displaced squeezed states were reported to achieve the smallest estimation variance with homodyne measurements providing an optimal strategy. In this section, we explore how the optimal strategy changes when we additionally estimate the imaginary squeezing component. We start by exploring the estimation strategy for the probe state $\rho(\boldsymbol{\varphi})$ introduced earlier, before focussing on specific pure and mixed Gaussian states.

The QCRB for each parameter may be achieved by performing measurements in the eigenbasis of the SLD operator, if its eigenvectors are locally independent of the parameter [Braunstein and

Caves, 1994; Braunstein et al., 1996]. The optimal quantum estimator that saturates the QCRB for φ_j is given by

$$\hat{O}(\varphi_j) = \varphi_j \mathbb{1} + \left[\left(\boldsymbol{\mathcal{I}}^{Q} \right)^{-1} \hat{\boldsymbol{\mathcal{L}}} \right]_j , \tag{6.28}$$

which is a projective measurement onto the eigenstates of the SLD [Paris, 2009]. The first term leads to the average estimate and the second the smallest covariance of the optimal measurement. The optimal measurement is therefore achieved by measuring in the eigenbasis of the SLD.

The traditional method for finding the SLD operator is to expand it in the eigenspace of density matrix. Defining the spectral decomposition of the evolved thermal probe state, $\rho(\boldsymbol{\varphi}) = \hat{V} \rho_{\text{th}} \hat{V}^{\dagger}$, with the set $\{p_j, |p_j\rangle\}$, the SLD takes the form

$$\left[\hat{\mathcal{L}}_j \right]_{mn} = \frac{2(\partial_j p_m)\delta_{mn}}{p_m + p_n} + \frac{2(p_m - p_n)\langle \partial_j p_m | p_n \rangle}{p_m + p_n}, \tag{6.29}$$

where $m, n \in \{1, 2, \ldots, s\}$, and $p_m + p_n \neq 0$. We saw in the previous chapter that we can rewrite this in terms of the local generator in φ_j, according to:

$$\left[\hat{\mathcal{L}}_j \right]_{mn} = \frac{2i(p_m - p_n)\langle p_m | \hat{V}^{\dagger} \hat{\mathcal{G}}_j \hat{V} | p_n \rangle}{p_m + p_n}, \tag{6.30}$$

which is Hermitian. This formulation of the SLD requires knowledge of both the generators and the spectral decomposition of the probe state, which are known.

Before investigating optimal measurements, we draw attention to the general non commutative structure of the SLD for each estimation parameter $[\hat{\mathcal{L}}_r, \hat{\mathcal{L}}_\vartheta] \neq 0$. The absence of a simultaneous eigenbasis for both operators rules out the possibility of simultaneously measuring in the eigenbases of the SLDs to achieve a simultaneously optimal estimate of complex squeezing in phase space. Additionally, there is no collective measurement that attains the QCRB asymptotically since $\langle [\hat{\mathcal{L}}_r, \hat{\mathcal{L}}_\vartheta] \rangle \neq 0$. The best option is to address the individual optimal measurement scheme for the indirect estimation of $\boldsymbol{\varphi}$. This is the objective in this section, where we consider specific pure and mixed single mode Gaussian states.

6.4.1 Pure state models

We start by considering single mode pure Gaussian states. This class of states closely models mixed states since the QFIM exhibits a convex property. Specifically, if we denote $\mathcal{I}$ as the set of achievable QFIMs, convexity entails that for any $I \in \mathcal{I}$ and $I' \in \mathcal{I}$, we know that $pI + (1-p)I' \in \mathcal{I}$ for all $0 \leq p \leq 1$.

Consider a rotated coherent state as the input probe such that such that the evolved state is written:

$$|\psi(\boldsymbol{\varphi})\rangle = \hat{S}_\xi |\psi(\mathbf{0})\rangle_{\text{in}} = \hat{S}_\xi \hat{R}_\Theta \hat{D}_\alpha |0\rangle , \tag{6.31}$$

This state is equivalent to the mixed state (6.9) with $\epsilon = 0$ and $p_n = 0$ for all $n \neq 0$. The QFIM for the squeezing parameters as a function of r and ϑ has the same dependency as that illustrated in figure 6.2. We argued in section 6.3 that this prohibited simultaneous optimal estimates variances for both parameters. To demonstrate this precisely, we now work in the SLD formalism since it is better suited to addressing this line of examination.

The SLD for a pure state is well known and is written $\hat{\mathcal{L}}_j = 2\partial_j \rho$ [Paris, 2009]. This form is sufficient to determine the commutator of the SLD for each parameter, but is not in a convenient form to describe the optimal measurement scheme. Instead, we express the operator as

$$\hat{\mathcal{L}}_j = 2\hat{\tilde{\mathcal{G}}}_j = 2\left(\hat{\mathcal{G}}_j - \left\langle \hat{\mathcal{G}}_j \right\rangle\right), \tag{6.32}$$

where the expectation value is with respect to the pure state (6.31). Note that the SLD is suitably Hermitian with zero trace. From the generators defined in Eq. (6.18) and Eq. (6.19), we have the following SLDs for complex squeezing

$$\begin{aligned} \hat{\mathcal{L}}_r(r) &= ie^{-i\vartheta}\hat{a}^2 - ie^{i\vartheta}\hat{a}^{\dagger 2} - 2\langle \hat{\mathcal{G}}_r \rangle, \\ \hat{\mathcal{L}}_\vartheta(r,\vartheta) &= \beta e^{-i\vartheta}\hat{a}^2 + \beta e^{i\vartheta}\hat{a}^{\dagger 2} + 2\alpha\hat{a}^\dagger\hat{a} + (\alpha - \langle \hat{\mathcal{G}}_\vartheta \rangle), \end{aligned} \tag{6.33}$$

where we recall that α and β are real constants defined in Eq. (6.20). Note that the SLD for amplitude squeezing depends on only its conjugate parameter, while the SLD for directional squeezing depends on both parameters. This is purely a consequence of how $\boldsymbol{\varphi}$ parameterises the Hamiltonian (6.17). The operators in Eq. (6.33) do not commute:

$$\left[\hat{\mathcal{L}}_r, \hat{\mathcal{L}}_\vartheta\right] = 4i\alpha\left(\exp\left[-i\vartheta\right]\hat{a}^2 + \exp\left[i\vartheta\right]\hat{a}^{\dagger 2}\right) \neq 0. \tag{6.34}$$

Since simultaneous optimal measurements are not possible, we attempt to find separable optimal measurements for r and ϑ separately. The optimal observable is determined from the second term in Eq. (6.28):

$$\hat{\boldsymbol{O}} = \left(\boldsymbol{\mathcal{I}}^{\mathrm{Q}}\right)^{-1}\hat{\boldsymbol{\mathcal{L}}}, \tag{6.35}$$

where we have defined $\hat{\boldsymbol{O}} = (\hat{O}_r, \hat{O}_\vartheta)^\top$ and $\hat{\boldsymbol{\mathcal{L}}} = (\hat{\mathcal{L}}_r, \hat{\mathcal{L}}_\vartheta)^\top$ for squeezing estimates. Through numerical values, the off-diagonal elements of the QFIM are not negligible when compared with the diagonal elements. This implies that the optimal observable for any one of the parameters depends on the SLD basis for both parameters.

Given the length of the expression for $\hat{\boldsymbol{O}}$, we do not write its specific form. However, to address the optimal measurement strategies, this is not necessary. Specifically, if we can describe a particular measurement strategy that reproduces the form of $\hat{O}_r$ then we are able to report an optimal implementation. Focussing on estimating the amplitude of squeezing, from Eq. (6.35) we write

$$\hat{O}_r = l_1 + l_2\hat{n} + l_3\hat{a}^{\dagger 2} + l_3^*\hat{a}^2, \tag{6.36}$$

where we have introduced the complex coefficients

$$l_1 = \left(\alpha - \langle \hat{\mathcal{G}}_\vartheta \rangle\right)[(\boldsymbol{\mathcal{I}}^{\mathrm{Q}})^{-1}]_{r\vartheta} - 2\langle \hat{\mathcal{G}}_r \rangle[(\boldsymbol{\mathcal{I}}^{\mathrm{Q}})^{-1}]_{rr}, \tag{6.37}$$

$$l_2 = 2\alpha[(\boldsymbol{\mathcal{I}}^{\mathrm{Q}})^{-1}]_{r\vartheta}, \tag{6.38}$$

$$l_3 = e^{i\vartheta}\left(\beta[(\boldsymbol{\mathcal{I}}^{\mathrm{Q}})^{-1}]_{r\vartheta} - i[(\boldsymbol{\mathcal{I}}^{\mathrm{Q}})^{-1}]_{rr}\right), \tag{6.39}$$

for further brevity, and where $[(\boldsymbol{\mathcal{I}}^{\mathrm{Q}})^{-1}]_{jk}$ denotes the element of the complex, symmetric QCRB in row j and column k. Our intention now is to find a measurement strategy that has the same form as Eq. (6.36).

Intensity measurements are a basic tool of quantum optics experiments. In general this can be implemented via correlated intensity measurements. However, since we have a single mode, we try writing the optimal observable as a photon counting measurement of some mode $\hat{b}$. Since we are trying to estimate the squeezing elements, an instinctive approach to realise the observable (6.36) is to apply a 'reverse' squeezer. Physically, the squeezed characteristics of an evolved state can be deduced by finding the values for ξ' that generates the original probe state. Hence, we investigate whether the optimal observable can be reproduced by applying a squeezer $\hat{S}_{\xi'}$ and then conducting intensity measurements. Specifically, this is described by

$$\begin{aligned}\hat{b}^\dagger\hat{b} &= \hat{S}^\dagger_{\xi'}\hat{a}^\dagger\hat{S}_{\xi'}\hat{S}^\dagger_{\xi'}\hat{a}\hat{S}_{\xi'} \\ &= \left(\cosh[r']^2 + \sinh[r']^2\right)\hat{a}^\dagger\hat{a} + e^{i\vartheta'}\cosh[r']\sinh[r']\hat{a}^{\dagger 2} \\ &\quad + e^{-i\vartheta'}\cosh[r']\sinh[r']\hat{a}^2 + \sinh[r']^2,\end{aligned} \tag{6.40}$$

where we have used the Bogolioubov transformation of the mode operators under a single mode squeezing operation

$$\hat{S}^\dagger_{\xi'}\hat{a}\hat{S}_{\xi'} = \cosh[r']\hat{a} + e^{i\vartheta'}\sinh[r']\hat{a}^\dagger, \tag{6.41}$$

and have expressed the result in normal order. The primed parameters are tuneable parameters of the squeezing operation. For this strategy to be optimal, we are required to determine the coefficients l_j for $j \in \{1,2,3\}$. Clearly this is underdetermined, which suggests that classical post-processing is additionally required. Any processing function of the experimental data is permitted, since this does not change the physical implementation. We choose to take the function: $\gamma\hat{b}^\dagger\hat{b}$. Taking this form and comparing coefficients with the optimal observable that we found in Eq. (6.36), we find that a reverse squeezer followed with intensity measurements is an optimal strategy if:

$$e^{2r'} = \frac{2\sqrt{l_1(l_2-l_1)}+l_2}{l_2-2l_1}, \tag{6.42}$$

$$e^{i\vartheta'} = \frac{l_3}{\sqrt{l_1(l_2-l_1)}}, \tag{6.43}$$

$$\gamma = -2l_1 + l_2, \tag{6.44}$$

where γ is the classical post-processing factor. Although these values are not unique, this does not alter the physical implementation. Hence the optimal measurement scheme is that described by Eq. (6.40) and is illustrated in figure 6.3.

Our discussion has so far focussed on the estimation of amplitude squeezing. However, by observing the form of the optimal observable in Eq. (6.35), we notice that $\hat{O}_\vartheta$ has the same dependence on the mode operators as $\hat{O}_r$, but with different definitions of the weightings l_j. This implies that the measurement scheme remains the same as that shown in figure 6.3, but with different values for r', ϑ' and γ. Hence, with the individual optimal measurement for both r and ϑ determined, we have provided a method to completely characterise the squeezing operation on single mode pure Gaussian states (6.31) using estimation theory. In the next section, we see how this changes when we consider mixed states.

6.4.2 Mixed state models

In the previous subsection, we derived the SLD for pure states using the generators of local translations. However, this method is much less convenient for general multi-mode Gaussian

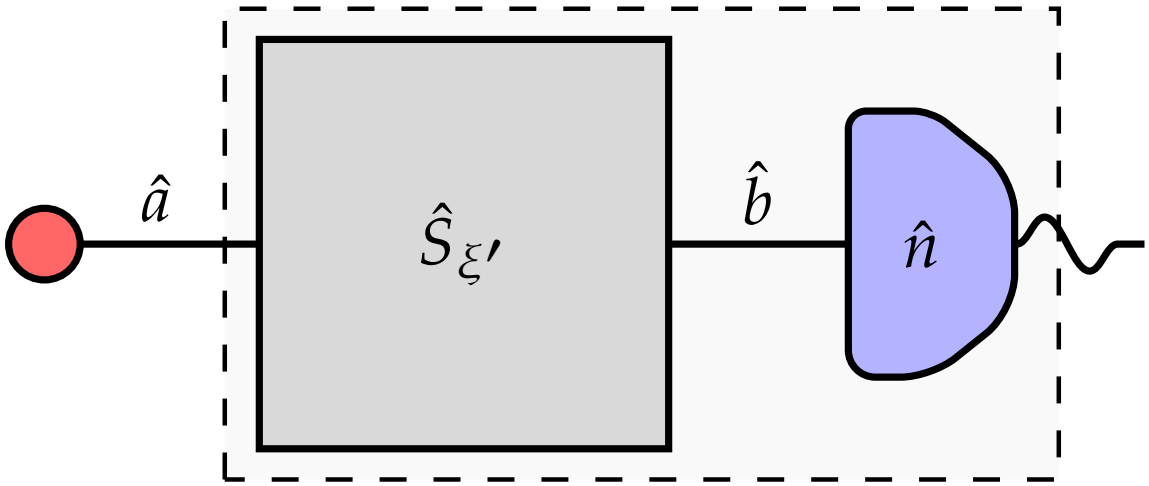

Figure 6.3: *Optimal measurement scheme that saturates the QCRB for the magnitude and direction of complex squeezing of a pure Gaussian models indicated with a dashed border. For some bosonic mode $\hat{a}$, the optimal measurement scheme is to perform a single-mode squeezer and follow up with intensity measurements of the emerging mode $\hat{b}$. Our objective is to find values of ξ' for which this measurement recovers the optimal observable for ξ. Note that classical processing of data is required to obtain the optimal estimates of squeezing.*

states. In this subsection, we use phase space methods to derive the SLDs for $\boldsymbol{\varphi}$ for single mode mixed Gaussian state. From this, we can address the optimal measurement scheme. Analogous to the pure state case in the preceding subsection, we consider the rotated, displaced thermal state

$$\rho_{\text{in}} = \hat{R}_\Theta \hat{D}_\alpha \rho_{\text{th}} \hat{D}_\alpha^\dagger \hat{R}_\Theta^\dagger, \tag{6.45}$$

as the input probe state. The squeezed state is then $\rho(\boldsymbol{\varphi}) = \hat{S}_\xi \rho_{\text{in}} \hat{S}_\xi^\dagger$, which is equivalent to the mixed state (6.9) with $\epsilon = 0$.

The SLD of a general n-mode Gaussian state in the phase space representation is written in terms of the vector of $2n$ canonical operators $\hat{\boldsymbol{R}} = (\hat{q}_1, \hat{p}_1, \ldots, \hat{q}_n, \hat{p}_n)^\top$ and its first two moments

$$\boldsymbol{\lambda} = \text{Tr}\left[\rho \hat{\boldsymbol{R}}\right], \quad \boldsymbol{\Sigma}_{jk} = \left\langle \left\{ \hat{\bar{R}}_j, \hat{\bar{R}}_k \right\} \right\rangle, \tag{6.46}$$

known as the mean and covariance respectively, where $\hat{\bar{R}}_j = \hat{R}_j - \langle \hat{R}_j \rangle$ are the zero mean operators. An equivalent expression for the SLD can be written in terms of the bosonic mode operators $\hat{\boldsymbol{a}} := (\hat{a}_1, \hat{a}_1^\dagger, \ldots, \hat{a}_n, \hat{a}_n^\dagger)^\top$. Several authors have developed and reviewed methods to calculate the QFI and the SLD using the phase space formalism [Monras, 2013; Gao and Lee, 2014; Jiang, 2014; Šafránek et al., 2015].

In this subsection, we use the approach detailed by Monras [2013][1], who derived a closed

[1] A different approach was developed by Y. Gao and H. Lee to also derive an exact form of the SLD. The result was summarised as [Gao and Lee, 2014]

$$\hat{\mathcal{L}}_j = \frac{1}{2} \mathfrak{M}^{-1}_{\gamma\kappa,\alpha\beta} \left(\partial_j \boldsymbol{\Sigma}^{\alpha\beta} \right) \left(\hat{\bar{a}}^\gamma \hat{\bar{a}}^\kappa - \boldsymbol{\Sigma}^{\gamma\kappa} \right) + \boldsymbol{\Sigma}^{-1}_{\mu\nu} \left(\partial_j \lambda^\nu \right) \hat{\bar{a}}^\mu,$$

where $\mathfrak{M} = \boldsymbol{\Sigma} \otimes \boldsymbol{\Sigma} + \boldsymbol{\Omega} \otimes \boldsymbol{\Omega}/4$, $\boldsymbol{\Omega}$ is the symplectic matrix defined in chapter 2. Assuming that the derivatives of the

form for the SLD as the solution to the Stein-equation to give

$$\hat{\mathcal{L}}_k = \frac{1}{2}\mathcal{A}^{(k)}_{\alpha\beta}\left\{\hat{\tilde{R}}^\alpha, \hat{\tilde{R}}^\beta\right\} + \mathcal{B}^{(k)}_\alpha \hat{\tilde{R}}^\alpha - \frac{1}{2}\mathrm{Tr}\left[\mathcal{A}^{(k)}\boldsymbol{\Sigma}\right], \tag{6.47}$$

where Greek indices imply Einstein summation convention and

$$\mathcal{A}^{(k)} = \sum_{j=0}^{\infty} \boldsymbol{F}^{\top j}\partial_k(\boldsymbol{\Sigma}^{-1})\boldsymbol{F}^j, \quad \mathcal{B}^{(k)} = 2\boldsymbol{\Sigma}^{-1}\partial_k\boldsymbol{\lambda}, \tag{6.48}$$

with $\boldsymbol{F} = (\boldsymbol{\Sigma}\boldsymbol{\omega})^{-1}$. The constant $\mathcal{A}^{(k)}$ is defined for non-singular ρ [Monras, 2013]. Note that due to the structure of Gaussian states, the SLD is at most quadratic in the canonical operators (or equivalently, the bosonic operators). Specifically, the first term in Eq. (6.47) is composed of bilinear contributions that corresponds to linear unitary operations. This describes passive devices such as beam-splitters, half and quarter wave plates, and phase-shifters. The quadratic contribution describes active devices such as squeezers and down-converters. The second term in Eq. (6.47) has a linear dependence on the operators. These operations describe displacements of Gaussian states in phase space. The coefficients $\mathcal{A}^{(k)}$ and $\mathcal{B}^{(k)}$ are completely determined from the first and second moments of the probe state and their derivatives. Using the definition of the moments in Eq. (6.46), we observe that the expectation value of the SLD is zero, as required. Eq. (6.47) is a general form of the SLDs for Gaussian states.

For the state in Eq. (6.45), the mean and covariance matrix of the state is given by

$$\boldsymbol{\lambda} = \boldsymbol{S}\boldsymbol{d}_\alpha, \quad \boldsymbol{\Sigma} = (2\overline{n}+1)\boldsymbol{S}\boldsymbol{S}^\top \tag{6.49}$$

respectively with the symplectic matrix $\boldsymbol{S} = \boldsymbol{S}_\xi \boldsymbol{R}_\Theta$. Both moments depend on the squeezing parameter ξ. Similar to the previous subsection, we write the SLD (6.47) in terms of the bosonic field operators $\hat{a}$. This requires mapping the transformed moments to the bosonic operator basis using the unitary map $\hat{\tilde{\boldsymbol{R}}} = \boldsymbol{s}\hat{\boldsymbol{a}}$, where

$$\boldsymbol{s} = \frac{1}{\sqrt{2}}\begin{pmatrix} 1 & 1 \\ -i & i \end{pmatrix}. \tag{6.50}$$

We find that the moments in this basis can be written as

$$\boldsymbol{\lambda}' = \boldsymbol{s}\boldsymbol{\lambda}, \quad \boldsymbol{\Sigma}' = \boldsymbol{s}\boldsymbol{\Sigma}\boldsymbol{s}^\top. \tag{6.51}$$

Substituting this into Eq. (6.47), we write the SLD in its final form:

$$\hat{\mathcal{L}}_k = \frac{1}{2}\mathscr{A}^{(k)}_{\alpha\beta}\left\{\hat{\tilde{\boldsymbol{a}}}^\alpha, \hat{\tilde{\boldsymbol{a}}}^\beta\right\} + \mathscr{B}^{(k)}_\alpha \hat{\tilde{\boldsymbol{a}}}^\alpha - \frac{1}{2}\mathrm{Tr}\left[\mathscr{A}^{(k)}\boldsymbol{\Sigma}\right], \tag{6.52}$$

where

$$\mathscr{A}^{(k)} = \boldsymbol{s}^\top\mathcal{A}^{(k)}\boldsymbol{s}, \quad \mathscr{B}^{(k)} = \mathcal{B}^{(k)}\boldsymbol{s}. \tag{6.53}$$

and $k \in \{r, \vartheta\}$. We now have a closed form for the SLD written in the bosonic mode basis. With the moments defined in Eq. (6.49), our task is one of determining the matrix coefficients $\mathscr{A}^{(k)}$ and

first and second moments exist, we can then determine the SLDs and the QFIM for any n-mode bosonic Gaussian system. However, the necessity of inverting large matrices is a drawback of this method.

$\mathscr{B}^{(k)}$. These coefficients are solutions to the Stein Eq. (F.21). We derive their explicit expressions in appendix F.3 and summarise the results as:

$$\frac{2\overline{n}(\overline{n}+1)}{2\overline{n}+1}\mathscr{A}^{r} = \begin{pmatrix} \cosh[2r]e^{-i\vartheta} & \sinh[2r] \\ \sinh[2r] & \cosh[2r]e^{i\vartheta} \end{pmatrix} \tag{6.54}$$

$$-\frac{2\overline{n}+1}{\sqrt{2}\,\alpha}\mathscr{B}^{r} = \begin{pmatrix} \cosh[r]e^{-i(\vartheta+\Theta)} + \sinh[r]e^{i\Theta} \\ \cosh[r]e^{i(\vartheta+\Theta)} + \sinh[r]e^{-i\Theta} \end{pmatrix} \tag{6.55}$$

$$\frac{4i\overline{n}(\overline{n}+1)}{2\overline{n}+1}\mathscr{A}^{\vartheta} = \begin{pmatrix} \sinh[2r]e^{-i\vartheta} & 0 \\ 0 & -\sinh[2r]e^{i\vartheta} \end{pmatrix} \tag{6.56}$$

$$\frac{i(2\overline{n}+1)}{\sqrt{2}\,\alpha\sinh[r]}\mathscr{B}^{\vartheta} = \begin{pmatrix} \sinh[2r]e^{i\Theta} - \cosh[2r]e^{-i(\vartheta+\Theta)} \\ \cosh[2r]e^{i(\vartheta+\Theta)} - \sinh[2r]e^{-i\Theta} \end{pmatrix} \tag{6.57}$$

Note that only the vector constants depend on the displacement term α and the rotation parameter Θ. This is due to the parameterisation of the transformed state moments. The constants $\mathscr{A}^{(k)}$ for $k \in \{r, \vartheta\}$ is singular for pure states $\overline{n} = 0$. Hence the SLD for pure state is not-defined using this approach. This is since the Stein Eq. (F.21) gives unique solutions for non-singular ρ, which excludes pure states.

Taking the commutator of the SLD for r and ϑ, we find they do not commute $[\hat{\mathcal{L}}_r, \hat{\mathcal{L}}_\vartheta] \neq 0$. To find the optimal POVM, we first determine the operators $\hat{\boldsymbol{O}} = [\boldsymbol{\mathcal{I}}^{\mathrm{Q}}]^{-1}\hat{\boldsymbol{\mathcal{L}}}$. For the amplitude of squeezing, we write

$$\hat{O}_r = l'_1 + l'_2\hat{n} + l'_3\hat{a}^\dagger + l'^{*}_3\hat{a} + l'_4\hat{a}^{\dagger 2} + l'^{*}_4\hat{a}^2. \tag{6.58}$$

Since the POVM is in normal order, it can be implemented through the intensity measurements $\hat{c}^\dagger\hat{c}$. In contrast to the optimal observable for the pure state, this has terms that are linear in the mode operators. The Bogolioubov transformation (6.41) of the mode operators must be updated accordingly. Specifically, we first squeeze then displace the operators where we have used the Bogolioubov transformation of the mode operators under a single mode squeezing operation

$$\hat{c} = \hat{b} + \alpha' = \cosh[r']\hat{a} + e^{i\vartheta'}\sinh[r']\hat{a}^\dagger + \alpha'. \tag{6.59}$$

Writing $\alpha' = r'_\alpha \exp[i\vartheta'_\alpha]$, we write:

$$\begin{aligned} e^{2r'} &= l'_2 - \sqrt{l'^2_2 - 1}\,, \\ e^{2i\vartheta'} &= \frac{4l'^2_4}{l'^2_2 - 1}, \\ 2r'^2_\alpha &= 1 - l'_2 + 2l'_1, \\ e^{i\vartheta'_\alpha} &= \frac{l'_3 e^r r_\alpha\left(2l'_2 - e^{2r} + 1\right)}{2(l'_2+1)r^2_\alpha} + \sqrt{\frac{l'^2_3 - 2e^{i\vartheta}r^2_\alpha\left(e^{2r} - l'_2\right)}{2(l'_2+1)r^2_\alpha}} \end{aligned} \tag{6.60}$$

The optimal measurement scheme for mixed squeezed states is illustrated in figure 6.4. It is a homodyne detection of a single-mode squeezer applied to the probe and an intense coherent source as inputs. Although no classical post-processing is required, this implementation still requires adaptive measurements. This may become prohibitive, especially if strong single-mode squeezing is demanded. The optimality of homodyne detection is consistent with the geometric argument provided by Monras [2013] for general Gaussian states.

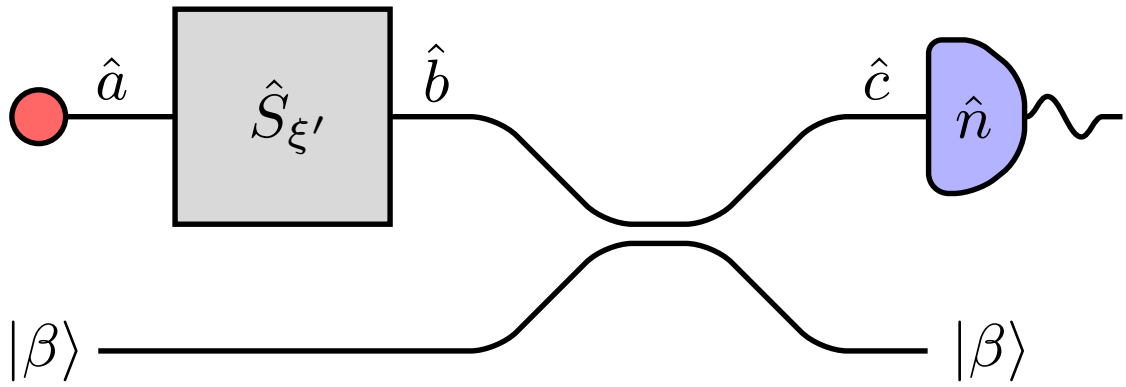

Figure 6.4: *Optimal measurement scheme that saturates the* qcrb *for the magnitude and direction of complex squeezing for mixed Gaussian states. For some bosonic mode $\hat{a}$, the optimal measurement scheme is to perform a mode squeezer, displaced by $\alpha' = r'_\alpha \exp[i\vartheta'_\alpha]$, and followed with intensity measurements. The displacement is achieved by using an intense laser source with $|\beta|^2 \gg 1$ as the second input to a beam splitter with unit transmissivity. The intensity measurements are performed on the output arm containing the displaced mode operators. The second output is just the same intense coherent state $|\beta\rangle$ and contains no information on the estimation parameters. Hence the arm that has the coherent state can be suitably ignored.*

6.5 Discussions and summary

The use of squeezed light as a quantum resource is ubiquitous in many applications across quantum optics. These states have formed an integral part of the drive towards realising quantum technologies, which promise to deliver practical advantages over classical strategies. However, an influential factor to a successful implementation of these applications is the level of squeezing in a light field. With this in mind, it is important to check whether the properties of experimentally-tailored squeezed states are indeed suitable for its intended implementation.

To address this, we have presented a means to completely characterise both the magnitude and direction of a squeezing operation. We approached this by estimating the two conjugate parameters of a squeezing operation. The quantum Cramér-Rao bound of the squeezing parameter ξ was calculated for arbitrary single mode Gaussian states. We demonstrated that the optimal observables for both parameters obey a non commutative nature which prohibits a simultaneous optimal measurement-even in the asymptotic limit. Despite this, we found the quantum optimal estimators for individual measurements of both parameters. Finally, we presented the measurement scheme that saturates these bounds for pure and mixed, single-mode Gaussian states. The work in this chapter is the first to address both the estimation bounds for complex squeezing and their optimal measurement schemes.

For future work, it would be interesting to explore simultaneous measurements of both the amplitude and direction of squeezing. Although both can not be measured optimally simultaneously, an open question in this work is how close simultaneous measurements can come to optimal by optimising the cost function of both parameters. To supplement this study, an estimate of the squeezing parameter values should be determined. This would require finding a suitable unbiased estimator that maximises the classical Fisher information. A further extension would explore how the estimation precision and optimal measurement scheme

changes for multi-mode Gaussian states.

Part 3

Summary and Outlook

In this final part of the thesis, we review what we have achieved. Potential avenues for future research that extend the scope of the work presented are also discussed.

Chapter 7

Summary and Outlook

In this thesis, we considered different applications of quantum estimation theory. We presented a framework for the detection and estimation of deformations applied to a grid of sources. This made progress towards multi-parameter quantum estimation theory and addressed two commonly visited problems in quantum metrology: source optimisation and source localisation. We also used estimation theory to provide better characterisation of squeezed states. Previous work in the literature has been limited to estimates of its amplitude. We extended this to include an estimate of the direction. This work is crucial for many applications in quantum optics and quantum information that use squeezed states to provide quantum enhancements. In this chapter, we provide a summary of the research conducted over the PhD, and detail ideas for future work.

7.1 Executive research summary

In chapter 4, we applied the theory of quantum estimation to an array of identical, stationary and equidistant emitters. The spatial uncertainty associated with the emitter position was characterised by a spatial Gaussian uncertainty profile. We explored how the estimation precision of the source separation distance d is effected with the choice of probe states. The quantum Fisher information (QFI) was chosen as a suitable metric to quantify the performance of the estimation. We derived the QFI for multi-mode thermal states $\mathcal{I}^{\mathrm{Q}}_{\mathrm{Bb}}$, coherent states $\mathcal{I}^{\mathrm{Q}}_{\mathrm{Coh}}$, single photon emitters $\mathcal{I}^{\mathrm{Q}}_{\mathrm{SPE}}$, and entangled sources of single photon emitters $\mathcal{I}^{\mathrm{Q}}_{\mathrm{E\text{-}SPE}}$. We conveniently summarise the analytic expression for each as

$$\mathcal{I}^{\mathrm{Q}}_{\mathrm{Bb}} = \frac{\xi_s^2 N(N^2-1)}{4s^2} = \frac{3}{2}\mathcal{I}^{\mathrm{Q}}_{\mathrm{Coh}} = 3\mathcal{I}^{\mathrm{Q}}_{\mathrm{SPE}} = 6\mathcal{I}^{\mathrm{Q}}_{\mathrm{E\text{-}SPE}}, \tag{7.1}$$

where s is the standard deviation of the Gaussian sources and N the number of emitters used. The photon number distributions for the black body and coherent states were set to one for fair comparison with the single photon emitters. We observed that the higher mode occupancies of the classical sources provided better estimates of d than single photon emitters. Hence, the classical black body states outperformed the single photon emitters for the estimation of source

separation distances. This can be seen from Eq. (7.1). The relative performance of these states held independent of the average photon number emitted at each array site. Consistent with other work in the literature, the optimal state was that constructed from the maximum and minimum eigenvectors of the generator governing dynamics in d. For regular arrays, this state is an extension of the NOON state, constructed from a superposition of all N photons emitted from the most extremal positions about the array centre O. The analytic results that were obtained are possible only if the sources are mutually independent. We demonstrated that this occurs when $d > 2s$. The optimal estimator that saturated the QCRB was finally presented. Photon number counting is found to be optimal. We also find the existence of a second optimal estimator, which motivates an open question into the uniqueness of optimal measurements.

In chapter 5, we considered a source localisation problem. We developed a framework for detecting arbitrary deformations applied to multi-dimensional grids of sources. This extended the work in chapter 4 to Hamiltonian dynamics beyond the phase-like Hamiltonians. We started by deriving the generators of arbitrary unitary evolutions and demonstrated that the result is a multi-parameter extension of previous results derived in the literature. These multi-parameter generators described changes to the expected mean positions of each source as a result of any grid deformation, but did not change the source variances. For any grid deformation, the generators describing dynamics in the parameters reduced to the set of commuting operators

$$\hat{G}_j = \sum_{k=1}^{N_t} E_{j,k} \left|\boldsymbol{n}\right\rangle \left\langle \boldsymbol{n}\right| , \tag{7.2}$$

where N_t is the total number of sources in the grid and the deformation is parameterised within the quantity $E_{j,k}$. Using this, we derived the QFIM of parameters that govern any arbitrary grid deformation. We considered the set of affine spatial maps, including composite stretches, shears, and, rotations, to provide numerical results. We demonstrated how changing the configuration of emitters in the grid enhanced the estimation sensitivity of the applied grid deformation. Specifically for rotations, we demonstrated an ability to arrange sources in a manner that eliminates an oscillatory dependence of the QFI. This implies that the QCRB is then attainable without the use of adaptive strategies.

The work completed in chapter 5 is applicable to many quantum estimation protocols. However, the application to grid metrology did not fully exercise the generality permitted by the formalism introduced, since we had a set of mutually commuting generators. This motivated a more general application in chapter 6, where we estimated the amplitude and direction of complex squeezing in phase space. This application is a true multi-parameter quantum estimation problem of incompatible observables. For some single mode squeezing $\xi = r\exp[i\vartheta]$, the generators

$$\hat{\mathcal{G}}_r(\vartheta) = \frac{i}{2}\left(e^{-i\vartheta}\hat{a}^2 - e^{i\vartheta}\hat{a}^{\dagger 2}\right), \tag{7.3}$$

$$\hat{\mathcal{G}}_\vartheta(r,\vartheta) = \alpha\left(\hat{n} + \frac{1}{2}\right) + \frac{\beta}{2}\left(e^{-i\vartheta}\hat{a}^2 + e^{i\vartheta}\hat{a}^{\dagger 2}\right), \tag{7.4}$$

for some $\alpha, \beta \in \mathbb{R}$ that depend on the amplitude of squeezing, do not commute. This prohibits simultaneous optimal joint estimates of both parameters, even in the asymptotic limit of large samples. As a result, we focussed on finding separable optimal estimates. The Cramér-Rao bound was determined to provide a theoretical benchmark on the bi-variate estimation precision for general single mode Gaussian probes. Using this, we presented the quantum optimal estimators of complex squeezing.

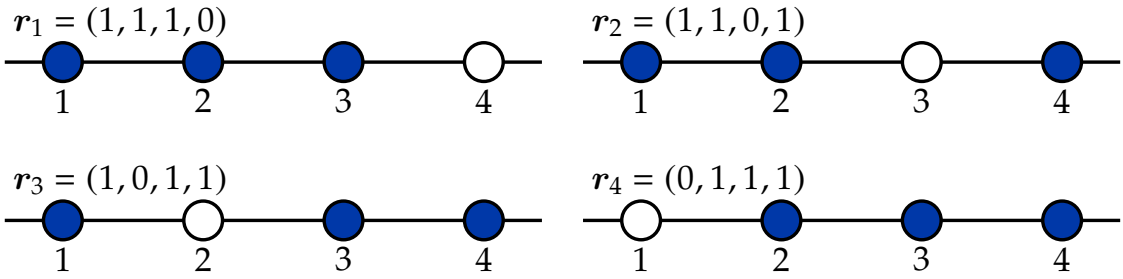

Figure 7.1: *For sources with efficiency $\eta < 1$, single photons will be emitted at some of the sources. Filled circles represent sources which successfully emit a photon and the unfilled represent the dormant ones. For $N = 4$, we illustrate the different arrangements of working-dormant sources for $m = 3$. There are $\binom{4}{3} = 4$ configurations, each illustrated above.*

7.2 Future work

There are some natural extensions that follow from the work in this thesis. For the grid metrology framework introduced in chapters 4 and 5, the need for spatially propagating the field to some far-field plane was circumvented by working in the near field of the sources. This was sufficient to analyse source optimisation for enhanced estimation precisions. However, a more practical treatment would treat the QFI in the far-field. This would provide a practical description by quantifing the quantum Fisher information over a subset in space. This is a possible method to consider the effects of incomplete detection of the state on the estimation precision of source separation distances.

We also assumed that the sources were stationary and positioned with equidistant spacing. It would be interesting to observe the effect that non-unit source efficiencies and temporal jitters has on the QFI. Through a quick calculation, we can motivate why this may be fruitful: Consider sources with operation efficiencies $\eta < 1$, then at a particular time t, only some of the sources will emit single photons. For some number of sources N along an array, and $m \in [0, N]$, of sources that emit a single photon, there exists $\binom{N}{m}$ number of possible configurations (see figure 7.1). Denoting the successful emission of a photon from a source with a '1' and dormant sources with a '0', the j^{th} configuration of operational sources may be characterised with the bit-vector $\boldsymbol{r}_j$. The probability of occurrence for each configuration $\boldsymbol{r}_j$ is $P(\boldsymbol{r}_j|N, m) = \eta^m(1-\eta)^{N-m}$. By considering an arbitrary number of photons, n_j, generated by source j, we can calculate the QFI for any arbitrary η. Since the QFI is additive, we have

$$\mathcal{I}^Q_{\text{SPE}}(\eta) = \sum_{j=1}^{\binom{N}{m}} \left[\mathcal{I}^Q_{\text{SPE}}(\eta)\right]_j = \frac{1}{s^2} \sum_{j=1}^{\binom{N}{m}} \sum_{i=1}^{N} \mu_i'^2 r_{j,i}^2. \tag{7.5}$$

The normalised QFI, $\overline{\mathcal{I}^Q_{\text{SPE}}} = \mathcal{I}^Q_{\text{SPE}}(\eta)/\mathcal{I}^Q_{\text{SPE}}(\eta = 1)$, has been illustrated in figure 7.2 with varying η. It demonstrates that our technique remains feasible even for low efficiency sources. Poor performing SPE can be compensated for by increasing the number of emitters.

In this thesis, we made extensive use of the Hamiltonian formulation of the QFI. The multi-parameter generators that we derived were all Hermitian. However, this is generally not the

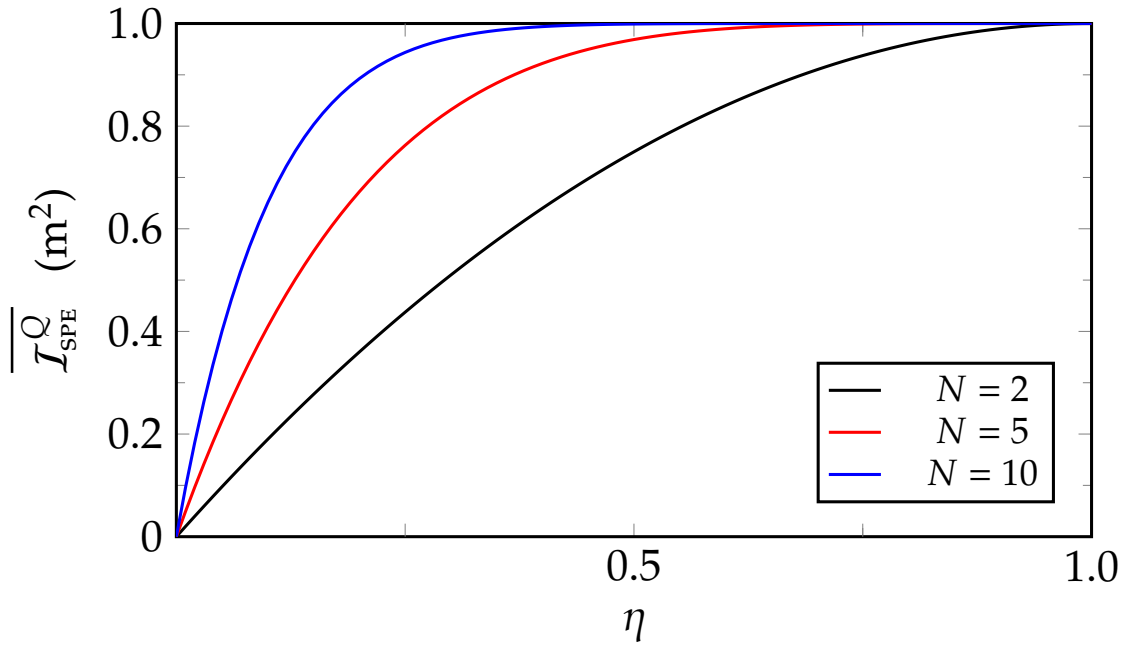

Figure 7.2: *The normalised QFI as a function of the source efficiencies, η. Each source is assumed to emit a single photon with efficiency η. As expected, it is 0 for $\eta = 0$ and reaches 1 for $\eta = 1$. We note that this technique improves for finite source efficiency as N increases. Even for poorly behaved sources, increasing N improves the estimation precision which motivates complete detection of all sources.*

case. This is a well know problem in quantum theory [Robertson, 1929; Luo, 2000], and it would be interesting to see the consequences this has for deriving generalised uncertainty relations for a pair of operators in terms their variances.

A final suggestion for future work is the existence of multiple optimal estimators. This was briefly discussed in chapter 4 and it motivates an open question into the uniqueness of optimal measurements. A related suggestion follows from our work in chapter 6. We found the separable optimal estimators for complex squeezing. A major step to experimentally realise the fundamental Cramér-Rao bound requires finding a measurement scheme that corresponds to the optimal estimators. This is typically difficult since the existence of such a map is not guaranteed.

Part 4

Appendices

Appendix A

Functional Analysis

Since quantum mechanics is defined on a complex vector space, we review the basic notion of a vector space. Most readers will have some familiarity and recognition of the basics of functional analysis, and so we review these only briefly. In this appendix, we will introduce the Hilbert space and some operations on it. For a more complete exposition, upon which this appendix is based, I encourage the reader to read the texts by Kreyszig [1989]; Debnath and Mikusinski [2005]; Clarke [2013]. In this section, we adopt a more mathematical tone to write a precise definition of the space and its properties.

A.1 Normed spaces

We assume that all vector spaces are over either the space of real numbers $\mathbb{R}$ or the space of complex numbers $\mathbb{C}$. Throughout the following, we denote the space $\mathbb{F}$ as either $\mathbb{R}$ or $\mathbb{C}$. Many problems in Physics and Mathematics involve dealing with infinite-dimensional vector spaces. Typically, the elements of such spaces are *functions*. Let S be a metric space, and $C(S)$ the set of continuous functions $f : S \to \mathbb{F}$, then $C(S)$, together with the addition and scalar multiplication defined as

$$\begin{aligned} (f+g)(x) &= f(x) + g(x), \quad \text{for} \quad f, g \in C(S), x \in S, \\ (\alpha f)(x) &= \alpha f(x) \qquad\quad \text{for} \quad \alpha \in \mathbb{F}, f \in C(S), x \in S, \end{aligned}$$

respectively, is a vector space. Axioms that define the vector space follow from these two operations. That is, for every $f, g, h \in C(S), x \in S$ and $\beta \in \mathbb{F}$ the following hold:

1. $f(x) + g(x) = g(x) + f(x)$ (*Commutative law*)
2. $(f(x) + g(x)) + h(x) = f(x) + (g(x) + h(x))$ (*Associative law*)
3. $0 + f(x) = f(x) + 0 = f(x)$ (*Existence of identity element for '+'*)
4. $f(x) + (-f(x)) = 0$ (*Existence of inverse for '+'*)

5. $\alpha(f(x)+g(x)) = \alpha f(x) + \alpha g(x)$ (*Distributive law*)
6. $(\alpha+\beta)f(x) = \alpha f(x) + \beta f(x)$ (*Distributive law*)
7. $1f(x) = f(x)1 = f(x)$ (*Existence of scalar multiplication*)
8. $(\alpha\beta)f(x) = \alpha(\beta f(x))$ (*Compatibility*)

A.2 Hilbert spaces

As we saw in chapter 2, the entire structure of quantum mechanics is formulated in terms of states and operations in Hilbert space. The state of a physical system is written as a vector in a complex vector space. Observables are linear Hermitian operators that operate in this complex space. The Hilbert space, named in honour of D. Hilbert, generalises the notion of Euclidean space. It is an abstract vector space (finite or not) possessing the structure of an inner product that allows length and angle to be measured. In this appendix, we will review the definition of this complex space, and the operators that act on it.

A.2.1 Inner products

The norm introduced in the preceding section on some vector space $\mathcal{V}$ over the field $\mathbb{F}$ gives a measure of distance. Similarly, inner products provide a measure of angle. The inner product of two vectors in $\mathcal{V}$ is a scalar that is defined through the map

$$\langle -, - \rangle : \mathcal{V} \times \mathcal{V} \to \mathbb{F}, \tag{A.1}$$

such that for any $\boldsymbol{u}, \boldsymbol{v}, \boldsymbol{w} \in \mathcal{V}$, and $\alpha, \beta \in \mathbb{F}$

1. $\langle \boldsymbol{u}, \alpha\boldsymbol{v} + \beta\boldsymbol{w} \rangle = \alpha\langle u, v\rangle + \beta\langle u, w\rangle$, (*Linearity of second argument*)
2. $\langle \boldsymbol{u}, \boldsymbol{v} \rangle = \langle \boldsymbol{v}, \boldsymbol{u} \rangle^*$, (*Hermitian symmetric*)
3. $\langle \boldsymbol{u}, \boldsymbol{u} \rangle \geq 0$ with equality if and only if $\boldsymbol{u} = \boldsymbol{0}$, (*Positive-definite*)

where $*$ denotes complex conjugation. We call a vector space with an inner product an *inner product space*.

To give an example, let $\boldsymbol{u}, \boldsymbol{v} \in \mathbb{C}^n$ with $\boldsymbol{u} = (x_1, \ldots, x_n)$ and $\boldsymbol{v} = (y_1, \ldots, y_n)$, then an inner product on $\mathbb{C}^n$ is defined by

$$\langle \boldsymbol{u}, \boldsymbol{v} \rangle = \sum_{j=1}^{n} x_j^* y_j = \boldsymbol{u}^\dagger \boldsymbol{v}. \tag{A.2}$$

The norm of a vector $\boldsymbol{u} \in \mathcal{V}$ is defined by

$$\|\boldsymbol{u}\| = \sqrt{\langle \boldsymbol{u}, \boldsymbol{u} \rangle}. \tag{A.3}$$

If $\|\boldsymbol{u}\| = 1$, the vector $\boldsymbol{u}$ is a *unit* vector. The set of unit vectors $\{\exp[i\varphi]\boldsymbol{u}\}$ with $\varphi \in [0, 2\pi)$ form a so-called *ray* in the linear vector space (consult postulate 1 of quantum mechanics in section 2.1). A linear vector space that is *complete* (as a normed vector space), with norm $\|\cdot\|$ is called a Hilbert space, and written $\mathcal{H}$.

For vector spaces with an inner product, the *Cauchy-Schwarz inequality* holds

$$|\langle \boldsymbol{u}, \boldsymbol{v} \rangle| \leq \|\boldsymbol{u}\| \cdot \|\boldsymbol{v}\| \tag{A.4}$$

for any $\boldsymbol{u}, \boldsymbol{v} \in \mathcal{V}$. This inequality is only saturated if one of the vectors is a constant multiple of the other. Since the inequality depends on only the inner product structure, it makes the Heisenberg uncertainty relation—that depends on it—generally valid. Combining Eq. (A.3) with the Cauchy-Schwarz inequality yields the *triangle inequality*:

$$\|\boldsymbol{u} + \boldsymbol{v}\|^2 = (\|\boldsymbol{u}\| + \|\boldsymbol{v}\|)^2, \tag{A.5}$$

and the *parallelogram law*:

$$\|\boldsymbol{u} + \boldsymbol{v}\|^2 + \|\boldsymbol{u} - \boldsymbol{v}\|^2 = 2(\|\boldsymbol{u}\| + \|\boldsymbol{v}\|)^2. \tag{A.6}$$

All complex vector spaces with an inner product is a Hilbert space if it is finite dimensional.

A.2.2 Orthonormal sets

We call two elements $\boldsymbol{u}, \boldsymbol{v} \in \mathcal{H}$ orthogonal, if their inner product is zero. If in addition they are also unit vectors, we say that they are orthonormal. In other words, $\boldsymbol{u}, \boldsymbol{v} \in \mathcal{H}, \boldsymbol{u}, \boldsymbol{v} \neq \mathbf{0}$are said to be orthonormal if

$$\begin{aligned} \langle \boldsymbol{u}, \boldsymbol{u} \rangle = \langle \boldsymbol{v}, \boldsymbol{v} \rangle = 1, \\ \langle \boldsymbol{u}, \boldsymbol{v} \rangle = 0. \end{aligned} \tag{A.7}$$

The process of constructing orthonormal sets from orthogonal sets is called normalisation. In quantum mechanics, this ensures that the total probability of a state sums to 1. To describe some further properties, we introduce the orthonormal set of vectors $\boldsymbol{e}_j \in \mathcal{H}, j \in \{1, 2, \ldots, n\}$ that are normalised for all j and are mutually orthogonal. The vectors $\{\boldsymbol{u}_j\}$ are said *linearly independent* if the only solution to the equation

$$\sum_j \alpha_j \boldsymbol{u}_j = \mathbf{0}, \ \alpha_j \in \mathbb{C} \tag{A.8}$$

is $\alpha_j = 0 \ \forall \ j$. The maximum number of linearly independent vectors in $\mathcal{H}$ is the dimension of $\mathcal{H}$. Constructing an orthonormal set of vectors from linearly independent vectors is called the *Gram-Schmidt orthonormalisation process*.

Gram-Schmidt orthonormalisation: *For the set of linearly independent vectors* $\{\boldsymbol{l}_n \in \mathcal{H} | n \in \mathbb{N}\}$, *we construct the orthonormal sequence of vectors* $\{\boldsymbol{e}_n \in \mathcal{H}\}$ *defined through*

$$\boldsymbol{e}_n = \frac{\boldsymbol{w}_n}{\|\boldsymbol{w}_n\|} \quad \textit{with} \quad \boldsymbol{w}_n = \boldsymbol{l}_n - \sum_{j=1}^{n-1} \langle \boldsymbol{e}_j, \boldsymbol{l}_n \rangle \boldsymbol{e}_j, \tag{A.9}$$

such that Span$\{\boldsymbol{e}_1, \ldots, \boldsymbol{e}_n\}$ = *Span*$\{\boldsymbol{l}_1, \ldots, \boldsymbol{l}_n\}$.

The span of some subset $\mathcal{S}$ of some vector space $\mathcal{V}$,

$$\text{Span}\{\alpha_1 \boldsymbol{l}_1 + \ldots, \alpha_n \boldsymbol{l}_n \mid \alpha_j \in \mathbb{F}, \boldsymbol{l}_j \in \mathcal{V}, n \in \mathbb{N}\}, \tag{A.10}$$

is defined as the smallest linear subspace of $\mathcal{V}$ that contains $\mathcal{S}$. ■

A maximal set of linearly independent vectors is said complete. For a Hilbert space $\mathcal{H}$, there always exists a complete set of orthonormal vectors $\{\boldsymbol{e}_j\}$. In particular, this set is a basis for $\mathcal{H}$, so that every vector $\boldsymbol{v} \in \mathcal{H}$ can be written as

$$\boldsymbol{v} = \sum_{j=1}^{n} c_j \boldsymbol{e}_j, \tag{A.11}$$

with $\langle \boldsymbol{e}_j, \boldsymbol{e}_k \rangle = \delta_{jk}$, and $c_j = \langle \boldsymbol{e}_j, \boldsymbol{v} \rangle$. We can take the inner product of $\boldsymbol{v}$ with any of the basis vectors $\boldsymbol{e}_k$ to obtain

$$\langle \boldsymbol{e}_k, \boldsymbol{v} \rangle = \sum_{j=1}^{n} c_j \langle \boldsymbol{e}_k, \boldsymbol{e}_j \rangle = \sum_{j=1}^{n} c_j \delta_{kj} = c_k. \tag{A.12}$$

This is a statement of Fourier's theory to determine the magnitude of each orthonormal vectors in the vector $\boldsymbol{v}$. Note that by substituting this result into Eq. (A.11) and using Eq. (A.2) gives

$$\boldsymbol{v} = \sum_{j=1}^{n} \boldsymbol{e}_j \boldsymbol{e}_j^{\dagger} \boldsymbol{v} \tag{A.13}$$

Therefore, we arrive at the resolution of identity $\sum_{j=1}^{n} \boldsymbol{e}_j \boldsymbol{e}_j^{\dagger} = \mathbb{1}$, which is clearly understood from the definition of $\boldsymbol{e}_j$ from Eq. (A.9). In Dirac's bracket notation, this can be recast in a more recognisable form

$$\sum_j \left|\psi_j\right\rangle \left\langle\psi_j\right| = \sum_j \hat{P}_j = \mathbb{1}. \tag{A.14}$$

where we defined the projector $\hat{P}_j$ that projects any vector onto the space spanned by the basis $\boldsymbol{e}_j$. This form hints that general operators on $\mathcal{H}$ can be written as sums over general matrices $|\chi\rangle \langle\xi|$. This will be the subject of the next subsection.

A.2.3 Linear operators in Hilbert space

Let $\boldsymbol{T} : \mathcal{H} \to \mathcal{V}$ be a linear map between two vector spaces. If $\mathcal{V} = \mathcal{H}$, then $\mathcal{L}(\mathcal{H})$ denotes the set of all linear operators on $\mathcal{H}$. That is, $\boldsymbol{T} \in \mathcal{L}(\mathcal{H})$ if and only if:

1. $\boldsymbol{T}(\boldsymbol{v} + \boldsymbol{w}) = \boldsymbol{T}(\boldsymbol{v}) + \boldsymbol{T}(\boldsymbol{w})$, for any $\boldsymbol{v}, \boldsymbol{w} \in \mathcal{H}$,
2. $\boldsymbol{T}(\alpha \boldsymbol{v}) = \alpha \boldsymbol{T}(\boldsymbol{v})$, for any $\alpha \in \mathbb{F}, \boldsymbol{v} \in \mathcal{H}$.

We dedicate capital typeset to denote linear operators $\boldsymbol{S}, \boldsymbol{T}, \ldots$. Let $\mathcal{L}(\mathcal{H})$ denote the set of linear operators in $\mathcal{H}$, then $\mathcal{L}(\mathcal{H})$ is a linear vector space on $\mathbb{C}$, where for any $\boldsymbol{S}, \boldsymbol{T} \in \mathcal{L}(\mathcal{H}), \alpha \in \mathbb{C}$, $\boldsymbol{v} \in \mathcal{H}$ the sum and scalar multiplication are defined as

1. $(\boldsymbol{S} + \boldsymbol{T})(\boldsymbol{v}) = \boldsymbol{S}(\boldsymbol{v}) + \boldsymbol{T}(\boldsymbol{v})$,
2. $(\alpha \boldsymbol{T})(\boldsymbol{v}) = \boldsymbol{T}(\alpha \boldsymbol{v})$

respectively. Moreover, for $S, T \in \mathcal{L}(\mathcal{H})$, we define their product ST as the operator on $\mathcal{H}$ given by

$$(ST)(v) = S(T(v)). \tag{A.15}$$

Note that, multiplication of two operators is generally *non-commutative*, with the difference between the two defined as the commutator

$$[S, T] = ST - TS. \tag{A.16}$$

The non-commutativity of operators satisfies matrix algebra. This conveniently motivates a matrix representation of linear operators. In quantum mechanics, the state of some physical system is denoted by some vector $|\phi\rangle \in \mathcal{H}$, and linear operators describe dynamics of the state $|\psi\rangle = T|\phi\rangle$. From the inner product of two vector elements of the complete orthonormal basis $|\psi_j\rangle$, $\langle\psi_j|T|\psi_k\rangle = T_{jk}$, the matrix form of operators is easy to observe. A description of the operation of T in $\mathcal{H}$ depends on the basis (we will discuss this in more detail in the next section). For the sequence of vectors $\{v_j\} \in \mathcal{H}$, $j = 1, 2, \ldots, n$, the action of any linear operator $Tv_k \in \mathcal{H}$ can be written as a linear combination of the vectors:

$$Tv_k = T_{kj}v_j, \tag{A.17}$$

where the Einstein summation rule is applied to repeated indices. Given this, how can the matrix representation of T be written in a different basis? Consider a change of basis from $\{v_j\}$ to $\{w_j\}$. Let

$$A \in \mathbb{C}^{2n} : T(\{v_j\}) \to T(\{w_j\}) \text{ for } j \in \{1, \ldots, n\} \tag{A.18}$$

denote some *invertible operator* that describes the basis transformation of T according to

$$A_{kj}v_j = w_k \Leftrightarrow v_k = A^{-1}_{kj}w_j. \tag{A.19}$$

Combining Eq. (A.19) with Eq. (A.18) yields

$$T(\{w\})w_j \overset{(A.19)}{=} A_{jk}T(\{v\})v_k \overset{(A.17)}{=} A_{jk}T_{kl}(\{v\})v_l \overset{(A.19)}{=} A_{jk}T_{kl}(\{v\})A^{-1}_{lm}w_m, \tag{A.20}$$

which gives

$$T(\{w\}) = AT(\{v\})A^{-1}. \tag{A.21}$$

This allows us to understand how a basis change affects the matrix representation of linear operators.

A.2.4 Adjoint and Hermitian operators

In this subsection, we introduce *adjoint* and *Hermitian* operators. To understand their properties, we first introduce introduce dual spaces and linear functionals.

A linear functional is defined as the *linear map* J of elements in any vector space to its field of scalars. For any element $v \in \mathcal{H}$, we define the *linear functional* $J_v : \mathcal{H} \to \mathbb{F}$ by:

$$J_v(z) = \langle v, z\rangle, \tag{A.22}$$

for any $z \in \mathcal{H}$. This map is bounded with norm $\|J_v\| = \|v\|$, which can be verified using the Cauchy-Schwarz inequality for $z \neq v$ and $z = v$. The set of all linear functionals from $\mathcal{H} \to \mathbb{F}$ forms a vector space that satisfies the operations of addition and scalar multiplication (section A.1). This space is called the *dual vector space* of $\mathcal{H}$ and is denoted $\mathcal{H}^*$. The following theorem establishes that every element of $\mathcal{H}^*$ can be uniquely written in the form in Eq. (A.22):

Riesz representation theorem: *Let $J_v : \mathcal{H} \to \mathbb{F}$ be some continuous linear map, then there exists a unique vector $v \in \mathcal{H}$ such that*

$$J_v(z) = \langle v, z \rangle \tag{A.23}$$

for any $z \in \mathcal{H}$.

Let $\{e_1, \ldots, e_n\}$ be an orthonormal basis for $\mathcal{H}$, then

$$z = \sum_{j=1}^{n} \langle e_j, z \rangle e_j. \tag{A.24}$$

To find the unique vector v that satisfies this we apply the functional J_v on Eq. (A.24) to give

$$J_v(z) = \sum_{j=1}^{n} \left\langle e_j, z \right\rangle J_v(e_j) = \sum_{j=1}^{n} \left\langle J_v^*(e_j) e_j, z \right\rangle = \left\langle \sum_{j=1}^{n} J_v^*(e_j) e_j, z \right\rangle, \tag{A.25}$$

where we used the conjugate-linearity of the inner product [1]. With comparison to Eq. (A.30) we have an expression for a unique element v that establishes a connection between the Hilbert space and its dual vector space. ■

We can now use this theorem to prove the existence of the *adjoint* of an operator. For some bounded linear operator T on a vector space $\mathcal{V}$, there exists an adjoint linear operator written $T^\dagger$ on $\mathcal{V}$ such that

$$\langle v, Tz \rangle = \left\langle T^\dagger v, z \right\rangle, \tag{A.26}$$

for any $v, z \in \mathcal{H}$. The adjoint has the following properties for some $S, T : \mathcal{H} \to \mathcal{H}$ and $\alpha, \beta \in \mathbb{F}$:

1. $(\alpha S + \beta T)^\dagger = \alpha^* S^\dagger + \beta^* T^\dagger$,
2. $(S^\dagger)^\dagger = S$,
3. $(ST)^\dagger = T^\dagger S^\dagger$.

At this point, we draw parallels between the Riesz representation theorem and quantum mechanics. In Dirac's notation, the vector elements $v \in \mathcal{H}$ are written as so-called *kets*: $|\psi\rangle, |\phi\rangle$ that describes the physical state of some system. The adjoints are called *bras*: $\langle\psi|, \langle\phi|$ and are elements of the dual space of $\mathcal{H}$. The inner product of both gives the overlap written by $\langle\psi|\phi\rangle$. These physical states obey all the conditions for inner products.

[1] The map $T : \mathcal{V} \to \mathcal{W}$ is termed *conjugate-linear* if $T(\alpha u + \beta v) = \alpha^* T(u) + \beta^* T(v)$, for $\alpha, \beta \in \mathbb{F}$ and $u, v \in \mathcal{V}$. If the two vector fields are described over the real space $\mathbb{F} = \mathbb{R}$, then the map is just linear.

A.3 Structure of vector spaces

An understanding of vector spaces can be achieved by observing the structure of its subspaces. In this subsection we describe how we can combine two linear vector spaces. This is important in understanding how linear operators operate on the Hilbert space.

Sometimes we can write a vector space $\mathcal{H}$ in terms of its subspaces $\mathcal{U}_1, \mathcal{U}_2, \ldots, \mathcal{U}_n$. More precisely, if $\mathcal{U}_j \cap \mathcal{U}_k = \{0\}$ for all $j, k \in \{1, 2, \ldots, n\}$, and for every element $v \in \mathcal{H}$, there exists the unique sum $v = u_1 + u_2 + \cdots + u_n$, where $u_j \in \mathcal{U}_j$, then we can write $\mathcal{H}$ as the *direct sum* of its subspaces:

$$\mathcal{H} = \bigoplus_{j=1}^{n} \mathcal{U}_j. \tag{A.27}$$

The dimension of $\mathcal{H}$ is then the sum of the dimensions of its subspaces:

$$\dim \mathcal{H} = \sum_{j=1}^{n} \dim \mathcal{U}_j. \tag{A.28}$$

We can use the notion of an inner product to construct interesting subspaces of $\mathcal{H}$. Let $\mathcal{S}$ be a *subset* of vectors in the Hilbert space $\mathcal{H}$, that is not necessarily a subspace[2]. We then define the *orthogonal complement* of $\mathcal{S}$ as the closed linear subspace of $\mathcal{H}$, containing the set of all vectors orthogonal to the vectors in $\mathcal{S}$:

$$\mathcal{S}^{\perp} = \{v \in \mathcal{H} \mid \langle s|v\rangle = 0 \text{ for all } s \in \mathcal{S}\}. \tag{A.29}$$

Projection theorem: *If $\mathcal{S}$ is a closed subspace of a Hilbert space $\mathcal{H}$, then the subspace and its orthogonal complement give a direct sum decomposition of the full space:*

$$\mathcal{H} = \mathcal{S} + \mathcal{S}^{\perp}. \tag{A.30}$$

This is not difficult to show. For any orthonormal basis of $\mathcal{S}$ $\{e_j\}$, we can trivially write any vector $v \in \mathcal{H}$ as

$$v = \left(\sum_{j=1}^{n} \langle e_j, v\rangle e_j\right) + \left(v - \sum_{j=1}^{n} \langle e_j, v\rangle e_j\right). \tag{A.31}$$

the first vector in parenthesis is clearly in $\mathcal{S}$ since it is written as a linear combination of e_j. The second vector is clearly in $\mathcal{S}^{\perp}$ as one can see that it is orthogonal to any vector in $\mathcal{S}$. Let $v \in \mathcal{S} \cap \mathcal{S}^{\perp}$. Then, since v is in $\mathcal{S}$ and in $\mathcal{S}^{\perp}$, it should satisfy $\langle v, v\rangle = 0$, which implies $v = \mathbf{0}$. Thus $\mathcal{S} \cap \mathcal{S}^{\perp} = \{\mathbf{0}\}$. This ensure the uniqueness of v. ■

This theorem guarantees the existence of the *orthogonal projection* map $\hat{P}_{\mathcal{S}} : \mathcal{H} \to \mathcal{S}$. That is, given a Hilbert space $\mathcal{H}$ and a closed linear subspace $\mathcal{S} \subseteq \mathcal{H}$, any element $v \in \mathcal{H}$ can be

[2] A subset of $\mathcal{S}$ is any set contained in $\mathcal{S}$. A subspace of $\mathcal{S}$ is any subset of $\mathcal{S}$ that inherits the spacial structure of the space $\mathcal{S}$. Hence a subspace of a vector space $\mathcal{V}$ is a subset of $\mathcal{V}$ that is also a vector space with the same operations. To verify that a subset $\mathcal{U}$ of $\mathcal{V}$ is a subspace you must check that $\mathcal{U}$ contains the zero vector $\mathbf{0}$, and that $\mathcal{U}$ is closed under addition and scalar multiplication.

written uniquely as the sum $\boldsymbol{v} = \boldsymbol{x} + \boldsymbol{y}$ where $\boldsymbol{x} \in \mathcal{S}$ and $\boldsymbol{y} \in \mathcal{S}^\perp$. The projector $\hat{P}$ then acts on the element $\boldsymbol{v}$ to give $\boldsymbol{x}$, from which it is clear that projectors are associated with subspaces. To understand this, consider some Euclidean space $\mathcal{E}^3$ spanned by the unit vectors $\{\boldsymbol{e}_1, \boldsymbol{e}_2, \boldsymbol{e}_3\}$. The projector then acts on any element in $\mathcal{E}^3$ and sets all components to zero besides those on the subspace it projects to. Projectors describe the 'collapse' of the state of some physical system onto some eigenspace of the measurement operator. Hence it is clear that from Eq. (A.31)

$$\hat{P}_{\mathcal{S}} \boldsymbol{v} = \boldsymbol{x} = \sum_{j=1}^{n} \langle \boldsymbol{e}_j, \boldsymbol{v} \rangle \boldsymbol{e}_j. \tag{A.32}$$

Note that the null space of $\hat{P}_{\mathcal{S}}$ is $\mathcal{S}^\perp$. Once projected to a subspace, a second operation of the same map should have no effect. It follows then that $\hat{P}_{\mathcal{S}}$ is a bounded linear map satisfying

$$\hat{P}_{\mathcal{S}}^2 = \hat{P}_{\mathcal{S}}. \tag{A.33}$$

This implies that the eigenvalues of $\hat{P}_{\mathcal{S}}$ is either zero or one, which corresponds to the orthonormal basis of $\mathcal{S}$ or $\mathcal{S}^\perp$ respectively. That is, for some $(n+m)$-dimensional space decomposed according to Eq. (A.30) with $\boldsymbol{e} = \{\boldsymbol{e}_1, \ldots, \boldsymbol{e}_n\}$ an orthonormal basis for $\mathcal{S}$ and $\boldsymbol{f} = \{\boldsymbol{f}_1, \ldots, \boldsymbol{f}_m\}$ for $\mathcal{S}^\perp$, a suitable orthonormal basis for $\mathcal{H}$ is spanned by $\boldsymbol{g} = \boldsymbol{e} \oplus \boldsymbol{f}$, then

$$\hat{P}_{\mathcal{S}} \boldsymbol{g} = \mathrm{diag}[1, \ldots, 1, 0, \ldots, 0] \boldsymbol{g}. \tag{A.34}$$

Note that the rank of the projector is related to the dimension of the space it operates on: $\mathrm{Tr}[\hat{P}_{\mathcal{S}}] = \dim[\mathcal{S}]$.

An alternative way to combine vector spaces $\mathcal{U}_j$ is through the *tensor product*:

$$\mathcal{H} = \bigotimes_{j=1}^{n} \mathcal{U}_j. \tag{A.35}$$

The dimension of $\mathcal{H}$ is then the multiplication of the dimensions of its subspaces:

$$\dim \mathcal{H} = \prod_{j=1}^{n} \dim \mathcal{U}_j. \tag{A.36}$$

The tensorial nature of the Hilbert space is heavily used in quantum theory. To see how, consider the elements of the Hilbert space $|\psi\rangle = \sum_j c_j |\psi_j\rangle \in \mathcal{U}_1$ and $|\phi\rangle = \sum_j d_j |\phi_j\rangle \in \mathcal{U}_2$, then the tensor product of these states is written

$$|\psi\rangle \otimes |\phi\rangle = \sum_{j,k} c_j d_k |\psi_j\rangle \otimes |\phi_k\rangle = \sum_{j,k} c_j d_k \left|\psi_j, \phi_k\right\rangle, \tag{A.37}$$

where we introduced convenient abbreviations for the tensor product notation. The inner product of two vectors that are tensor products is

$$\langle \psi_1, \phi_1 | \psi_2, \phi_2 \rangle = \langle \psi_1 | \psi_2 \rangle \langle \phi_1 | \phi_2 \rangle. \tag{A.38}$$

Operators also obey the tensor product structure $(A \otimes B)(C \otimes D) = (AC \otimes BD)$. We note that every operator sticks to its own Hilbert space. General rules for tensor products of operators are:

1. $(\boldsymbol{A}_1 + \boldsymbol{A}_2) \otimes \boldsymbol{B} = \boldsymbol{A}_1 \otimes \boldsymbol{B} + \boldsymbol{A}_2 \otimes \boldsymbol{B}$,
2. $\boldsymbol{A} \otimes \boldsymbol{0} = \boldsymbol{0} \otimes \boldsymbol{A} = \boldsymbol{0}$,
3. $\mathbb{1} \otimes \mathbb{1} = \mathbb{1}$,
4. $\alpha\boldsymbol{A} \otimes \beta\boldsymbol{B} = (\alpha\beta)\boldsymbol{A} \otimes \boldsymbol{B}$,
5. $(\boldsymbol{A} \otimes \boldsymbol{B})^{-1} = \boldsymbol{A}^{-1} \otimes \boldsymbol{B}^{-1}$,
6. $(\boldsymbol{A} \otimes \boldsymbol{B})^{\dagger} = \boldsymbol{A}^{\dagger} \otimes \boldsymbol{B}^{\dagger}$,
7. $\mathrm{Tr}[\boldsymbol{A} \otimes \boldsymbol{B}] = \mathrm{Tr}[\boldsymbol{A}]\mathrm{Tr}[\boldsymbol{B}]$,

where we will define the trace $\mathrm{Tr}[\cdot]$ of an operator in subsection A.4.

A.4 The trace and determinant of an operator

Before concluding this appendix, we mention two special functions of operators that are heavily used in linear vector spaces. These operations are the *trace* and *determinant* and for any operator $\boldsymbol{T}$ are denoted by $\mathrm{Tr}[\boldsymbol{T}]$ and $\det \boldsymbol{T}$, respectively. The trace map is the simplest operation related to measurements. In the matrix representation of linear operators, the trace of the operator can be understood as the sum of the diagonal elements:

$$\mathrm{Tr}[\boldsymbol{T}] = \boldsymbol{T}_{jj}, \tag{A.39}$$

where we remind ourselves that repeat indices implies a sum over the index. Similarly, the determinant of some operator $\boldsymbol{T}$ can be defined though:

$$\det \boldsymbol{T} = \sum_{\sigma \in S_n} \left[\mathrm{sgn}(\sigma) \prod_{j=1}^{n} \boldsymbol{T}_{j,\sigma(j)} \right] \tag{A.40}$$

where the sign function '$\mathrm{sgn}(\sigma)$' returns $+1$ (-1) for even (odd) permutations in the permutation group S_n (see appendix E for details). This is the *Leibniz* or *Laplace formula*. Note that both operations are conveniently written using the matrix representation of the operator $\boldsymbol{T}$. However, since the trace is in fact basis independent, we should be able to write $\mathrm{Tr}[\boldsymbol{T}]$ without specifying the basis. To understand this, we use the result for the basis change we obtained in Eq. (A.21):

$$\mathrm{Tr}[\boldsymbol{T}(\{\boldsymbol{v}\})] = \boldsymbol{T}_{jj}(\{\boldsymbol{v}\}) = \boldsymbol{A}_{jk}\boldsymbol{T}_{kl}(\{\boldsymbol{w}\})\boldsymbol{A}^{-1}_{lj} = \delta_{lk}\boldsymbol{T}_{kl}(\{\boldsymbol{w}\}) = \mathrm{Tr}[\boldsymbol{T}(\{\boldsymbol{w}\})], \tag{A.41}$$

where we used $\boldsymbol{A}^{-1}_{lj}\boldsymbol{A}_{jk} = \delta_{lk}$. Hence we see that the trace of some linear operator is basis independent. The same property is also true for the determinant which can be easily demonstrated through:

$$\det \boldsymbol{T}(\{\boldsymbol{v}\}) = \det[\boldsymbol{A}] \det[\boldsymbol{T}(\{\boldsymbol{w}\})] \det\left[\boldsymbol{A}^{-1}\right] = \det \boldsymbol{T}(\{\boldsymbol{w}\}), \tag{A.42}$$

where we used the property $\det[\boldsymbol{A}]\det[\boldsymbol{A}^{-1}] = \det[\boldsymbol{A}\boldsymbol{A}^{-1}] = 1$.

Appendix B

Operator ordering methods in quantum optics

Operators in quantum mechanics satisfy matrix algebra, which implies that two operators do not necessarily commute. Hence there is an ambiguity in the definition of any function of non-commuting operators. In this appendix we discuss common operator ordering conventions. These conventions have lead to the introduction of associated quasiprobability distributions that describe quantum-classical correspondences, which have been used to solve many problems in quantum optics. We then explain how certain operator orderings help solve the vacuum expectation values (VEVs). This was an important part of calculating the quantum Fisher information as we observed in chapters 4 and 5. We define a function in Mathematica that can deal with this. We note that the SNEG package developed by Ž. Rok [Žitko, 2011] built for commutation algebra is not complete and can not handle specific operations.

B.1 Types of operator orderings

For non commuting operators, there is an ambiguity in the definitions of operator functions in quantum mechanics. This is implicit in the definition of the number operator, which was defined as $\hat{n} = \hat{a}^\dagger \hat{a} \neq \hat{a}\hat{a}^\dagger$. For functions of $\hat{a}$ and $\hat{a}^\dagger$ (and hence of any operator function), there are three operator orderings, referred to as *normal*, *antinormal*, and *symmetric* (or *Weyl*). To describe each, we introduce the operator string $\hat{\boldsymbol{a}} = \hat{a}^{\dagger p}\hat{a}^q$ for $p, q \in \mathbb{R}$. Then, the normal ordered form of the number operator raised to power $\hat{\boldsymbol{a}}$ is written

$$: \hat{\boldsymbol{a}} := \hat{a}^{\dagger p}\hat{a}^q, \tag{B.1}$$

which remains unchanged. There is another method to obtain the normal ordered form of the operator, which we denote through $\mathcal{N}[\hat{\boldsymbol{a}}]$. We postpone a discussion of the difference between these operations for the next section, but the result leaves *all* creation operators to the left of annhilation operators. Antinormal ordering instead places all annhilation operators to the left of creation operators and is written

$$\vdots \hat{\boldsymbol{a}} \vdots = \hat{a}^q \hat{a}^{\dagger p}. \tag{B.2}$$

Ordering	Notation	Description
Normal	$\mathcal{N}$ or $:\hat{n}^l:$	All $\hat{a}^\dagger$'s to left of $\hat{a}$'s
Antinormal	$\mathcal{A}$ or $\vdots\hat{n}^l\vdots$	All $\hat{a}$'s to left of $\hat{a}^\dagger$'s
Symmetric	$S(\hat{n}^l)$	Symmetric ordering

Table B.1: *Different operator orderings used in quantum optics for non-commuting operators. We use the number operator as an example, but since any operator may be re-expressed in terms of the operators* $\{\hat{a}, \hat{a}^\dagger\}$*, this is true for any operator function. Achieving each type of ordering is described in the text. The difference between the two operations achieving normal ordering will be described in section B.2.*

Similar to normal ordering, there is an alternative function $\mathcal{A}$ that returns the antinormal ordered form of an operator: $\mathcal{A}[\hat{\boldsymbol{a}}]$. The symmetric or Weyl ordering is the complete symmetrisation of the creation and annhilation operators. That is, the symmetrised operator of $\hat{\boldsymbol{a}}$ can be written as the sum of all permutations of $p\hat{a}^\dagger$'s and $q\hat{a}$'s, weighted by the number of terms. We write this as:

$$S\left(\hat{\boldsymbol{a}}\right) = \binom{p+q}{q}^{-1} \sum_{\sigma} \prod_{j=1}^{n} \hat{\boldsymbol{a}}_{\sigma(j)}, \tag{B.3}$$

where the sum over permutation elements was defined in appendix E and the Binomial coefficient $\binom{a}{b} = a!/[(a-b)!b!]$ is the number of permutations of arranging a operators given b indistinguishable (same-mode) operators. Note that for $p = q = 1$, $\hat{\boldsymbol{a}} = \hat{n}$, then $S[\hat{\boldsymbol{a}}] = \{\hat{a}, \hat{a}^\dagger\}/2$.

Table B.1 summarises the three operator orderings. Since certain operator orderings are more suited to specific problems, mapping between them is important. This is beyond the scope of this thesis, but the reader is recommended to consult section 3.3 of [Barnett and Radmore, 2005].

B.2 Normal ordering method

As discussed in the previous section, the normal ordered form of a boson operator, where all creation operators appear to the left of annihilation operators, was developed to address the operator ordering ambiguity. The two well-defined procedures on the boson operators that yield a normally ordered form are known as the normal ordering $\mathcal{N}$ operation, and the double-dot $:\cdot:$ operation. Both normal ordering methods are appropriate to calculate *vacuum expectation values* (VEV) of a string of operators, which is the average value of the operator string in the ground state. This is since the VEV of a normally ordered operator string is zero.

B.2.1 Different normal ordering strategies

For any general boson operator string written $g(\hat{a}, \hat{a}^\dagger)$, normal ordering by means of the $\mathcal{N}$ operation is achieved by repeated use of commutation relations until all creation operators appear to the left of annihilation operators. In the double-dot operation, the normally ordered form of $g(\hat{a}, \hat{a}^\dagger)$ is achieved by assuming the creation and annihilation operators commute. The operator is in general changed, with an equivalence maintained only if the operation is performed on a normally ordered string: $\mathcal{N}[g(\hat{a}, \hat{a}^\dagger)] = :\mathcal{N}[g(\hat{a}, \hat{a}^\dagger)]:$. From these definitions, we can immediately understand the two operations that achieve antinormal ordered operators: $\mathcal{A}$, and the triple dot $\vdots\cdot\vdots$ operation. The operation $\mathcal{A}$ uses the same commutation relations as $\mathcal{N}$, but has the effect of ordering all annihilation operators before creation operators.

The normal ordering problem is solved when the following is satisfied:

$$g(\hat{a}, \hat{a}^\dagger) = \mathcal{N}\left[g(\hat{a}, \hat{a}^\dagger)\right] =: g(\hat{a}, \hat{a}^\dagger) : . \tag{B.4}$$

To exemplify the difference between both operations, it is meaningful to compare the normal ordered forms of operator string $\hat{a}^j(\hat{a}^\dagger)^k$. The double dot operation readily gives

$$: \hat{a}^j(\hat{a}^\dagger)^k := (\hat{a}^\dagger)^k \hat{a}^j. \tag{B.5}$$

Through repeated use of the commutation relation $[\hat{a}, \hat{a}^\dagger] = 1$, then it can be shown that [Blasiak et al., 2007]:

$$\hat{a}^j(\hat{a}^\dagger)^k = \mathcal{N}\left[\hat{a}^j(\hat{a}^\dagger)^k\right] = \sum_{l=0}^{j} \binom{j}{l} k^{\underline{l}} (\hat{a}^\dagger)^{k-l} \hat{a}^{j-l}, \tag{B.6}$$

where we have defined the *falling factorial* $k^{\underline{l}} = k(k-1)\cdots(k-l+1)$. In general, normal ordered operators have attracted a lot of attention in quantum optics and quantum field theory. One application of this ordering an operator in this manner is that we can immediately write its coherent state matrix elements. That is, for the operator string in Eq. (B.4) we have:

$$\left\langle \alpha' \middle| g(\hat{a}, \hat{a}^\dagger) \middle| \alpha \right\rangle = \langle \alpha' | \alpha \rangle \, g(\alpha, \alpha'^*) \tag{B.7}$$

More specifically, the two operations achieving normal ordered operators have attracted their individual applications. This is easy to understand: the two operations have different meanings. The double-dot operation changes the physical nature of the operator string. However, this procedure for normally-ordering Hamiltonians has attracted significant attention in quantum field theory, since it ensures the ground state energy is zero [Peskin and Schroeder, 1995]. To understand this, we recall from chapter 2, Eq. (2.63) that the quantised Hamiltonian

$$\hat{\mathcal{H}} \propto \frac{1}{2}\left(\hat{a}^\dagger\hat{a} + \hat{a}\hat{a}^\dagger\right) = \left(\hat{a}^\dagger\hat{a} + \frac{1}{2}\right) \tag{B.8}$$

had energies $E_n = n + 1/2$ for all $n = 0, 1, 2, \ldots$, from which it is clear that the ground state energy is non-zero. In quantum field theory, any field is considered as an infinite collection of harmonic oscillators. The contribution of the zero point energies from each oscillator would predict an unphysical field with infinite energy. The work-around is to define the ground state to have zero energy by subtracting the zero point energy from each oscillator:

$$\hat{\mathcal{H}}_0 \propto : \frac{1}{2}\left(\hat{a}^\dagger\hat{a} + \hat{a}\hat{a}^\dagger\right) := \frac{1}{2}\left(\hat{a}^\dagger\hat{a} + \hat{a}\hat{a}^\dagger\right) - \frac{1}{2}\langle 0|\left(\hat{a}^\dagger\hat{a} + \hat{a}\hat{a}^\dagger\right)|0\rangle \equiv \hat{a}^\dagger\hat{a}. \tag{B.9}$$

By subtracting the zero point energy, we obtain a new Hamiltonian that is generated from the double-dot operation of the original Hamiltonian: $\hat{\mathcal{H}}_0 =: \hat{\mathcal{H}} :$.

In certain cases, the use of commutation relations for normal ordering through the operation $\mathcal{N}$ is preferred. This is since it does not change the interpretation of the operator despite having a different functional appearance. In this thesis, we have considered only this approach, and will continue to do so for the remainder of this appendix. From Eq. (B.6) we observe that this approach yields many terms. A systematic approach to address all of the combinatorics associated with *any* operator string is through *Wicks theorem*[1]. A wide variety of numerical packages provide some ease to this difficulty for polynomial expressions. However, this becomes increasingly cumbersome for increasing operator string lengths and the computational time grows exponentially. The normal ordering problem for non trivial operator strings of arbitrary lengths remains an open area of research with notable contribution made by Blasiak et al. [2007]. However, these methods have assumed commutation relations for discrete systems: $[\hat{a}, \hat{a}^\dagger] = 1$. In this thesis we work with continuous variable systems. Evaluated VEVs is then a bit more involved. Luckily, we encounter a very specific form for the operator string that helps generalise the result.

In the following, we use the Bargmann representation to approach the normal ordering problem [Bargmann, 1961]. It converts a boson operator string into one of multiplicative factors of a formal dummy variable η and its derivative by making the following transformations:

$$\hat{a}_j^\dagger \to \eta_j \quad \text{and} \quad \hat{a}_j \to \frac{\partial}{\partial \eta_j}. \tag{B.10}$$

The commutation relation is preserved and this transformation makes the evaluation of vacuum expectation values of boson operator strings easier. Under this transformation map, the action of the annihilation operator $\hat{a}(k_j)\,|0\rangle = 0$ is reproduced if the vacuum $|0\rangle$ maps to unity: $\partial/\partial\eta_j \cdot 1 = 0$. We use this representation to derive some results that have been used in the thesis.

In section 4.2.1 we determined the dependence of the QFI on the source separation distance by allowing a relaxation of the assumption that sources are mutually independent. The following vacuum expectation value was encountered:

$$\langle 0| \prod_{j=1}^{N} \hat{b}(x_j) \prod_{j=1}^{N} \hat{b}^\dagger(x'_j) |0\rangle = \sum_{\sigma} \prod_{j=1}^{N} \delta\left(x_j - x'_{\sigma(j)}\right). \tag{B.11}$$

The permutation sum identifies all the possible combinations of source overlaps along the array. This expression becomes increasingly cumbersome to determine for more complicated boson strings as encountered when using the generator to determine the QFI. Hence, to simplify the evaluation after this, we assumed mutual independence for different sources. By use of the Bargmann representation, we derive the following two expectation values:

$$\langle 0|\hat{b}_j(k'_j)^{n_j}\hat{n}_j(k''_j)\hat{b}_j^\dagger(k_j)^{n_j}|0\rangle = n_j! n_j \delta\left(k'_j - k''_j\right)\delta\left(k''_j - k_j\right)\delta\left(k_j - k'_j\right)^{n_j-1} \tag{B.12}$$

and

$$\langle 0|\hat{b}_j(k'_j)^{n_j}\hat{n}_j(k''_j)\hat{n}_j(k'''_j)\hat{b}_j^\dagger(k_j)^{n_j}|0\rangle = n_j! n_j^2 \delta\left(k'_j - k''_j\right)\delta\left(k''_j - k_j\right)\delta\left(k_j - k'_j\right)^{n_j-1}. \tag{B.13}$$

[1] Wicks theorem reduces the operation $\mathcal{N}$ to a sum of double dot operations on all contractions of the operator string. The term contraction refers to the removal of a pair of $\hat{a}$ and $\hat{a}^\dagger$ such that $\hat{a}$ always precedes $\hat{a}^\dagger$.

These vacuum expectation values are used to evaluate the variance of the generator. Specifically, the absence of the summation over all permutations reflects the use of updated commutation relations, which treat each source as distinct and mutually independent.

B.2.2 Normal ordering on continuous variable systems

In the following *Mathematica* code we generate a means of expressing the vacuum expectation values associated with continuous variable systems. The commutator used is

$$\left[\hat{a}(k_m), \hat{a}^{\dagger}(k_n)\right] = \delta(k_m - k_n). \tag{B.14}$$

It returns the only surviving terms once the ground state expectation values has been determined.

```
In[1]:= (*Normalization<0|0> =1*)
        correlate[]=1;

        (* Commutation relation: [a(k1),a†(k2)]=δ(k1-k2) *)
        correlate[left___,a[k1_],ad[k2_],right___]:=
        correlate[left,ad[k2],a[k1],right]+δ[k1-k2] correlate[left,right];

        (* Commutation relations: [a(k1),a(k2)]=[a†(k1),a†(k2)]=0 *)
        correlate[left___,a[k1_],a[k2_],right___]/;!OrderedQ[{k2,k1}]:=
        correlate[left,a[k2],a[k1],right];

        correlate[left___,ad[k1_],ad[k2_],right___]/;!OrderedQ[{k2,k1}]:=
        correlate[left,ad[k2],ad[k1],right];

        (* Annihilation of vacuum state: <0|a† and a|0> =0 *)
        correlate[___,a[_]]:=0;
        correlate[ad[_],___]:=0;


In[2]:= correlate[a[k10],a[k9],ad[k8],a[k7],ad[k6],a[k5],ad[k4],ad[k3]]

Out[2]= δ[-k4+k5] δ[-k6+k7] δ[k10-k8] δ[-k3+k9]+
        δ[-k3+k5] δ[-k6+k7] δ[k10-k8] δ[-k4+k9] +
        δ[-k4+k5] δ[-k3+k7] δ[k10-k8] δ[-k6+k9] +
        δ[-k3+k5] δ[-k4+k7] δ[k10-k8] δ[-k6+k9] +
        δ[-k4+k5] δ[k10-k6] δ[-k3+k7] δ[-k8+k9] +
        δ[-k3+k5] δ[k10-k6] δ[-k4+k7] δ[-k8+k9] +
        δ[k10-k4] δ[-k3+k5] δ[-k6+k7] δ[-k8+k9] +
        δ[k10-k3] δ[-k4+k5] δ[-k6+k7] δ[-k8+k9].
```

Appendix C

Operator identities

In this appendix we go through some of the identities that have been commonly used throughout the work in this thesis. All of the identities summarised in this appendix have been based on material that can be found in the classic quantum optics textbooks by Scully and Zubairy [1997]; Barnett and Radmore [2005]; Sakurai and Napolitano [2017]. For proof of the identities, the reader is referred to these texts.

Sum of nested commutators - Jacobi Identity:

$$\left[\hat{A},\left[\hat{B},\hat{C}\right]\right]+\left[\hat{B},\left[\hat{C},\hat{A}\right]\right]+\left[\hat{C},\left[\hat{A},\hat{B}\right]\right]=0. \tag{C.1}$$

This can be generalised operators of arbitrary length.

Expansion of commutators - Leibniz's law:

$$\begin{aligned}\left[\hat{A},\hat{B}\hat{C}\right]&=\left[\hat{A},\hat{B}\right]\hat{C}+\hat{B}\left[\hat{A},\hat{C}\right],\\ \left[\hat{A}\hat{B},\hat{C}\right]&=\left[\hat{A},\hat{C}\right]\hat{B}+\hat{A}\left[\hat{B},\hat{C}\right].\end{aligned} \tag{C.2}$$

If two operators have a unit commutator, then a more general property exists for the expansion of their commutators.

Bosonic operator function commutators: *For $\alpha\in\mathbb{C}$ and the creation and annihilation operators $\hat{a}^\dagger$ and $\hat{a}$ respectively satisfying the commutator $[\hat{a},\hat{a}^\dagger]=\mathbb{1}$, we have the following identities:*

$$\left[\hat{a},f(\hat{a},\hat{a}^\dagger)\right]=\frac{\partial f}{\partial\hat{a}^\dagger}, \tag{C.3}$$

$$\left[\hat{a}^\dagger,f(\hat{a},\hat{a}^\dagger)\right]=-\frac{\partial f}{\partial\hat{a}}, \tag{C.4}$$

$$\exp\left[-\alpha\hat{a}^\dagger\hat{a}\right]f(\hat{a},\hat{a}^\dagger)\exp\left[\alpha\hat{a}^\dagger\hat{a}\right]=f(\hat{a}\exp[\alpha],\hat{a}^\dagger\exp[-\alpha]). \tag{C.5}$$

Operator functions: *For any Hermitian operator $\hat{A}$ with the spectrum $\{a_j, |a_j\rangle\}$, then the operation of any well-behaved function f on $\hat{A}$ may be written*

$$f(\hat{A}) = \sum_j f(a_j) \left|a_j\right\rangle \left\langle a_j\right|, \tag{C.6}$$

which follows from matrix properties. This can alternatively be shown from the Maclaurin operator expansion of $f(\hat{A})$:

$$f(\hat{A}) = \sum_{j=0}^{\infty} \frac{f^{(j)}(\mathbf{0})}{j!} \hat{A}^j. \tag{C.7}$$

A common function encountered in quantum optics is the exponential function since exponentiating any Hermitian operator yields a unitary operator. Since the number operator is Hermitian, we can immediately exemplify the use of Eq. (C.7) by considering the expansion of some number $\alpha \in \mathbb{C}$ raised to the power of $\hat{n}$:

$$\alpha^{\hat{a}^\dagger \hat{a}} = \exp\left[\hat{a}^\dagger \hat{a} \ln \alpha\right] = \sum_n \exp\left[n \ln \alpha\right] |n\rangle \langle n| , \tag{C.8}$$

where we used the Fock-basis as a complete, orthonormal set of the number operator. In fact, using the Maclaurin expansion for the exponential function, we can prove the *Hadamard Lemma*, which for *any* two operators $\hat{A}$ and $\hat{B}$ reads:

Hadamard Lemma: *For some $\alpha \in \mathbb{C}$:*

$$\exp\left[\alpha \hat{A}\right] \hat{B} \exp\left[-\alpha \hat{A}\right] = \hat{B} + \alpha \left[\hat{A}, \hat{B}\right] + \frac{\alpha^2}{2!} \left[\hat{A}, \left[\hat{A}, \hat{B}\right]\right] + \ldots. \tag{C.9}$$

Alternative derivations for this lemma can be seen in section 1.4.1 of Kok and Lovett [2010]. This lemma was used to generalise the form of the generator of dynamics in chapter 5. It is also used to generate operator ordering theorems, such as the following Baker-Campbell-Hausdorff formula:

Baker-Campbell-Hausdorff formula: *If $\left[\hat{A}, \left[\hat{A}, \hat{B}\right]\right] = \left[\hat{B}, \left[\hat{A}, \hat{B}\right]\right] = 0$, then:*

$$\begin{aligned} \exp\left[\hat{A} + \hat{B}\right] &= \exp\left[\hat{A}\right] \exp\left[\hat{B}\right] \exp\left[-\frac{1}{2}\left[\hat{A}, \hat{B}\right]\right] \\ &= \exp\left[\hat{B}\right] \exp\left[\hat{A}\right] \exp\left[\frac{1}{2}\left[\hat{A}, \hat{B}\right]\right]. \end{aligned} \tag{C.10}$$

This formula is often used to show different operator orderings. To understand this, we follow the argument presented by Barnett and Radmore. Consider the jth term in the Maclaurin expansion of the left hand side of Eq. (C.10): $(\hat{A} + \hat{B})^j$. For non-commuting $\hat{A}$ and $\hat{B}$, this expansion is ambiguous. While we defer further discussion of operator orderings until appendix B, we appreciate that for certain problems in quantum optics, it may be useful to express the expansion such that all occurrences of $\hat{A}$ appear to the left of $\hat{B}$. This can be achieved through

repeated use of the assumed commutator between the operators to re-arrange their ordering. Hence, the resulting power series can be written as the product of a function of $\hat{A}$, a function of $\hat{B}$, and a function of their commutator $[\hat{A}, \hat{B}]$. This is exactly the Baker-Campbell-Hausdorff formula, which can also be used to place all occurrences of $\hat{B}$ before $\hat{A}$. In this thesis, this formula was used to express different forms of the characteristic function, which gives rise to different quasiprobability distributions.

For completeness, we mention the existence of other operator ordering formulas that derive from this. These can be reviewed in appendix 5 of [Barnett and Radmore, 2005, p. 236–239].

Appendix D

Statistical distance measures

Distance measures are central to quantum estimation theory and quantum information theory. They provide a means to quantify distinguishability and similarity between two statistical objects. There are many intuitive applications of distance measures, such as the Euclidean distance is a common measure for distances. In classical information, the distinguishability between two messages could be the difference between two bit strings that encode a message. In parameter estimation, we will see that the Fisher information gives a statistical distance measure between two probability distributions generated from two different values of a parameter to estimate. In this appendix, we define the axioms for statistical distance measures. We will see that the arbitrariness of these definitions allow for its easy extension to the quantum mechanical case. Notable contributions to this extension were made by Wooters [1981]; Hilgevoord and Uffink [1991]; Braunstein and Caves [1994]. We limit our review to *static* distance measures, which measure the similarity between two objects. This is in contrast to *dynamic* measures which quantifies the information content preserved during the dynamical process [Nielsen and Chuang, 2010].

D.1 Distance measures for probability distributions

In this section, we present a precise definition of distance measures. A metric is a distance function that defines the distance between any two elements of a set. Any set with an associated metric is called a metric space. More precisely, for some metric space S, a *metric* on the set X is the distance function

$$d : X \times X \to [0, \infty), \tag{D.1}$$

where $[0, \infty)$ is the set of non-negative real numbers, which for all $\boldsymbol{x}, \boldsymbol{y}, \boldsymbol{z} \in S$ satisfies the following three axioms.

1. $d(\boldsymbol{x}, \boldsymbol{y}) = d(\boldsymbol{y}, \boldsymbol{x})$ (*Symmetric*)
2. $d(\boldsymbol{x}, \boldsymbol{y}) \geq 0$ with equality iff $\boldsymbol{x} = \boldsymbol{y}$ (*Positivity*)

3. $d(\boldsymbol{x}, \boldsymbol{z}) \leq d(\boldsymbol{x}, \boldsymbol{y}) + d(\boldsymbol{y}, \boldsymbol{z})$ (*Triangle inequality*)

The distance function $d(\boldsymbol{p}, \boldsymbol{q})$ between the points $\boldsymbol{p}$ and $\boldsymbol{q}$ is valid if it satisfies all the following properties which defines a metric for all $\boldsymbol{p}, \boldsymbol{q}$:

The vectors $\boldsymbol{p}$ and $\boldsymbol{q}$ in the two dimensional Euclidean space, $\mathbb{R}^2$, can be seen to satisfy the properties of a metric. We will now consider different distance measures.

D.2 Distance measures for classical information

Some shit here to motivate the rest of this section.

D.2.1 Hamming distance

The Hamming distance for classical codes is the *minimum* number of bit flips required to transform a bit string into another. For

$$\begin{aligned} \boldsymbol{x} &= 1\,0\,1\,0 \\ \boldsymbol{y} &= 0\,1\,1\,0, \end{aligned} \tag{D.2}$$

we have $H(\boldsymbol{p}, \boldsymbol{q}) = 2$. This code distance determines the maximum number of errors that can be detected, $(d-1)$, where d is the *code distance* [Nielsen and Chuang, 2010]. This measure is not capable of describing more complex information sources over general probability distributions.

D.2.2 The classical fidelity

For two classical random variables, X and Y described by the *probability distributions* $\{x_i\}$ and $\{y_i\}$, the fidelity is defined

$$\mathscr{F}_C(\boldsymbol{x}, \boldsymbol{y}) = \left[\sum_i \sqrt{x_i y_i}\right]^2 := B(\boldsymbol{x}, \boldsymbol{y})^2, \tag{D.3}$$

where $\boldsymbol{x} = \{x_i\}$ and $\boldsymbol{y} = \{y_i\}, i \in [1, d]$ with d being the dimension of the metric space. The classical fidelity can be understood as the inner product of the vectors $\{x_1, x_2, \ldots, x_d\}$ and $\{y_1, y_2, \ldots, y_d\}$ in the d–dimensional Euclidean space. The conventional definitions provided in [Bengtsson and Zyczkowski, 2008; Nielsen and Chuang, 2010] is the *non-squared* version of the above. The *Bhattacharyya distance* can be defined as $D_{\text{Bhatt}} = \cos^{-1} B(\boldsymbol{x}, \boldsymbol{y})$, with the *Bhattacharyya coefficient* defined on the RHS of Eq. (D.3).

D.2.3 Trace distance

The *classical* trace distance,

$$d_C(\boldsymbol{p}, \boldsymbol{q}) = \frac{1}{2}\sum_i |p_i - q_i|, \tag{D.4}$$

also provides a tool to distinguish between the two probability distributions $\{p_i\}$ and $\{q_i\}$. This procedure can be extended to distinguish between two quantum states ρ and σ provided

$$d_Q(\rho, \sigma) = \frac{1}{2}\mathrm{Tr}\left[|\rho - \sigma|\right], \tag{D.5}$$

where the modulus requires the positive square root such that $|A| = \sqrt{A^\dagger A}$. This is the quantum analogue of Eq. (D.4) and this can be shown to reduce to the classical trace distance under appropriate criteria as required by the correspondence principle. Namely, the two general states ρ and σ (pure or mixed) commute in the classical limit and hence are diagonal in the same basis such that $\rho = \sum_i \rho_i |i\rangle\langle i|$, $\sigma = \sum_i \sigma_i |i\rangle\langle i|$. Hence Eq. (D.5) becomes

$$\begin{aligned} d_Q(\rho,\sigma) &= \frac{1}{2}\mathrm{Tr}\left[\left|\sum_i (\rho_i - \sigma_i)|i\rangle\langle i|\right|\right] = \frac{1}{2}\mathrm{Tr}\left(\sum_i |\rho_i - \sigma_i| \cdot |i\rangle\langle i|\right) = \frac{1}{2}\sum_i |\rho_i - \sigma_i| \\ &= d_C(\boldsymbol{\rho},\boldsymbol{\sigma}), \end{aligned} \tag{D.6}$$

where we define $\boldsymbol{\rho}$ as the vector of eigenvalues associated with the spectral decomposition of the state ρ. The quantum trace distance is observed to be a suitable metric since it meets all four of the requirements listed earlier.

D.2.4 The quantum fidelity

Similarly, a quantum fidelity can be assigned to quantify the similarity between quantum states. The QFI can then be written in terms of the quantum fidelity – also known as the *Uhlmann fidelity*, $\mathscr{F}_Q$ – according to [Fuentes et al., 2014]

$$\mathcal{I}_Q = \frac{8}{d\theta^2}(1 - \mathscr{F}(\rho_\theta, \rho_{(\theta+d\vartheta)})) \tag{D.7}$$

where the quantum fidelity for two states ρ and σ is defined by

$$\mathscr{F}_Q(\rho,\sigma) = \left(\mathrm{Tr}\sqrt{\sqrt{\rho}\,\sigma\sqrt{\rho}}\right)^2. \tag{D.8}$$

In the case of a pure state $|\psi\rangle$ such that $\rho = |\psi\rangle\langle\psi|$ and an arbitrarily state σ, the quantum fidelity becomes

$$\mathscr{F}_Q(|\psi\rangle,\sigma) = \left(\mathrm{Tr}\sqrt{|\psi\rangle\langle\psi|\sigma|\psi\rangle\langle\psi|}\right)^2 = \langle\psi|\sigma|\psi\rangle = \mathrm{Tr}(\sigma|\psi\rangle\langle\psi|). \tag{D.9}$$

In the evaluation we made use of the fact that $\rho = \hat{U}D\hat{U}^\dagger = \sqrt{\rho}\sqrt{\rho} = \left(\hat{U}\sqrt{D}\,\hat{U}^\dagger\right)\left(\hat{U}\sqrt{D}\,\hat{U}^\dagger\right)$, where we have expressed the state ρ in its spectral decomposition with $\hat{U}$ being the matrix of eigenvectors and where D has as its diagonal the corresponding eigenvalues. Hence $\sqrt{\rho} = \hat{U}\sqrt{D}\,\hat{U}^\dagger$, which requires only the eigenvalues be square-rooted upon spectral decomposition of ρ.

Note that Eq. (D.8) reduces to the classical fidelity in the classical limit, $\rho = \sum_i \rho_i |i\rangle\langle i|$, $\sigma = \sum_i \sigma_i |i\rangle\langle i|$. In this case Eq. (D.8) becomes

$$\begin{aligned} \mathscr{F}_Q(\rho,\sigma) &= \left[\mathrm{Tr}\left(\sqrt{\sum_{i,j}\sqrt{\rho_i}|i\rangle\langle i|\sigma_j|j\rangle\langle j|\sqrt{\rho_i}|i\rangle\langle i|}\right)\right]^2 = \left[\mathrm{Tr}\left(\sqrt{\sum_j \rho_j\sigma_j|j\rangle\langle j|}\right)\right]^2 \\ &= \left[\mathrm{Tr}\left(\sum_j \sqrt{\rho_j\sigma_j}|j\rangle\langle j|\right)\right]^2 = \left[\sum_j \sqrt{\rho_j\sigma_j}\right]^2 = \mathscr{F}_C(\boldsymbol{\rho},\boldsymbol{\sigma}), \end{aligned} \tag{D.10}$$

which concludes our expectation. The quantum fidelity is more extensively used than the trace distance, but it is *not* a metric on the space of density operators. We are able to transform Eq. (D.8) to rectify this [Nielsen and Chuang, 2010]:

Theorem 1 (Uhlmann's Theorem)**.** *Let ρ and σ be two states of a system X, then we introduce Y as the copy of X such that*

$$\mathscr{F}_Q(\rho,\sigma) = \max_{|\psi\rangle,|\varphi\rangle} |\langle\psi|\varphi\rangle|^2, \tag{D.11}$$

where the maximisation is performed over all of the purifications $|\psi\rangle$ of the state ρ and $|\varphi\rangle$ of σ into the combined system XY. ■

To recast the quantum fidelity as a metric, we define

$$\mathscr{A}(\rho,\sigma) = \cos^{-1}\left(\sqrt{\mathscr{F}_Q(\rho,\sigma)}\right) \tag{D.12}$$

as the angle between the states ρ and σ. It can be observed that this obeys all of the criteria of a metric. A geometric interpretation for $\mathscr{F}_Q$ has been provided in [Jones and Kok, 2010]. Further, having defined the quantum fidelity, we are now in a position to exemplify the operational requirements of distinguishability measures for probability distribution.

Example 1 (Operational requirements of distinguishability measures for probability distributions)**.** *The Bhattacharyya coefficient introduced in section D.2.2 can also be understood as the minimisation of the quantum fidelity over all possible POVMs. To understand this and to motivate the quantum fidelity as a suitable distinguishability measure, we pose the question: Which of the two states ρ and σ best describes an unknown general quantum system ξ? Practically, this would require a measurement POVM $\hat{\mathscr{E}}^d$ with elements $\hat{E}_i$. If $\xi = \rho$ (or $\xi = \sigma$), then the measurement outcome would yield the outcome i with probability $\rho_i = \mathrm{Tr}[\rho\hat{E}_i]$ ($\sigma_i = \mathrm{Tr}[\sigma\hat{E}_i]$). Hence distinguishing between the two states ρ and σ amounts to estimating the state by determining the frequency distribution of the measurement outcomes, i.e. distinguishing between the probability distributions $\boldsymbol{\rho} = \{\rho_i\}$ and $\boldsymbol{\sigma} = \{\sigma_i\}$, such that*

$$\mathscr{F}_Q(\rho,\sigma) = \min_{\hat{E}_i} \mathscr{F}_C(\boldsymbol{\rho},\boldsymbol{\sigma}). \tag{D.13}$$

We note that the Law of large numbers ensures that as the number of measurements $\to \infty$, the measured probability distribution $\to$ the true distribution [Bengtsson and Zyczkowski, 2008]. ■

D.2.5 The relative entropy

The Shannon entropy of a probability distribution P,

$$S_s(P) = -k\sum_{i=1}^{N} p_i \ln p_i, \tag{D.14}$$

defines certain attributes of a probability distribution[1]. This makes it unsuitable for a distinguishability measures. We make use of the *Kullback-Leibler* entropy

$$S_{kl}(P||Q) = \sum_{i=1}^{N} p_i \ln \frac{p_i}{q_i}, \tag{D.15}$$

as a remedy to this. Whilst this is not a metric since it is not symmetric under exchange of p_i and q_i, it remains sufficient as a distinguishability measure between the two distributions. Operationally, Eq. (D.15) describes how the length of a bit string grows. Equivalently it quantifies the rate at which measured probability distributions *not* equivalent to the true distribution, vanish with the number of measurements taken (consult Example 1) [Bengtsson and Zyczkowski, 2008].

D.3 Statistical geometry and the Fisher-Rao metric

For this section, we follow the procedure in [Bengtsson and Zyczkowski, 2008] to formulate an appropriate metric on the space of probability distributions. A similar procedure is taken in [Kok and Lovett, 2010; Jones and Kok, 2010]. The *Fisher–Rao metric* (FR), defined as:

$$\mathrm{d}s^2 = \sum_{i,j} \mathrm{d}p^i \, \mathrm{d}p^j g_{ij} = \sum_{i=1}^{N} \frac{\mathrm{d}p^i \, \mathrm{d}p^i}{4p_i} \iff g_{ij} = \frac{\delta_{ij}}{4p^i}, \tag{D.16}$$

defines the statistical distance metric between two probability distributions in the *probability simplex*[2]. This is the infinitesimal form for the FR metric – a consequence of being derived from discrete probability distributions for sake of simplicity. The generalisation of this for *continuous probability distributions* of the form $p(x)$ can be written as [Bengtsson and Zyczkowski, 2008]

$$g_{ab} = \frac{1}{4} \int_{\Omega} \mathrm{d}x \frac{\partial_a p(x) \partial_b p(x)}{p(x)}, \tag{D.17}$$

where Ω is required to define a *finite dimensional sub–manifold* of the probability simplex with coordinates ϑ^a. All of the properties required to discuss probability distributions may be sufficiently described by the discrete form with which we shall adhere to for the remainder of this section.

Eq. (D.16) can be re–expressed in a more convenient way, and in doing so related to the classical fidelity distance measure from section D.2.2, if we introduce a new coordinate system $(x^i)^2 = p^i$. This transforms the FR metric according to

$$\mathrm{d}s^2 = \sum_{i=1}^{N} \mathrm{d}x^i \, \mathrm{d}x^i, \tag{D.18}$$

[1] We note that k is the Boltzmann constant and in natural units is often set to 1. However, for information theory it is conventional to set $k = 1/\ln 2$ which transforms Eq. (D.14) according to $S_s(P) = -\sum_{i=1}^{N} p_i \log_2 p_i$, which is more suited to measurements in units of bits. This is because each qubit can take one of two values and so for a bit string of length a, there are $N = 2^a$ possible combinations. If each combination is considered equally probable then the entropy is maximum: $S_s = \log_2 N = a$.

[2] We have omitted the very informative derivative of Eq. (D.16) since we shall only concern ourselves with its uses in this review. For a thorough derivation, the reader is recommended to view [Bengtsson and Zyczkowski, 2008; Kok and Lovett, 2010].

and is illustrated in Fig D.1. However this does not provide an operational significance for the FR metric and so we seek to instead formulate the metric in terms of the relative entropy that was deliberately introduced in section D.2.5 for this purpose. A Taylor expansion to first order of the ln term in Eq. (D.15) yields

$$S_{kl}(P||P+\mathrm{d}P) = \sum_{i=1}^{N} p^i \ln \frac{p^i}{p^i + \mathrm{d}p^i} \approx \sum_i \frac{\mathrm{d}p^i\,\mathrm{d}p^i}{2p^i}. \tag{D.19}$$

We are required to make several notes to make ourselves comfortable with this [Bengtsson and Zyczkowski, 2008]:

1. We consider the vector $\boldsymbol{q} = \{q^i\}$ to lie outside an ellipsoid centered on $\boldsymbol{p}$ and containing all of the probability vectors between $\boldsymbol{p} + \mathrm{d}\boldsymbol{p}$ within the probability simplex.

2. When the central term of Eq. (D.19) is compared to the relative entropy, all of the indices have been raised. This does not affect our results, but is a requirement for the usage of differential geometry.

3. The same result can be obtained from the Taylor expansion of $S_{kl}(P + \mathrm{d}P||P)$ which is surprising since we commented earlier that the relative entropy is not symmetric. This is a consequence of having expanded the 'ln' to first order.

4. To within a constant, the relative entropy has been shown to be the square distance in Eq. (D.16). This reduces the task to the evaluation of this entropy, though generally this can be a difficult task also.

5. In a similar manner, the FR metric can be expressed in terms of the Shannon entropy – hence the Fisher information matrix is positive definite.

We conclude this section with some of the uses of the FR metric in quantum imaging. The metric arises by considering the geometry of classical probability distributions alone; it is a natural description for classical observables. It can be related to the classical FI by use of Eq. (D.16) such that

$$\frac{\mathrm{d}s}{\mathrm{d}\vartheta} \equiv \frac{\sqrt{\mathcal{F}(\vartheta)}}{2}, \tag{D.20}$$

where the factor of 2 arises due to our use of the convention used in [Bengtsson and Zyczkowski, 2008]. In fact we can determine the distinguishability criterion for two probability distributions $p(x|\vartheta_1)$ and $p(x|\vartheta_2)$ by use of a Maclauren expansion of $s(\vartheta)$ to first order and the CRB developed in Eq. (3.21) to yield $\mathrm{d}s^2 \geq 1/N$ [Kok and Lovett, 2010].

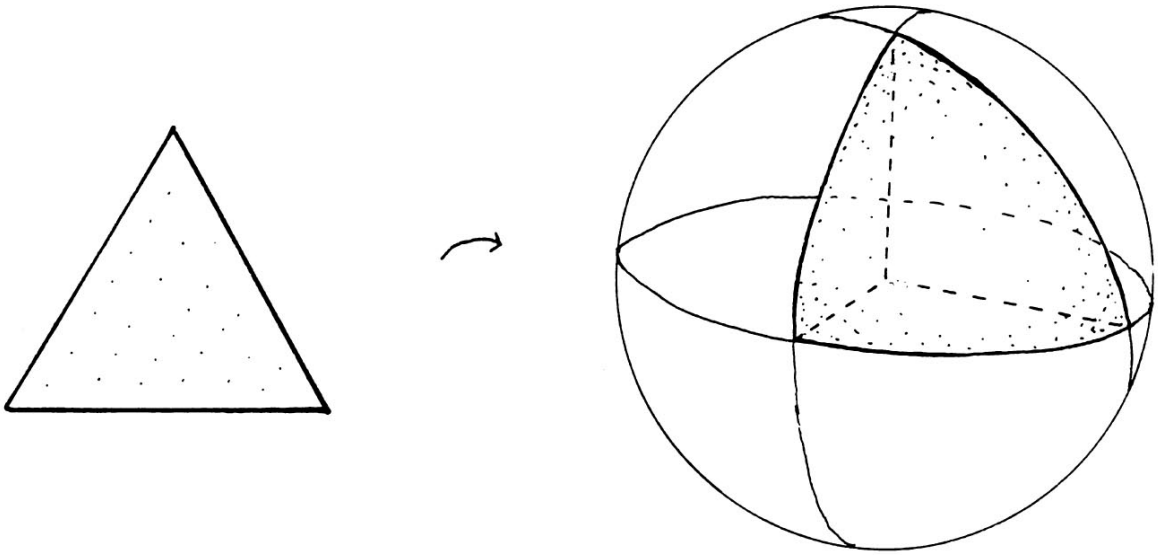

Figure D.1: *The coordinate transformation in fact transforms a flat geometry of the probability simplex to a round geometry on the surface of a sphere. The transformation does not affect the area, and the resulting sphere is required to have a unit radius. This constraint owes itself to the normalisation of the probability distributions, i.e.* $\sum_{i=1}^{N} dx^i dx^i = \sum_{i=1}^{N} p^i = 1$. *Image taken from [Bengtsson and Zyczkowski, 2008].*

Appendix E

The permutation group

In this appendix we explain the permutation group. For some set S_N of finite size N, the permutation group is the finite group P whose elements are permutations of S_N. There exists $N!$ elements—each a bijection $\sigma : M \to M$. Hence, for $M \in \{1, 2, \ldots, N\}$, each permutation can be written using Cauchy's two-line notation [John D. Dixon, 1996]

$$\sigma = \begin{pmatrix} 1 & 2 & 3 & \cdots & N \\ \sigma(1) & \sigma(2) & \sigma(3) & \cdots & \sigma(N) \end{pmatrix},$$

which contains the elements of the set S_N along the first row and the permutation image along the second. A cyclic notation is also commonly used. All finite groups can be represented as a group of permutations of a suitable set. In this work, when allowing for different sources to overlap, the contribution of different source pairings to the QFI becomes important. The permutation group is used to describe the combinatorics of this pairing. In the remainder of this section, we list identities associated with the mean source positions that were used when discussing the numerical results in section 4.2. Let μ_j define the expected position of the jth source that was introduced in chapter 4. Since each permutation is bijective,

$$\sum_{j=1}^{N} \mathfrak{G}\left[\mu_{\sigma(j)}\right] = \sum_{j=1}^{N} \mathfrak{G}\left[\mu_j\right], \tag{E.1}$$

for some arbitrary well-defined operation $\mathfrak{G}$ on the elements of the permutation sets. A consequence of the same reasoning is the following

$$\sum_{j=1}^{N} \mu'_{\sigma(j)} \mu_{\sigma(j)} = \sum_{j=1}^{N} \mu'_j \mu_j, \tag{E.2}$$

where we recall $\mu'_j = \partial_d \mu_j$. Further, the evaluation of the QFI requires integrating over the continuous variable x which runs along the source array. This operation becomes difficult to perform when the subscript contains a permutation element. To overcome this difficulty, we

generate a "shift" property. For any group G the inverse is a bijection of the set S_N. Hence, the inverse $\sigma^{-1} \in P$ such that for the sum over all permutations we have the following equality

$$\sum_{\sigma} \sum_{j=1}^{N} \left[\mu_j'(x_{\sigma(j)} - \mu_j) \right] = \sum_{\sigma} \sum_{j=1}^{N} \left[\mu_j'(x_{\sigma^{-1}(j)} - \mu_j) \right]. \tag{E.3}$$

From property (E.1) and the identity permutation $\sigma\sigma^{-1}(j) = \sigma^{-1}\sigma(j) = j$, we may re-write the right-hand side such that

$$\sum_{\sigma} \sum_{j=1}^{N} \left[\mu_j'(x_{\sigma(j)} - \mu_j) \right] = \sum_{\sigma} \sum_{j=1}^{N} \left[\mu_{\sigma(j)}'(x_j - \mu_{\sigma(j)}) \right], \tag{E.4}$$

where we notice that the subscript σ is shifted from the integration variable. Finally, for the form of the source positions used in this report we have

$$\sum_{\sigma} \left[\sum_{j=1}^{N} \mu_j \mu_{\sigma(j)} \right] = 0. \tag{E.5}$$

This may be seen by changing the order of the summation and that for each j there are $(N-1)!$ terms with $\sigma(j) = k$ such that

$$(N-1)! \sum_{j=1}^{N} \mu_j \sum_{k=1}^{N} \mu_k = 0. \tag{E.6}$$

The properties identified in Eqs (E.1)-(E.6) were used in Section 4.2, where we derived the dependence of the QFI with the source separation distance d. There, the permutation symbol naturally arose to describe all of the possible source pairings along the array.

Appendix F

Calculations for squeezing estimations

In this appendix, we provide supplemental work for chapter 6. In the first section, we will derive the generators for complex squeezing, since there construction is not straightforward. Following that, we derive and list a complete set of expectation values of normally ordered bosonic mode operators. These were required to calculate the QFIM.

F.1 Derivation of the squeezing generators

In this section we derive the generators of squeezed parameters. Recall the definition of the single mode squeezing operator:

$$\hat{S}_\xi = \exp\left[-i\hat{\mathcal{H}}\right] = \exp\left[\frac{1}{2}\left(\xi^*\hat{a}^2 - \xi\hat{a}^{\dagger 2}\right)\right] \tag{F.1}$$

where we write the squeezing Hamiltonian

$$\hat{\mathcal{H}} = \frac{i}{2}\left(\xi^*\hat{a}^2 - \xi\hat{a}^{\dagger 2}\right). \tag{F.2}$$

Since $\xi = r\exp[i\vartheta]$, we can see that the amplitude term r appears as a multiplicative factor to the Hamiltonian. Hence we can readily find the generator for the amplitude of squeezing:

$$\hat{\mathcal{G}}_r = i\left(\mu'^*\hat{a}^2 - \mu'\hat{a}^{\dagger 2}\right), \tag{F.3}$$

where we have defined $\mu = \xi/2$ and $\mu' = \partial\mu/\partial r$. In contrast, the directional term is not a multiplicative term in the Hamiltonian (F.2). Therefore, we have to use the machinery introduced in chapter 5 to write

$$\hat{\mathcal{G}}_\vartheta = \sum_{n=0}^{\infty} \frac{(-i)^n}{(n+1)!} C^{(n)}_{\hat{\mathcal{H}}}(\hat{\mathcal{H}}_\vartheta), \tag{F.4}$$

where we defined the Hamiltonian derivative $\hat{\mathcal{H}}_\vartheta = \partial\hat{\mathcal{H}}/\partial\vartheta$. This requires calculating the nested commutation relations $C^{(n)}_{\hat{\mathcal{H}}}(\hat{\mathcal{H}}_\vartheta)$ between the Hamiltonian and its derivative

$$\hat{\mathcal{H}} = i\left(\mu^*\hat{a}^2 - \mu\hat{a}^{\dagger 2}\right), \quad \hat{\mathcal{H}}_\vartheta = \left(\mu^*\hat{a}^2 + \mu\hat{a}^{\dagger 2}\right), \tag{F.5}$$

respectively, where we introduced $\mu = \xi/2$ for brevity. We list the first four nested commutation relations in normal order (using the operation $\mathcal{N}$ from subsection B.2.2):

$$C^{(0)}_{\hat{\mathcal{H}}} = \hat{\mathcal{H}}_\vartheta, \tag{F.6}$$

$$C^{(1)}_{\hat{\mathcal{H}}} = 8i|\mu|^2\left(\hat{a}^\dagger\hat{a} + \frac{1}{2}\right), \tag{F.7}$$

$$C^{(2)}_{\hat{\mathcal{H}}} = -16|\mu|^2\hat{\mathcal{H}}_\vartheta, \tag{F.8}$$

$$C^{(3)}_{\hat{\mathcal{H}}} = -128i|\mu|^4\left(\hat{a}^\dagger\hat{a} + \frac{1}{2}\right). \tag{F.9}$$

By normally ordering, it is immediately evident that the structure of all the 'even' nested commutation terms have the same functional dependence on $\hat{\mathcal{H}}_\vartheta$, with different coefficients. Similarly, all the 'odd' terms have the same functional dependence on the number operator. Hence we separate the generator (F.4) for even and odd n. Generalising the nth nested commutation between the Hamiltonian and its derivative, we find

$$\hat{\mathcal{G}}_\vartheta = \frac{1}{\sqrt{16|\mu|^2}}\sum_{n=1,3,5,\ldots}^{\infty}\frac{\left(\sqrt{16|\mu|^2}\right)^n}{n!}\hat{\mathcal{H}}_\vartheta + \sum_{n=2,4,6,\ldots}^{\infty}\frac{\left(\sqrt{16|\mu|^2}\right)^n}{2n!}\left(\hat{a}^\dagger\hat{a} + \frac{1}{2}\right). \tag{F.10}$$

Now, by writing the Maclaurin series for the hyperbolic functions

$$\sinh[x] = \sum_{n=0}^{\infty}\frac{x^{2n+1}}{(2n+1)!} = \sum_{n=1,3,5,\ldots}^{\infty}\frac{x^n}{n!}, \tag{F.11}$$

$$\cosh[x] = \sum_{n=0}^{\infty}\frac{x^{2n}}{(2n)!} = 1 + \sum_{n=2,4,6,\ldots}^{\infty}\frac{x^n}{n!}, \tag{F.12}$$

we can re-write the generator in Eq. (F.10). This gives the final form of the result presented in chapter 6:

$$\hat{\mathcal{G}}_\vartheta = \alpha\left(\hat{n} + \frac{1}{2}\right) + \beta\left(\mu^*\hat{a}^2 + \mu\hat{a}^{\dagger 2}\right), \tag{F.13}$$

where

$$\alpha = \frac{1}{2}\left(\cosh[4|\mu|] - 1\right), \quad \beta = \frac{1}{4|\mu|}\sinh[4|\mu|]. \tag{F.14}$$

This concludes the derivation for the generator of local translations in $\boldsymbol{\varphi} = (r, \vartheta)$.

F.2 Bogoliubov expectation values

In section 6.3 we saw that calculating the QFIM for complex squeezing required evaluation of expectation values of the mode operators $\langle\hat{a}^{\dagger l}\hat{a}^m\rangle_{jk}$, $\{l, m\} \in \{0, 1, 2, \ldots\}$, with respect to the jth

and kth eigenstate of the evolved probe state. Since the eigenspectrum of the evolved probe state may be determined from a Bogoliubov transformation of the field operators, we refer to the calculation of these expectation values in this thesis as *Bogoliubov expectation values*. Doing so reminds the reader that expectation values with unbalanced boson strings, with $l \neq m$, exist. In this section, we explain how we write the results used in calculating the QFIM.

Consider the Gaussian evolved thermal state

$$\rho(\boldsymbol{\varphi}) = \hat{V}\rho_{\text{th}}\hat{V}^\dagger, \tag{F.15}$$

where

$$\hat{V} = \hat{S}_\xi \hat{R}_\vartheta \hat{S}_\epsilon \hat{D}_\alpha. \tag{F.16}$$

This unitary can be described as a Bogoliubov transformation of the thermal state mode operators, such that $\hat{V}^\dagger \hat{a} \hat{V} = \mathcal{A}\hat{a}^\dagger + \mathcal{B}\hat{a} + C$ with the complex numbers defined through

$$\begin{aligned}
\mathcal{A} &= -\left(e^{i(\vartheta_\epsilon - \Theta)} \cosh r \sinh r_\epsilon + e^{i(\vartheta+\Theta)} \cosh r_\epsilon \sinh r\right), \\
\mathcal{B} &= e^{-i\Theta} \cosh r \cosh r_\epsilon + e^{i(\vartheta+\Theta-\vartheta_\epsilon)} \sinh r \sinh r_\epsilon, \\
C &= \alpha\mathcal{B} + \alpha^*\mathcal{A}.
\end{aligned} \tag{F.17}$$

Now, from the unitarity of the transformation $\hat{V}^\dagger\hat{V} = \hat{V}\hat{V}^\dagger = \mathbb{1}$, we can write

$$\left\langle \hat{a}^{\dagger l}\hat{a}^m \right\rangle_{jk} = \left\langle n_j \middle| \left(\hat{V}^\dagger\hat{a}^\dagger\hat{V}\right)^l \left(\hat{V}^\dagger\hat{a}\hat{V}\right)^m \middle| n_k \right\rangle. \tag{F.18}$$

Expanding, normally ordering, using $\langle n_j|\hat{n}|n_j\rangle = n_j$ and $\langle n_j|\hat{a}^{\dagger 2}\hat{a}^2|n_j\rangle = n_j(n_j-1)$, we obtain the following 'diagonal' ($j = k$) Bogoliubov expectation values:

$$\begin{aligned}
\left\langle \hat{a}^4 \right\rangle_{jj} &= 6\mathcal{A}^2\mathcal{B}^2 n_j^2 + \left(6\mathcal{A}^2\mathcal{B}^2 + 12\mathcal{A}\mathcal{B}C^2\right) n_j + 3\mathcal{A}^2\mathcal{B}^2 + 6\mathcal{A}\mathcal{B}C^2 + C^4, \\
\left\langle \hat{a}^{\dagger 2}\hat{a}^2 \right\rangle_{jj} &= \left(|\mathcal{B}|^4 + |\mathcal{A}|^4 + 4|\mathcal{A}|^2|\mathcal{B}|^2\right) n_j^2 \\
&\quad + \left(4|\mathcal{A}|^2|\mathcal{B}|^2 + 2C^2\mathcal{A}^*\mathcal{B}^* + 2C^{*2}\mathcal{A}\mathcal{B} + 3|\mathcal{A}|^4 - |\mathcal{B}|^4 + 4|\mathcal{B}|^2|C|^2 + 4|\mathcal{A}|^2|C|^2\right) n_j \\
&\quad + |\mathcal{A}|^2|\mathcal{B}|^2 + \mathcal{A}^*\mathcal{B}^*C^2 + 2|\mathcal{A}|^4 + 4|\mathcal{A}|^2|C|^2 + C^{*2}\mathcal{A}\mathcal{B} + |C|^4, \\
\left\langle \hat{a}^\dagger\hat{a}^3 \right\rangle_{jj} &= 3\left(\mathcal{A}|\mathcal{B}|^2\mathcal{B} + |\mathcal{A}|^2\mathcal{A}\mathcal{B}\right) n_j^2 + \left(3|\mathcal{B}|^2C^2 + 6|\mathcal{A}|^2\mathcal{A}\mathcal{B} + 3|\mathcal{A}|^2C^2 + 6\mathcal{A}\mathcal{B}|C|^2\right) n_j \\
&\quad + 3|\mathcal{A}|^2\mathcal{A}\mathcal{B} + 3|\mathcal{A}|^2C^2 + 3\mathcal{A}\mathcal{B}|C|^2 + |C|^2C^2, \\
\left\langle \hat{a}^\dagger\hat{a} \right\rangle_{jj} &= \left(|\mathcal{A}|^2 + |\mathcal{B}|^2\right) n_j + |\mathcal{A}|^2 + |C|^2, \\
\left\langle \hat{a}^2 \right\rangle_{jj} &= 2\mathcal{A}\mathcal{B}n_j + \mathcal{A}\mathcal{B} + C^2.
\end{aligned} \tag{F.19}$$

The 'off-diagonal' ($j \neq k$) Bogoliubov expectation values can similarly be determined. Together with Eq. (F.19), the QFIM for any arbitrary single mode Gaussian state can be completely defined. In chapter 6, we use these results to apply quantum estimation theory to estimate squeezing with specific states.

F.3 Coefficients for the Gaussian mixed state SLD

In this section, we detail how to derive the coefficients for the SLD for mixed Gaussian states that were encountered in subsection 6.4.2 of the thesis. For convenience, we write the form of the SLD as follows:

$$\hat{\mathcal{L}}_k = \frac{1}{2}\mathcal{A}^{(k)}_{\alpha\beta}\left\{\hat{\tilde{R}}^{\alpha}, \hat{\tilde{R}}^{\beta}\right\} + \mathcal{B}^{(k)}_{\alpha}\hat{\tilde{R}}^{\alpha} - \frac{1}{2}\mathrm{Tr}\left[\mathcal{A}^{(k)}\boldsymbol{\Sigma}\right], \tag{F.20}$$

where greek indices imply Einstein summation convention and

$$\mathcal{A}^{(k)} = \sum_{j=0}^{\infty} \boldsymbol{F}^{\top j}\partial_k(\boldsymbol{\Sigma}^{-1})\boldsymbol{F}^{j}, \quad \mathcal{B}^{(k)} = 2\boldsymbol{\Sigma}^{-1}\partial_k\boldsymbol{\lambda}, \tag{F.21}$$

with $\boldsymbol{F} = (\boldsymbol{\Sigma}\boldsymbol{\omega})^{-1}$. We can solve these parameters using *Mathematica*.

We start by introducing the function *kronmat*, which is used to define the covariance matrices associated with multi-mode states. Since we are working with single modes, we take $n = 1$, and the code reads:

```
In[3]:= ClearAll["Global`*"]
        kronmat_n_[mat_] := Nest[KroneckerProduct[mat, #] &, mat, n - 1]
        n = 1;
```

We now define the coefficient of the quadratic contribution to the SLD. The following four cells evaluates the matrix $\mathscr{A}^{(k)}$ by evaluating the Stein equation:

```
In[4]:= (*Symplectic transformations for rotation and one mode squeezing*)
        R[Θ_] := {{Cos[Θ], Sin[Θ]}, {-Sin[Θ], Cos[Θ]}};
        Sξ[r_, θ_] := {{Cosh[r] - Sinh[r] Cos[θ], - Sinh[r] Sin[θ]},
                       {-Sinh[r] Sin[θ], Cosh[r] + Sinh[r] Cos[θ]}};
```

```
In[5]:= (*Final state, Σf, covariance matrix of single mode*)
        Γ[r_, θ_, Θ_, ν_] := (2ν + 1) Dot[Sξ[r, θ], R[Θ], Transpose[R[Θ]],
                                 Transpose[Sξ[r, θ]]];
        x = Γ[r, θ, Θ, ν][[1, 1]] // FullSimplify;
        y = Γ[r, θ, Θ, ν][[1, 2]] // FullSimplify;
        z = Γ[r, θ, Θ, ν][[2, 2]] // FullSimplify;
        Σf = {{x, y}, {y, z}};
```

```
In[6]:= (*Write derivatives of the inverse of the final covariance matrix
           Σf:*)
        DInverseΣf = D[Inverse[Σf], r];
        tx = DInverseΣf[[1, 1]] // FullSimplify;
        ty = DInverseΣf[[1, 2]] // FullSimplify;
        tz = DInverseΣf[[2, 2]] // FullSimplify;
        T = {{tx,ty},{ty,tz}};
        ω = i {{0, 1}, {-1, 0}};
        F = Inverse[Σf.ω] // FullSimplify;
        Ar = Sum[MatrixPower[Transpose[F], k].T. MatrixPower[F, k],
                {k, 0, ∞, 1}] // Simplify;
```

```
In[7]:= (*Write in bosonic basis*)
        s = 1/Sqrt[2] {{1, 1}, {-i, i}};
        Arboson = Transpose[s].Ar.s // Simplify;
```

To define the coefficient of the linear contribution, $\mathscr{B}^{(k)}$, to the SLD we use the moments of the evolved probe state definition in Eq. (6.49). This is implemented as follows:

```
In[8]:= (*Final state first moment [Weedbrook, 2012]*)
        xf[r_, θ_, Θ_, α_] := Sξ[r, θ].R[Θ].{Re[α], Im[α]};

In[9]:= (*Now we set up the coefficient B from Monras*)
        B[δ_] := 2 Inverse[Σf].{D[xf[r, θ, Θ, α][[1]], δ],
                                D[xf[r, θ, Θ, α][[2]], δ]};

In[10]:= (*Write linear contribution constant for Lrξ in bosonic basis*)
         Brboson = B[r].s // Simplify;
```

Similarly, we now define the constant term to the SLD:

```
In[11]:= constr = -1/2 Tr[Arboson.Σf];
```

By simplifying the output, we arrive at the final form of the constants $\mathscr{A}^k$ and $\mathscr{B}^k$. Armed with these coefficients, we have a final form of the SLD for the state

$$\rho(\boldsymbol{\varphi}) = \hat{S}_\xi \rho_{\text{in}} \hat{S}_\xi^\dagger, \quad \text{with} \quad \rho_{\text{in}} = \hat{R}_\Theta \hat{D}_\alpha \rho_{\text{th}} \hat{D}_\alpha^\dagger \hat{R}_\Theta^\dagger. \tag{F.22}$$

This is then used to construct the optimal measurement scheme that saturates the QCRB.

References

[Aasi et al., 2013] J. Aasi, J. Abadie, B. P. Abbott, R. Abbott, T. D. Abbott, M. R. Abernathy, C. Adams, T. Adams, P. Addesso, R. X. Adhikari, et al. Enhanced sensitivity of the ligo gravitational wave detector by using squeezed states of light. *Nat. Photon.*, 7:613–619, July 2013. doi: 10.1038/nphoton.2013.177.

[Abadie et al., 2011] J. Abadie, B. P. Abbott, R. Abbott, T. D. Abbott, M. Abernathy, C. Adams, R. Adhikari, C. Affeldt, B. Allen, G. S. Allen, et al. A gravitational wave observatory operating beyond the quantum shot-noise limit. *Nat. Phys. Lett.*, 7(12):962–965, August 2011. doi: 10.1038/nphys2083.

[Abbe, 1873] E. Abbe. Beiträge zur theorie des mikroskops und der mikroskopischen wahrnehmung. *Arch. Mikroskop. Anatomie*, 9(1):413–468, 1873. ISSN 0176-7364. doi: 10.1007/BF02956173.

[Abbott et al., 2004] B. Abbott, R. Abbott, R. Adhikari, A. Ageev, B. Allen, R. Amin, S. B. Anderson, W. G. Anderson, M. Araya, H. Armandula, et al. First upper limits from ligo on gravitational wave bursts. *Phys. Rev. D*, 69(10):102001, May 2004. doi: 10.1103/PhysRevD.69.102001.

[Abouraddy et al., 2001] A. F. Abouraddy, B. E. A. Saleh, A. V. Sergienko, and M. C. Teich. Role of entanglement in two-photon imaging. *Phys. Rev. Lett.*, 87(12):123602, August 2001. doi: 10.1103/PhysRevLett.87.123602.

[Adesso et al., 2014] G. Adesso, S. Ragy, and A. R. Lee. Continuous variable quantum information: Gaussian states and beyond. *Open Syst. Inf. Dyn.*, 21(01n02):1440001, 2014. doi: 10.1142/S1230161214400010.

[Agarwal and Wolf, 1970] G. S. Agarwal and E. Wolf. Calculus for functions of noncommuting operators and general phase-space methods in quantum mechanics. i. mapping theorems and ordering of functions of noncommuting operators. *Phys. Rev. D*, 2(10):2161–2186, November 1970. doi: 10.1103/PhysRevD.2.2161.

[Alipour et al., 2014] S. Alipour, M. Mehboudi, and A. T. Rezakhani. Quantum metrology in open systems: Dissipative cramér-rao bound. *Phys. Rev. Lett.*, 112(12):120405, March 2014. doi: 10.1103/PhysRevLett.112.120405.

[Amari and Nagaoka, 2007] S.-I. Amari and H. Nagaoka. *Methods of Information Geometry*, volume 191 of *Translations of Mathematical Monographs*. American Mathematical Society, April 2007. ISBN 9780821843024.

[Andersen et al., 2009] U. L. Andersen, G. Leuchs, and C. Silberhorn. Continuous-variable quantum information processing. *Laser & Photon. Rev.*, 4(3):337–354, July 2009. doi: 10.1002/lpor.200910010.

[Andersen et al., 2016] U. L. Andersen, T. Gehring, C. Marquardt, and G. Leuchs. 30 years of squeezed light generation. *Phys. Scr.*, 91(5):053001, April 2016. doi: 10.1088/0031-8949/91/5/053001.

[Anisimov et al., 2010] P. M. Anisimov, G. M. Raterman, A. Chiruvelli, W. N. Plick, S. D. Huver, H. Lee, and J. P. Dowling. Quantum metrology with two-mode squeezed vacuum: Parity detection beats the heisenberg limit. *Phys. Rev. Lett.*, 104(10):103602, March 2010. doi: 10.1103/PhysRevLett.104.103602.

[Ansmann et al., 2009] M. Ansmann, H. Wang, R. C. Bialczak, M. Hofheinz, E. Lucero, M. Neeley, A. D. O'Connell, D. Sank, M. Weides, J. Wenner, A. N. Cleland, and J. M. Martinis. Violation of bell's inequality in josephson phase qubits. *Nature*, 461:504–506, September 2009. doi: 10.1038/nature08363.

[Aoki et al., 2009] T. Aoki, G. Takahashi, T. Kajiya, J.-i. Yoshikawa, S. L. Braunstein, P. van Loock, and A. Furusawa. Quantum error correction beyond qubits. *Nat. Phys.*, 5:541–546, June 2009. doi: 10.1038/NPHYS1309.

[Aspect et al., 1982] A. Aspect, J. Dalibard, and G. Roger. Experimental test of bell's inequalities using time-varying analyzers. *Phys. Rev. Lett.*, 49(25):1804–1807, December 1982. doi: 10.1103/PhysRevLett.49.1804.

[Bagan et al., 2006] E. Bagan, M. A. Ballester, R. D. Gill, A. Monras, and R. Muñoz Tapia. Optimal full estimation of qubit mixed states. *Phys. Rev. A*, 73(3):032301, March 2006. doi: 10.1103/PhysRevA.73.032301.

[Bargmann, 1961] V. Bargmann. On a hilbert space of analytic functions and an associated integral transform part i. *Commun. Pure Appl. Math.*, 14(3):187–214, 1961. doi: 10.1002/cpa.3160140303.

[Barnett and Radmore, 2005] S. M. Barnett and P. M. Radmore. *Methods in Theoretical Quantum Optics*. Oxford University Press, Great Britain, 2005. ISBN 9780198563617.

[Baumgratz and Datta, 2016] T. Baumgratz and A. Datta. Quantum enhanced estimation of a multidimensional field. *Phys. Rev. Lett.*, 116:030801, January 2016. doi: 10.1103/PhysRevLett.116.030801.

[Beau and del Campo, 2017] M. Beau and A. del Campo. Nonlinear quantum metrology of many-body open systems. *Phys. Rev. Lett.*, 119(1):010403, July 2017. doi: 10.1103/PhysRevLett.119.010403.

[Belavkin, 1976] V. P. Belavkin. Generalized uncertainty relations and efficient measurements in quantum systems. *Theoret. Math. Phys.*, 26(3):213–222, March 1976. doi: 10.1007/BF01032091.

[Beltrán and Luis, 2005] J. Beltrán and A. Luis. Breaking the heisenberg limit with inefficient detectors. *Phys. Rev. A*, 72:045801, October 2005. doi: 10.1103/PhysRevA.72.045801.

[Bengtsson and Zyczkowski, 2008] I. Bengtsson and K. Zyczkowski. *Geometry of Quantum States: An Introduction to Quantum Entanglement*. Cambridge University Press, New York, 1 edition, 2008. ISBN 9780521891400.

[Berni et al., 2015] A. A. Berni, T. Gehring, B. M. Nielsen, V. Händchen, M. G. A. Paris, and U. L. Andersen. Ab initio quantum-enhanced optical phase estimation using real-time feedback control. *Nat. Photon.*, 9:577–582, August 2015. doi: 10.1038/NPHOTON.2015.139.

[Berrada et al., 2013] T. Berrada, S. van Frank, R. Bücker, T. Schumm, J.-F. Schaff, and J. Schmiedmayer. Integrated mach–zehnder interferometer for bose–einstein condensates. *Nat. Commun.*, 4:2077, June 2013. ISSN 2041-1723. doi: 10.1038/ncomms3077.

[Berry and Wiseman, 2000] D. W. Berry and H. M. Wiseman. Optimal states and almost optimal adaptive measurements for quantum interferometry. *Phys. Rev. Lett.*, 85(24):5098–5101, December 2000. doi: 10.1103/PhysRevLett.85.5098.

[Berry and Wiseman, 2002] D. W. Berry and H. M. Wiseman. Adaptive quantum measurements of a continuously varying phase. *Phys. Rev. A*, 65(4):043803, March 2002. doi: 10.1103/PhysRevA.65.043803.

[Berry et al., 2015] D. W. Berry, M. Tsang, M. J. W. Hall, and H. M. Wiseman. Quantum bell-ziv-zakai bounds and heisenberg limits for waveform estimation. *Phys. Rev. X*, 5(3):031018, August 2015. doi: 10.1103/PhysRevX.5.031018.

[Betzig et al., 2018] E. Betzig, S. W. Hell, and W. E. Moerner. Advanced information. nobelprize.org., September 2018. URL `https://www.nobelprize.org/prizes/chemistry/2014/advanced-information/`.

[Blasiak et al., 2007] P. Blasiak, A. Horzela, K. A. Penson, A. I. Solomon, and G. H. E. Duchamp. Combinatorics and boson normal ordering: A gentle introduction. *Am. J. Phys.*, 75(7):639–646, 2007. doi: 10.1119/1.2723799.

[Boixo et al., 2007] S. Boixo, S. T. Flammia, C. M. Caves, and J. Geremia. Generalized limits for single-parameter quantum estimation. *Phys. Rev. Lett.*, 98:090401, February 2007. doi: 10.1103/PhysRevLett.98.090401.

[Bollinger et al., 1996] J. J. . Bollinger, W. M. Itano, D. J. Wineland, and D. J. Heinzen. Optimal frequency measurements with maximally correlated states. *Phys. Rev. A*, 54:R4649–R4652, December 1996. doi: 10.1103/PhysRevA.54.R4649.

[Boto et al., 2000] A. N. Boto, P. Kok, D. S. Abrams, S. L. Braunstein, C. P. Williams, and J. P. Dowling. Quantum interferometric optical lithography: Exploiting entanglement to beat the diffraction limit. *Phys. Rev. Lett.*, 85(13):2733–2736, September 2000. doi: 10.1103/PhysRevLett.85.2733.

[Bradshaw et al., 2017] M. Bradshaw, S. M. Assad, and P. K. Lam. A tight cramér-rao bound for joint parameter estimation with a pure two-mode squeezed probe. *Physics Letters A*, 381(32):2598 – 2607, 2017. doi: https://doi.org/10.1016/j.physleta.2017.06.024.

[Braun et al., 2018] D. Braun, G. Adesso, F. Benatti, R. Floreanini, U. Marzolino, M. W. Mitchell, and S. Pirandola. Quantum enhanced measurements without entanglement. *Rev. Mod. Phys*, 90(3): 035006, September 2018. doi: 10.1103/RevModPhys.90.035006.

[Braunstein, 1992] S. L. Braunstein. Quantum limits on precision measurements of phase. *Phys. Rev. Lett.*, 69(25):3598–3601, December 1992. doi: 10.1103/PhysRevLett.69.3598.

[Braunstein, 2005] S. L. Braunstein. Squeezing as an irreducible resource. *Phys. Rev. A*, 71(5):055801, May 2005. doi: 10.1103/PhysRevA.71.055801.

[Braunstein and Caves, 1994] S. L. Braunstein and C. M. Caves. Statistical distance and the geometry of quantum states. *Phys. Rev. Lett.*, 72(22):3439–3443, May 1994. doi: 10.1103/PhysRevLett.72.3439.

[Braunstein and Kimble, 1998] S. L. Braunstein and H. J. Kimble. Teleportation of continuous quantum variables. *Phys. Rev. Lett.*, 80(4):869–872, January 1998. doi: 10.1103/PhysRevLett.80.869.

[Braunstein and van Loock, 2005] S. L. Braunstein and P. van Loock. Quantum information with continuous variables. *Rev. Mod. Phys.*, 77(2):513–577, June 2005. doi: 10.1103/RevModPhys.77.513.

[Braunstein et al., 1996] S. L. Braunstein, C. M. Caves, and G. Milburn. Generalized uncertainty relations: Theory, examples, and lorentz invariance. *Ann. Phys.*, 247(1):135 – 173, 1996. doi: http://dx.doi.org/10.1006/aphy.1996.0040.

[Breuer and Petruccione, 2002] H. P. Breuer and F. Petruccione. *The Theory of Open Quantum Systems*. Oxford University Press, June 2002. ISBN 9780198520634.

[Brody and Graefe, 2013] D. C. Brody and E.-M. Graefe. Information geometry of complex hamiltonians and exceptional points. *Entropy*, 15(9):3361–3378, August 2013. doi: 10.3390/e15093361.

[Brown and Twiss, 1956a] R. H. Brown and R. Q. Twiss. Correlation between photons in two coherent beams of light. *Nature*, 177, 1956a. doi: http://dx.doi.org/10.1038/177027a0.

[Brown and Twiss, 1956b] R. H. Brown and R. Q. Twiss. A test of a new type of stellar interferometer on sirius. *Nature*, 178:1046–1048, 1956b. doi: 10.1038/1781046a0.

[Brown and Twiss, 1957] R. H. Brown and R. Q. Twiss. Interferometry of the intensity fluctuations in light - i. basic theory: the correlation between photons in coherent beams of radiation. *Proc. R. Soc. Lond. (Ser. A)*, 242(1230):300–324, November 1957. doi: 10.1098/rspa.1957.0177.

[Brown and Twiss, 1958a] R. H. Brown and R. Q. Twiss. Interferometry of the intensity fluctuations in light. ii. an experimental test of the theory for partially coherent light. *Proc. R. Soc. Lond. (Ser. A)*, 243(1234):291–319, January 1958a. doi: 10.1098/rspa.1958.0001.

[Brown and Twiss, 1958b] R. H. Brown and R. Q. Twiss. Interferometry of the intensity fluctuations in light iii. applications to astronomy. *Proc. R. Soc. Lond. (Ser. A)*, 248(1253):199–221, November 1958b.

[Carmichael, 2002] H. J. Carmichael. *Statistical Methods in Quantum Optics 1*. Springer, Berlin, 1 edition, 2002. ISBN 9783642081330.

[Carmichael et al., 1980] H. Carmichael, P. Drummond, D. Walls, and P. Meystre. Photon antibunching in resonance fluorescence in the presence of atomic number fluctuations. *Optica Acta Int. J. Opt.*, 27(5):581–586, 1980. doi: 10.1080/713820289.

[Carolan et al., 2015] J. Carolan, C. Harrold, C. Sparrow, E. Martín-López, N. J. Russell, J. W. Silverstone, P. J. Shadbolt, N. Matsuda, M. Oguma, M. Itoh, et al. Universal linear optics. *Science*, 349(6249): 711–716, August 2015. doi: 10.1126/science.aab3642.

[Caron et al., 1995] B. Caron, A. Dominjon, F. Marion, L. Massonnet, R. Morand, B. Mours, M. Yvert, D. Babusci, H. Fang, G. Giordano, et al. Status of the virgo experiment. *Nucl. Instrum. Methods Phys. Res. A*, 360(1):258 – 262, 1995. ISSN 0168-9002. doi: 10.1016/0168-9002(94)01613-5.

[Caves, 1980] C. M. Caves. Quantum-mechanical radiation-pressure fluctuations in an interferometer. *Phys. Rev. Lett.*, 45(2):75–79, July 1980. doi: 10.1103/PhysRevLett.45.75.

[Caves, 1981] C. M. Caves. Quantum-mechanical noise in an interferometer. *Phys. Rev. D*, 23(8):1693–1708, April 1981. doi: 10.1103/PhysRevD.23.1693.

[Chang et al., 2014] D. E. Chang, V. Vuletić, and M. D. Lukin. Quantum nonlinear optics — photon by photon. *Nat. Photon.*, 8:685–694, August 2014. doi: 10.1038/NPHOTON.2014.192.

[Chin et al., 2012] A. W. Chin, S. F. Huelga, and M. B. Plenio. Quantum metrology in non-markovian environments. *Phys. Rev. Lett.*, 109(23):233601, December 2012. doi: 10.1103/PhysRevLett.109.233601.

[Chiribella et al., 2006a] G. Chiribella, G. M. D'Ariano, and M. F. Sacchi. Joint estimation of real squeezing and displacement. *J. Phys. A: Math. Gen.*, 39(9):2127, 2006a. URL `http://stacks.iop.org/0305-4470/39/i=9/a=009`.

[Chiribella et al., 2006b] G. Chiribella, G. M. D'Ariano, and M. F. Sacchi. Optimal estimation of squeezing. *Phys. Rev. A*, 73(6):062103, June 2006b. doi: 10.1103/PhysRevA.73.062103.

[Cirac and Zoller, 1995] J. I. Cirac and P. Zoller. Quantum computations with cold trapped ions. *Phys. Rev. Lett.*, 74(20):4091–4094, May 1995. doi: 10.1103/PhysRevLett.74.4091.

[Clarke, 2013] F. Clarke. *Functional Analysis, Calculus of Variations and Optimal Control*. Graduate Texts in Mathematics. Springer, 2013. ISBN 9781447148197.

[Cramér, 1999] H. Cramér. *Mathematical Methods of Statistics*. Princeton University Press, 1999. ISBN 978-0691005478.

[Crowley et al., 2014] P. J. D. Crowley, A. Datta, M. Barbieri, and I. A. Walmsley. Tradeoff in simultaneous quantum-limited phase and loss estimation in interferometry. *Phys. Rev. A*, 89(2):023845, February 2014. doi: 10.1103/PhysRevA.89.023845.

[de L. Kronig and Penney, 1931] R. de L. Kronig and W. G. Penney. Quantum mechanics of electrons in crystal lattices. *Proc. R. Soc. Lond. (Ser. A)*, 130:499–513, 1931. doi: 10.1098/rspa.1931.0019.

[Debnath and Mikusinski, 2005] L. Debnath and P. Mikusinski. *Introduction to Hilbert Spaces with Applications*. Academic Press, 3 edition, November 2005. ISBN 9780122084386.

[Degen et al., 2017] C. L. Degen, F. Reinhard, and P. Cappellaro. Quantum sensing. *Rev. Mod. Phys.*, 89 (3):035002, July 2017. doi: 10.1103/RevModPhys.89.035002.

[Demkowicz-Dobrzański and Maccone, 2014] R. Demkowicz-Dobrzański and L. Maccone. Using entanglement against noise in quantum metrology. *Phys. Rev. Lett.*, 113(25):250801, 2014. doi: 10.1103/PhysRevLett.113.250801.

[Demkowicz-Dobrzański et al., 2012] R. Demkowicz-Dobrzański, J. Kołodyński, and M. Guţă. The elusive heisenberg limit in quantum-enhanced metrology. *Nat. Commun.*, 3:1063, September 2012. doi: 10.1038/ncomms2067.

[Demkowicz-Dobrzanski et al., 2009] R. Demkowicz-Dobrzanski, U. Dorner, B. J. Smith, J. S. Lundeen, W. Wasilewski, K. Banaszek, and I. A. Walmsley. Quantum phase estimation with lossy interferometers. *Phys. Rev. A*, 80:013825, July 2009. ISSN 1050-2947. doi: 10.1103/PhysRevA.80.013825.

[Dieks and Lam, 2008] D. Dieks and S. Lam. Complementarity in the einstein-bohr photon box. *Am. J. Phys.*, 76(9):838–842, 2008. doi: 10.1119/1.2919740.

[Dirac, 1988] P. A. M. Dirac. *The Principles Of Quantum Mechanics*. Monographs On Physics. Oxford University Press, 4 edition, January 1988. ISBN 9780198520115.

[Dirac and Bohr, 1927] P. Dirac and N. Bohr. The quantum theory of the emission and absorption of radiation. *Proc. R. Soc. Lond. (Ser. A)*, 114(767):243–265, March 1927. doi: 10.1098/rspa.1927.0039.

[Dirac, 2003] P. A. M. Dirac. *Lectures on Quantum Mechanics*. Dover Publications Inc., March 2003. ISBN 9780486417134.

[Dooley et al., 2016] S. Dooley, W. J. Munro, and K. Nemoto. Quantum metrology including state preparation and readout times. *Phys. Rev. A*, 94(5):052320, November 2016. doi: 10.1103/PhysRevA.94.052320.

[Dorner et al., 2009] U. Dorner, R. Demkowicz-Dobrzanski, B. J. Smith, J. S. Lundeen, W. Wasilewski, K. Banaszek, and I. A. Walmsley. Optimal quantum phase estimation. *Phys. Rev. Lett.*, 102(4): 040403, January 2009. doi: 10.1103/PhysRevLett.102.040403.

[Dyson, 1949] F. Dyson. The radiation theories of tomonaga, schwinger, and feynman. *Phys. Rev.*, 75(3), February 1949.

[Ercolessi and Schiavina, 2013] E. Ercolessi and M. Schiavina. Symmetric logarithmic derivative for general n-level systems and the quantum Fisher information tensor for three-level systems. pages 1–9, 2013.

[Escher et al., 2011a] B. M. Escher, R. L. de Matos Filho, and L. Davidovich. General framework for estimating the ultimate precision limit in noisy quantum-enhanced metrology. *Nature*, 7:406, March 2011a. doi: 10.1038/nphys1958.

[Escher et al., 2011b] B. M. Escher, R. L. de Matos Filho, and L. Davidovich. General framework for estimating the ultimate precision limit in noisy quantum-enhanced metrology. *Nat. Phys.*, 7: 406–411, March 2011b. doi: 10.1038/NPHYS1958.

[Escher et al., 2012] B. M. Escher, L. Davidovich, N. Zagury, and R. L. de Matos Filho. Quantum metrological limits via a variational approach. *Phys. Rev. Lett.*, 109(19):190404, November 2012. doi: 10.1103/PhysRevLett.109.190404.

[Eymard et al., 2000] R. Eymard, T. Gallouët, and R. Herbin. *Handbook of Numerical Analysis*, volume 7. Elsevier, 1 edition, November 2000. ISBN 9780444503503. doi: 10.1016/S1570-8659(00)07005-8.

[Fairhurst, 2011] S. Fairhurst. Source localization with an advanced gravitational wave detector network. *Classical and Quantum Gravity*, 28(10):105021, April 2011. URL `http://stacks.iop.org/0264-9381/28/i=10/a=105021`.

[Falaye et al., 2017] B. J. Falaye, A. G. Adepoju, A. S. Aliyu, M. M. Melchor, M. S. Liman, O. J. Oluwadare, M. D. González-Ramírez, and K. J. Oyewumi. Investigating quantum metrology in noisy channels. *Sci. Rep.*, 7(1):16622, November 2017. doi: 10.1038/s41598-017-16710-w.

[Fano, 1957] U. Fano. Description of states in quantum mechanics by density matrix and operator techniques. *Rev. Mod. Phys.*, 29(1):74–93, January 1957. doi: 10.1103/RevModPhys.29.74.

[Fei et al., 1997] H.-B. Fei, B. M. Jost, S. Popescu, B. E. A. Saleh, and M. C. Teich. Entanglement-induced two-photon transparency. *Phys. Rev. Lett.*, 78:1679–1682, March 1997. doi: 10.1103/PhysRevLett.78.1679.

[Ferraro et al., 2005] A. Ferraro, S. Olivares, and M. G. A. Paris. Gaussian states in continuous variable quantum information. March 2005.

[Fraïsse and Braun, 2017] J. M. E. Fraïsse and D. Braun. Enhancing sensitivity in quantum metrology by hamiltonian extensions. *Phys. Rev. A*, 95(6):062342, June 2017. doi: 10.1103/PhysRevA.95.062342.

[Friis et al., 2015] N. Friis, M. Skotiniotis, I. Fuentes, and W. Dür. Heisenberg scaling in gaussian quantum metrology. *Phys. Rev. A*, 92:022106, August 2015. doi: 10.1103/PhysRevA.92.022106.

[Friis et al., 2018] N. Friis, O. Marty, C. Maier, C. Hempel, M. Holzäpfel, P. Jurcevic, M. B. Plenio, M. Huber, C. Roos, R. Blatt, and B. Lanyon. Observation of entangled states of a fully controlled 20-qubit system. *Phys. Rev. X*, 8(2):021012, April 2018. doi: 10.1103/PhysRevX.8.021012.

[Fuentes et al., 2014] I. Fuentes, G. Adesso, M. Ahmadi, D. E. Bruschi, C. Sabin, and G. Adesso. Relativistic quantum metrology: Exploiting relativity to improve quantum measurement technologies. *Sci. Rep.*, 4:1–10, May 2014. doi: 10.1038/srep04996.

[Fujiwara, 1994] A. Fujiwara. Multi-parameter pure state estimation based on the right logarithmic derivative. *METR 94-9*, 1994.

[Fujiwara, 2001] A. Fujiwara. Quantum channel identification problem. *Phys. Rev. A*, 63(March):042304, March 2001. doi: 10.1103/PhysRevA.63.042304.

[Fujiwara and Nagaoka, 1995] A. Fujiwara and H. Nagaoka. Quantum fisher metric and estimation for pure state models. *Phys. Lett. A*, 201(2):119 – 124, 1995. doi: 10.1016/0375-9601(95)00269-9.

[Furusawa et al., 1998] A. Furusawa, J. L. Sørensen, S. L. Braunstein, C. A. Fuchs, H. J. Kimble, and E. S. Polzik. Unconditional quantum teleportation. *Science*, 282(5389):706–709, October 1998. doi: 10.1126/science.282.5389.706.

[Gaiba and Paris, 2009] R. Gaiba and M. G. Paris. Squeezed vacuum as a universal quantum probe. *Phys. Lett. A*, 373(10):934 – 939, March 2009. doi: 10.1016/j.physleta.2009.01.026.

[Gao and Lee, 2014] Y. Gao and H. Lee. Bounds on quantum multiple-parameter estimation with gaussian state. *Eur. Phys. J. D*, 68(11):1–7, 2014. doi: 10.1140/epjd/e2014-50560-1.

[Gardiner and Zoller, 2004] C. Gardiner and P. Zoller. *Quantum Noise*. Springer, 2 edition, August 2004. ISBN 9783540223016.

[Gehring et al., 2015] T. Gehring, V. Händchen, J. Duhme, F. Furrer, T. Franz, C. Pacher, R. F. Werner, and R. Schnabel. Implementation of continuous-variable quantum key distribution with composable and one-sided-device-independent security against coherent attacks. *Nat. Commun.*, 6:8795, October 2015. doi: 10.1038/ncomms9795.

[Genoni et al., 2013] M. G. Genoni, M. G. A. Paris, G. Adesso, H. Nha, P. L. Knight, and M. S. Kim. Optimal estimation of joint parameters in phase space. *Phys. Rev. A*, 87(1):012107, January 2013. doi: 10.1103/PhysRevA.87.012107.

[Gerry and Knight, 2004] C. C. Gerry and P. L. Knight. *Introductory Quantum Optics*. Cambridge University Press, United Kingdom, 1 edition, 2004. ISBN 9780521527354.

[Geyer, 2013] C. J. Geyer. *Asymptotics of Maximum Likelihood without the LLN or CLT or Sample Size Going to Infinity*, volume 10. IMS Collection, September 2013. doi: 10.1214/12-IMSCOLL1001.

[Giovannetti et al., 2004] V. Giovannetti, S. Lloyd, and L. Maccone. Quantum-enhanced measurements: Beating the standard quantum limit. *Science*, 306(5700):1330–1336, 2004. doi: 10.1126/science.1104149.

[Giovannetti et al., 2006] V. Giovannetti, S. Lloyd, and L. Maccone. Quantum metrology. *Phys. Rev. Lett.*, 96(1):010401, January 2006. ISSN 0031-9007. doi: 10.1103/PhysRevLett.96.010401.

[Giovannetti et al., 2011] V. Giovannetti, S. Lloyd, and L. Maccone. Advances in quantum metrology. *Nat. Photon.*, 5:222–229, April 2011. doi: 10.1038/nphoton.2011.35.

[Glauber, 1963a] R. J. Glauber. Coherent and incoherent states of the radiation field. *Phys. Rev.*, 131(6): 2766–2788, September 1963a. doi: 10.1103/PhysRev.131.2766.

[Glauber, 1963b] R. J. Glauber. The quantum theory of optical coherence. *Phys. Rev.*, 130(6):2529–2539, June 1963b. doi: 10.1103/PhysRev.130.2529.

[Glauber, 1963c] R. J. Glauber. Photon correlations. *Phys. Rev. Lett.*, 10(3):84–86, February 1963c. doi: 10.1103/PhysRevLett.10.84.

[Glauber, 2005] R. J. Glauber. Nobel lecture: One hundred years of light quanta. *Nobelprize.org.*, pages 75–98, October 2005. URL `http://www.nobelprize.org/nobel_prizes/physics/laureates/2005/glauber-lecture.html`.

[Gottesman, 1997] D. Gottesman. *Stabilizer Codes and Quantum Error Correction*. PhD thesis, California Institute of Technology, California Institute of Technology, May 1997.

[Grabchak, 2013] M. Grabchak. A note on the multivariate clt and convergence of levy processes at long and short times. *ArXiv*, June 2013.

[Griffiths, 1998] D. J. Griffiths. *Introduction To Electrodynamics*. Pearson, 3 edition, December 1998.

[Griffiths, 2016] D. J. Griffiths. *Introduction to Quantum Mechanics*. Cambridge University Press, 2 edition, August 2016. ISBN 9781107179868.

[Grynberg et al., 2010] G. Grynberg, A. Aspect, and C. Fabre. *Introduction to Quantum Optics: From the Semi-classical Approach to Quantized Light*. Cambridge University Press, 1 edition, 2010. ISBN 9780521551120.

[Hartshorne, 2010] R. Hartshorne. *Deformation Theory*. Graduate Texts in Mathematics. Springer, 2010. ISBN 9781441915955. doi: 10.1007/978-1-4419-1596-2.

[Hayashi, 2005] M. Hayashi. *Asymptotic Theory of Quantum Statistical Inference*. World Scientific Publishing, February 2005. ISBN 9789812560155.

[Hayashi and Matsumoto, 2008] M. Hayashi and K. Matsumoto. Asymptotic performance of optimal state estimation in qubit system. *J. Math. Phys.*, 49(10):102101, 2008. doi: https://doi.org/10.1063/1.2988130.

[Heinze et al., 2015] D. Heinze, D. Breddermann, A. Zrenner, and S. Schumacher. A quantum dot single-photon source with on-the-fly all-optical polarization control and timed emission. *Nat. Commun.*, 6:8473, October 2015. doi: http://dx.doi.org/10.1038/ncomms9473.

[Heller et al., 2013] I. Heller, G. Sitters, O. D. Broekmans, G. Farge, C. Menges, W. Wende, S. W. Hell, E. J. G. Peterman, and G. J. L. Wuite. Sted nanoscopy combined with optical tweezers reveals protein dynamics on densely covered dna. *Nat. Methods*, 10:910–916, August 2013. doi: 10.1038/nmeth.2599.

[Helstrom, 1968] C. Helstrom. The minimum variance of estimates in quantum signal detection. *IEEE Trans. Inf. Theory*, 14(2):234–242, March 1968. doi: 10.1109/TIT.1968.1054108.

[Helstrom, 1973] C. W. Helstrom. Cramér-rao inequalities for operator-valued measures in quantum mechanics. *Int. J. Theor. Phys.*, 8(5):361–376, September 1973. doi: 10.1007/BF00687093.

[Helstrom, 1976] C. W. Helstrom. *Quantum Detection and Estimation Theory*. Academic Press Inc., 1976. ISBN 9780123400505.

[Higgins et al., 2007] B. L. Higgins, D. W. Berry, S. D. Bartlett, H. M. Wiseman, and G. J. Pryde. Entanglement-free heisenberg-limited phase estimation. *Nature*, 450:393, November 2007. doi: 10.1038/nature06257.

[Higgins et al., 2009] B. L. Higgins, D. W. Berry, S. D. Bartlett, M. W. Mitchell, H. M. Wiseman, and G. J. Pryde. Demonstrating heisenberg-limited unambiguous phase estimation without adaptive measurements. *New J. Phys.*, 11(7):073023, July 2009. doi: 10.1088/1367-2630/11/7/073023.

[Hilgevoord and Uffink, 1991] J. Hilgevoord and J. Uffink. Uncertainty in prediction and in inference. *Found. Phys.*, 21(3):323–341, 1991. doi: 10.1007/BF01883638.

[Holevo, 2011] A. S. Holevo. *Probabilistic and Statistical Aspects of Quantum Theory*. Springer, 1 edition, 2011. ISBN 9788876423758. doi: 10.1007/978-88-7642-378-9.

[Holevo, 1978] A. Holevo. Estimation of shift parameters of a quantum state. *Reports on Mathematical Physics*, 13(3):379 – 399, 1978. doi: https://doi.org/10.1016/0034-4877(78)90065-4.

[Huang et al., 2015] J. Huang, X. Qin, H. Zhong, Y. Ke, and C. Lee. Quantum metrology with spin cat states under dissipation. *Sci. Rep.*, 5(17894), December 2015.

[Huelga et al., 1997] S. F. Huelga, C. Macchiavello, T. Pellizzari, A. K. Ekert, M. B. Plenio, and J. I. Cirac. Improvement of frequency standards with quantum entanglement. *Phys. Rev. Lett.*, 79(20): 3865–3868, November 1997. doi: 10.1103/PhysRevLett.79.3865.

[Humphreys et al., 2013] P. C. Humphreys, M. Barbieri, A. Datta, and I. A. Walmsley. Quantum enhanced multiple phase estimation. *Phys. Rev. Lett.*, 111(7):070403, August 2013. doi: 10.1103/PhysRevLett.111.070403.

[ichi Amari, 2016] S. ichi Amari. *Information Geometry and Its Applications*, volume 194 of *Applied Mathematical Sciences*. Springer, 1 edition, February 2016. ISBN 9784431559771.

[Jackson, 1998] J. D. Jackson. *Classical Electrodynamics*. John Wiley Sons, 3 edition, December 1998. ISBN 9780471309321.

[Jeong et al., 2014] H. Jeong, Y. Lim, and M. S. Kim. Coarsening measurement references and the quantum-to-classical transition. *Phys. Rev. Lett.*, 112(1):010402, January 2014. doi: 10.1103/PhysRevLett.112.010402.

[Jiang, 2014] Z. Jiang. Quantum fisher information for states in exponential form. *Phys. Rev. A*, 89: 032128, March 2014. doi: 10.1103/PhysRevA.89.032128.

[John D. Dixon, 1996] B. M. John D. Dixon. *Permutation Groups*, volume 163 of *Graduate Texts in Mathematics*. Springer New York, 1996. ISBN 978-1-4612-6885-7. doi: 10.1007/978-1-4612-0731-3.

[Jones and Kok, 2010] P. J. Jones and P. Kok. Geometric derivation of the quantum speed limit. *Phys. Rev. A*, 82(March):022107, August 2010. doi: 10.1103/PhysRevA.82.022107.

[Jordan, 1964] T. F. Jordan. Operators for observables in quantum optics. *Phys. Lett.*, 11(4):289–291, August 1964. doi: https://doi.org/10.1016/0031-9163(64)90331-2.

[Kadianakis and Travlopanos, 2016] N. Kadianakis and F. I. Travlopanos. Infinitesimally affine deformations of a hypersurface. *Math. Mech. Solids*, December 2016. doi: 10.1177/1081286516680261.

[Kahn and Guţă, 2009] J. Kahn and M. Guţă. Local asymptotic normality for finite dimensional quantum systems. *Commun. Math. Phys.*, 289(2):597–652, July 2009. doi: 10.1007/s00220-009-0787-3.

[Kay, 1993] S. Kay. *Fundamentals of Statistical Signal Processing, Volume I: Estimation Theory (v. 1)*. Prentice Hall, United States, 1 edition, 1993. ISBN 9780133457117.

[Kimble et al., 1977] H. J. Kimble, M. Dagenais, and L. Mandel. Photon antibunching in resonance fluorescence. *Phys. Rev. Lett.*, 39(11):691–695, September 1977. doi: 10.1103/PhysRevLett.39.691.

[Knight et al., 2003] P. L. Knight, E. A. Hinds, M. B. Plenio, D. J. Wineland, M. Barrett, J. Britton, J. Chiaverini, B. DeMarco, W. M. Itano, B. Jelenković, et al. Quantum information processing with trapped ions. *Philos. Trans. R. Soc. Lond. A: Math., Phys. Eng. Sci.*, 361(1808):1349–1361, July 2003. doi: 10.1098/rsta.2003.1205.

[Knill et al., 2001] E. Knill, R. Laflamme, and G. J. Milburn. A scheme for effcient quantum computation with linear optics. *Nature*, 409:46–52, January 2001. URL http://dx.doi.org/10.1038/35051009.

[Knott et al., 2016] P. A. Knott, T. J. Proctor, A. J. Hayes, J. F. Ralph, P. Kok, and J. A. Dunningham. Local versus global strategies in multiparameter estimation. *Phys. Rev. A*, 94(6):062312, December 2016. doi: 10.1103/PhysRevA.94.062312.

[Kok, 2016] P. Kok. Photonic quantum information processing. *Contemp. Phys.*, 57(4):526–544, May 2016. doi: 10.1080/00107514.2016.1178472.

[Kok, 2018] P. Kok. *A First Introduction to Quantum Physics*. Springer, 1 edition, August 2018. ISBN 9783319922065.

[Kok and Lovett, 2010] P. Kok and B. W. Lovett. *Introduction to Optical Quantum Information Processing*. Cambridge University Press, Cambridge, UK, 1 edition, 2010. ISBN 978-0521519144.

[Kok et al., 2007] P. Kok, W. J. Munro, K. Nemoto, T. C. Ralph, J. P. Dowling, and G. J. Milburn. Linear optical quantum computing with photonic qubits. *Rev. Mod. Phys.*, 79(1):135–174, January 2007. doi: 10.1103/RevModPhys.79.135.

[Kok et al., 2017] P. Kok, J. Dunningham, and J. F. Ralph. Role of entanglement in calibrating optical quantum gyroscopes. *Phys. Rev. A*, 95(1):012326, January 2017. doi: 10.1103/PhysRevA.95.012326.

[Kolenderski and Demkowicz-Dobrzański, 2008] P. Kolenderski and R. Demkowicz-Dobrzański. Optimal state for keeping reference frames aligned and the platonic solids. *Phys. Rev. A*, 78(5):052333, November 2008. doi: 10.1103/PhysRevA.78.052333.

[Kolobov, 2007] M. I. Kolobov. *Quantum Imaging*. Springer, 1 edition, 2007. ISBN 9780387338187. doi: 10.1007/0-387-33988-4.

[Kołodyński and Demkowicz-Dobrzański, 2010] J. Kołodyński and R. Demkowicz-Dobrzański. Phase estimation without a priori phase knowledge in the presence of loss. *Phys. Rev. A*, 82(5):053804, November 2010. doi: 10.1103/PhysRevA.82.053804.

[Kołodyński and Demkowicz-Dobrzański, 2013] J. Kołodyński and R. Demkowicz-Dobrzański. Efficient tools for quantum metrology with uncorrelated noise. *New J. Phys.*, 15(7):073043, July 2013. doi: 10.1088/1367-2630/15/7/073043.

[Kreyszig, 1989] E. Kreyszig. *Introductory Functional Analysis With Applications*. John Wiley Sons, 1989. ISBN 9780471504597.

[Lee et al., 2002] H. Lee, P. Kok, and J. P. Dowling. A quantum rosetta stone for interferometry. *J. Mod. Opt.*, 49(14-15):2325–2338, April 2002. doi: 10.1080/0950034021000011536.

[Leibfried et al., 2004] D. Leibfried, M. D. Barrett, T. Schaetz, J. Britton, J. Chiaverini, W. M. Itano, J. D. Jost, C. Langer, and D. J. Wineland. Toward heisenberg-limited spectroscopy with multiparticle entangled states. *Science*, 304(5676):1476–1478, June 2004. doi: 10.1126/science.1097576.

[Leonhardt, 2010] U. Leonhardt. *Essential Quantum Optics: From Quantum Measurements to Black Holes*. Cambridge University Press, 1 edition, February 2010. ISBN 9780521145053.

[Li et al., 2016] D. Li, B. T. Gard, Y. Gao, C.-H. Yuan, W. Zhang, H. Lee, and J. P. Dowling. Phase sensitivity at the heisenberg limit in an su(1,1) interferometer via parity detection. *Phys. Rev. A*, 94 (6):063840, December 2016. doi: 10.1103/PhysRevA.94.063840.

[Liu et al., 2014] J. Liu, X. Jing, W. Zhong, and X. Wang. Quantum fisher information for density matrices with arbitrary ranks. *Comms. in Theo. Phys.*, 61(1):45, 2014. doi: 10.1088/0253-6102/61/1/08.

[Liu et al., 2015] J. Liu, X.-X. Jing, and X. Wang. Quantum metrology with unitary parametrization processes. *Sci. Rep.*, 5:8565, February 2015. doi: 10.1038/srep08565.

[Liu et al., 2016] J. Liu, J. Chen, X.-x. Jing, and X. Wang. Quantum fisher information and symmetric logarithmic derivative via anti-commutators. *J. Phys. A: Math. Theoret.*, 49(27):275302, May 2016. doi: 10.1088/1751-8113/49/27/275302.

[Lloyd, 2008] S. Lloyd. Enhanced sensitivity of photodetection via quantum illumination. *Science*, 321: 1463–1466, September 2008. doi: 10.1126/science.1160627.

[Loudon and Knight, 1987] R. Loudon and P. L. Knight. Squeezed light. *J. Mod. Opt.*, 34(6-7):709–759, 06 1987. doi: 10.1080/09500348714550721.

[Loudon, 2000] R. Loudon. *The Quantum Theory of Light*. Oxford University Press, 3 edition, November 2000. ISBN 9780198501763.

[Luff et al., 1998] B. Luff, J. Wilkinson, J. Piehler, U. Hollenbach, J. Ingenhoff, and N. Fabricius. Integrated optical mach–zehnder biosensor. *J. Lightwave Technol.*, 16(4):583–592, April 1998. doi: 10.1109/50.664067.

[Luo, 2000] S. Luo. Quantum fisher information and uncertainty relations. *Lett. Math. Phys.*, 53(3): 243–251, August 2000. doi: 10.1023/A:1011080128419.

[Macintosh et al., 2014] B. Macintosh et al. First light of the gemini planet imager. *Proc. Natl. Acad. Sci.*, 111(35):12661–12666, September 2014. doi: 10.1073/pnas.1304215111.

[Magesan et al., 2013] E. Magesan, A. Cooper, H. Yum, and P. Cappellaro. Reconstructing the profile of time-varying magnetic fields with quantum sensors. *Phys. Rev. A*, 88(3):032107, September 2013. doi: 10.1103/PhysRevA.88.032107.

[Marian and Marian, 2012] P. Marian and T. A. Marian. Uhlmann fidelity between two-mode gaussian states. *Phys. Rev. A*, 86(2):022340, August 2012. doi: 10.1103/PhysRevA.86.022340.

[Markov, 2014] I. L. Markov. Limits on fundamental limits to computation. *Nature*, 512:147–154, August 2014. doi: 10.1038/nature13570.

[Matsukevich et al., 2008] D. N. Matsukevich, P. Maunz, D. L. Moehring, S. Olmschenk, and C. Monroe. Bell inequality violation with two remote atomic qubits. *Phys. Rev. Lett.*, 100(15):150404, April 2008. doi: 10.1103/PhysRevLett.100.150404.

[Matsumoto, 2002] K. Matsumoto. A new approach to the cramér-rao-type bound of the pure-state model. *J. Phys. A: Math. Gen.*, 35(13):3111, March 2002. doi: http://stacks.iop.org/0305-4470/35/i=13/a=307.

[Menicucci et al., 2006] N. C. Menicucci, P. van Loock, M. Gu, C. Weedbrook, T. C. Ralph, and M. A. Nielsen. Universal quantum computation with continuous-variable cluster states. *Phys. Rev. Lett.*, 97(11):110501, September 2006. doi: 10.1103/PhysRevLett.97.110501.

[Menicucci et al., 2007] N. C. Menicucci, S. T. Flammia, H. Zaidi, and O. Pfister. Ultracompact generation of continuous-variable cluster states. *Phys. Rev. A*, 76(1):010302, July 2007. doi: 10.1103/PhysRevA.76.010302.

[Moerner, 2007] W. E. Moerner. New directions in single-molecule imaging and analysis. *Proc. Natl. Acad. Sci.*, 104(31):12596–12602, July 2007. doi: 10.1073/pnas.0610081104.

[Monras, 2013] A. Monras. Phase space formalism for quantum estimation of gaussian states. March 2013.

[Monras and Illuminati, 2011] A. Monras and F. Illuminati. Measurement of damping and temperature: Precision bounds in gaussian dissipative channels. *Phys. Rev. A*, 83:012315, January 2011. doi: 10.1103/PhysRevA.83.012315.

[Mukai and Yamamoto, 1981] T. Mukai and Y. Yamamoto. Noise characteristics of semiconductor laser amplifiers. *Electron. Lett.*, 17(1):31–33, January 1981. doi: 10.1049/el:19810024.

[Nair and Tsang, 2015] R. Nair and M. Tsang. Quantum optimality of photon counting for temperature measurement of thermal astronomical sources. *Astrophysical J.*, 808(2):125, August 2015. doi: 10.1088/0004-637X/808/2/125.

[Napolitano et al., 2010] M. Napolitano, M. Koschorreck, B. Dubost, N. Behbood, R. J. Sewell, and M. W. Mitchell. Interaction-based quantum metrology showing scaling beyond the heisenberg limit. *Nature*, 471:486–489, December 2010. ISSN 0028-0836. doi: 10.1038/nature09778.

[Nielsen and Chuang, 2010] M. A. Nielsen and I. L. Chuang. *Quantum Computation and Quantum Information*. Cambridge University Press, 10th edition, 2010. ISBN 9781107002173.

[Northup and Blatt, 2014] T. E. Northup and R. Blatt. Quantum information transfer using photons. *Nat. Photon.*, 8:356–363, April 2014. doi: 10.1038/NPHOTON.2014.53.

[O'Brien et al., 2003] J. L. O'Brien, G. J. Pryde, A. G. White, T. C. Ralph, and D. Branning. Demonstration of an all-optical quantum controlled-not gate. *Nature*, 426:264–267, November 2003. URL `http://dx.doi.org/10.1038/nature02054`.

[O'Brien, 2007] J. L. O'Brien. Optical quantum computing. *Science*, 318(5856):1567–1570, December 2007. doi: 10.1126/science.1142892.

[Oppel et al., 2012] S. Oppel, T. Büttner, P. Kok, and J. von Zanthier. Superresolving multiphoton interferences with independent light sources. *Phys. Rev. Lett.*, 109(23):233603, December 2012. doi: 10.1103/PhysRevLett.109.233603.

[Ou et al., 1992] Z. Y. Ou, S. F. Pereira, H. J. Kimble, and K. C. Peng. Realization of the einstein-podolsky-rosen paradox for continuous variables. *Phys. Rev. Lett.*, 68(25):3663–3666, June 1992. doi: 10.1103/PhysRevLett.68.3663.

[Pang and Brun, 2014] S. Pang and T. A. Brun. Quantum metrology for a general hamiltonian parameter. *Phys. Rev. A*, 90(2):022117, August 2014. doi: 10.1103/PhysRevA.90.022117.

[Pang and Brun, 2016] S. Pang and T. A. Brun. Erratum: Quantum metrology for a general hamiltonian parameter [phys. rev. a 90, 022117 (2014)]. *Phys. Rev. A*, 93(5):059901, May 2016. doi: 10.1103/PhysRevA.93.059901.

[Paris, 2009] M. G. A. Paris. Quantum estimation for quantum technologies. *Int. J. Quantum Inf.*, 7: 125–137, 2009. doi: 10.1142/S0219749909004839.

[Pearce et al., 2015] M. E. Pearce, T. Mehringer, J. von Zanthier, and P. Kok. Precision estimation of source dimensions from higher-order intensity correlations. *Phys. Rev. A*, 92:043831, October 2015. doi: 10.1103/PhysRevA.92.043831.

[Pearce et al., 2017] M. E. Pearce, E. T. Campbell, and P. Kok. Optimal quantum metrology of distant black bodies. *Quantum*, 1:21, July 2017. doi: 10.22331/q-2017-07-26-21.

[Peskin and Schroeder, 1995] M. E. Peskin and D. V. Schroeder. *An Introduction To Quantum Field Theory*. CRC Press, 1 edition, October 1995. ISBN 9780201503975.

[Pezzé and Smerzi, 2014] L. Pezzé and A. Smerzi. Quantum theory of phase estimation. *Atom Interferometry, Proc. Int. School Phys. Enrico Fermi, Course 188 Amsterdam*, page 691, November 2014.

[Pinel et al., 2013] O. Pinel, P. Jian, N. Treps, C. Fabre, and D. Braun. Quantum parameter estimation using general single-mode gaussian states. *Phys. Rev. A*, 88(4):040102, October 2013. doi: 10.1103/PhysRevA.88.040102.

[Pinel et al., 2012] O. Pinel, J. Fade, D. Braun, P. Jian, N. Treps, and C. Fabre. Ultimate sensitivity of precision measurements with intense gaussian quantum light: A multimodal approach. *Phys. Rev. A*, 85(1):010101, January 2012. doi: 10.1103/PhysRevA.85.010101.

[Pittman et al., 1995] T. B. Pittman, Y. H. Shih, D. V. Strekalov, and A. V. Sergienko. Optical imaging by means of two-photon quantum entanglement. *Phys. Rev. A*, 52(5):R3429–R3432, November 1995. doi: 10.1103/PhysRevA.52.R3429.

[Porzio et al., 2007] A. Porzio, V. D'Auria, P. Aniello, M. Paris, and S. Solimeno. Quantum communication exploiting above threshold opo intensity correlations and polarization encoding. *Opt. Lasers Eng.*, 45(4):463 – 467, April 2007. doi: https://doi.org/10.1016/j.optlaseng.2005.07.012.

[Purcel, 1956] E. M. Purcel. The question of correlation between photons in coherent light rays. *Nature*, 178:1449–1450, 12 1956. URL `http://dx.doi.org/10.1038/1781449a0`.

[Ragy et al., 2016] S. Ragy, M. Jarzyna, and R. Demkowicz-Dobrzański. Compatibility in multiparameter quantum metrology. *Phys. Rev. A*, 94(5):052108, November 2016. doi: 10.1103/PhysRevA.94.052108.

[Ralph et al., 2002] T. C. Ralph, N. K. Langford, T. B. Bell, and A. G. White. Linear optical controlled-not gate in the coincidence basis. *Phys. Rev. A*, 65(6):062324, June 2002. doi: 10.1103/PhysRevA.65.062324.

[Rayleigh, 1879] L. Rayleigh. Investigations in optics, with special reference to the spectroscope. *Philos. Mag. Ser.*, 8(49):261–274, 1879. doi: 10.1080/14786447908639684.

[Reid and Drummond, 1988] M. D. Reid and P. D. Drummond. Quantum correlations of phase in nondegenerate parametric oscillation. *Phys. Rev. Lett.*, 60(26):2731–2733, June 1988. doi: 10.1103/PhysRevLett.60.2731.

[Rigovacca et al., 2017] L. Rigovacca, A. Farace, L. A. M. Souza, A. De Pasquale, V. Giovannetti, and G. Adesso. Versatile gaussian probes for squeezing estimation. *Phys. Rev. A*, 95(5):052331, May 2017. doi: 10.1103/PhysRevA.95.052331.

[Robertson, 1929] H. P. Robertson. The uncertainty principle. *Phys. Rev.*, 34(1):163–164, July 1929. doi: 10.1103/PhysRev.34.163.

[Roy and Braunstein, 2008] S. M. Roy and S. L. Braunstein. Exponentially enhanced quantum metrology. *Phys. Rev. Lett.*, 100:220501, June 2008. doi: 10.1103/PhysRevLett.100.220501.

[Ruppert et al., 2016] L. Ruppert, V. C. Usenko, and R. Filip. Estimation of the covariance matrix of macroscopic quantum states. *Phys. Rev. A*, 93(5):052114, May 2016. doi: 10.1103/PhysRevA.93.052114.

[Sabìn et al., 2014] C. Sabìn, D. E. Bruschi, M. Ahmadi, and I. Fuentes. Phonon creation by gravitational waves. *New J. Phys.*, 16(8):085003, 2014. ISSN 1367-2630.

[Sakurai and Napolitano, 2017] J. J. Sakurai and J. Napolitano. *Modern Quantum Mechanics*. Cambridge University Press, 2 edition, 2017. ISBN 9781108422413.

[Sanders and Milburn, 1995] B. C. Sanders and G. J. Milburn. Optimal quantum measurements for phase estimation. *Phys. Rev. Lett.*, 75(16):2944–2947, October 1995. doi: 10.1103/PhysRevLett.75.2944.

[Santori et al., 2001] C. Santori, M. Pelton, G. Solomon, Y. Dale, and Y. Yamamoto. Triggered single photons from a quantum dot. *Phys. Rev. Lett.*, 86(8):1502–1505, February 2001. doi: 10.1103/PhysRevLett.86.1502.

[Sarovar and Milburn, 2006] M. Sarovar and G. J. Milburn. Optimal estimation of one-parameter quantum channels. *J. Phys. A: Math. Gen.*, 39(26):8487, June 2006. URL `http://stacks.iop.org/0305-4470/39/i=26/a=015`.

[Schleich, 2001] W. P. Schleich. *Quantum Optics in Phase Space*. Wiley VCH, 1 edition, February 2001. ISBN 9783527294350.

[Schumaker, 1986] B. L. Schumaker. Quantum mechanical pure states with gaussian wave functions. *Phys. Rep.*, 135(6):317–408, April 1986.

[Scully and Zubairy, 1997] M. O. Scully and S. Zubairy. *Quantum Optics*. Cambridge University Press, 1 edition, 1997. ISBN 9780524235959.

[Seveso and Paris, 2017] L. Seveso and M. G. A. Paris. Estimation of hamiltonian parameters beyond the quantum cramér-rao bound. *ArXiv*, December 2017.

[Shchukin and Vogel, 2005] E. V. Shchukin and W. Vogel. Nonclassical moments and their measurement. *Phys. Rev. A*, 72(4):043808, October 2005. doi: 10.1103/PhysRevA.72.043808.

[Shields, 2007] A. J. Shields. Semiconductor quantum light sources. *Nat. Photon.*, 1:215, April 2007. doi: http://dx.doi.org/10.1038/nphoton.2007.46.

[Sidhu and Kok, 2017] J. S. Sidhu and P. Kok. Quantum metrology of spatial deformation using arrays of classical and quantum light emitters. *Phys. Rev. A*, 95(6):063829, June 2017. doi: 10.1103/PhysRevA.95.063829.

[Sidhu and Kok, 2018] J. S. Sidhu and P. Kok. Quantum fisher information for general spatial deformations of quantum emitters. *ArXiv*, February 2018.

[Simon et al., 1988] R. Simon, E. C. G. Sudarshan, and N. Mukunda. Gaussian pure states in quantum mechanics and the symplectic group. *Phys. Rev. A*, 37(8):3028–3038, April 1988. doi: 10.1103/PhysRevA.37.3028.

[Skotiniotis et al., 2015] M. Skotiniotis, P. Sekatski, and W. Dür. Quantum metrology for the ising hamiltonian with transverse magnetic field. *New J. Phys.*, 17(7):073032, July 2015. doi: 10.1088/1367-2630/17/7/073032.

[Slusher et al., 1985] R. E. Slusher, L. W. Hollberg, B. Yurke, J. C. Mertz, and J. F. Valley. Observation of squeezed states generated by four-wave mixing in an optical cavity. *Phys. Rev. Lett.*, 55(22): 2409–2412, November 1985. doi: 10.1103/PhysRevLett.55.2409.

[Spedalieri et al., 2013] G. Spedalieri, C. Weedbrook, and S. Pirandola. A limit formula for the quantum fidelity. *J. Phys. A: Math. Theoret.*, 46(2):025304, December 2013. doi: 10.1088/1751-8113/46/2/025304.

[Spring et al., 2017] J. B. Spring, P. L. Mennea, B. J. Metcalf, P. C. Humphreys, J. C. Gates, H. L. Rogers, C. Söller, B. J. Smith, W. S. Kolthammer, P. G. R. Smith, and I. A. Walmsley. Chip-based array of near-identical, pure, heralded single-photon sources. *Optica*, 4(1):90–96, January 2017. doi: 10.1364/OPTICA.4.000090.

[Sreenivasan, 2017] S. V. Sreenivasan. Nanoimprint lithography steppers for volume fabrication of leading-edge semiconductor integrated circuits. *Microsystems & Nanoengineering*, 3(17075):17075–17094, September 2017. doi: 10.1038/micronano.2017.75.

[Stobińska et al., 2008] M. Stobińska, G. J. Milburn, and K. Wódkiewicz. Wigner function evolution of quantum states in the presence of self-kerr interaction. *Phys. Rev. A*, 78(1):013810, July 2008. doi: 10.1103/PhysRevA.78.013810.

[Strauss, 2008] W. A. Strauss. *Partial Differential Equations: An Introduction*. John Wiley Sons, 2 edition, January 2008. ISBN 9780470054567.

[Takeuchi et al., 2003] S. Takeuchi, R. Okamoto, and K. Sasaki. A single photon source using parametric down conversion. In *2003 European Quantum Electronics Conference. EQEC 2003 (IEEE Cat No.03TH8665)*, page 320, June 2003. doi: 10.1109/EQEC.2003.1314177.

[Tan et al., 2008] S.-H. Tan, B. I. Erkmen, V. Giovannetti, S. Guha, S. Lloyd, L. Maccone, S. Pirandola, and J. H. Shapiro. Quantum illumination with gaussian states. *Phys. Rev. Lett.*, 101(25):253601, December 2008. doi: 10.1103/PhysRevLett.101.253601.

[Thiel et al., 2007] C. Thiel, T. Bastin, J. Martin, E. Solano, J. von Zanthier, and G. S. Agarwal. Quantum imaging with incoherent photons. *Phys. Rev. Lett.*, 99(13):133603, September 2007. doi: 10.1103/PhysRevLett.99.133603.

[Tilma et al., 2010] T. Tilma, S. Hamaji, W. J. Munro, and K. Nemoto. Entanglement is not a critical resource for quantum metrology. *Phys. Rev. A*, 81(2):022108, February 2010. doi: 10.1103/PhysRevA.81.022108.

[Tóth and Apellaniz, 2014] G. Tóth and I. Apellaniz. Quantum metrology from a quantum information science perspective. *J. Phys. A: Math. Theoret.*, 47(42):424006, October 2014. doi: 10.1088/1751-8113/47/42/424006.

[Tsang, 2008] M. Tsang. Fundamental quantum limit to the multiphoton absorption rate for monochromatic light. *Phys. Rev. Lett.*, 101:033602, July 2008. doi: 10.1103/PhysRevLett.101.033602.

[Tsang, 2015] M. Tsang. Quantum limits to optical point-source localization. *Optica*, 2(7):646–653, July 2015. doi: 10.1364/OPTICA.2.000646.

[Tsang et al., 2011] M. Tsang, H. M. Wiseman, and C. M. Caves. Fundamental quantum limit to waveform estimation. *Phys. Rev. Lett.*, 106(9):090401, March 2011. doi: 10.1103/PhysRevLett.106.090401.

[Urizar-Lanz et al., 2013] I. Urizar-Lanz, P. Hyllus, I. L. Egusquiza, M. W. Mitchell, and G. Tóth. Macroscopic singlet states for gradient magnetometry. *Phys. Rev. A*, 88(1):013626, July 2013. doi: 10.1103/PhysRevA.88.013626.

[Vaneph et al., 2013] C. Vaneph, T. Tufarelli, and M. G. Genoni. Quantum estimation of a two-phase spin rotation. *Quantum Measurements and Quantum Metrology*, 1:12, June 2013. doi: 10.2478/qmetro-2013-0003.

[Vidrighin et al., 2014] M. D. Vidrighin, G. Donati, M. G. Genoni, X.-M. Jin, W. S. Kolthammer, M. Kim, A. Datta, M. Barbieri, and I. A. Walmsley. Joint estimation of phase and phase diffusion for quantum metrology. *Nat. Commun.*, 5:3532, April 2014. doi: 10.1038/ncomms4532.

[von Neumann, 1996] J. von Neumann. *Mathematical Foundations of Quantum Mechanics*. Princeton University Press, October 1996. ISBN 9780691028934.

[Šafránek et al., 2015] D. Šafránek, A. R. Lee, and I. Fuentes. Quantum parameter estimation using multi-mode gaussian states. *New J. Phys.*, 17(7):073016, July 2015. doi: 10.1088/1367-2630/17/7/073016.

[Walls and Milburn, 2008] D. Walls and G. J. Milburn. *Quantum Optics*. Springer-Verlag Berlin Heidelberg, 2 edition, 2008. ISBN 9783540285731.

[Wang et al., 2007] X.-B. Wang, T. Hiroshima, A. Tomita, and M. Hayashi. Quantum information with gaussian states. *Phys. Rep.*, 448(1):1–111, August 2007. doi: https://doi.org/10.1016/j.physrep.2007.04.005.

[Weedbrook et al., 2012] C. Weedbrook, S. Pirandola, R. García-Patrón, N. J. Cerf, T. C. Ralph, J. H. Shapiro, and S. Lloyd. Gaussian quantum information. *Rev. Mod. Phys.*, 84(2):621–669, May 2012. doi: 10.1103/RevModPhys.84.621.

[Weihs et al., 1998] G. Weihs, T. Jennewein, C. Simon, H. Weinfurter, and A. Zeilinger. Violation of bell's inequality under strict einstein locality conditions. *Phys. Rev. Lett.*, 81(23):5039–5043, December 1998. doi: 10.1103/PhysRevLett.81.5039.

[Wetterich, 2009] C. Wetterich. Emergence of quantum mechanics from classical statistics. *J Phys.: Conf. Ser.*, 174(1):012008, 2009. doi: 10.1088/1742-6596/174/1/012008.

[Wilcox, 1967] R. M. Wilcox. Exponential operators and parameter differentiation in quantum physics. *J. Math. Phys.*, 8(4):962–982, 1967. doi: 10.1063/1.1705306.

[Wolfgramm et al., 2013] F. Wolfgramm, C. Vitelli, F. A. Beduini, N. Godbout, and M. W. Mitchell. Entanglement-enhanced probing of a delicate material system. *Nat. Photon.*, 7:28–32, October 2013. ISSN 1749-4885. doi: 10.1038/nphoton.2012.300.

[Wooters, 1981] W. K. Wooters. Statistical distance and hilbert space. *Physical Review D*, 23:357–362, January 1981. doi: 10.1103/PhysRevD.23.357.

[Wu et al., 1986] L.-A. Wu, H. J. Kimble, J. L. Hall, and H. Wu. Generation of squeezed states by parametric down conversion. *Phys. Rev. Lett.*, 57(20):2520–2523, November 1986. doi: 10.1103/PhysRevLett.57.2520.

[Yang et al., 2001] C. Yang, A. Wax, M. S. Hahn, K. Badizadegan, R. R. Dasari, and M. S. Feld. Phase-referenced interferometer with subwavelength and subhertz sensitivity applied to the study of cell membrane dynamics. *Opt. Lett.*, 26(16):1271–1273, March 2001. doi: 10.1364/OL.26.001271.

[Yao et al., 2014] Y. Yao, L. Ge, X. Xiao, X. Wang, and C. P. Sun. Multiple phase estimation for arbitrary pure states under white noise. *Phys. Rev. A*, 90(6):062113, December 2014. doi: 10.1103/PhysRevA.90.062113.

[Yonezawa and Furusawa, 2010] H. Yonezawa and A. Furusawa. Continuous variable quantum information processing with squeezed states of light. *Optics and Spectroscopy*, 108(2):288–296, February 2010. doi: 10.1134/S0030400X10020189.

[Yonezawa et al., 2012] H. Yonezawa, D. Nakane, T. A. Wheatley, K. Iwasawa, S. Takeda, H. Arao, K. Ohki, K. Tsumura, D. W. Berry, T. C. Ralph, H. M. Wiseman, E. H. Huntington, and A. Furusawa. Quantum-enhanced optical-phase tracking. *Science*, 337(6101):1514–1517, September 2012.

[Yuan, 2016] H. Yuan. Sequential feedback scheme outperforms the parallel scheme for hamiltonian parameter estimation. *Phys. Rev. Lett.*, 117(16):160801, October 2016. doi: 10.1103/PhysRevLett.117.160801.

[Yuan and Fung, 2015] H. Yuan and C.-H. F. Fung. Optimal feedback scheme and universal time scaling for hamiltonian parameter estimation. *Phys. Rev. Lett.*, 115(11):110401, September 2015. doi: 10.1103/PhysRevLett.115.110401.

[Yue et al., 2014] J.-D. Yue, Y.-R. Zhang, and H. Fan. Quantum-enhanced metrology for multiple phase estimation with noise. *Sci. Rep.*, 4:5933, August 2014. doi: 10.1038/srep05933.

[Yuen and Lax, 1973] H. Yuen and M. Lax. Multiple-parameter quantum estimation and measurement of nonselfadjoint observables. *IEEE Trans. Inf. Theory*, 19(6):740–750, November 1973. doi: 10.1109/TIT.1973.1055103.

[Yurke et al., 1986] B. Yurke, S. L. McCall, and J. R. Klauder. Su(2) and su(1,1) interferometers. *Phys. Rev. A*, 33(6):4033–4054, June 1986. doi: 10.1103/PhysRevA.33.4033.

[Zhang and Fan, 2014] Y.-R. Zhang and H. Fan. Quantum metrological bounds for vector parameters. *Phys. Rev. A*, 90(4):043818, October 2014. doi: 10.1103/PhysRevA.90.043818.

[Zhou et al., 2018] J. Zhou, D. Huang, and Y. Guo. Long-distance continuous-variable quantum key distribution using separable gaussian states. *Phys. Rev. A*, 98(4):042303, October 2018. doi: 10.1103/PhysRevA.98.042303.

[Žitko, 2011] R. Žitko. Sneg–mathematica package for symbolic calculations with second-quantization-operator expressions. *Comput. Phys. Commun.*, 182(10):2259–2264, 2011. doi: https://doi.org/10.1016/j.cpc.2011.05.013.

[Zwierz et al., 2010] M. Zwierz, C. A. Pérez-Delgado, and P. Kok. General optimality of the heisenberg limit for quantum metrology. *Phys. Rev. Lett.*, 105(18):180402, October 2010. doi: 10.1103/PhysRevLett.105.180402.

[Zwierz et al., 2012a] M. Zwierz, C. A. Pérez-Delgado, and P. Kok. Ultimate limits to quantum metrology and the meaning of the Heisenberg limit. *Physical Review A*, 85, January 2012a. doi: 10.1103/PhysRevA.85.042112. URL `http://arxiv.org/abs/1201.2225`.

[Zwierz et al., 2012b] M. Zwierz, C. A. Pérez-Delgado, and P. Kok. Ultimate limits to quantum metrology and the meaning of the heisenberg limit. *Phys. Rev. A*, 85(4):042112, April 2012b. ISSN 1050-2947. doi: 10.1103/PhysRevA.85.042112.

Index